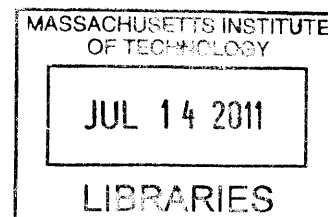


***Citrobacter rodentium* Induced Liver Changes in C57BL/6 Mice:
Animal Model of Acute Inflammatory Stress and Injury**

by

Arkadiusz R. Raczynski

B.A. Biology, Biochemistry
Carleton College, 2002



SUBMITTED TO THE DEPARTMENT OF BIOLOGICAL ENGINEERING IN PARTIAL
FULLFILLMENT OF THE REQUIREMENTS FOR THE DEGREE OF


DOCTOR OF PHILOSOPHY IN MOLECULAR AND SYSTEMS TOXICOLOGY AND
PHARMACOLOGY

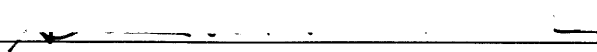
AT THE
MASSACHUSETTS INSTITUTE OF TECHNOLOGY

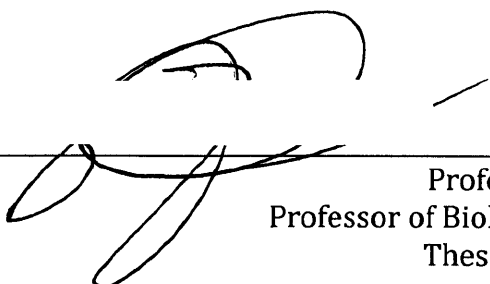
ARCHIVES

JUNE 2011

© 2011 Massachusetts Institute of Technology. All rights reserved

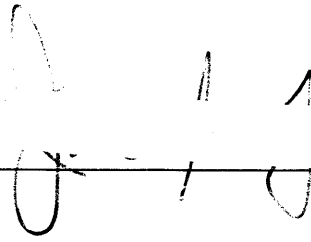
Signature of Author 
Biological Engineering
April 25th, 2011

Certified by 
Professor Steven R. Tannenbaum
Professor of Biological Engineering
Thesis Advisor

Accepted by 
Professor Linda Griffith
Professor of Biological Engineering
Thesis Committee Chair

This doctoral thesis has been examined by a committee of the Department of Biological Engineering as follows:

Certified by



Professor James G. Fox, MIT
Department of Comparative Medicine

Certified by



Dr. Eric R. Fedyk
Director of Immunobiology and Toxicology
Millennium Pharmaceuticals: A Takada Company

***Citrobacter rodentium* Induced Liver Changes in C57BL/6 Mice: Animal Model of Acute Inflammatory Stress and Injury**

By
Arkadiusz R. Raczynski

Submitted to the Department of Biological Engineering on April 25th, 2011
In Partial Fulfillment of the Requirements
For the Degree of Doctor of Philosophy in Molecular and Systems Toxicology and
Pharmacology

Abstract

The activation of inflammatory responses, while critical for host defense, contributes to hepatic injury in numerous acute and chronic liver disease states as well as drug-induced liver injury (DILI). The interactions that mediate susceptibility to liver injury and disease, however, are still poorly understood, underscored by the complexity of immune interactions and the diverse cellular composition and functions of the liver. Using *Citrobacter rodentium*, a well characterized rodent-specific enteric pathogen as a source of extrahepatic inflammatory stress; host liver responses, metabolic dysregulation, and susceptibility to injury in C57BL/6 mice were investigated. For the first time, we show altered liver pathology during the early course of *C. rodentium* infection, characterized by periportal necrosis indicative of thrombic ischemic injury, correlating with distinct circulating and tissue specific cytokine/chemokine profiles.

Using Acetaminophen (APAP), a widely used analgesic and well-characterized hepatotoxin, we evaluated liver responses in isolation and in the context of host inflammation to gain insight into the role of live bacterial infection in altering liver metabolism and susceptibility to DILI. We combined systemic and tissue-specific cytokine/chemokine levels, clinical serum chemistries, and histopathological assessments of hepatic and enteric inflammation and necrosis to measure molecular-level responses to treatment and their physiological effect. Using principal components analysis (PCA), clustering, partial least squares regression (PLSR), and a combination mutual-information-correlation network, enabled detection and visualization of both linear and nonlinear dependencies between molecules and physiological states across tissues and timepoints.

C. rodentium-induced inflammatory stress was finally investigated for its potential in altering drug pharmacokinetics (PK) of substrates varying in their metabolic biotransformation and clearance mechanisms. Infection resulted in increased systemic oral exposure (AUC) of clinically relevant xenobiotics such as verapamil, propranolol, and digoxin. Functionally, these changes were not found dependent on CYP-mediated biotransformation of parent compounds; rather, they appear driven more by proposed gut barrier compromise.

In conclusion, gastrointestinal infection with *C. rodentium* alters systemic and hepatocytes specific responses, not previously appreciated from this enteric pathogen, making it a useful model for studying host-pathogen interactions under acute hepatic inflammatory stress and injury.

Thesis Supervisor: Steven R. Tannenbaum
Title: Professor of Biological Engineering

Acknowledgments

I would like to dedicate my PhD to the late Dr. David Schauer, without his mentorship and support this work would not have been possible. His vision and incredible wisdom has been an inspiration throughout my tenure as a graduate student and this will surely carry on throughout my career. I am also in great debt to my parents Marek and Irena who made tremendous sacrifices in allowing me to pursue advanced studies. The support of Jeanette Raczynski, Derin Tugal, and other family and close friends has also been amazing throughout this process - their love and patience were invaluable.

My deepest thanks go to Steven Tannenbaum who was instrumental in not only his guidance, but also his efforts to continue my support after David's passing. Furthermore, he was extremely flexible in allowing my relocation to Cleveland towards the later part of the thesis write-up - for this I am extremely grateful and most appreciative.

Furthermore, I would like to extend my thanks to the remaining members of the committee: Dr. James Fox, Dr. Linda Griffith, and Dr. Eric Fedyk. Their suggestions and insight were extremely valuable towards a deeper understanding of the work and critical in guiding experiments and conclusions.

Thanks of course go to the Department of Biological Engineering and all of its members. I would like to particularly thank Marcia Weir, Amy Francis, Marcia Ross, JoAnn Sorrento, Roni Dudley-Cowans, and Dalia Fares and all other administrators for their assistance at MIT, and Doug Lauffenburger for all his efforts towards making research in this department so enjoyable and rewarding.

During my time at MIT I was also fortunate to work and collaborate with numerous scientists (and friends) that not only listened during experimental struggles, but whose advice was so valuable to me. These include Megan McBee, Diana Borenshtein, Adrienne Li, Alex Sheh, David Weingeist, Laure-anne Venterous, Luke Robinson, Mark Bathe, Robbie Barbero, Jaime Rivera, Jeremy Rock, and Justin Pritchard. Many thanks to Emily Miraldi who was instrumental in helping with computational approaches with the APAP-related work and Charles Knutson for his efforts and collaboration in the MGH project. I would like to also acknowledge the support of Biogen Idec, specifically Tonika Bohnert and Lawrence Gan for their efforts and intellectual contributions towards the pharmacokinetics project.

Also, the Department of Comparative Medicine (DCM) has been so incredibly supportive in many aspect of this thesis. From Gladys Valeriano in orchestrating animals space and time to Melissa Mobley and Amanda Potter for their technical

expertise, and Sureshkumar Muthupalani for his pathological assessments and research advice.

Prior to MIT, there is a tremendous amount of guidance that was vital in cultivating a desire to continue a scientific career. At Millennium Pharmaceuticals, Vilmos Csizmadia was instrumental in motivating me as a scientist. It was truly a privilege to have you as a mentor and I know it will undoubtedly continue for years to come. Passing on his depth of knowledge and expertise helped tremendously in my scientific endeavors at MIT. I would also like to thank Vito Sasseville, Scott Barros, Cindy Xia, Mingxiang Liao, and Vic Kadambi for their insightful discussions and guidance as a young scientist. And of course Peter Smith for giving me a chance to intern at MLNM fresh out of college – an invaluable research experience that has opened so many opportunities.

I would like to acknowledge the support of the ISN grant 6915549, and support from the Toxicology Training Grant (ES-070220) and Nitric Oxide Project Program Grant (P01 CA026731).

A final thanks to the support and effort from all those I may have omitted.

Table of Contents

ABSTRACT	3
ACKNOWLEDGMENTS	4
TABLE OF CONTENTS	6
LIST OF FIGURES	9
LIST OF TABLES	14
CHAPTER 1: INTRODUCTION	1-16
STRESS RESPONSE AND INFLAMMATION	1-16
INNATE IMMUNE SYSTEM IN STRESS AND INFLAMMATION.....	1-16
LIVER STRUCTURE AND FUNCTION	1-18
INFLAMMATION AND LIVER DISEASES	1-18
DRUG-INDUCED LIVER INJURY (DILI).....	1-19
ACETAMINOPHEN-INDUCED LIVER INJURY	1-20
ANIMAL MODELS OF LIVER INJURY	1-21
<i>CITROBACTER RODENTIUM</i>	1-22
CONCLUDING REMARKS:	1-23
FIGURES AND TABLES	1-25
CHAPTER 2: ENTERIC INFECTION WITH <i>CITROBACTER RODENTIUM</i> INDUCES HEPATIC INFLAMMATION AND COAGULATIVE LIVER NECROSIS PRIOR TO PEAK INFECTION AND COLONIC DISEASE	2-26
2.1 INTRODUCTION	2-27
2.2 RESULTS	2-28
2.3 DISCUSSION	2-32
2.4 SELECTED METHODS.....	2-35
2.5 FIGURES AND TABLES.....	2-39
CHAPTER 3: SYSTEMS ANALYSIS OF ACETAMINOPHEN-INDUCED LIVER INJURY UNDER CONDITIONS OF <i>CITROBACTER RODENTIUM</i>-INDUCED INFLAMMATORY STRESS	3-57
3.1 INTRODUCTION	3-58
3.2 RESULTS	3-60
3.3 DISCUSSION	3-67
3.4 SELECTED METHODS.....	3-75
3.5 FIGURES AND TABLES.....	3-81
CHAPTER 4: EFFECT OF SYSTEMIC INFLAMMATION FROM GASTROINTESTINAL INFECTION WITH <i>CITROBACTER RODENTIUM</i> ON ORAL DRUG EXPOSURE	4-98
4.1 INTRODUCTION	4-99
4.2 RESULTS	4-100
4.3 DISCUSSION	4-103
4.4 SELECTED METHODS.....	4-106
4.5 FIGURES AND TABLES.....	4-108
CHAPTER 5: CONCLUSIONS AND FUTURE WORK	5-115

APPENDIX A: GENERAL METHODS	A-117
MEDIA AND BACTERIAL STRAINS.....	A-117
QUANTITATIVE REAL-TIME PCR.....	A-117
APPENDIX B: EFFECT OF <i>CITROBACTER RODENTIUM</i> ON EARLY SERUM AND LIVER RESPONSES	B-118
B.1 INTRODUCTION.....	B-119
B.2 RESULTS.....	B-120
B.3 DISCUSSION.....	B-121
B.4 SELECTED METHODS.....	B-123
B.5 FIGURES AND TABLES.....	B-124
APPENDIX C: BIOMARKERS OF INFLAMMATORY BOWEL DISEASE	C-129
C.1 INTRODUCTION.....	C-130
C.2 RESULTS.....	C-131
C.3 DISCUSSION.....	C-133
C.4 SELECTED METHODS.....	C-134
C.5 FIGURES AND TABLES.....	C-136
APPENDIX D: SERUM AND KIDNEY CYTOKINE ANALYSIS OF STX-EXPRESSING <i>CITROBACTER RODENTIUM</i>	D-142
D.1 INTRODUCTION.....	D-143
D.2 RESULTS.....	D-144
D.3 DISCUSSION.....	D-145
D.4 SELECTED METHODS.....	D-146
D.5 SELECTED FIGURES.....	D-147
APPENDIX E: ABBREVIATIONS	E-149
APPENDIX F: REFERENCES	F-150

LIST OF FIGURES

Figure 1-1. Acetaminophen Metabolism and Elimination.....	1-25
Figure 2-1. Infection kinetics and body weight changes in C57BL/6 mice infected with <i>C. rodentium</i>	2-39
Figure 2-2. <i>C. rodentium</i> -induced colonic effects in C57BL/6 mice.	2-40
Figure 2-3. <i>C. rodentium</i> -induced necrosis and histological liver changes in C57BL/6 mice.....	2-41
Figure 2-4. Activated caspase 3 and KI-67 in <i>C. rodentium</i> -induced liver lesions	2-42
Figure 2-5. <i>C. rodentium</i> significantly increases Ki-67 ⁺ labeling index in livers....	2-43
Figure 2-6. Signal transduction changes in liver due to <i>C. rodentium</i> infection....	2-44
Figure 2-7. STAT3 activation in livers of <i>C. rodentium</i> inoculated C57BL/6 mice.....	2-45
Figure 2-8. Serum specific PLS-DA analysis of <i>C. rodentium</i> infected C57BL/6 mice at 3 DPI	2-46
Figure 2-9. Serum specific OPLS analysis of <i>C. rodentium</i> infected animals at 3 DPI..	2-47
Figure 2-10. Liver specific PLS-DA analysis of <i>C. rodentium</i> infected C57BL/6 mice at 3 DPI	2-48
Figure 2-11. Liver specific OPLS analysis of <i>C. rodentium</i> infected animals at 3 DPI..	2-49
Figure 2-12. Most influential variables in serum and liver for PLS-DA (necrosis versus no necrosis) and OPLS (ALT) models ranked by Variable in Projection (VIP) values.	2-51
Figure 3-1. Experimental design evaluating APAP-induced liver injury under <i>C. rodentium</i> -induced inflammatory stress.	3-81

Figure 3-2. <i>C. rodentium</i> and APAP-induced liver lesions evaluated by H&E at 3 DPI	3-82
Figure 3-3. PLS-DA analysis at 3 DPI:	3-83
Figure 3-4. <i>C. rodentium</i> and APAP-induced liver H&E and inflammation at 7 DPI.	3-84
Figure 3-5. PLS-DA analysis at 7DPI	3-85
Figure 3-6. OPLS results for prediction of ALT levels for all APAP treated mice. 3-86	
Figure 3-7. OPLS model for prediction of ALT levels for <i>Citro</i> (3DPI) treated mice...	3-87
Figure 3-8. Cytokine changes at 3 and 7 DPI with high ALT correlation for <i>Citro</i> or APAP alone.....	3-88
Figure 3-9. Correlations and Mutual information of targets for liver pathologies....	3-89
Figure 3-10. Mutual information and correlation maps for liver inflammation and necrosis.....	3-90
Figure 4-1. Effects of <i>C. rodentium</i> infection of Acetaminophen (5mg/kg) exposure.	4-108
Figure 4-2. Effects of <i>C. rodentium</i> infection on Fexofenadine (5mg/kg) exposure...	4-108
Figure 4-3. Effect of <i>C. rodentium</i> infection on Propranolol and Digoxin exposure...	4-109
Figure 4-4. Effects of <i>C. rodentium</i> infection on Verapamil (5mg/kg) exposure.....	4-110
Figure 4-5. Verapamil metabolites monitored after 5mg/kg PO dose	4-111
Figure 4-6. Method description and LC/MS/MS results of verapamil metabolite levels.....	4-111
Figure 4-7. Effect of <i>C. rodentium</i> on metabolites of verapamil (5mg/kg).....	4-112

SUPPLEMENTAL FIGURES

Supplemental Figure 2-1. Serum chemistry changes in C57BL/6 mice inoculated with <i>C. rodentium</i>	2-52
Supplemental Figure 2-2. Systemic cytokine and chemokine changes induced by <i>C. rodentium</i> infection in C57BL/6 mice.....	2-53
Supplemental Figure 2-3. Liver cytokine and chemokine changes induced by <i>C. rodentium</i> infection in C57BL/6 mice.....	2-54
Supplemental Figure 2-4. PLS-DA analysis of 3 and 7 DPI animals.....	2-55
Supplemental Figure 3-1. Affinity propagation clustering of all measurements.....	3-92
Supplemental Figure 3-2. Animals and measurements clustered by affinity propagation using Z-score values.....	3-93
Supplemental Figure 3-3. Mutual information and correlation network at 3 DPI.....	3-94
Supplemental Figure 3-4. Mutual information and correlation network at 7 DPI.....	3-95
Supplemental Figure 3-5. Sub-network diagram highlighting interactions for liver IL-1 β	3-96

APPENDIX FIGURES

Figure B-1. Signal transduction in liver lysates of <i>C. rodentium</i> infected animals at 12 and 24 HPI.....	B-124
Figure B-2. qRT-PCR for acute phase and liver targets due to <i>C. rodentium</i> infection.....	B-125
Figure B-3. <i>C. rodentium</i> induced systemic cytokines changes at early timepoints..	B-126
Figure B-4. Infection kinetics of DBS 9, DBS 120, and DBS255 in C57BL/6 mice.....	B-127
Figure B-5. STAT3 activation in livers of DBS9, DBS120, and DBS255 livers.....	B-127
Figure C-1. OPLS for disease score: Ulcerative colitis using active and inactive patients (STUDY 1&2).....	C-136

Figure C-2. Observed versus predicted disease score: Ulcerative colitis active and inactive patients (STUDY 1&2)	C-137
Figure C-3. OPLS for disease score: Crohn's using active and inactive patients (STUDY 1&2).....	C-138
Figure C-4. Observed versus predicted disease score: Crohn's active and inactive patients (STUDY 1&2).....	C-139
Figure C-5. Mann-Whitney of ESR and CRP values for UC active and inactive patients.....	C-140
Figure C-6. Potential biomarkers of disease activity obtained from OPLS analysis... ..	C-140
Figure C-7. Total scores for UC and CD patients based on VIP scores obtained from OPLS.....	C-141
Figure D-1. Serum cytokine and chemokine changes in C57BL/6 mice exposed to intimin-deficient and STX-expressing <i>C. rodentium</i>	D-147
Figure D-2. Quantitative RT-PCR for expression of kidney cytokines and chemokines transcript in C57BL/6 mice inoculated with STX-expressing <i>C. rodentium</i>	D-148

LIST OF TABLES

Table 1-1. Target modulation and susceptibility to APAP-induced toxicity in experimental models.....	1-25
Table 2-1. PLS-DA and OPLS component contributions to discrimination ($R^2 Y$) and variance (Q^2) of necrosis at 3 DPI.....	2-50
Table 3-1. Data compendium including animal numbers and measurements collected.....	3-91
Table 4-1. Summary of compound exposure under <i>C. rodentium</i> -induced inflammatory stress.....	4-113
Table 4-2. LC/MS/MS Results of propranolol metabolites with and without <i>C. rodentium</i> Infection.....	4-114

Chapter 1: Introduction

Stress Response and Inflammation

Acute stress primes immune functions by stimulating cell trafficking from lymphoid organs into systemic circulation and sites of infection. In humans, exposure to even short term stress, like public speaking, results in increased numbers of certain populations of circulating lymphocytes and briefly increase natural-killer-cell activity [1]. Innate immune cells mediate early cytokine release (IL-1 β , TNF- α , IL-6) promoting the acute phase response, which is critical to appropriately deal with infection and trauma. As an essential response to harmful stimuli such as chemical injury and microbial pathogens, however, inflammatory activation must be tightly coupled with regulatory mechanisms that bring about its own resolution [2]. A failure to properly regulate inflammatory processes can result in sustained collateral damage to healthy cells and tissues (cytokine storms, septic shock), as demonstrated by numerous knockout (KO) models as well as disease states with both genetic and environmental components. Indeed, persistent and aberrant inflammation plays a key role in many, if not most, serious human diseases including atherosclerosis, autoimmune disorders, inflammatory bowel disease, neurodegenerative disease, obesity/diabetes, chronic infection, and cancer [3, 4].

Recently, research groups have begun to address the role of various stressors on liver responses (apoptosis/necrosis) and metabolic function. Such stressors include endotoxin-induced inflammation (lipopolysaccharide (LPS)) [5, 6], pathogenic bacterial infection [7, 8], caging stress [9], temperature [10], electric foot shock [11], and various other 'generic' stress conditions. Infection with pathogenic bacteria is one stress that can lead to inflammation, resulting in the stimulation and recruitment of immune regulators and release of various cytokines and chemokines at local and systemic levels with concomitant release of bacterial antigens that can activate innate and adaptive immune responses.

Innate Immune System in Stress and Inflammation

Pattern recognition receptors (PRRs), and their recognition of highly conserved pathogen-associated molecular patterns (PAMPs), as well as endogenous stress signals termed damage-associated molecular pattern molecules (DAMPs), allow the innate immune system to discriminate a variety of potential pathogens and injuries, furthermore, to coordinate appropriate responses [12]. PRRs include toll-like receptors (TLRs), NOD-like receptors (NLRs), C-type lectin receptors (CLRs), and several others, which contribute to immune activation in response to diverse stimuli, including infection and tissue injury. PRR expression can include the cell

surface, cytoplasm, and endosomal compartments, with levels and expression of receptors varying by cell type. Interestingly, despite a variety of TLR ligands, signaling converges to activation of nuclear factor-kappa B (NF- κ B), mitogen-activated protein kinases (MAPKs), extracellular signal-regulated kinase (ERK), p38, and c-Jun N-terminal kinase (JNK). Adapter molecules are also critical in mediating effector function, and of the TLR adaptor proteins identified (MyD88, Mal, TRIF, TRAM, and SARM), MyD88 is utilized by most TLRs (and some NLRs) to regulate cytokine and major histocompatibility (MHC) molecule production through NF- κ B [13]. Repressors of MyD88 signaling have also been discovered, specifically IRAK-M, expressed only in monocytes and macrophages, has been implicated in LPS tolerance in sepsis, and can suppress innate immunity mechanistically due to dampened Nf- κ B activation [14, 15].

Recently, NLR proteins (NALPs, IPAF) have been reported to form caspase-1-activating complexes called inflammasomes, the process of which has recently been reviewed in depth [16]. Inflammasomes appear to play a critical role in leading to the activation of pro IL-1 β and IL-18, key early mediators in inflammation and cell responses. It has also been proposed that NALP inflammasomes may also contribute to antimicrobial defense by inducing the apoptosis of infected cells [17]. In macrophages, IL-1 β production requires double stimulation with TLR ligands, which induce gene transcription, and NLR agonists (such as ATP or muramyl dipeptide (MDP)) that activate the inflammasome and subsequently activate pro-IL-1 β . Interestingly, monocytes can release active IL-1 β upon stimulation with TLR ligands alone [18]. Conceptually, it has been proposed that TLR signaling in the absence of NLRs may result in a 'yellow' alert, indicating for example gut barrier compromise, and in conjunction with activation of inflammasome NLRs, may trigger a 'red alert', indicating exposure to more virulent pathogens [19]. This signal processing is complicated further by an emerging number of molecules known as DAMPs, a group naturally expressed in the cytosol or nucleus, and currently includes S100 proteins, heat-shock proteins (HSPs) and HMGB1, and when released extracellularly, induce signals to the host of tissue damage [20, 21]. HMGB1 is of particular interest, as its release can be active, secreted by macrophages and monocytes (as well as NK cells [22]) in response to exogenous and endogenous inflammatory stimuli (LPS, TNF- α , IL-1, and IFN- γ), or passive during necrosis, in both cases mediates innate and adaptive inflammatory responses to infection and injury. Recently, a reactive oxygen species (ROS), hydrogen peroxide (H₂O₂), was shown to induce both active (at low dose) and passive (high dose) HMGB1 release from macrophages and monocytes, a mechanism abrogated by JNK and MEK inhibition [23]. While there is clear diversity in PRRs, PAMPs, and DAMPs, downstream signaling through conserved signaling nodes indicates that the network state might be resolved by interrogating a select number of downstream effectors (ex Nf- κ B, JNK, MAPK, JAK-STAT) and gain insight by correlating these states to cellular responses as well as pathophysiological outcomes.

Liver Structure and Function

Functionally complex, the liver plays critical roles in metabolism, lipid and protein synthesis, as well as detoxifying functions. The liver is unique in its anatomical proximity affording it continuous blood flow through the sinusoids from the gastrointestinal tract, and diverse in cellular composition; host to metabolically active hepatocytes, non-parenchymal cells (biliary, Kupffer, sinusoidal endothelial, and stellate cells) and various innate and adaptive immune cell populations (neutrophils (PMN), monocytes, dendritic cells (DCs), and lymphocytes (T, B, NK, and NKT cells) that can enter via hepatic arteries or the portal vein [24]. Within this heterogeneous tissue, cytokines and chemokines, small molecular-weight messengers that act in autocrine, paracrine, and endocrine fashion, are critical in mediating effector functions of resident and distal immune cells, as well as intracellular hepatic signaling responses that modulate liver homeostasis [25]. While indispensable in its metabolic function, the liver is also a key "immunological" organ, underscored by its constant perfusion of blood from the gastrointestinal tract which is highly enriched with potential antigens, providing an early line of defense against microbes and toxins crossing the intestinal barrier [26]. The immune cells mentioned above have the potential to initiate both innate and adaptive immune responses, as in the case of infection in response to high levels of systemic LPS or bacterial superantigens, while balancing immunological tolerance in the case of low levels of LPS and innocuous antigens.

Inflammation and Liver Diseases

The activation of the inflammatory response, while critical for pathogen defense, contributes to hepatic injury in numerous cases of liver diseases including alcoholic liver disease (ALD), non-alcoholic fatty liver disease (NAFLD), ischemia/reperfusion (I/R) injury, autoimmune hepatitis and viral hepatitis. Generally it is accepted that acute injury is driven primarily by a Th1 cytokine response, among these tumor necrosis factor- α (TNF- α), in combination with additional pathophysiological factors, seems to play a central role in liver damage by induction of hepatocyte apoptosis, although oncotic necrosis, typically a consequence of acute metabolic perturbation characterized by ATP depletion and mitochondrial dysfunction, can also predominate [27]. Indeed, pure apoptosis or necrosis might just represent extremes in the spectrum of so called "necroapoptotic" responses, and that the more typical response of liver cells to injury might be a mixture of events associated with apoptosis, necrotic cell death, and inflammation. Recently, necrotic mechanisms have been described, indicating a process more regulated than originally thought [28]. It has also become evident that hepatocyte responses to TNF- α are context-dependent, promoting pleiotropic cell responses such as apoptosis, proliferation, or survival [29]. Such seemingly disparate outcomes demonstrate dependence on autocrine loops, and sustained intracellular signaling (ex Nf- κ B, JNK activation).

Decision processes of cell fate in tissues are also likely intricately linked to the presence and coordinated signaling of PAMPS, DAMPS, and local and systemic cytokine levels. HMGB1, for example engages its receptor RAGE, and results in cooperation with TLR2/4 in inducing inflammatory responses. The role of TLR4 dependent signaling in resident cell types has gained considerable attention, and while it has been generally accepted that Kupffer cells, a TLR4 expressing cell, are critical mediators of liver inflammation, recent findings demonstrate that hepatic stellate cells also express TLR4, and furthermore, are the predominant target through which TLR4 ligands promote fibrosis [30].

Drug-induced Liver Injury (DILI)

Drug induced liver injury (DILI) is a major pharmaceutical and clinical concern that can result in last stage discontinuation of drug development, limit the use and distribution of effective therapeutics, and even lead to market withdrawal [31]. DILI is the leading cause of acute liver failure (ALF) in the United States, accounting for about half of all cases [32]. Drugs that cause severe DILI in humans do not show clear hepatotoxicity in currently used animal models, generally lack dose-related toxicity, and typically demonstrate low rates of severe injury in humans (1 in 5,000 to 10,000 or less). In the US alone, DILI accounts for more than 50% of cases of ALF, with ~39% due to acetaminophen and ~13% resulting from idiosyncratic drug reactions (IDRs) [32]. Such IDRs could be a reflection on host factors and individual susceptibility, as the majority of patients do not demonstrate adverse drug reactions to these agents[33]. Whether they are the result of genetic or acquired differences has not yet been established, and to date no genetic, metabolic, or other characteristic has been found to predict severe DILI in an individual.

While inflammation is intricately associated with numerous liver diseases, its importance is also appreciated in DILI: proposed mechanisms include the Hapten and Danger hypotheses as a model for allergic reactions observed with some drugs (ex penicillin) [34]. Others hypothesize that variable host factors such as endotoxin leakage from the gut, for example during pathogenic infection or gut barrier compromise (alcohol ingestion), or underlying inflammatory conditions (ex hepatitis, arthritis) can promote increased basal levels of local or systemic inflammatory cytokine, chemokines, or other soluble factors that predispose the liver to injury[6, 35, 36]. The role of bacteria and cytokines on the regulation of hepatic metabolic enzyme activity, such as cytochrome P450s and more recently drug transporters have been demonstrated and recently well reviewed [37]. These changes are believed to be regulated by altering nuclear receptor activities (PXR, CAR, FXR, RXR, LXR) which drive expression of phase I, II, and III metabolic enzymes. While critical for biotransformation and clearance, the changes in metabolic enzymes do not fully explain idiosyncratic effects observed in humans[33].

Acetaminophen-Induced Liver Injury

Acetaminophen (APAP) is the world's most commonly used analgesic and antipyretic, responsible for approximately a third of cases related to DILI [38]. Under normal liver conditions, ~90% of APAP is metabolized to non-toxic conjugated metabolites APAP-glucuronide and APAP-sulfate and ~10% of APAP metabolism occurs via cytochrome P450 oxidation (CYP 2E1, 3A4, and to a lesser extent 1A2) to form N-acetyl-p-benzoquinoneimine (NAPQI), a highly reactive electrophilic metabolic intermediate [39]. Detoxification of NAPQI normally proceeds by conjugation with intracellular glutathione, either spontaneously or catalyzed by glutathione-S-transferase (GST), the majority of which is excreted into bile via multidrug resistance-associated protein 2 (Mrp2) [40]. When doses exceed glutathione stores, free NAPQI can covalently modify thiol (SH) groups on cellular proteins (summarized in **Figure 1-1**). While long thought that covalent protein adducts are the cause of liver injury [41], it has been recently suggested that adduct formation is a necessary initiating factor in cell death but not sufficient, requiring amplification through intracellular signaling [42]. In this regard there is a central role for sustained JNK activation [43], a serine/threonine kinase important in responding to environmental stresses, growth factors, and cytokines [44]. Important intracellular activators of JNK are ROS such as H₂O₂ generated from mitochondria and other sources [45, 46]. Indeed APAP-induced ROS from mitochondria is a necessary requirement for APAP induced toxicity, demonstrated by upstream knockout of ASK1, JNK knockout, and JNK specific inhibitors [42, 47].

Altering the host's ability to properly balance both protoxicant and hepatoprotective processes has also been shown to alter susceptibility to APAP-induced injury. Germline KO for IL-13 [48], IL-10 [49], IL-6 [50], cyclooxygenase-2 (COX-2) [51], C-C chemokine receptor 2 (CCR2: receptor for MCP-1), and Nrf2 all demonstrate increased susceptibility to APAP-induced liver injury, while CX-chemokine receptor 2 (CXCR2: receptor for KC and MIP-2) KO is protective [52]. Furthermore, the importance of innate immune cells in mediating injury as demonstrated by Kupffer cell depletion using liposomal clodronate treatment, which confers protection at early time points after APAP treatment [53], but can lead to more severe injury at later time points [54]. While mechanistically not completely understood, depletion dramatically reduced transcript levels of IL-10 and IL-6, corroborating their importance demonstrated in KO studies. Functionally, IL-10 limits inducible nitric oxide synthase (iNOS) expression [49, 55] and peroxynitrite-induced liver injury after APAP overdose, while IL-6 promotes regeneration. Others have found that APAP toxicity results in liver infiltration of a macrophage (IM) population derived from circulating monocytes, distinct from resident Kupffer cells. The IMs exhibit a phenotype consistent with that of alternatively activated macrophages, with ability to phagocytize apoptotic cells and induce apoptosis of neutrophils. Furthermore, in the absence of the IMs, the resolution of hepatic damage following APAP-induced hepatotoxicity was delayed in CCR2 KO mice at 48 and 72 hours [56], however, necrosis and circulating ALT were comparable at earlier time points (10 and 24 hrs post dose). These animals demonstrated reductions in infiltrating macrophages.

These findings implicate IMs in the processes of tissue repair, including dampening inflammation and promoting angiogenesis.

The role of PRRs has also been examined, and TLR4 is involved in APAP-induced hepatotoxicity, as C3H/HeN (TLR4+/+) mice demonstrated more severe histological lesions, significantly higher ALT, and higher liver and plasma TNF- α levels than C3H/HeJ (TLR4-/-) [57]. Interestingly, endotoxin pretreatment of male C3H/OuJ mice 24hr prior to APAP treatment (400mg/kg) afforded protection but not in male C3H/HeJ, furthermore, protection was mimicked with pretreatment with IL-1 α alone in both strains [58]. LPS binding protein (LPB) KO mice also show protection to APAP-induced liver injury, and a recently used LPB inhibitory peptide demonstrated protection against APAP-induced hepatotoxicity in C57BL/6 mice [59, 60]. LPB is known to assist binding of LPS to receptors CD14 [61] and TLR4/MD2, promoting inflammatory cytokine production. Furthermore, while the effect of LPS delivery 24 prior to APAP has been shown protective, potentially via suppression of CYPs associated with APAP bioactivation, a distinctly different local and systemic cytokine profile than may be experienced with APAP delivery 2 hrs-post LPS [62], where LPS pretreatment moved the dose response curve to the left, sensitizing animals to injury. Collectively, this indicates a complex role for LPS signaling and predisposition to injury may be context or time dependent.

More recently, C57BL/6 mice deficient in TLR9, a key receptor for bacterial DNA, as well as modified mammalian DNA, demonstrated protection to APAP-induced hepatotoxicity [63]. Mammalian DNA in cells undergoing apoptosis can be modified by caspase-activated DNase-mediated (CAD-mediated) cleavage [64], as well as methylation [65], and oxidative damage [66], modifications shown to increase its ability to activate TLR9 [67]. Downstream targets of TLR9, including components of the inflammasome (Nalp3, apoptosis-associated speck-like protein containing a CARD (ASC), and caspase-1) when knocked out, decreased susceptibility to APAP-induced liver injury and mortality to a normally toxic dose. Mechanistically, it was demonstrated that activation of TLR9 and subsequent caspase-1 activation via inflammasome components, resulted in processing of pro-IL-1 β and pro-IL-18 to their respective active forms. APAP appeared to have a 2-signal requirement (TLR9 and Nalp3 inflammasome) mediating toxicity, analogous to the 'red' alert hypothesis of innate immune activation. Although not mentioned by the authors, JNK activation is downstream of TLR4, TLR9, and IL-1R [43], a key mediator of APAP toxicity downstream of metabolic activation.

Animal Models of Liver Injury

LPS is found in the outer membrane of gram-negative bacteria. It contains Lipid A, a hydrophobic anchoring protein also known as endotoxin, a potent PAMP known to activate TLR4. LPS is commonly used to induce an inflammatory state to interrogate the role of host factors to explain the susceptibility of certain individuals to idiosyncratic drug reactions[36]. Specifically, numerous papers from Roth et al.

demonstrate that drugs such as Ranitidine and Trovafloxacin, which result in idiosyncratic injury in humans, synergize with a subtoxic iv dose of LPS resulting in hepatotoxicity in rats and mice, while innocuous when treated with either drug or LPS alone [68, 69]. Mechanistically, subsequent studies demonstrated critical roles for TNF- α [70, 71], neutrophils [72], and the coagulation pathway [73], in mediating the toxic response. Although, it has been noted that levels of LPS in this model are not physiologically relevant to what would be observed in clinical patients [33], and the profile of toxicity in these studies is similar to high dose LPS treatment alone. While the use of LPS has helped greatly in the understanding of cytochrome P450 regulation under inflammatory conditions, it may not accurately predict enzyme regulation and cell responses under live bacterial infections, which results in complex pathogen host interactions, and release of diverse PAMPs other than LPS. Moreover, a bolus injection of LPS is unlikely to be physiologically relevant.

Citrobacter rodentium

Citrobacter rodentium is an enteric bacterial pathogen that results in varying degrees of intestinal inflammation, acute colitis, hyperplasia, and edema in numerous strains of inbred and outbred laboratory mice [74, 75]. Sharing numerous virulence factors with the human infecting enteropathogenic *Escherichia coli* (EPEC) and enterohemorrhagic *E. coli* (EHEC), as well demonstrating superior pathogenicity to the former in mice, have made *C. rodentium* infection a highly utilized and robust model for studying the pathogenesis of attaching and effacing (A/E) lesion forming pathogens. In experimentally infected mice, large numbers of bacteria colonize the distal colon and are observed adhering to the epithelial surface. Although highly dependent on mouse strain, peak colonization and hyperplasia can be seen as early as 4 days post inoculation (DPI), with maximal colonic thickening observed between 10 and 12 dpi. In adult C57BL/6, disease recovery and full clearance of *C. rodentium* occurs by 4 weeks post infection (WPI) and full resolution of colonic lesions by 6 wpi [74, 76].

Recent work by Richardson et al demonstrates that *C. rodentium* infection alters mRNA levels of phase I (cytochrome P450s) and phase II (UGTs) metabolic enzymes in liver and kidney, as well as hepatic cytokine levels [7, 8]; a time course of regulation that followed colonic inflammation and bacterial colonization, peaking at 7-10 dpi, and returning to normal by 15-24 dpi. Interestingly, when the role of toll-like-receptor 4 (TLR4) was examined in the regulation of hepatic and renal mRNA changes using C3H/HeJ (TLR4 $^{-/-}$) and C3H/HeN (TLR4 $+/+$) mice, the majority of transcriptional changes were TLR4 independent. Subsequent study comparing IV versus oral infection with *C. rodentium* resulted in both quantitatively and qualitatively different responses in regulation of P450 enzymes [77]. What remains unclear, is the role of potential cross-talk from other TLR receptors, as well as NLRs on regulating hepatic transcriptional changes in this model, furthermore, if cytokine and chemokine secretion due to pathogenic bacterial detection in the gut and subsequent transport to liver via portal blood flow is primarily driving these

changes, and not bacterial antigens leaking from the gut. Furthermore, whether there is a consequential change on drug exposure and clearance under infection conditions.

Concluding Remarks:

While inflammation plays a critical role in liver homeostasis and response to xenobiotics, clear biomarkers that predict host susceptibility factors for hepatotoxicity are currently lacking. Its diverse cellular constituents as well as its many functions critical for host survival underscore the complexity of the liver as a tissue and early responder to pathogenic infection. This includes a population of innate and adaptive immune regulators under constant flux, balancing proper responses to deal with host stress and insult, while also mediating its resolution and eventual homeostasis. Local responses in the liver to intestinal stimuli are a substantial source of circulating cytokines [77], attributable to portal blood (potentially containing bacterial components, cytokines/chemokines etc) draining from the intestines for liver filtration prior to entering systemic circulation. A balance between the gut and liver axis may be critical in mediating host-pathogen equilibrium, a failure of which can result in detrimental consequences in both intestinal, liver, and systemic health [4, 78]. It is possible that these cytokine responses are general to the presence of bacterial products, but may also indicate a liver response to distal infection in the gut. A combination of cytokines, PRRs, DAMPs, and intracellular stress may all synergize to induce such hepatic injury, however, depending on the time course of expression may also contribute to resistance and resolution of injury via immune mechanisms. Particularly interesting is the potential for molecular mimicry of host components (mammalian DNA) as well as active and passive release of HMGB1 that have cross-talk with PRRs, resulting in altered kinetics of signaling, potentially critical in understanding and predicting toxic disposition or resolution of injury. While *in vitro* attempts to understand these processes have been immensely helpful, to truly understand the complexity may require systems-wide interrogation *in vivo* using a reproducible physiological model of pathogenic inflammation using multiplex capabilities and computational tools.

Here we have utilized *C. rodentium* infection, a model of EPEC and EHEC infection and IBD in humans, to interrogate both systemic and liver-specific effects of gastrointestinal infection in C57BL/6 mice. Using a physiologically relevant source of systemic inflammation and acute stress, we measured liver responses at various pathological states of infection, pathogen-host interactions under conditions of drug-induced-liver injury, and systemic effects on drug clearance across a diverse class of xenobiotics that vary in their biotransformation and clearance mechanisms. Furthermore, using a computational approaches such as PCA, PLSR, affinity propagation, and mutual information, we have attempted to build a model of interactions that help not only visualize this interactive landscape, but show both linear and non-linear interactions using a compilation of systemic and tissue specific cytokine/chemokine levels, serum chemistries, histological scoring metrics.

My first aim (reviewed in **Chapter 2**) focused on taking a systems-level approach in characterizing both systemic and liver-specific changes that occur over the course of *C. rodentium* infection kinetics using multiplex assays and multivariate computational modeling approaches. This resulted in the novel discovery and characterization of an infection-induced liver necrosis in the absence of clinically relevant colonic injury, paralleled by local and circulating cytokine and chemokine changes indicative of a host inflammatory component to the injury. In subsequent work, we demonstrated that *C. rodentium* induces systemic and local changes in liver signaling as early as 12 hours post inoculation (**Appendix Chapter B**). The second aim, and focus of **Chapter 3**, involved superimposing drug treatment on gastrointestinal infection in order to evaluate the potential effect of local and systemic cytokine changes induced by *C. rodentium* to synergize or protect animals from drug-induced injury. Using APAP treatment at a mildly hepatotoxic dose in the presence and absence of *C. rodentium*-induced inflammatory stress, a compendium of measurements were generated including systemic and local cytokine levels (colon and liver), serum chemistries, as well as pathological assessment of inflammation and necrosis for both liver and colonic sections. We not only confirmed our initial findings of *C. rodentium* induced liver lesions during early course of infections, but determined through computational approaches such as mutual information and partial least squares (PLS), signatures characteristics of both infection-induced and drug-induced liver injury. In the final aim (**Chapter 4**), we evaluated the effect of gastrointestinal infection on altering oral bioavailability of clinically relevant xenobiotics. *C. rodentium* resulted in increased systemic exposure (AUC) to commonly used pharmaceutical agents, such as verapamil, propranolol with paralleled increases in their metabolites. Mechanistically, it appears that *C. rodentium* acts to increase intestinal absorption, perhaps through alteration of the mucosal barrier, as a principle mode of PK alteration. In summary, these findings are important in helping to build our understanding of the dynamic interplay between inflammation and systemic/tissue-level homeostasis during enteric infection. Future work focusing on neutralizing antibodies or conditional KO's may help to confirm and expand on the importance of numerous targets implicated.

Figures and Tables

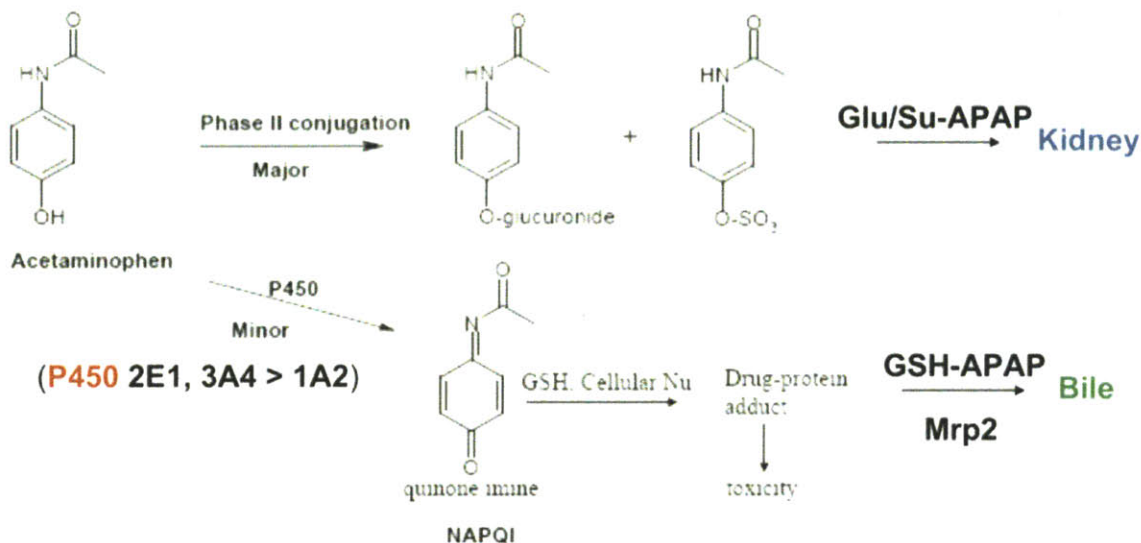


Figure 1-1. Acetaminophen Metabolism and Elimination.

Acetaminophen biotransformation proceeds by phase II glucuronidation or sulphation with subsequent elimination via renal excretion. A minor pathway (10%) involves oxidation via cytochrome p450s (2E1, 3A4 > 1A2) to a reactive quinone imine (NAPQI), followed by detoxification by glutathione stores and biliary elimination via Mrp2. Under conditions of glutathione depletion or overdose, NAPQI reacts with hepatic proteins and nucleic acids resulting in subsequent toxicity. Figure obtained from Steven R. Tannenbaum and amended to include details of P450 activation and elimination pathways.

Table 1-1. Target modulation and susceptibility to APAP-induced toxicity in experimental models. (Modified and updated table from Kaplowitz 2004 [79])

Decreased Susceptibility	ref	Increased Susceptibility	ref
GST-Pi ^{-/-}	[80]	IL-6 ^{-/-}	[50]
CYP 2E1 ^{-/-}	[81]	IL-10 ^{-/-}	[49]
IFN- γ ^{-/-}	[82]	IL-4/IL-10 (highly sensitive)	[55]
NALP3 ^{-/-}	[63]	IL-13 ^{-/-}	[48]
TLR9 ^{-/-}	[63]	CCR2 (MCP-1 receptor)	[83, 84]
CXCR2 ^{-/-} (KC and MIP-2 receptor)	[52]	COX-2 ^{-/-}	[51]
NK/NKT depletion	[85]	JNK ^{-/-} (and inhibition)	[43]
IL-1 α (24 hrs prior)	[58]	MIP-2 inhibition	[86]
LPS binding protein	[60]	LPS delivery (2 hrs prior)	[62]
LPS delivery (24 hrs prior)	[58]		

Chapter 2: Enteric Infection with *Citrobacter rodentium* Induces Hepatic Inflammation and Coagulative Liver Necrosis Prior to Peak Infection and Colonic Disease

Arek Raczynski¹, Katherine Schlieper¹, Sureshkumar Muthupalani², Steven Tannenbaum¹, David Schauer^{1,2}

¹Department of Biological Engineering, ²Division of Comparative Medicine, Massachusetts Institute of Technology, Cambridge, MA, USA

An abridged version of this chapter is to be submitted to *Infection and Immunity*

2.1 Introduction

Liver responses under acute and chronic forms of inflammation have gained considerable interest, particularly due to the role of inflammation in non-alcoholic steatohepatitis (NASH) [87, 88] and drug induced liver injury (DILI). While genetic manipulation and pharmacological inhibition has helped greatly in our understanding of hepatic homeostasis under inflammatory stress conditions, there still exist few animal models that can properly predict these pathologies in the human case. Furthermore, understanding the host response to environmental pathogens is critical in order to study how exposure to chemicals amplifies, synthesizes with, or mitigates environmentally induced disease.

Citrobacter rodentium (*C. rodentium*) is an enteric bacterial pathogen that causes varying degrees of intestinal inflammation, acute colitis, hyperplasia, and edema in numerous strains of mice [74-76]. As a murine homolog of enteropathogenic *Escherichia coli* (*E. coli*) and enterohemorrhagic *E. coli* (EPEC and EHEC respectively), *C. rodentium* has become a highly utilized animal model of these human infections, providing a reproducible, robust, and physiologically relevant model of inflammation. More recently, it has demonstrated organ-specific effects distal to the main site of attachment and disease with alterations of phase I (cytochrome P450s) and phase II (UGTs) metabolic enzymes in liver and kidney, as well as increases in hepatic cytokine transcript [7, 8]; a time course of regulation that follows colonic inflammation and bacterial colonization, peaking at 7-10 days post inoculation (DPI), and returning to normal by 15-24 DPI. Such changes in local and systemic cytokines could lead to metabolic dysregulation or alter susceptibility to injury and disease. Furthermore, altered phase I and II metabolic enzymes, which catalyze the biosynthesis and catabolism of endogenous substrates and metabolic clearance of pharmaceuticals, could be of clinical impact for patients presenting inflammatory bowel syndromes (IBS) or pathogenic gastrointestinal infections.

Here we examined the host response to *C. rodentium* at various stages in the course of enteric infection, focusing particularly on systemic and liver-specific cytokine protein profiles. For the first time, we show distinct liver pathology associated with enteric infection with *C. rodentium* in C57BL/6 mice, characterized by periportal necrotic lesions indicative of thrombotic ischemic injury during the early course of pathogenic infection. Histologic liver changes in inflammation and injury correlate with serum elevation of liver transaminases, systemic and liver resident cytokines, as well as signal transduction changes and liver inflammation prior to peak bacterial colonization and colonic disease. *C. rodentium* infection in C57BL/6 mice appears to be a useful new model to study acute liver injury and inflammatory stress under conditions of gastrointestinal infection analogous to pathogenic *E.coli* infection in humans.

2.2 Results

Infection kinetics and body weight changes

As previously reported, fecal shedding of *C. rodentium* in C57BL/6 mice reached a maximum of $\sim 10^9$ CFU/g feces [89], with detectable levels 3 DPI, peaking 7 DPI, with clearance beginning as early as 10 DPI (**Figure 2-1A**). Although dependent on mouse strain, bacterial load in the colon peaks at 5-14 DPI with approximately 10^9 colony-forming units [74]. Body weight changes were not significant over the course of infection, although variable with some animals losing close to 20% of their initial body weight (**Figure 2-1B & C**), in line with previous findings that *C. rodentium* infection in adult C57BL/6 mice results in self-limiting disease with minimal incidence of morbidity and mortality [74, 76, 90].

***C. rodentium*-induced histological colonic changes**

Infection and disease was confirmed by colonic histological changes assessed by H&E with sections scored by a veterinary pathologist blinded to study treatment groups (**Figure 2-2**). The integrity of epithelial and goblet cells appear intact in control animals but as early as 3 DPI, epithelial defects, colonic foci of inflammation, edema, and hyperplasia were noted (**Figure 2-2A and B**) with statistically significant increases in inflammation, edema, and epithelial defects by 7 DPI ($p < 0.05$, Kruskal Wallis with Dunn's post test), appearing maximal by 14 DPI (**Figure 2-2C and D**). Statistically significant changes in crypt atrophy and hyperplasia were only observed at 14 DPI (**Figure 2-2D**) ($p < 0.05$ and $p < 0.01$ respectively). Although highly dependent on mouse strain, peak colonization and hyperplasia can be seen as early as 4 DPI, with maximal colonic thickening observed between 10 and 12 DPI. In adult C57BL/6, disease peaks approximately 2 weeks post inoculation (WPI) with recovery and full clearance of *C. rodentium* occurs by 4 WPI and resolution of colonic lesions by 6 WPI [74, 76, 91].

***C. rodentium*-induced histological liver changes**

While the effect of *C. rodentium* infection has been well characterized with respect to colonic changes, we decided to examine in greater detail the effect of pathogenic enteric infection on liver homeostasis. Liver sections were formalin fixed, paraffin embedded, and stained by H&E for pathological assessment (**Figure 2-3**). *C. rodentium* induced statistically significant histological changes as early as 3 DPI (lobular inflammation) in liver sections and most significant at 7 DPI (portal inflammation, lobular inflammation, interface inflammation, # lobes with >5 inflammatory foci, and hepatitis index), with moderate improvement by 14 DPI (**Figure 2-3E**). Control livers had no observable histological abnormalities, however, at 3 DPI, the appearance of foci of inflammation indicated a pro-inflammatory state with multifocal vascular coagulative necrosis observed in 3/6 mice (**Figure 2-3A-D**). Necrotic lesions presented primarily with a periportal pattern of distribution (**Figure 2-3G**) and indicative of thrombic ischemic injury with the presence of portal venular fibrin thrombi. Necrotic regions contained

hepatocytes with eosinophilic cytoplasm, appearance of pyknotic or absent nuclei, and loss of normal cellular structure. To confirm and measure the extent of necrosis, serum was processed for alanine amino transferase (ALT), and aspartate amino transferase (AST), two accepted markers of hepatic injury. Hepatic necrosis score correlated with increased ALT at 0 vs 3 DPI = ($28.60 \pm 2.358 \text{ U L}^{-1} \text{ N}=5$ versus $415.2 \pm 250.4 \text{ U L}^{-1} \text{ N}=6$). Mice presenting lesions had ALT levels 56, 16, and 13-fold higher than average control values (ALT = 1603, 464, and 359 U L^{-1} respectively), while non-lesions bearing animals at 3 DPI were comparable to controls (**Figure 2-3 F**). To our knowledge, this is the first reported liver lesion of this kind reported as a result of *C. rodentium* infection and have been repeated and confirmed in subsequent studies (**Chapter 3**).

Further characterization of necrotic livers by immunohistological staining for activated caspase 3 and Ki-67 revealed labeling index in periportal areas of injury for both markers indicating heterogeneous cell death and active proliferation (**Figure 2-4**). Livers harboring lesions at 3 DPI contained a higher incidence of positively stained cells for Ki-67, as compared to controls and non-lesions bearing mice at 3 DPI, indicating a proliferative state in these livers with a comparable increase in labeling index at 7 and 14 DPI (**Figure 2-5A and B**). Animals at 7 and 14 DPI did not harbor obvious necrotic lesions, however, the presence of large hepatocytes and areas of necro-granulomatous inflammation indicate prior lesions in these animals may have resolved via inflammatory and proliferative mechanisms.

Serum cytokine and chemistry changes due to *C. rodentium* infection

C. rodentium has been shown to induce numerous immune regulators at both systemic and local levels, and generally associated with a mucosal TH1/Th17-mediated response in C57BL/6 mice ([92, 93]). Recently, serum and colon matched cytokines were analyzed in *C. rodentium* infected C57BL/6 mice at peak colonic disease (14 DPI), demonstrating correlations of colon and systemic levels associated with disease severity [94]. Here we decided to measure both serum specific changes in cytokines/chemokines (23-PLEX Luminex bead-based ELISA) as well as serum chemistries in multiplex at early, peak, and resolving timepoints of bacterial clearance (**Supplementary Figures 2-1 and 2-2**). We determined numerous circulating cytokines and chemokines to be significantly induced at 3, 7, and 14 DPI. Findings at 3 DPI are particularly interesting as they correlate with our histological findings in the liver and precede peak colonic bacterial colonization and disease. Circulating cytokines were significantly elevated for IL-2, G-CSF, GM-CSF, MCP-1, MIP-1b, and RANTES at 3 DPI as a group ($p < 0.05$, by one way ANOVA with Tukey's multiple comparison test). Elevations in IL-10 and KC were noted but missed significance. For the majority of targets measured, mice at 7 DPI appeared to have the highest circulating cytokines and chemokines, correlating with peak bacterial burden as assessed by fecal shedding (**Supplementary 2-1**), which included elevations in pro-inflammatory (IL1b, IL-6, and TNF- α), immunomodulatory (IL-2, IL-12p70, IL-17), TH2 (IL-4, INF-gamma), and macrophage chemotaxis/activation (GM-CSF, MIP-1b) ($p < 0.001$ as compared to controls).

Serum cholesterol levels also increased significantly at 3 DPI and continued to rise until 14 DPI. It has been shown that *C. rodentium* can alter the transcriptional levels of certain phase I (cytochrome P450s) and phase II metabolic enzymes in both liver and kidney, key in metabolism of endogenous and pharmaceutical substrates [7, 8]. Cholesterol clearance from circulations is partially mediated by oxidation via CYP7A1, and we have shown decreases in CYP7a1 in liver infected with *C. rodentium* (**Appendix Chapter B**). LPS has also been shown to induce expression of ATP-binding cassette transporter A1 (ABCA1), a transporter known to promote apolipoprotein-dependent cholesterol efflux from cells, with cholesterol participating in the removal of an immunostimulatory bacterial lipid, lipopolysaccharide (LPS)[95]. Others have also shown that acute phase proteins such as serum amyloid A are loaded into HDL vesicles for transport, indicating a mechanism for cholesterol in host defense that have previously not been appreciated. Cholesterol homeostasis is complex, and while interesting in this model, would require considerable follow-up to understand the mechanism for its increased serum levels in this infection model. Other serum chemistries and electrolytes, including albumin and glucose, were normal and did not vary significantly across times monitored (**Supplementary Figure 2-1**).

Liver cytokine and signaling changes due to *C. rodentium* infection

To determine if systemic cytokine and chemokine profiles correlated with local levels in the liver, we analyzed lysates using the 23-plex cytokine/chemokine panels and discovered numerous targets increased in serum demonstrated similar up-regulation in livers at 3 DPI (**Supplemental Figure 2-3**). Liver levels of IL-1 β (L), G-CSF (L), KC (L), MCP-1 (L), MIP-1a (L), and RANTES (L) showed upregulation at 3 DPI. Cytokines are known signaling molecules in signal transduction pathways, so we also measured signal transduction in liver lysates using multiplex phospho-kits monitoring both total and phosphorylated forms of JNK, AKT, ERK1/2, p38, I κ B α , and STAT3 (phosphorylated only). STAT3 showed increases in livers harboring necrotic lesions as confirmed by western analysis, with lower but sustained activation at 7 and 14 DPI (**Figure 2-7**). Akt activation as assessed by the ratio of phosphorylated/total Akt was statistically significantly upregulated at 14 DPI, although levels were comparably elevated at 3 and 7 DPI but missed significance (**Figure 2-7**). Phosphorylation of I κ B α , which results in proteasome-mediated degradation and subsequent activation of Nf- κ B, was increased in animals bearing necrotic lesions, indicating potential activation of pro-inflammatory and tissue repair mechanisms associated with this transcription factor.

Multivariate analysis uncovers serum and tissue cytokines and chemokines discriminate necrosis

Analyzing data based on averages in representative groups can cause an investigator to miss important correlations on an individual animal basis. Based on this, we decided to take a multivariate computational approach in determining features that covary best in our data compendium leveraging its multiplex nature. PLS-DA (Partial Least Squares Projection to Latent Structures - Discriminant

Analysis) and OPLS (Orthogonalized Partial Least Squares Regression) were used to determine variables with the highest discriminatory power for lesion bearing animals at 3DPI, furthermore, to determine features that correlate best with serum ALT, a known biomarkers of liver necrosis. We developed non-invasive models (serum targets only), tissue level model (liver targets only), and a combined model using both types of features. The serum PLS-DA model resulted in good separation of lesion bearing vs non-lesion bearing animals (**Figure 2-8A**), with dummy variables (Y) based on this classification covarying with serum targets that make up the principal components plane (**Figure 2-8B**). Their relative importance as discriminators was assessed by their variables in projection (VIPs) score for the principle component 1, where values >1 are have positive influence in discriminating between classes and VIP <1 are less influential (**Figure 2-8C and D**). Similarly using OPLS regression, which reduces dimensions on the basis of their covariance with a specified dependent variable (Y, serum ALT) (principal component 1 - predictive), while ignoring targets orthogonal to this vector (principal component 2 - orthogonal) also resulted in clear separation of animals based on this classifier (**Figure 2-9**). PLS-DA serum models uncover ALT, AST, immune modulators (IL-6, IL-10), monocytes chemokines/activators (MIP-1a, MCP-1), neutrophil chemokines/activators (G-CSF, KC), and t-cell activation (RANTES) as enriched in lesion bearing animals (**Figure 2-8 C-D**).

This method was repeated for tissue markers (**Liver PLS-DA Figures 2-10, and OPLS Figure 2-11**) and resulted in a large overlap with the serum specific targets; immune modulators (IL-1 α (L), IL-6 (L), IL-12p40 (L)), monocytes chemokines/activators (MIP-1a (L), MIP-1b (L), MCP-1 (L)), neutrophil chemokines/activators (G-CSF (L), KC (L)), and t-cell activation (RANTES (L)) as enriched in lesion bearing animals resulting in enrichment of liver PLS-DA and OPLS models generated using serum targets, liver targets, and combined targets are summarized (**Table 2-1**). Overall, both serum and tissue models were highly effective at discriminating both necrosis state prediction of necrosis severity. The tissue models were slightly better independently than the serum models, and the combine (serum + tissue) gave the highest R²Y (cumulative) and Q² (cumulative) with the least number of components. The less non-invasive method of serum cytokine detection makes this a more attractive method even with a modest lost in model prediction.

2.3 Discussion

In the present study we have characterized the systemic and liver effects of *C. rodentium* infection in female C57BL/6 mice at early, peak, and resolving timepoints of bacterial clearance. We demonstrated systemic targets (cytokines/chemokines and serum chemistry markers) that differentiated animals by PLS-DA. Systemic elevations in ALT, AST, with an upregulation of immune modulators (IL-6, IL-10), monocytes chemokines/activators (MIP-1a, MCP-1), neutrophil chemokines/activators (G-CSF, KC), and t-cell activation (RANTES) at 3PDI correlated with coagulative liver necrosis, lesions predominantly periportal in nature and associated with fibrin thrombi. Mice harboring lesions also demonstrated induction of STAT3 and I κ B α phosphorylation, coupled with liver specific protein elevations of IL-1 β (L), IL-6 (L) G-CSF (L), KC (L), IL-12p40 (L), MCP-1 (L), MIP-1a (L), and RANTES (L).

***C. rodentium*-induced histological liver changes**

Pathological assessment of livers discovered that 50% of mice at 3 DPI harbored periportal necrotic lesions that have not been observed and/or reported to our knowledge in this murine model of enteric infection and colonic hyperplasia. This may be due in part to the fact that 3 DPI is early in disease pathogenesis coupled by our interest in investigating an organ distal to the primary site of disease pathology and bacterial colonization. Bacterial translocation due to inflammation or overgrowth of commensal bacteria has been shown to occur, with translocation of luminal bacteria to other organs [96, 97], in some cases resulting in sepsis and the subsequent death. Furthermore, *C. rodentium* has demonstrated translocation to MLNs during infection course [98]. We did not plate liver tissues to determine *C. rodentium* liver load but follow-up experiments staining liver sections using a *C. rodentium* specific antibody could confirm this. *C. rodentium* has been associated with disruption of tight junctions and barrier function in intestinal epithelial cells *in vitro* and *in vivo* ([99, 100]). As liver lesions were predominantly periportal in their pattern of distribution, and indicative of thrombotic ischemic injury with portal vein thrombi present, it is possible that bacterial components, or *C. rodentium* (live or dead) at the early stages of bacterial colonization, translocated from the gut lumen via portal blood to the liver inducing a systemic and local inflammatory response. LPS, for example, through interaction with LPS-binding protein has been demonstrated to induce fibrin clots in tissues. Others have proposed that the liver may act to trap LPS, along with other bacterial components as a protective mechanism to prevent systemic spread of bacteria. As a regenerative organ, minimal necrosis via coagulative mechanisms could be manageable. The presence of necrogranulomatous inflammation at later timepoints indicates perhaps of residual effects of clearance mechanisms of prior injury in these animals. The lack of circulating ALT indicates that active necrosis was likely not occurring.

Cytokine/chemokines correlations with necrotic lesions

Using PLS-DA and OPLS modeling, we demonstrate an upregulation of targets associated with necrosis at 3 DPI (for total list see **Figure 2-12**). G-CSF (S/L), MCP-1 (S), KC (S/L), IL-6 (S/L), IL-10 (S), and RANTES (S/L) were highly predictive for animals harboring liver lesions and demonstrated high covariation with ALT. Neutrophil activation is commonly observed at the sight of tissue injury. Indeed, G-CSF, a chemokine known for neutrophil recruitment and activation, was elevated in serum and liver homogenates. G-CSF is also known to promote the survival, proliferation, differentiation, and function of both precursor and mature neutrophils. The increased levels of G-CSF may also account for the induction of STAT3 and Akt levels found in the liver. Interestingly, IL-6 can inhibit the inflammatory induced by neutrophil-activating chemokines by facilitating neutrophils apoptotic clearance [101, 102]. Mechanistically, this has been demonstrated a result of STAT-3 activation in a model of acute peritoneal infection [103]. Deregulation of gp130 (IL-6 receptor) signaling in this model did not affect the initial CXCL1/KC-driven neutrophil recruitment, indicating early induction of these chemokines is IL-6 independent. IL-10 (S) was also elevated in necrotic bearing mice in our model, a cytokine with known hepatoprotective affects in drug-induced liver injury. IL-10 can regulate KC levels *in vivo* attributable to modulation of STAT 1 and STAT3 (non- gp130 mediated) signaling [104], as well as iNOS levels in an APAP-induced model of liver injury [49, 55].

C. rodentium also induced cytokines MCP-1 and MIP-1a in necrosis-bearing mice, targets implicated in the process of hepatic inflammation, known to recruit monocytes and lymphocytes during liver injury. MCP-1 is primarily secreted by monocytes, macrophages, and dendritic cells and demonstrates activation for macrophages and chemotactic activity for monocytes [105] and basophils but not for neutrophils or eosinophils. MCP-1 is also associated with numerous models of fibrosis, and shown to activate hepatic stellate cells, which play a major role in hepatic fibrosis. Here the occurrence of portal vein thrombi in liver lesion-bearing animals parallel increases in serum and liver MCP-1 and PLS-DA analysis at 3 DPI also showed covariation with P-I κ B α ; a known regulator of Nf- κ B transcription. It has also shown to work in an autocrine loop with RANTES, and demonstrates high correlation with MCP-1 ($R^2 = 0.84$) in our study (**Supplemental Figure 2-4** comparing 3 and 7 DPI networks). Collectively, the regulatory control by both STAT and Nf- κ B mediated transcription deserve further exploration in precise roles in mediating the responses to early infection and liver inflammation/injury in this model.

It is interesting that liver responses detected in animals at 3 DPI overlapped many of the targets associated with acute colitis and disease severity such as chemokines MCP-1, MIP-1a, MIP-1b, RANTES, and KC and neutrophil/Th17-related targets such as KC, IL- 1b, IL-6, IL-12/23p40, G-CSF. Local responses in the liver to intestinal stimuli are a substantial source of circulating cytokines [77], attributable to portal

blood (potentially containing bacterial components, cytokines/chemokines etc) draining from the intestines for liver filtration prior to entering systemic circulation [78]. It is possible that these cytokine responses are general to the presence of bacterial products, but may also indicate a liver response to distal infection in the gut. While indispensable as a metabolic organ, the liver is also a key “immunological” organ, underscored by its constant perfusion of blood from the gastrointestinal tract which is highly enriched with potential antigens, providing an early line of defense against microbes and toxins crossing the intestinal barrier [26]. Whatever the source or stimuli for these local and systemic changes, they clearly correlate with observed pathologies determined by PLS modeling in a complex data set, but also predictive for known biomarkers of injury such as serum ALT for liver necrosis.

Future analysis would hope to confirm the phenotype of liver injury at early timepoints of *C. rodentium* infection. Indeed, subsequent work from our lab has confirmed it as reproducible in work to be published (**Chapter 3**). Specifically, the incidence of necrotic injury at 3 DPI was increased in our hands to 5/6 animals with an overnight fast prior to necropsy, with lesion resolution again by 7 DPI. To better understand the temporal kinetics of injury, collecting serial bleeds from animals preceding, during, and under conditions of resolving liver injury could be extremely helpful in understating the kinetics of cytokine release and whether such targets are precursors to injury or simply a consequence. Furthermore, use of neutralizing antibodies or conditional knockout studies may also help to elucidate the importance of these markers in the predisposition and severity of injury.

In conclusion, we show for the first time, to our knowledge, distinct liver pathology associated with enteric infection with *C. rodentium* in C57BL/6 mice, characterized increased inflammation and hepatitis index as well as periportal necrotic lesions indicative of thrombic ischemic injury during the early course of pathogenic infection. Histologic changes correlate with serum elevation of liver transaminases, systemic and local cytokine and chemokine changes, as well as signal transduction changes prior to peak bacterial colonization and colonic disease. *C. rodentium* infection in C57BL/6 mice appears to be a useful new model to study acute liver injury and inflammatory stress under conditions of gastrointestinal infection analogous to pathogenic *E. coli* infection in humans.

2.4 Selected methods

Mouse Infections

24 female 8-10 week-old, specific pathogen free C57BL/6 mice were (The Jackson Laboratory, Bar Harbor, ME) were housed and maintained as described in Appendix A (General Methods). Infectious colitis was induced by intragastric inoculation with $\sim 1 \times 10^9$ CFU of DBS120 in 3% sodium bicarbonate (in PBS, pH 7.4) using a 100uL volume. Control animals (0 DPI) were sacrificed within 1hr of inoculation while the 3, 7, and 14 DPI animals were monitored for fecal shedding (3,7,10,14 DPI) and body weight changes as indicated and euthanized and necropsied at their respective timepoints as described in Appendix A.

Histopathology

Tissues were processed as described in Appendix A. Colons and livers were sectioned and stained by H&E for histological assessment by a veterinary pathologist blinded to study treatment groups. Disease severity of colonic sections was based on an existent method assessing inflammation, edema, epithelial defects, crypt atrophy, hyperplasia, and dysplasia and graded on a scale from 0 to 4. Livers were assessed for both inflammatory and necrotic parameters. Degree of hepatic inflammation was graded on a scale from 0 to 4 based on region (lobular, portal, and interface), and the number of lobes with greater than 5 inflammatory foci was noted. The summation of these categorical inflammatory scores resulted in a hepatitis index; mice with a score ≥ 4 were defined as having hepatitis.

A modified scoring criterion was developed to define the extent, degree, and pattern of liver necrosis. The degree of necrosis was scored from 0 to 4 and the pattern of injury was evaluated as centrilobular, midzonal, or periportal in nature (# = low, ## = medium, ### = high). The distribution of necrosis was evaluated as follows: 0 - none, 1 - focal, 2 - multifocal, 3 - translobular, 4 - submassive, involving multiple lobules or entire lobe.

Immunohistochemistry

Formalin-fixed paraffin-embedded livers and intestinal sections were stained to assess the degree of proliferation (Ki-67) and apoptosis (activated caspase 3). Anti-activated caspase 3 (Cell Signaling Technologies, Inc., Beverly, MA) and anti-Ki-67 antibodies were used as specified by the manufacturer. Antibodies were detected with biotinylated goat anti-rabbit IgG (Sigma-Aldrich, St. Louis, MO) and sections visualized with diaminobenzidine and hematoxylin counterstained.

Clinical Chemistries

Serum samples were thawed on ice and diluted 1:4 in water and processed on an Olympus AU 400e serum chemistry analyzer (Beckman Coulter, Inc., Brea, CA) for 18 serum chemistry targets. All samples were run against internal standards and machine calibrated prior to use as specified by the manufacturer.

Multiplex Detection of Serum Cytokines and Chemokines:

Mouse serum collected at necropsy was processed using mouse 23-plex cytokine panels (Bio-Rad, Hercules, CA) as specified by the manufacturer. Briefly, serum was diluted in species-specific sample diluent (1:4) and 50uL of sample or premixed standards were incubated with pre-washed target capture antibody-conjugated microspheres provided and incubated for 30 minutes with orbital shaking (300 rpm) in a 96-well plate. Upon washing, beads were incubated with detection antibody (30 min), washed, and subsequently incubated with streptavidin-PE (10 min). Beads were washed and resuspended with 125uL assay buffer and read on the Luminex 200 suspension array system using the low RP1 target setting (High PMT) for maximum sensitivity. Data analysis was carried out with the Bio-Plex Manager™ 5.0 software and cytokine or chemokine concentrations calculated against an 8 point standard curve generated by either 4PL or 5PL curve fitting.

Multiplex Detection of Liver Cytokines, Chemokines, and Phospho-Signaling

Colon and livers were thawed on ice and ~30-50 mg of liver was briefly washed with 500uL ice-cold cell wash buffer (Bio-Rad, Hercules, CA). Livers were then transferred to a clean pre-weighed eppendorf tube and resuspended 12X the tissue weight with cell lysis buffer (Bio-Rad, Hercules, CA). Tissues were homogenized on ice for 1 minute with a Tissue Tearor™ and subsequently frozen to -80°C overnight. Tissues were then thawed on ice and sonicated on level 5 with 5 short (~3 sec) bursts. Upon sonication, lysates were centrifuged for 10 minutes (5,000 rpm, 4°C). Resultant supernatant was carefully removed, protein quantified by BCA protein assay (Thermo Scientific, Rockford, IL), and adjusted to 1ug/uL with 1X PBS + 0.5% BSA (w/v). 50uL of adjusted lysate was subsequently loaded on to a Mouse Group I: 23-Plex panel (Bio-Rad, Hercules, CA) and standards resuspended in the appropriate matrix. Samples were subsequently processed as specified above for serum cytokines and chemokines analysis using the Bio-Plex array system and software manager.

Immunoblot of Phospho-proteins:

Tissues were thawed on ice, suspended in Bio-Rad cell lysis buffer with provided phosphatase and protease inhibitors, and homogenized with a Tissue Tearor™ for 1 minute. Upon freeze thawing (-80°C), samples were sonicated on level 5 for three 10 second bursts, incubated on ice for 20 minutes, and centrifuged at 4°C at 5000 rpm for 15 minutes to precipitate insolubles. Supernatants were protein quantified by BCA (Thermo Scientific, Rockford, IL) and adjusted to 2ug/uL with Bio-Rad lysis buffer. Equal volumes of 2X SDS loading buffer was added and 20uL loaded (20ug/well) onto 10% SDS Tris-glycine gels (Invitrogen, Carlsbad, BA). Upon transfer to immobolin^{PQ} PVDF membranes, blots were incubated with antibodies (1:2000 P-STAT-3, 1:2000 anti-rabbit monoclonal, Cell Signaling Technologies) in TBST-5%BSA, incubated with Santa Cruz luminal reagent, exposed by Kodak MR film, and quantified by NIH imageJ.

Statistical Analysis:

Statistical significance in body weight change, bacterial load, disease indices, cytokine changes, clinical chemistries, and mRNA expression levels was determined by comparing control or experimental groups by either student's T-test or by two-way analysis of variance (ANOVA) followed by Tukey's post tests. Data that demonstrated non-normal distributions or categorical in nature were assessed by Kruskal-Wallis non-parametric test with Dunn's multiple comparison test against controls unless otherwise indicated. If only two groups were analyzed, Mann Whitney was utilized. All analyses were done using GraphPad Prism software, version 4.0 and *P* values of <0.05 were considered significant.

PCA and PLSR Analysis

The data was mean centered, variance scaled, \log_{10} transformed, and analyzed by multivariate analysis using SIMCA-P 11.5 software (Umetrics Inc., Kinnelon, New Jersey). PCA analysis was used to reduce the dimensionality of the data set and to assess the covariation of variance across measured targets. PLS-DA analysis was used to determine the features that best differentiated between selected groups of animals designated as classes (ex. mice harboring necrosis vs non-harboring mice). OPLS analysis was used to determine the features that best correlated with a desired Y variable, such as ALT levels or degree of necrosis/hepatitis, resulting in variable importance in the projection (VIP). VIPs greater ≥ 1 were considered significant in their contribution to the model predicting the dependent variable (Y) of interest. Model quality was assessed and reported using the following parameters: R^2 Y, the fraction of the sum of squares of all Y variables explained by the component of the model, and R^2 Y cumulative, the cumulative sum of squares of all Y variables explained by all components of the model. Q^2 is the fraction of the total variation in Y variables that can be predicted by the component, and Q^2 cumulative is the cumulative Q^2 of the Y variables for all components in the model. An R^2 cumulative and Q^2 cumulative of 1 indicate a perfect fit, with 100% of the relationship between X variables and Y variables explained.

2.5 Figures and Tables

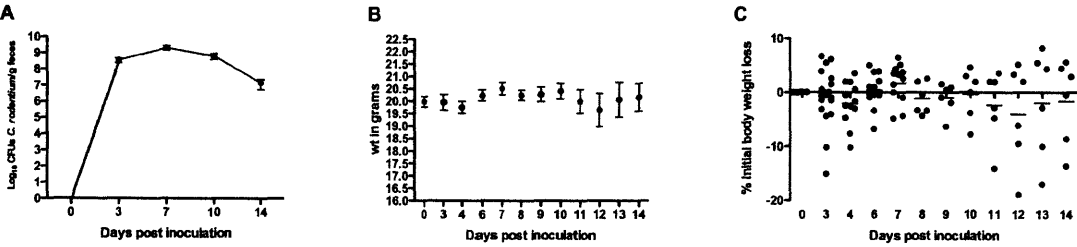


Figure 2-1. Infection kinetics and body weight changes in C57BL/6 mice infected with *C. rodentium*.

C. rodentium bacterial burden (A) was detectable by 3DPI and maximal around 7 dpi with clearance beginning by 10 dpi. Monitoring of body weights (B) demonstrated no statistically significant weight loss over the course of infection, however % body weight loss (C) was variable across animals with some approaching 20% loss of their initial weight.

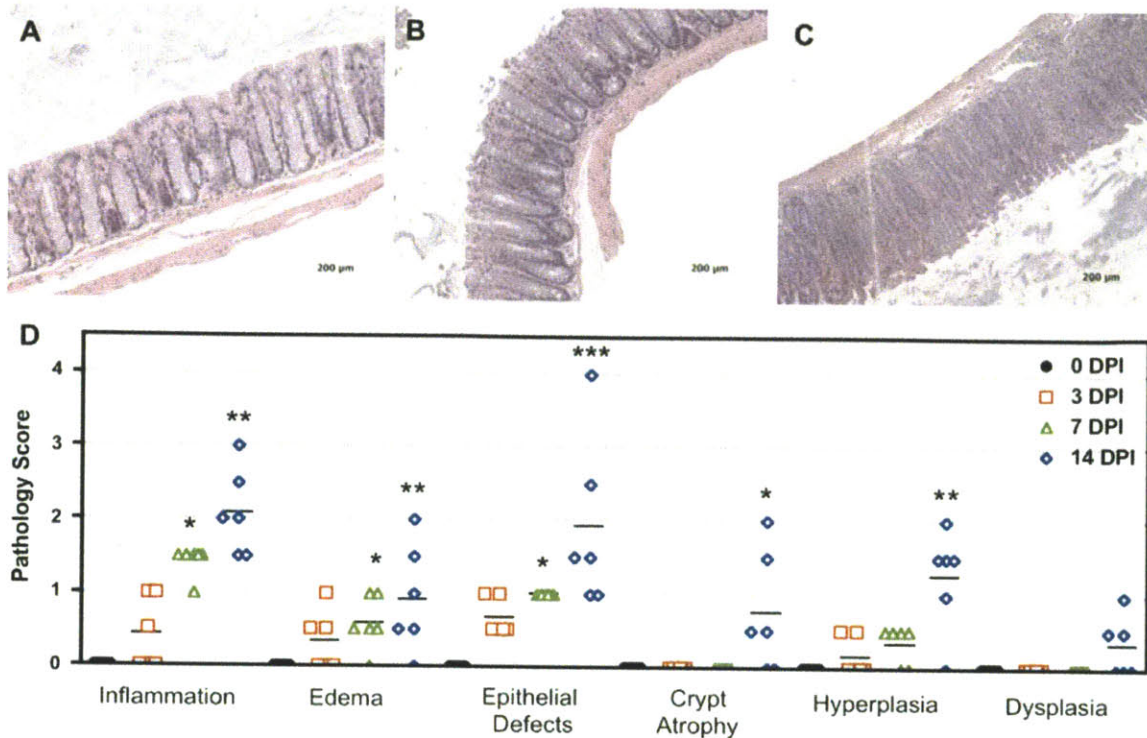


Figure 2-2. *C. rodentium*-induced colonic effects in C57BL/6 mice.

(A) Mock inoculated animals at 0 DPI with normal colonic architecture where epithelial integrity and goblet cells appear intact. (B) Colon at 3DPI showing epithelial defects at the top of the crypt. (C) Colon at 14 DPI demonstrating hyperplastic crypts and depletion of goblet cells. (D) *C. rodentium* induced statistically significant histological changes as early as 7 DPI (inflammation, edema, epithelial defects) in colonic sections and found to be most dramatic at 14 DPI. Crypt atrophy and dysplasia were only noticeable at 14 DPI. There were observed changes in inflammation, edema, epithelial defects, and hyperplasia as early as 3 DPI but did not reach statistical significance (Kruskal Wallis non-parametric test with Dunn's multiple comparison test: * $p < 0.05$, ** $p < 0.01$, *** $p < 0.001$). Symbols indicate individual animals and lines indicate group means.

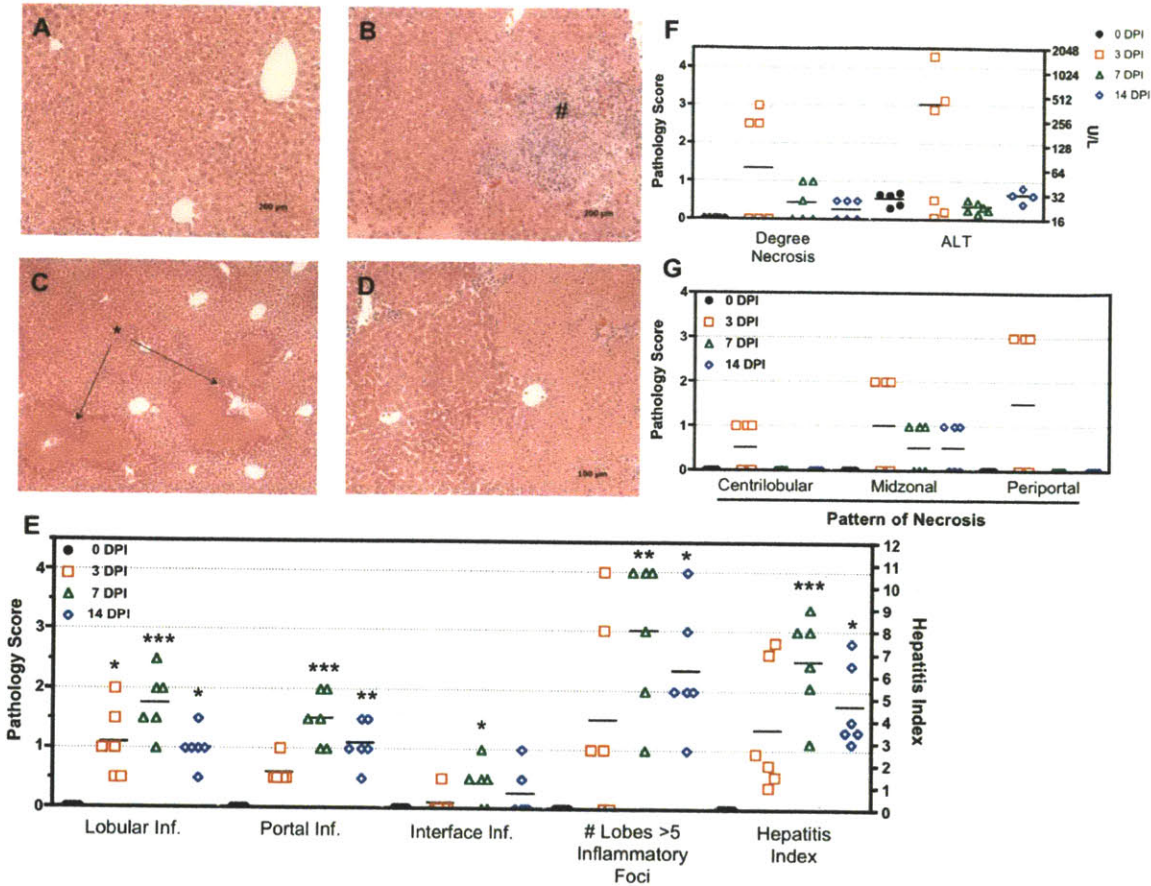


Figure 2-3. *C. rodentium*-induced necrosis and histological liver changes in C57BL/6 mice.

(A) Control livers appeared normal with no observable histology. (B) At 3 DPI the appearance of small injury of inflammation indicating a pro-inflammatory state (indicated by #). (C) Multifocal vascular coagulative necrosis (indicated by *) was observed at 3 DPI demonstrating periportal injury to hepatocytes indicative of thrombic eschismic injury (D) 400X view of necrotic injury containing hepatocytes with eosinophilic cytoplasm, appearance of pyknotic or absence of hepatic nuclei, and loss of normal cellular structure. (E) *C. rodentium* induced statistically significant histological changes as early as 3 DPI (lobular inflammation) in liver sections and most significant at 7 DPI (portal, lobular, interface inflammation, # lobes with >5 inflammatory foci, and hepatitis index score), with moderate improvement by 14 DPI. (F) The degree of necrosis determined by pathological assessment as well as serum ALT measurements (G) The pattern of necrosis was assessed as centrilobular, midzonal, or periportal in distribution. (Kruskal-Wallis with Dunn's post test compared to controls: * $p < 0.05$, ** $p < 0.01$, *** $p < 0.001$). Symbols indicate individual animals and lines indicate group means.

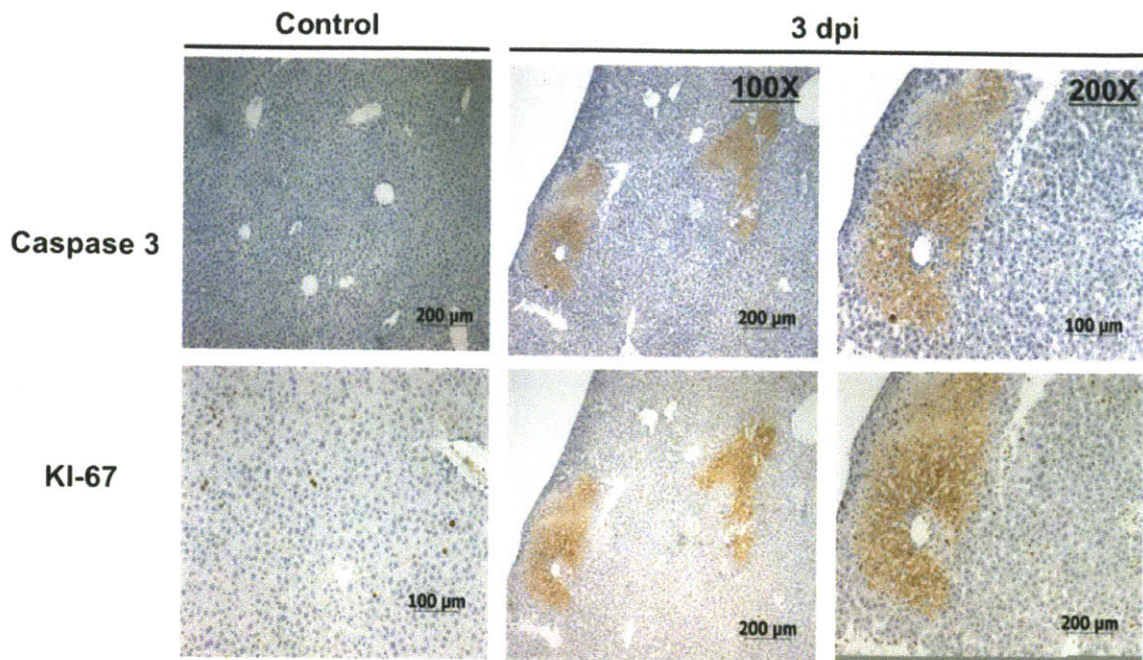


Figure 2-4. Activated caspase 3 and KI-67 in *C. rodentium*-induced liver lesions

Control livers showed minimal staining for the apoptotic marker activated caspase 3, and proliferative marker KI-67 (far left panels), while lesion-bearing livers at 3 DPI stained positively for both markers with a periportal pattern of distribution (middle (100X) and far right (200X)). Pictured is an indicative liver section sliced twice and stained independently for each cell marker.

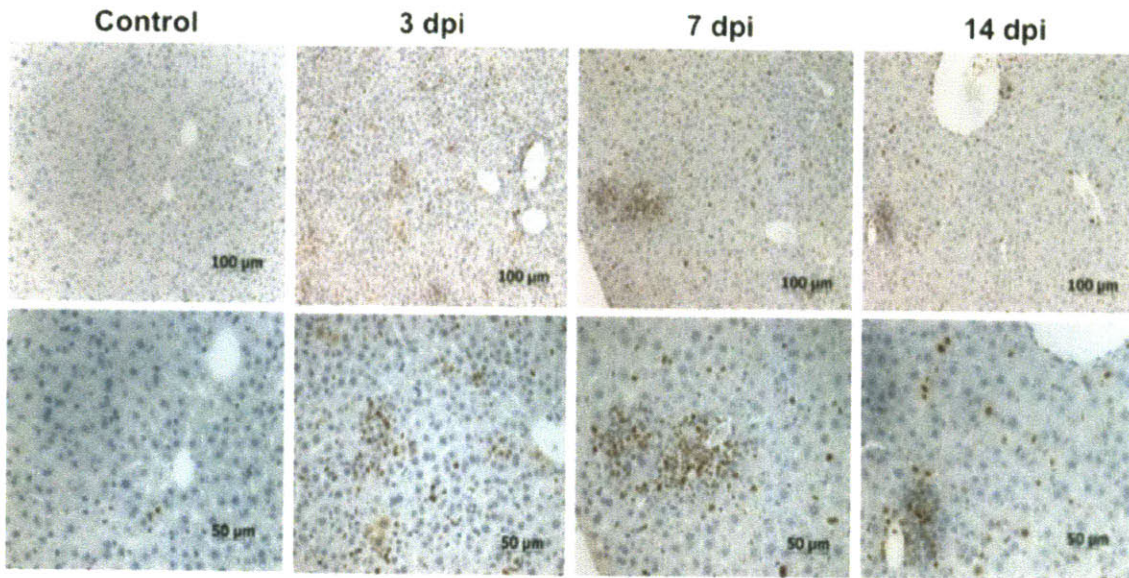
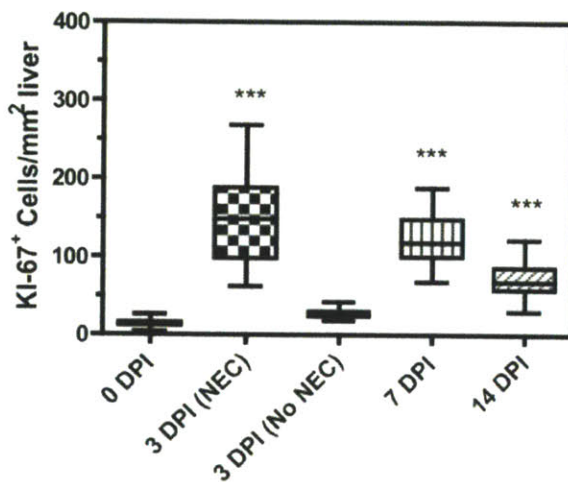
A**B**

Figure 2-5. *C. rodentium* significantly increases Ki-67+ labeling index in livers

(A) Top panels are 200X and lower panels are 400X views of the same frame. A brown-colored pigment indicates positively stained cells for Ki-67. (B) Average number of Ki-67+ cells/mm² liver determined in 15 fields (magnification, ×400, 3 fields/lobe) per mouse ($n = 3$ for 0, 7, and 14 DPI; $n = 2$ for 3 DPI (NEC); $n=1$ for 3 DPI (No NEC)). Data is represented as box-whisker plots, where boxes represent the first to third quartile and a horizontal line indicates the median. Bars represent ranges. (One-way ANOVA with Tukey's multiple comparison test: *** $p < 0.001$)

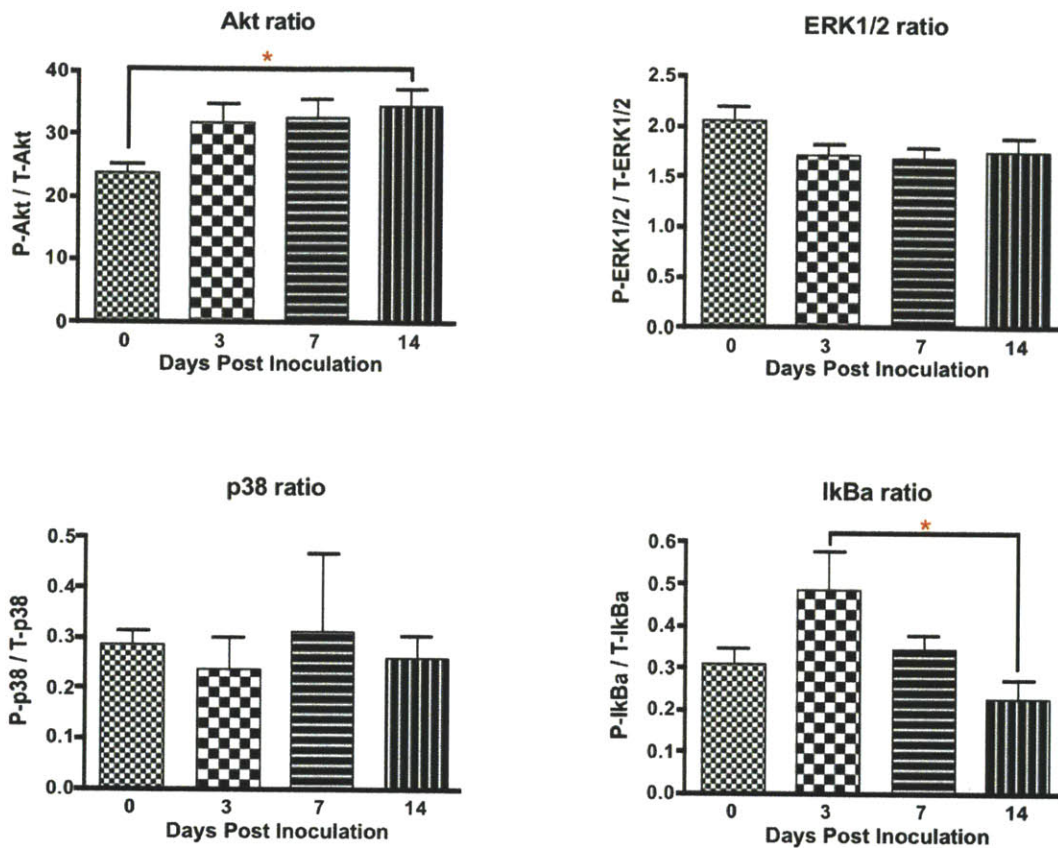


Figure 2-6. Signal transduction changes in liver due to *C. rodentium* infection.

The phosphorylated/total mean fluorescence units (MFI) ratios were determined for liver lysates (5ug total protein) harvested from animals over the course of *C. rodentium* infection. Average Akt activation was significantly increased at 14 DPI with comparable elevations at 3 and 7 DPI missing statistical significance. Elevations were observed in IκBα phosphorylation, particularly in liver lesion-bearing mice, demonstrating statistical significance as a group versus 14 DPI livers. ERK1/2 and p38 failed to demonstrate changes over the course of *C. rodentium* infection in livers (One-way ANOVA with Tukey's multiple comparison test: * p < 0.05, ** p < 0.01, *** p < 0.001). Data presented are mean ± SEM.

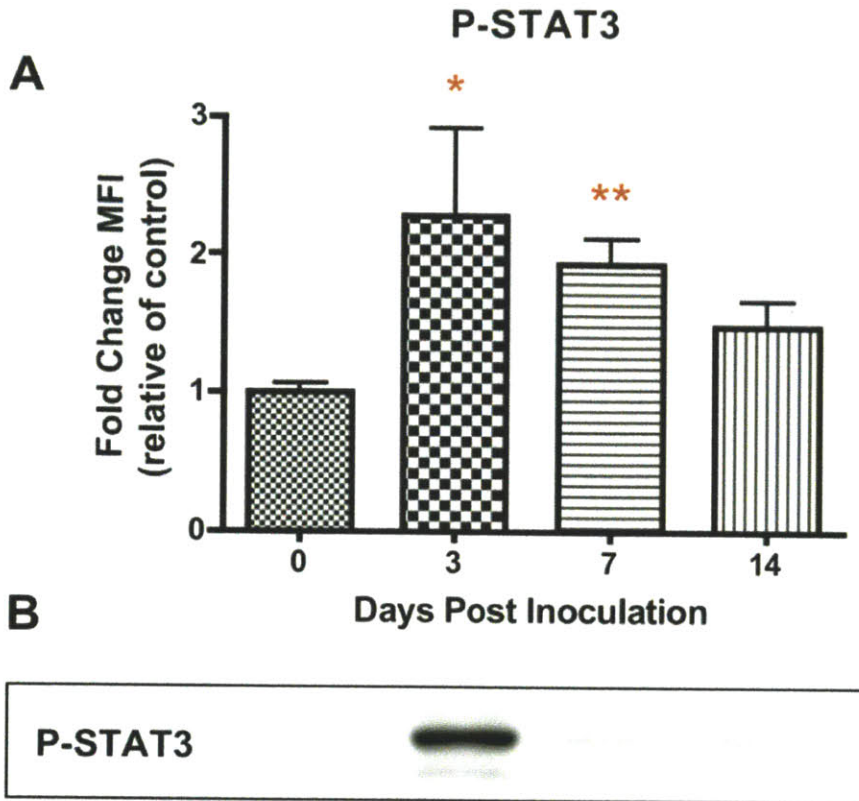


Figure 2-7. STAT3 activation in livers of *C. rodentium* inoculated C57BL/6 mice. (A) P-STAT3 levels were detected by Bio-Rad phospho panel and expressed as a fold changes of mean fluorescence intensity (MFI) relative to control animals. STAT3 was statistically significantly activated in livers of mice inoculated with *C. rodentium* at 3 and 7 DPI (Kuskal-Wallis test with Dunn's multiple comparisons test: *p < 0.05, ** p < 0.01). (B) Western detecting P-STAT3 levels in liver lysate (20ug/lane) from one animal per time point. Mouse 08-5648 (3DPI) is shown and presented the most severe necrotic injury and highest ALT levels, correlating with largest P-STAT3 MFI fold-change (5.3-fold). Data presented are mean \pm SEM.

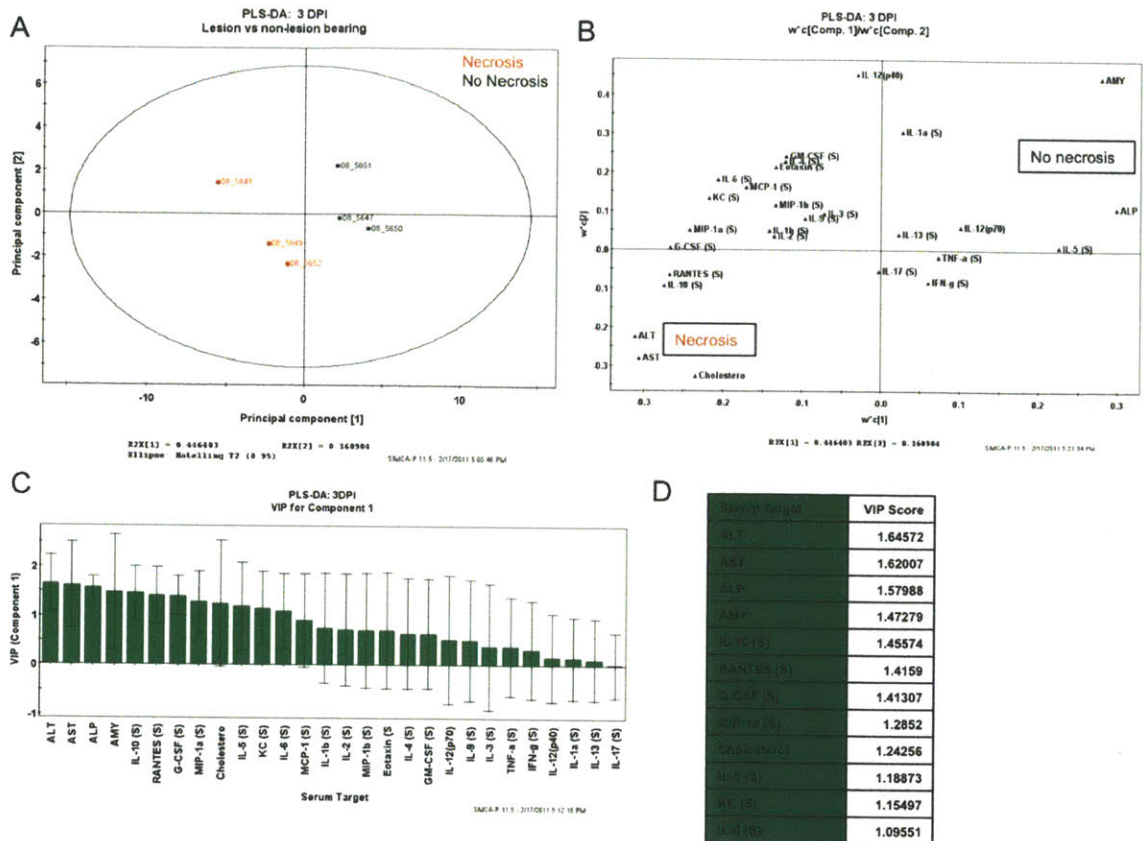


Figure 2-8. Serum specific PLS-DA analysis of *C. rodentium* infected C57BL/6 mice at 3 DPI

(A) Partial least squares discriminate analysis (PLS-DA) showing separation of lesion and non-lesion bearing mice using the first two principal components (B) Cytokine covariation based on class discrimination using cytokine targets as independent variables (X) and pathological states (presence of absence of necrotic lesions) as the dependent dummy variables (Y). (C) Variables in projection (VIPs) for the principle component 1, where values >1 are have positive influence in discriminating between classes and VIP <1 have less influence (D) Table representing the serum specific VIPs and their respective scores that best discriminate necrotic from non-necrotic mice at 3 DPI

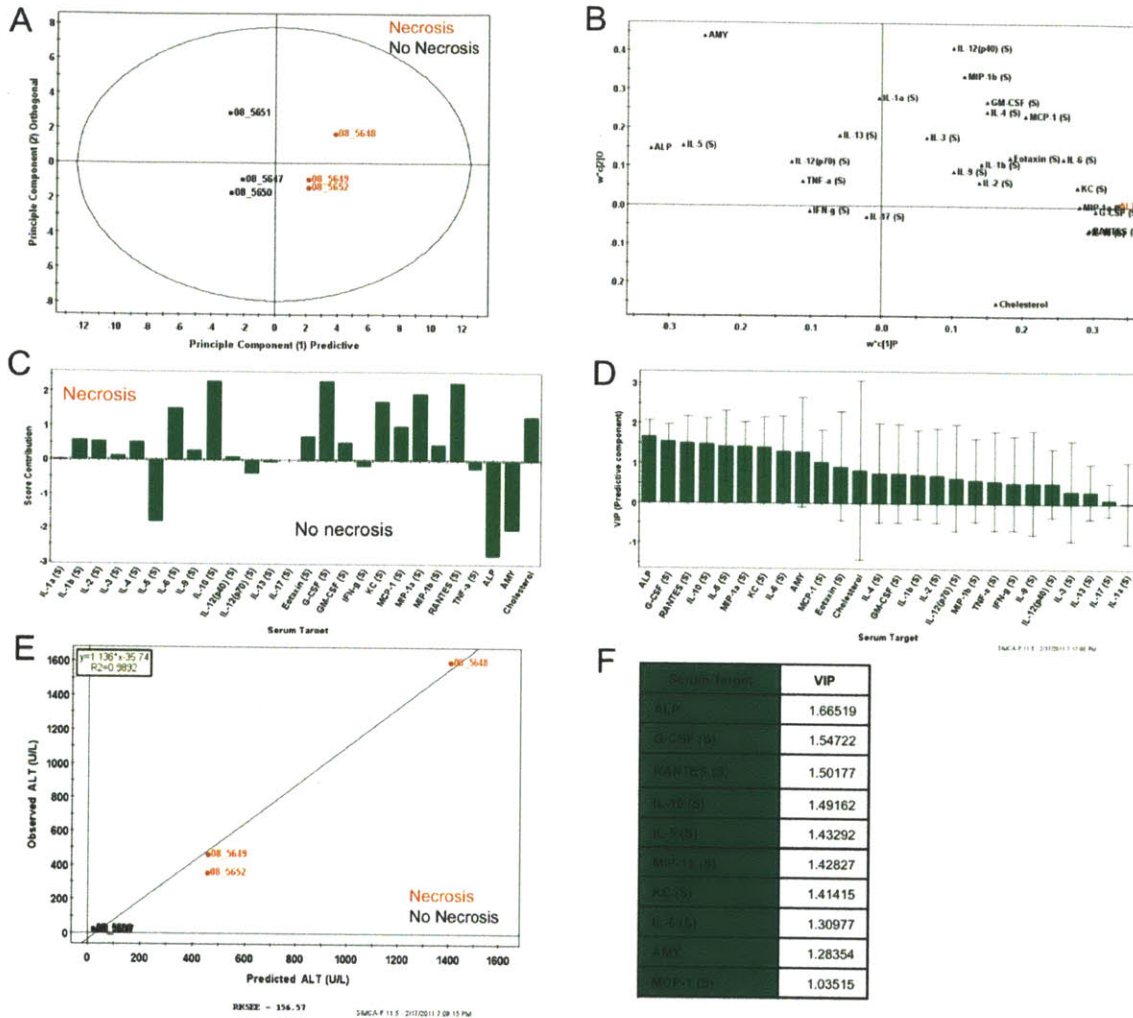


Figure 2-9. Serum specific OPLS analysis of *C. rodentium* infected animals at 3 DPI
 OPLS analysis of *C. rodentium* infected animals at 3 DPI using serum cytokines and chemistries (X) for prediction of ALT levels (Y) (A) Mice segregated well in the predictive component (Principle component 1) with an $R^2X(1) = 0.35$, indicating this component captured ~35% of the variance present in the X variables. (B) The predictive weight and covariation of serum targets (black triangles) in relation to serum ALT (red square). (C) The variables that best separate the two pathological states in relation to the predictive component (D) Variables in projection (VIPs) for the predictive component where values >1 have positive influence in determining ALT levels, and $VIP < 1$ have less predictive influence (E) Observed vs predicted plot for ALT resulted in a $R^2 = 0.9892$ indicating a highly predictive model based on serum cytokines. (F) Table representing the VIPs for the predictive component for serum ALT.

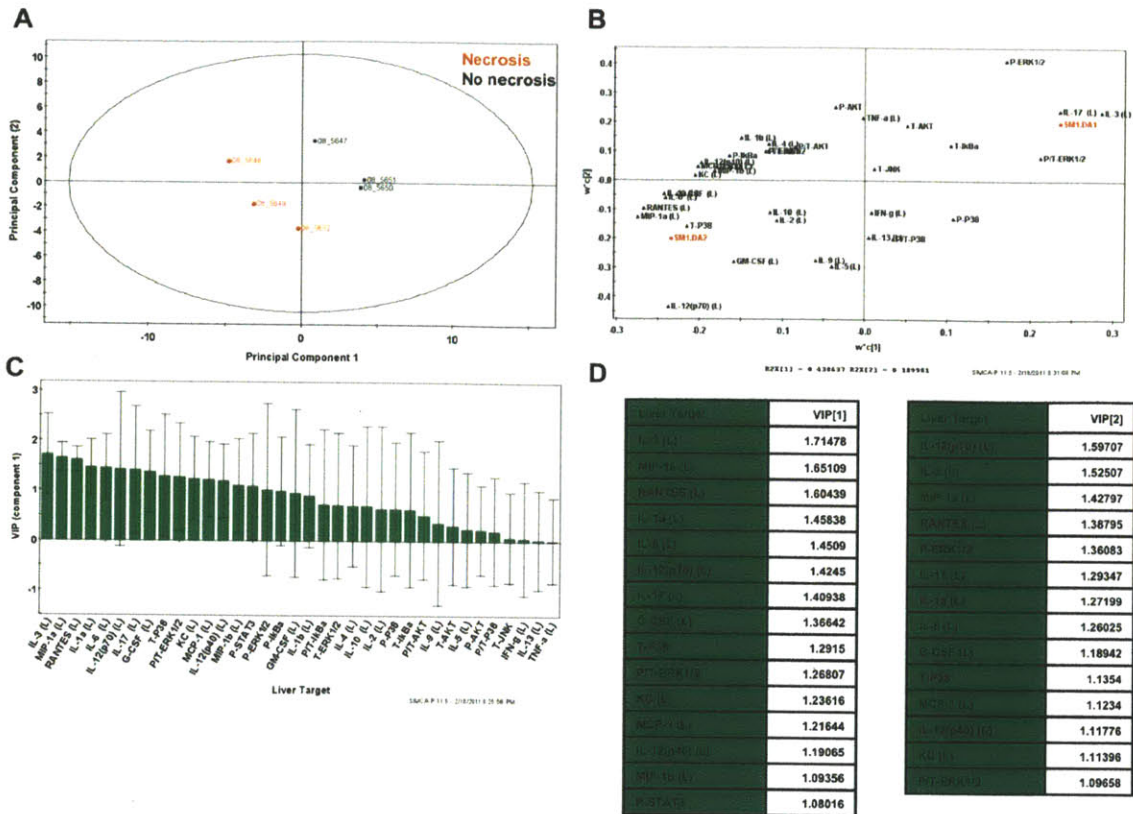


Figure 2-10. Liver specific PLS-DA analysis of *C. rodentium* infected C57BL/6 mice at 3 DPI

(A) Partial least squares discriminate analysis (PLS-DA) showing separation of lesion and non-lesion bearing mice using the first two principal components (B) Cytokine covariation based on class discrimination using cytokine targets as independent variables (X) and pathological states (presence of absence of necrotic lesions) as the dependent dummy variables (Y). (C) Variables in projection (VIPs) for the principle component 1, where values >1 are have positive influence in discriminating between classes and VIP <1 have less influence (D) Table representing the serum specific VIPs and their respective scores that best discriminate necrotic from non-necrotic mice at 3 DPI. The contribution of both components was listed in this model.

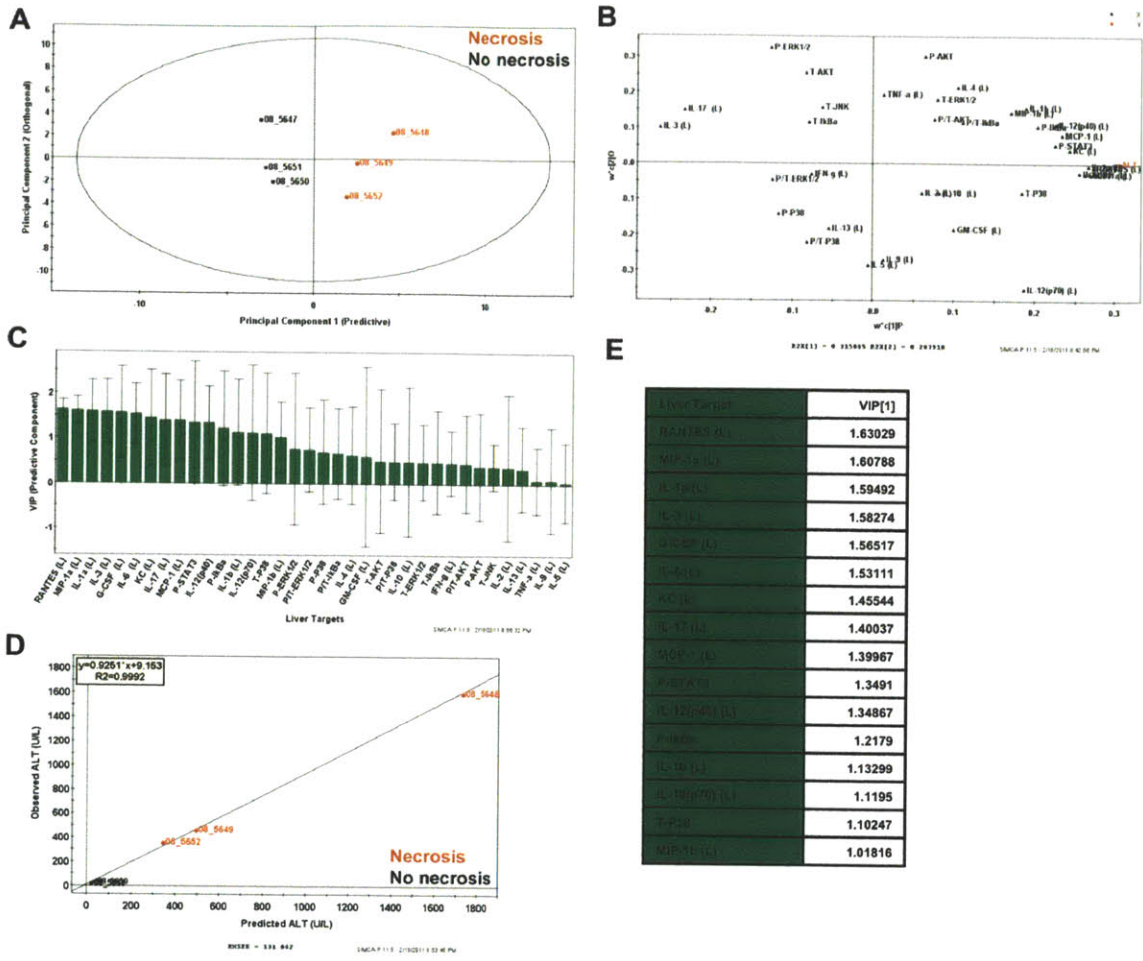


Figure 2-11. Liver specific OPLS analysis of *C. rodentium* infected animals at 3 DPI
 OPLS analysis of *C. rodentium* infected animals at 3 DPI using serum cytokines and chemistries (X) for prediction of ALT levels (Y) (A) Mice segregated well in the predictive component (Principle component 1) with an $R^2X(1) = 0.35$, indicating this component captured ~35% of the variance present in the X variables. (B) The predictive weight and covariation of serum targets (black triangles) in relation to serum ALT (red square). (C) The variables that best separate the two pathological states in relation to the predictive component (D) Variables in projection (VIPs) for the predictive component where values >1 are have positive influence in determining ALT levels, and $VIP < 1$ have less predictive influence (E) Observed vs predicted plot for ALT resulted in a $R^2 = 0.9892$ indicating a highly predictive model based on serum cytokines. (F) Table representing the VIPs for the predictive component for serum ALT.

Table 2-1. PLS-DA and OPLS component contributions to discrimination ($R^2 Y$) and variance (Q^2) of necrosis at 3 DPI.

Both PLS-DA and OPLS models were utilized to interrogate serum features that best discriminate between lesion-bearing and non-lesion bearing mice at 3 DPI. Model results are indicated based on using serum or tissue targets as well as the combined models using the top variables from each independent model.

Serum Model					Model Type
Component	$R^2 Y$	$R^2 Y$ (cumulative)	Q^2	Q^2 (cumulative)	
1	0.789	0.789	0.441	0.441	
2	0.168	0.957	-0.336	0.385	
3	0.0299	0.987	0.343	0.596	PLS-DA: 3DPI
1 (P)	0.842	0.842	0.547	0.547	
2 (O)	0.0809	0.923	0.137	0.684	
3 (O)	0.0563	0.980	0.198	0.882	OPLS: 3DPI (ALT)

Liver Model					Model Type
Component	$R^2 Y$	$R^2 Y$ (cumulative)	Q^2	Q^2 (cumulative)	
1	0.735	0.735	0.492	0.492	
2	0.248	0.984	0.656	0.825	
3	0.0154	0.999	0.86	0.976	PLS-DA: 3DPI
1 (P)	0.783	0.783	0.522	0.522	
2 (O)	0.208	0.990	0.234	0.756	
3 (O)	0.0065	0.997	0.132	0.888	OPLS: 3DPI (ALT)

Combined					Model Type
Component	$R^2 Y$	$R^2 Y$ (cumulative)	Q^2	Q^2 (cumulative)	
1+2 (27 targets)	0.983	0.983	0.987	0.917	PLS-DA: 3 DPI
1+2 (13 targets)	0.994	0.994	0.976	0.976	PLS-DA: 3DPI
P+(O) (26 Targets)	0.996	0.996	0.96	0.96	OPLS: 3 DPI (ALT)

PLS-DA :3 DPI (**necrosis**)

Serum and Liver Combined

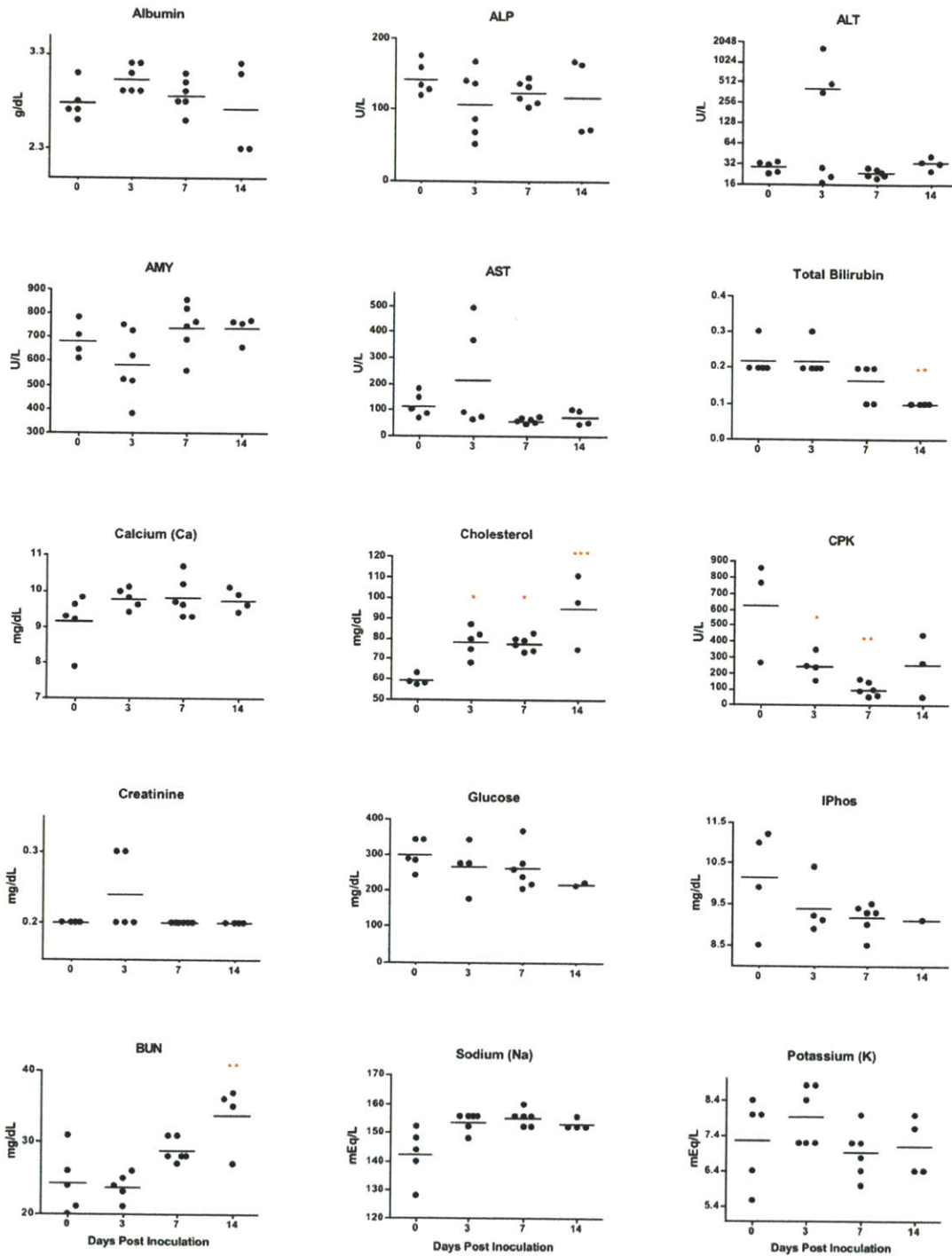
Var. ID (Primary)	M1.VIP[1]
ALT	1.25074
AST	1.23125
ALP	1.2007
IL-3 (L)	1.198
AMY	1.11931
MIP-1a (L)	1.11084
IL-10 (S)	1.10635
RANTES (S)	1.07608
G-CSF (L)	1.07408
G-CSF (S)	1.07393
RANTES (L)	1.05493
IL-1a (L)	1.01725
IL-12(p70) (L)	1.01065
MIP-1a (S)	0.976747
IL-6 (L)	0.96033
IL-17 (L)	0.953303
Cholesterol	0.944339
KC (L)	0.912226
IL-6 (S)	0.903432
KC (S)	0.877771
PT-ERK1/2	0.864734
IL-6 (S)	0.832581
MCP-1 (L)	0.830224
IL-12(p40) (L)	0.818783
P-STAT3	0.805327
T-PPR	0.776951
MIP-1b (L)	0.741268

OPLS: 3DPI (ALT)

Serum and Liver Combined

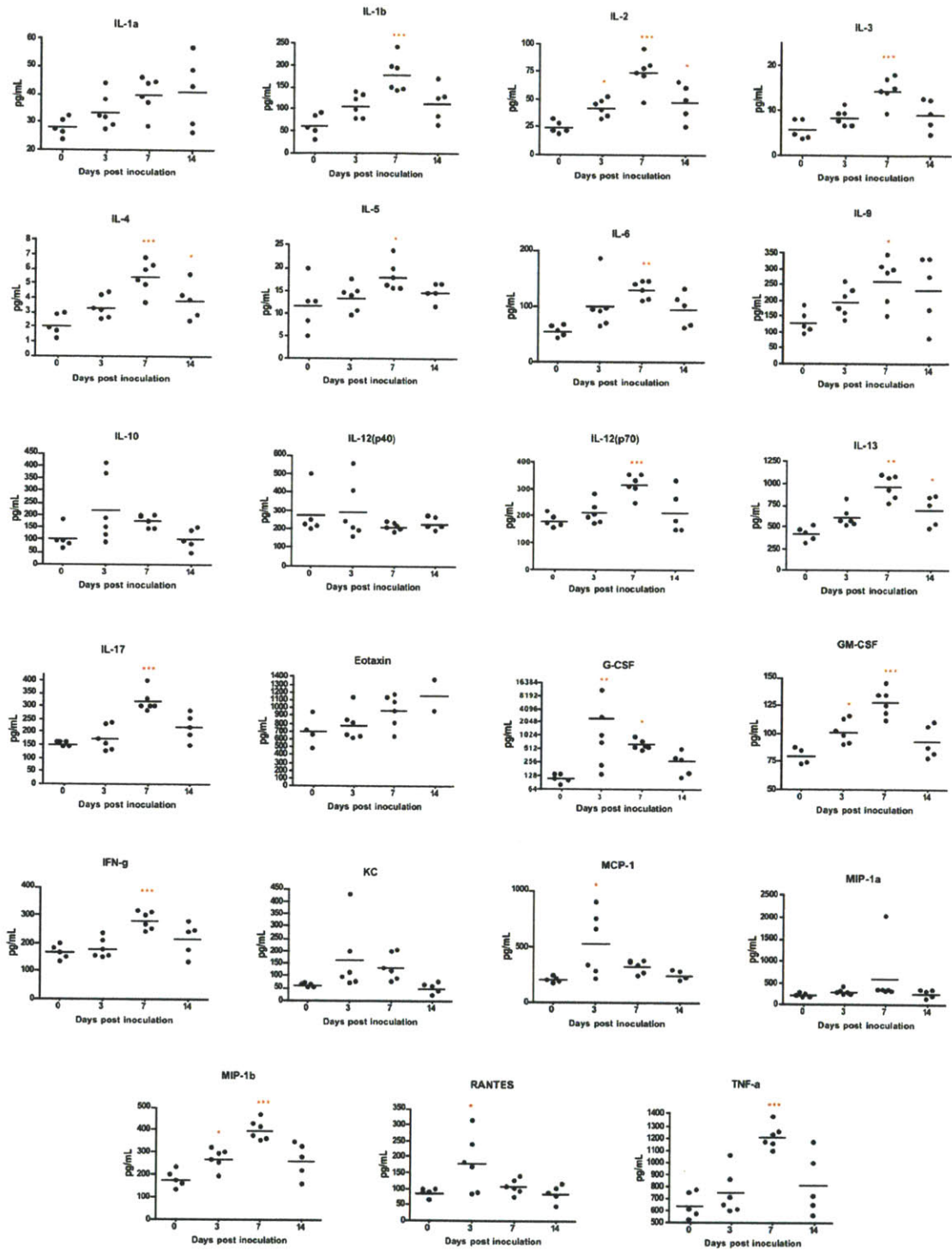
Var. ID (Primary)	M1.VIP[1]
ALP	1.22602
G-CSF (L)	1.16202
G-CSF (S)	1.13907
IL-3 (L)	1.13121
IL-1a (L)	1.12531
RANTES (S)	1.10328
IL-10 (S)	1.09756
MIP-1a (L)	1.08626
IL-6 (L)	1.05872
MIP-1a (S)	1.0562
IL-5 (S)	1.05235
KC (S)	1.04214
RANTES (L)	1.03743
KC (L)	1.00582
P-STAT3	0.974117
IL-6 (S)	0.971058
IL-17 (L)	0.952548
MCP-1 (L)	0.946976
AMY	0.941791
IL-12(p40) (L)	0.918754
IL-12(p70) (L)	0.876672
PT-ERK	0.875737
MCP-1 (S)	0.762724
IL-1b (L)	0.761612
IL-6 (S)	0.749626
MIP-1b (L)	0.705092

Figure 2-12. Most influential variables in serum and liver for PLS-DA (**necrosis** versus no necrosis) and OPLS (ALT) models ranked by Variable in Projection (VIP) values. Targets highlighted in white are those that were found influential in both serum and liver.



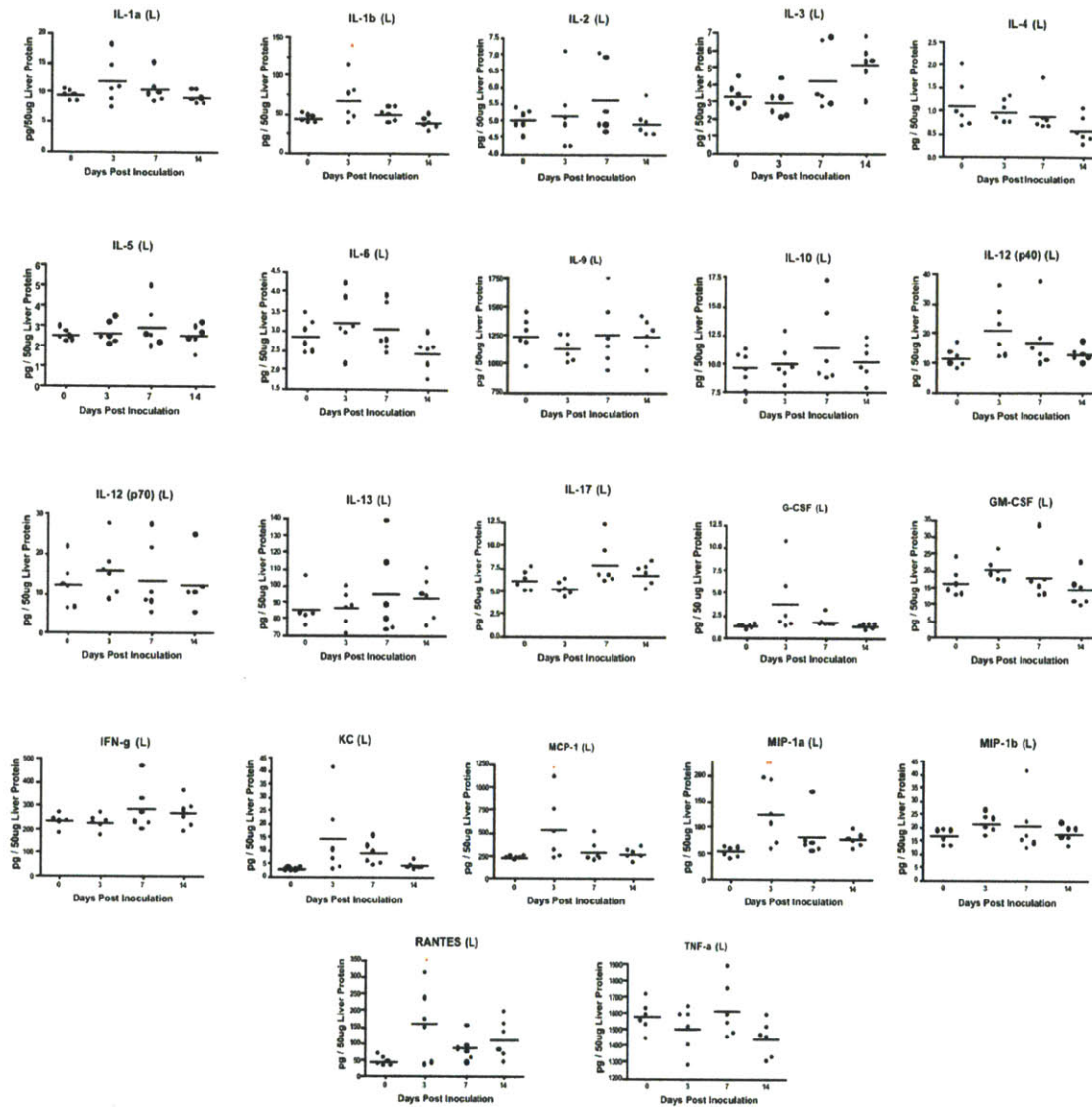
Supplemental Figure 2-1. Serum chemistry changes in C57BL/6 mice inoculated with *C. rodentium*.

Systemic parameters assessing liver function (ALT, AST, ALP, total bilirubin), kidney function (creatinine, BUN, CPK) and electrolytes (Ca, Cl, Na, K) were measured at 0, 3, 7, and 14 DPI. (One-way ANOVA with Tukey's multiple comparison test: * $p < 0.05$, ** $p < 0.01$, *** $p < 0.001$). Lines indicate group means.



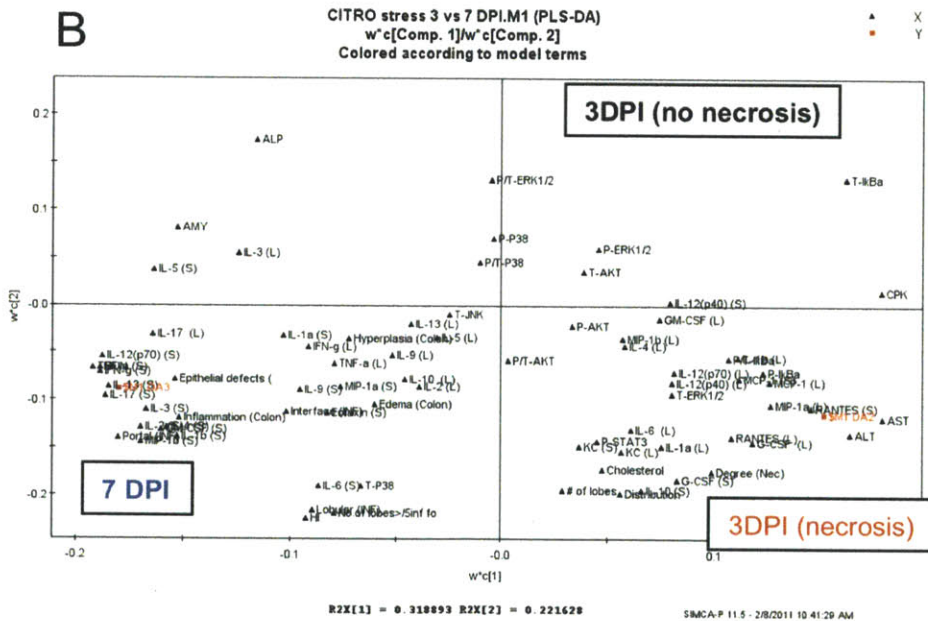
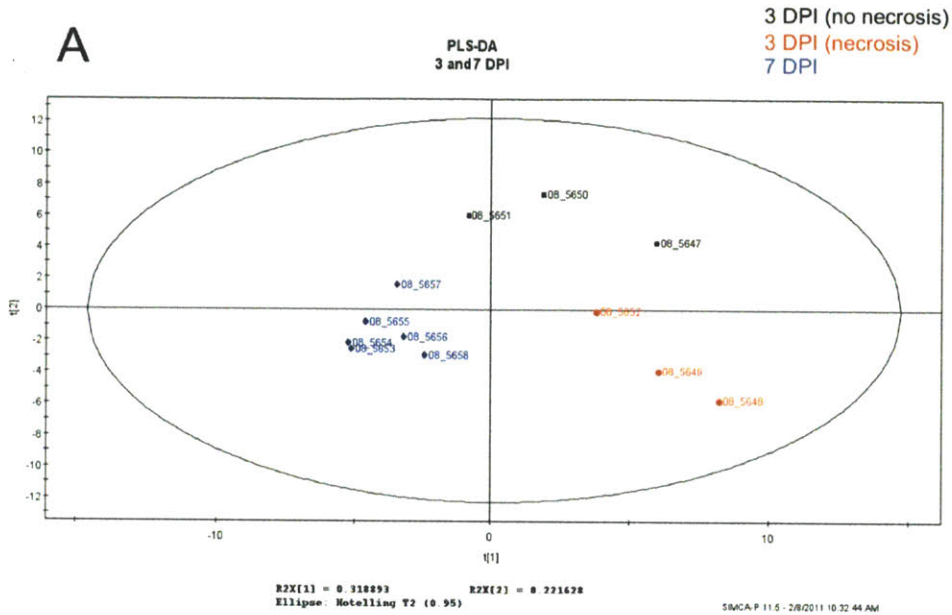
Supplemental Figure 2-2. Systemic cytokine and chemokine changes induced by *C. rodentium* infection in C57BL/6 mice

Serum cytokines and chemokines were measured by quantitative multiplex analysis using Luminex technology. (One-way ANOVA with Tukey's multiple comparison test: * p < 0.05, ** p < 0.01, *** p < 0.001). Lines indicate group means (n= 5 to 6 animals per timepoint).



Supplemental Figure 2-3. Liver cytokine and chemokine changes induced by *C. rodentium* infection in C57BL/6 mice

Liver cytokines and chemokines were measured by quantitative multiplex analysis using Luminex technology. Statistically significant changes as a group were only found for IL-1 β (L), MCP-1 (L), MIP-1a (L), and RANTES (L) (One-way ANOVA with Dunnett's multiple comparison test comparing all columns to controls: * p < 0.05, ** p < 0.01, *** p < 0.001). Lines indicate group means (n=6 animal livers per timepoint).



Supplemental Figure 2-4. PLS-DA analysis of 3 and 7 DPI animals.

Animals were assigned one of three classes; 1) 3 DPI (no necrosis), **3 DPI (necrosis)**, and **7 DPI**. Animal separation based on the first two principal components (A). Target covariation using all serum target, liver targets, and histological scores (B).

Chapter 3: Systems analysis of Acetaminophen-induced liver injury under conditions of *Citrobacter rodentium*-induced inflammatory stress

Arek Raczynski¹, Emily Miraldi¹, Katherine Schlieper¹, Sureshkumar Muthupalani², Steven Tannenbaum¹, David Schauer^{1,2}

¹Department of Biological Engineering, ²Division of Comparative Medicine, Massachusetts Institute of Technology, Cambridge, MA, USA

An abridged version of this chapter is to be submitted to *PLOS Biology*

3.1 Introduction

Drug induced liver injury (DILI) is the leading cause of acute liver failure (ALF) in the United States, characterized by low incidence, mechanisms independent of therapeutic target, and is poorly predicted for in animal models. From a pharmaceutical and clinical perspective, DILI is a major concern that can result in last stage discontinuation of drug development, limit the use and distribution of effective therapeutics, and even lead to market withdrawal [31]. Inflammation is one host susceptibility factor contributing to DILI, evidenced by numerous knockout studies and endotoxin-induced inflammation (LPS), demonstrating increased predisposition to injury under immune dysregulation and inflammatory stress [6, 34, 71]. Immune mediators such as cytokines and chemokines are recognized pro- and anti-inflammatory players involved in the progression and regression of DILI and critical in mediating liver homeostasis and repair.

Acetaminophen (*N*-acetyl-para-aminophenol (APAP)) is a well-studied hepatotoxin, responsible for approximately a third of cases related to DILI [38]. Toxicity is dependent on cytochrome P450 bioactivation of parent molecule to a highly reactive quinone imine (NAPQI), which under high doses depletes hepatic glutathione resulting in protein adducts, with subsequent mitochondrial dysfunction, formation of reactive oxygen species (ROS) and peroxynitrite, and eventual liver necrosis. This process shows dependence on intracellular signal transduction of JNK, with sustained activation promoting APAP-induced injury [106]. More recently, pattern recognition receptors (PRR's) TLR9 and components of the inflammasome (Nalp3)[63] implicate damage associated molecular patterns (DAMPs) such as mitochondrial DNA from necrotic cells, as playing a role in APAP injury, with potential for cross talk with Toll-like receptors (TLRs) and pattern associated molecular patterns (PAMPs) such as LPS, which can also modulate susceptibility to APAP [58, 62]. Furthermore, both innate [85, 107] and adaptive immune responses can alter the susceptibility of APAP injury; moreover, APAP treatment alone can induce levels of inflammatory mediators (ie cytokines and chemokines) both locally and systemically [108]. Collectively, this all points to the importance of inflammatory state in mitigating responses associated with APAP-induced liver injury.

Citrobacter rodentium (*C. rodentium*) is an enteric bacterial pathogen that results in varying degrees of intestinal inflammation, acute colitis, hyperplasia, and edema in numerous strains of mice [74, 75]. As a human homolog of enteropathogenic *Escherichia coli* (*E. coli*) and enterohemorrhagic *E. coli* (EPEC and EHEC respectively), *C. rodentium* has become a highly utilized animal model of these human infections, providing a reproducible, robust, and physiologically relevant model of inflammation. More recently, it has demonstrated organ specific effects distal to the site of attachment and disease with alterations of phase I (cytochrome P450s) and phase II (UGTs) metabolic enzymes in liver and kidney, as well as increases in hepatic cytokine transcript [7, 8]; a time course of regulation that

follows colonic inflammation and bacterial colonization, peaking at 7-10 days post inoculation (DPI), and returning to normal by 15-24 DPI.

Previously, we observed *C. rodentium*-induced coagulative liver necrosis at 3 DPI, paralleled by increased ALT and both serum and liver cytokine changes associated with monocytes and neutrophils chemotaxis/activation as well a Th1 predominant cytokine environment. Whereas, at 7 DPI, infection results in maximal systemic cytokine induction and hepatic inflammation, correlating with peak bacterial load with induction of Th17 environment characterized by serum IL-17, IL-6 and IL-1 β (**Chapter 2**). As host inflammation and disease state have been implicated as a susceptibility factors for DILI, we evaluated APAP-induced liver injury (200 mg/kg IP) during early and peak stages of *C. rodentium*-induced inflammatory stress (3 and 7 DPI). Furthermore, we took a systems-level approach in determining the role of pathogenic enteric infection on altering the response of DILI induced by APAP using both linear (PLS-based) and non-linear dependent (mutual information) computational approaches. These methods were applied to a multi-parameter data compendium that included tissue-resident and circulating cytokine/chemokine targets measured in multiplex, clinical serum chemistries, and pathological liver and colonic assessments of inflammation and necrosis. Specifically, we evaluated potential biomarkers and inflammatory signatures that correlate with the type (sterile (APAP) vs microbially-induced (*C. rodentium*)) and extent of liver damage induced under inflammatory and drug-induced scenarios, furthermore, compared them to standard biomarkers for hepatic injury such as serum ALT/AST.

Here, we demonstrate distinct signatures associated with both types of injury, furthermore, modulation of inflammatory patterns when treatments were superimposed. While moderate APAP protection was demonstrated at early stages of *C. rodentium* infection (3 DPI), statistically significant increases in circulating ALT and additive serum and tissue markers were observed at later time points associated with an increased inflammatory state (7 DPI). This demonstrates a dynamic interplay between sterile and microbial-induced injury and inflammation with implications in understanding liver homeostasis under acute inflammatory stress.

3.2 Results

Experimental design

Based on previous studies, we evaluated APAP-induced liver injury during early and peak stages of *C. rodentium*-induced inflammatory stress (3 and 7 DPI), timepoints based on liver and serum cytokine and chemokine changes in this model. For the remainder of the chapter we will use *C. rodentium* and *Citro* interchangeably when describing study groups. The experimental design is presented in **Figure 3-1**. Briefly, at day 0, 8-10 week old female C57BL/6 mice were infected with either *C. rodentium* ($\sim 10^9$) or sodium bicarbonate (vehicle control) by intragastric inoculation. At 2 DPI, animals were fasted 14-16 hrs to uniformly deplete hepatic glutathione stores, and delivered either vehicle (0.9% saline solution) or 200mg/kg APAP solution delivered via intraperitoneal injection (IP) at an infusion volume of 100mL/kg. 24hrs after IP injection, animals were sacrificed and blood/tissues harvested and processed for H&E (pathological assessment), serum and tissue cytokines quantification using multiplex panels, serum chemistry analysis, and liver total glutathione and serum total bile salts. The process was repeated for animals at 6 DPI. The resulting data compendium included over 4,500 data points and is detailed in **Table 3-1**.

Histopathology of *Citro*, APAP, and APAP+*Citro*-induced liver inflammation and injury

Upon examination of liver sections by H&E at 3 DPI, we observed *C. rodentium*-infected animals (5/6) with periportal multi-focal coagulative necrosis, accompanied with thrombi of injury primarily in the portal vein (**Figure 3-2A,C**) (degree of necrosis, p-value = 0.026, Mann-Whitney compared to vehicle controls). Necrotic regions contained hepatocytes with eosinophilic cytoplasm, appearance of pyknotic or absent nuclei, and loss of normal cellular structure. *C. rodentium* treatment alone resulted in a statistically significant increase in portal inflammation (p<0.01), with a pattern of necrosis predominantly midzonal/periportal in distribution (**Figure 3-2B,D**). We first reported this novel pathological finding in a prospective study examining systemic and liver effects of *C. rodentium* in C57BL/6 mice at various stages of infection course. The incidence of necrotic liver lesions in that study was 50% (**Chapter 2**). Although speculative, it is possible that fasting may have increased the incidence in the current study. APAP treatment alone at 3 DPI resulted in liver necrosis with characteristic centrilobular injury, coupled with elevations in lobular inflammation and significant increases in interface inflammation, # of foci of inflammation, and hepatitis index (p<0.05, p<0.01, p<0.05 respectively) (**Figure 3-2 A, B, and D**). APAP+*Citro* livers at 3DPI, at least grossly, appeared similar to APAP treatment alone and were comparable in inflammatory categories scored (**Figure 3-2 A-D**), except for a decreased trend in periportal inflammation.

The degree of liver necrosis was corroborated by paralleled increases in the serum liver transaminases alanine aminotransferase (ALT) (control = 34 ± 5.92 , *Citro* = 178 ± 110 , APAP = 5391 ± 6700 , APAP+*Citro* = 1193 ± 1372 (mean (U/L) \pm SD)) (Figure 3-2C). Surprisingly, at 3 DPI, superimposing a hepatotoxic dose of APAP on *Citro*-induced liver injury and moderate hepatic inflammation did not result in an additive or synergistic outcome, rather, demonstrated decreased levels of necrosis and serum ALT, albeit just missing significance as a group ($p = 0.083$ for ALT, APAP vs APAP+*Citro* (one-way ANOVA with Bonferroni post test)). When we superimposed drug treatment at 7 DPI, however, we found a statistically significant increase in circulating ALT levels ($p < 0.01$, ANOVA with Tukey multiple comparison test) with comparable degree of necrosis by pathological assessment between APAP and APAP+*Citro* groups (Figure 3-4C). Pathological scores for categories of liver inflammation were similar between APAP and APAP+*Citro* groups and comparable to 3DPI, but due to the larger samples size at 7 DPI ($n = 10-12$ per group) reached higher levels of statistical stringency (Figure 3-4B). *Citro* treatment alone at 7 DPI did not induce serum ALT (control = 33.33 ± 6.08 vs *Citro* = 22.30 ± 4.67 (mean (U/L) \pm SD)) as it did at 3 DPI, however, there was a significant increase in portal inflammation ($p < 0.01$), hepatitis index ($p < 0.05$), and increased regions of inflammatory infiltrates (Figure 3-4A and B).

Multivariate analysis of serum and tissue markers associated with APAP and *Citro*-induced liver injury and inflammation

As mentioned in our previous evaluation of *C. rodentium* induced liver changes (Chapter 2), we found robust changes in both serum and liver cytokines at 3 and 7DPI in C57BL/6 mice, and using computational tools, determined variables highly discriminatory for both liver pathological state (necrosis and inflammation) and markers correlative for serum ALT. Analyzing data based on average responses can result in an investigator missing important variables driving inter-animal differences. Based on this, we decided to again take a multivariate computational approach in determining features that covary best in our data compendium leveraging its multiplex nature. PLS-DA (Partial Least Squares Discriminant Analysis) was used to determine features with highest discriminatory power for lesion-bearing animals and treatment conditions at 3 and 7 DPI, furthermore, to distinguish features most strongly associated with microbial-induced (*Citro*) and drug-induced (APAP) liver injury. Using OPLS (Orthogonalized Partial Least Squares Regression), we determine features that correlate best with serum ALT (dependent variable (Y)), an established serum biomarker of liver necrosis, with serum and tissue measurements (independent variables (X)). As serum is the most easily accessible compartment for biomarker evaluation, we developed non-invasive models (serum targets) and combined models (tissue & serum targets).

PLS-DA analysis at 3 and 7 DPI:

The effect of underlying *C. rodentium* infection on APAP-induced circulating ALT varied at 3 and 7 DPI, furthermore, liver pathology associated with *C. rodentium* infection is distinct at these two timepoints, prompting us to initially evaluate 3 and 7 DPI groups independently. Using PLA-DA, we used all tissue and serum targets in

model generation, but paid particular attention to serum targets as they represent the most accessible compartment for biomarker use. PLS-DA at 3 DPI resulted in an expected separation of treatment groups with moderate overlap of animals in the *Citro* and APAP+*Citro* groups (**Figure 3-3 A**). This could be attributable to certain animals presenting a more dominant *C. rodentium* than APAP signature. The first principle component (PC1, 27% of variance) was dominated by features that separated best APAP-only treated animals and *Citro* infected groups, while the second principal component (PC2, 11% of variance) appeared to capture best the differences between *Citro* and APAP+*Citro* cohorts. The representative scores plot shows covariation of targets responsible for class discrimination (**Figure 3-3 B**). By highlighting animals in representative groups, we were able to generate weighted score plots of the features driving class separation in the principal component plane (**Figure 3-3 C and D**). Examining APAP vs *Citro* at 3 DPI (**Figure 3-3 C**), we find that APAP treated animals are dominant for IL-4 (L, S), IL-6 (L, S), MCP-1 (L), TNF- α (L), AST, and ALT levels, while *Citro* animals were discriminated best by targets such as IL-1 α (L, S), IL-1 β (L), IL-10 (S), IL-12p40 (L), G-CSF (S), MIP-1a (L), and RANTES (L, S), IL-17 (CO), KC (CO). We repeated the analysis for APAP vs APAP+*Citro* (**Figure 3-3 D**). Interesting, while ALT/AST, IL-4 (S) and IL-4 (L) MCP-1 (L), were highly discriminate for APAP alone, they did not have much importance in APAP+*Citro*; if these target were equally important between groups its weighted score would be close to zero. The variable weight, however, did drop in intensity, indicating potential attenuation under infection conditions. Indeed, examining those targets independently by one-way ANOVA showed a significant suppression of IL-4 in both liver and serum under conditions of *Citro* infection at both timepoints (**Figure 3-8 C**) (APAP vs APAP+*Citro* (3DPI) = $p < 0.05$, APAP vs APAP+*Citro* (7 DPI) = $p < 0.001$). These changes are in the context of observed changes in ALT/AST with *Citro* infection (**Figure 3-2 C**). Furthermore, the importance of IL-6 (S) was larger for APAP rather than APAP+*Citro*, and its relative contribution compared to MCP-1 changed greatly at 3 DPI (**Figure 3-3 C and D**).

We also analyzed animals at 7 DPI by PLS-DA and obtained clear separation of treatment groups and resultant scores plot for the principal component plane (**Figure 3-5 A and B**). We obtained a similar pattern for IL-4, however this time, IL-6 (L, S), MCP-1 (L), ALT and AST were better at discriminating APAP+*Citro* animals, confirming our ANOVA results where animals treated with APAP under *Citro* infection at 7 DPI had significantly elevated ALT levels (**Figure 3-4 C**). We also noticed increased weight for targets IL-10 (L), IL-13 (L), and IFN- γ (L) in APAP treatment alone over APAP+*Citro* at 7 DPI, indicating that those cytokines were down-regulated in the latter cohort (**Figure 3-4 D**). This demonstrates that both APAP and *Citro* can induce cytokine and chemokine changes in numerous compartments (liver, serum, colon), furthermore, that superimposition of APAP and *Citro* results in cytokine changes that coincide with ALT changes.

OPLS for ALT: *Citro* versus APAP-induced necrosis:

APAP-induced liver necrosis

We were curious if the features that predict serum ALT elevations were different between drug-induced and pathogen-induced injury and utilized OPLS using serum and tissue targets as independent (X) variables and ALT, a surrogate for liver necrosis, as our dependent (Y) variable. OPLS analysis using all normal and APAP-only treated animals at both timepoints (3 and 7 DPI) resulted in good separation of animals in the predictive component and a strong $R^2 = 0.9611$ for ALT (**Figure 3-6 A & E**). Some of the targets that correlate best with ALT were total serum bile acids, pathologically scored degree of necrosis, MCP-1 (L, S), IL-4 (L, S), and KC (L, S) and glucose. These features had some of the highest VIPs (>1) listed for both liver and serum-specific targets (**Figure 3-6 D**). MCP-1 is one cytokine that has consistently demonstrates high correlation with severity of APAP injury clinically [109]. Hepatic levels of MCP-1 are greatly increased during acute liver inflammation, and CCR2^{-/-} (MCP-1 receptor) mice are markedly more sensitive to the hepatotoxic effects of APAP [84]. MCP-1 has also been associated with late monocytes recruitment in APAP injury [56, 83].

Citro-induced liver necrosis

As ALT increases were only detectable in *C. rodentium* treated animals at 3 DPI, we developed an OPLS model to determine features that correlate best with circulating ALT at this time point, providing correlates of microbial-mediated liver injury. OPLS analysis resulted in separation along the predictive axis with cytokines superimposed on the predictive plane, generating a model with an $R^2 = 0.7446$ using the predictive component and one orthogonormalized rotation (**Figure 3-7 A, B, and E**). Variables with the highest VIP include targets associated with neutrophils chemotaxis and activation (G-CSF (L, S) and KC (L, S)), monocytes /macrophage activation and chemotaxis (MCP-1 (L, S), MIP-1b (L, S)), Th1 cytokines (IL-1 α/β (L), IL-12p40 (L), RANTES (L)), and immunomodulatory targets (IL-10 (S)). This is in line and confirms previous target associations with *Citro*-induced liver injury (**Chapter 2**). While there is clear overlap of targets between APAP and *Citro*-induced liver injury, differences are apparent. Mainly, total bile acids, MCP-1, and KC are correlated with ALT in both types of injury, indicating potentially a shared response to necrosis or liver injury in general. For APAP-alone, however, IL-4 appears to play a much larger role in predicting ALT than in *Citro*-induced liver injury, where RANTES, G-CSF, IL-1 α/β , and IL-10 are more dominant. Furthermore, relative to APAP treatment, the induction of ALT was minor in *Citro* treated animals at 3 DPI, however, the induction of G-CSF and IL-10, and MCP-1 was far more robust in comparison, with G-CSF (S) and IL-10 (S) showing higher correlation for ALT in *Citro*-induced than APAP-induced necrosis (**Figure 3-8 A and B**).

Affinity Propagation, Network Diagrams, and Mutual Information

While PLS-based modeling is a powerful tool for determining linear relationships in large datasets, occasionally, biological targets are not linear in their behavior due to negative feedback and context-dependent responses. Furthermore, our data set contains numerous values below the range of our standard curve, especially for control animals, as well as groups that may show no variance (such as some pathological scores) for certain treatment conditions. PLS accommodates such cases by excluding or interpolating their contribution and importance to the model. PLS is also sensitive to outliers (common with animals data), and VIP-score-based model reduction is not maximally insightful; resulting in numerous PLS planes to digest where target redundancy is difficult to determine.

Mutual information uses a general framework of variable dependence. The method involves initially discretizing data into optimal levels of separation (quantile discretization), converting continuous data into discrete counterparts. This helps accommodate measurement values below the detectable range to be set as the lowest discretization level while values above the detectable range are set to the highest (**See methods for detailed description**). Unlike PLS-based modeling, mutual information makes no assumptions about linear variable dependence, thereby allowing more diverse detection of functional relationship [110], furthermore, is amenable to missing or out of range data and outliers, and provides calculated dependence between categorical labels (ie pathology) and numerical values (ie. cytokine target) using permutation methods to determine statistical significance. For our dataset, we discretized our measurements into optimal levels for comparison between treatment classes. The one caveat with mutual information is that class membership must be set a priori in developing the model. In our case, we determined 6 discrete classes based on pathological endpoints and treatment groups; 1) Control, 2) APAP only (3 and 7 dpi combined) 3) *Citro* 3 DPI (necrotic lesions+ALT elevations) 4) APAP+*Citro* 3 DPI, 5) *Citro* 7 DPI (no obvious lesions or ALT elevations), and 6) APAP+*Citro* 7 DPI.

Given the size of the current data set, we wanted to generate visualizations that best represent the architecture of interactions and dependencies in our data compendium. We first generated a correlation-based matrix using affinity propagation, a robust clustering algorithms that minimizes the error involved in cluster generation compared to other methods. We determined measurement vs measurement correlations as well as measurement vs animal correlations for the purpose of visualizing the overall structure of our dataset (**Supplemental Figures 3-1 and 3-2**). This resulted in clear clusters of treatment conditions as and targets associated with scored pathological endpoints (APAP treatment). For the purpose of visualizing connectivity, we next generated network interaction diagrams using mutual information and ANOVA correlations (p-value ≤ 0.001) for both 3 DPI and 7DPI timepoints based on our 6 treatment classes (**Supplemental Figures 3-4 and 3-5**). Navigating such a complex web of interactions can be difficult, furthermore, if one is interested in a specific target and its interaction partners, we encoded the ability to highlight target sub-networks using MatLab (Example highlighting IL-1 β

(L) interactions at 3 DPI, **Supplemental Figure 3-6**). Deciphering causality from such visualizations is not necessarily possible due to the nature of our data set; however, affinity propagation and network diagrams help present features of our data that covary with one another, as well as specific treatment groups and pathologies making our data amenable to inferring relationships. Furthermore, such visualizations and network diagrams provide associations across the data compendium at a quick glance; which is not easily obtained using PLS-based methods, where digesting multiple principal component planes is necessary.

Mutual information with Liver Pathologies

We first harnessed mutual information to show dependence of our quantitative measurements (tissue and serum cytokines, chemistries etc) with pathological endpoints for liver inflammation and necrosis, but also wanted to find targets able to differentiate between our 6 classes of treatment conditions. Using permutation testing, we incorporated a statistical test to determine those features most significant in their ability to predict pathological states and treatment class from our multivariate dataset. The targets that resulted are presented in a heatmap based on their correlation with the specified treatment class and a subset evaluated by one-way ANOVA (**Figure 3-9 A and B**). We then used these targets and generated a correlation based heat map for liver pathologies, as well as a mutual information heat map colored by Log_{10} p-value for each target association (**Figure 3-10 A and B**). Targets that demonstrate very high mutual information for general degree of necrosis include ALT, AST, IL-4 (S, L), total cholesterol, and MCP-1 (L), MIP-1b (S), and all of these also demonstrate high correlation for degree of necrosis except for IL-4 (S, L). If we examine the pathological manifestations of portal vein thrombi, some of the targets that demonstrate high mutual information and correlation include MCP-1 (S, L), a target that correlated well with both APAP-induced and *Citro*-induced liver injury by OPLS. MCP-1 is a major target involved in monocyte chemotaxis and activation; furthermore, monocytes are a major source of tissue factor (TF), a key component in thrombin formation. Others have also correlated TF and MCP-1 with liver necrosis and markers of graft rejection [111].

One key advantage of this approach is that targets that demonstrate little to no correlation but have high mutual information for a particular pathology indicate a potential non-linear relationship. This is exemplified by liver and serum IL-4 levels, which show extremely high mutual information for degree of necrosis, but very little correlation for liver necrosis across the data set (**Figure 3-10 A and B**). Indeed, IL-4 levels were highly induced in animals treated with APAP alone, and paralleled levels of ALT, however, at 7DPI, APAP+*Citro* animals had significantly elevated ALT elevated compared to APAP alone, but IL-4 levels were attenuated greatly (**Figure 3-9 A and B**). This could indicate that IL-4's potential role in hepatic injury may be dependent on the cytokine environment. Indeed IL-4 has been implicated as both protective and deleterious with respect to hepatic inflammation and injury in various models. For example, IL-4 promotes hepatitis after concanavalin-A (ConA) treatment, but is protective against damage associated with ischemia/reperfusion (I/R) [112, 113]. One could imagine that under an already induce inflammatory

state, associated with neutrophils accumulation and activation (ex high KC, G-CSF), that additional IL-4 could further augment both of these processes, resulting in undesirable collateral damage. Furthermore, IL-4 has been associated with DILI in the case of dicloxacillin-induced hepatic injury, where neutralization of IL-4 in mice was hepatoprotective [114]. And more recently, dual roles for IL-4 have been proposed in the pathogenesis of immune-mediated DILI; including 1) suppressing auto-antigen-induced regulatory responses and 2) promoting hapten-induced pro-inflammatory responses [115]. Clearly, continued study into the role of IL-4 in DILI is warranted, particularly in its role in both innate and adaptive function in liver homeostasis.

Fibrosis associated signature with *C. rodentium* (3DPI):

Affinity propagation demonstrated strong correlation with the occurrence of portal vein thrombi in animals expressing elevated IL-1 α (L), IL-1 β (L), IL-12(p40) (L), RANTES (L), and MIP-1a (L) at 3DPI (**Supplemental Figure 3-1**). These animals also presented with coagulative necrosis resulting from *C. rodentium* infection at this early time point based on observed ALT increases and pathological assessment. Three of these targets demonstrated high mutual information for liver pathology and correlated highly with *Citro* 3 DPI. Under conditions of APAP treatment at this timepoint, however, these targets (RANTES (L), IL-1 α (L), IL-12p40 (L)) demonstrate down-regulation (**Figure 3-9 A and B**). While IL-1 β (L) missed statistical significance based on mutual information, it can still be evaluated in its ANOVA-based sub-network and shows correlation in this pathological finding (**Supplemental Figure 3-4 A and B**). These targets are associated with Th1-mediated response, whereas IL-4 is a prototypical Th2 cytokine. Based on this, there appears to be a neutralization of these two T helper cell polarizing cytokine subtypes in the APAP+*Citro* case at 3 DPI.

***C. rodentium* infection at 7 DPI aggravates APAP-induced liver injury**

Based on the mutual information heat map, there also appeared targets associated with APAP+*Citro* treatment (7 DPI) that had dependences for liver pathology and discriminatory across all treatment classes. Such targets appeared to be down-regulated (MCP-1 (S), IL-4 (L, S)) or up-regulated in this treatment group (KC (L), G-CSF (S, L), and IL-17 (CO), bile acids, and cholesterol) compared to APAP alone or APAP+*Citro* at 3 DPI. Peak bacterial colonization and infection with *C. rodentium* is associated with a characteristic Th17 response, characterized by elevations in colonic and systemic IL-17 [94]. The role of IL-17 has been recently examined in the context in liver injury and in a ConA model of hepatitis; IL-17 plays a role in modifying Nf- κ B mediated responses in a STAT3 dependent manner [116]. Using multiplex assays for colonic cytokines, we found robust induction of IL-1 β , IL-6, KC, IL-17, G-CSF, targets that show high covariation and cluster by affinity propagation (**Supplemental Figures 3-2 and 3-2**). KC in particular appeared to demonstrate synergy at 7 DPI as *Citro* alone was unable to induce levels, but APAP+*Citro* resulted in robust responses that resulted in statistical significance when APAP treatment alone did not (**Figure 3-9 B**).

3.3 Discussion

Most animal models of DILI involve exposure to extremely high levels of chemical stress with subsequent expression changes of cytokines such as TNF α , HMGB-1, IL-6, IL-10 and IL-1 β , potentially misrepresentative of the majority of cases of liver injury observed clinically [117-119]. Here we investigated moderately hepatotoxic doses of APAP in the presence and absence of physiological acute stress induced by gastrointestinal infection with *C. rodentium* in C57BL/6 mice, an animal model of *E. coli* infection and IBD in humans. Using computational approaches such as PLS based modeling and mutual information, we present unique cytokine signatures associated with APAP-induced and microbially-induced liver necrosis, furthermore, altered cytokine patterns under superimposition of drug treatment and enteric infection.

C. rodentium infection at 3DPI was moderately protective against APAP-induced liver injury, correlating with decreased serum and liver cytokines (IL-4, IL-6), liver transaminases (ALT, AST), and histological disease scores as well as elevations in MCP-1 (S), MIP-1b (L), G-CSF (L, S), and IL-10 (S). At 7 DPI, however, superimposing pathogenic enteric infection augmented APAP-induced liver injury characterized by elevated ALT, correlating with decreased IL-4 (L, S), IL-6, and increased levels of G-CSF (L, S) and KC (L, S), and IL-17 (S, CO). It is important to note that despite the association between greatly elevated ALT levels and hepatocellular diseases, the absolute height of the ALT elevation does not necessarily correlate with the extent of liver cell damage [118]. Thus altered ALT levels under infection conditions could also be attributable to altered kinetics of injury potentially slowing or accelerating progression or recovery. Future work following individual animals over time prior to and after 24hrs-post APAP treatment seems warranted in this regard.

The role of anti-inflammatory cytokines has been investigated in fasted transgenic C57BL/6 mice lacking targets such as IL-4, IL-6, IL-10, IL-13, and MIF, dosed with a comparable levels of APAP (200-300 mg/kg, IP), and demonstrate increased susceptibility to APAP-induced liver injury [48-50, 55]. These data suggest a hepatoprotective role for anti-inflammatory mediators and that the balance between the Th1 and Th2 responses is an important determinant for APAP-induced liver injury. Indeed, here we demonstrate an induction of circulating IL-1 α/β , IL-4, IL-6, IL-10, RANTES, IL-12(p40), G-CSF, KC, MCP-1, in animals harboring *C. rodentium*-induced necrotic lesions at 3DPI, indicating that microbially-induced hepatic injury 'primed' the liver, making it less susceptible to injury with APAP treatment. It is also possible that up-regulating protective factors prior to APAP administration allowed for faster resolution of APAP-induced necrosis, possibly altering the signaling landscape and attenuating the extent of liver necrosis. Follow up study measuring liver signaling states would help support this. *C. rodentium* is known to activate Th1/Th17 responses in various strains of mice, potentially skewing the systemic balance of cytokines and altering the extent of APAP damage.

Indeed, strain susceptibility has been investigated; demonstrating C57B/6 mice are more sensitive to APAP-induced liver injury than BALB/c mice, which are characteristically Th2 in their response to treatment compared to their C57BL/6 counterpart [120]. However, the study in question did not examine the role of an already activated and Th1/Th17-skewed environment prior to dosing as investigated here. Furthermore, we evaluated this cytokine environment at early and late stages of enteric infection, under conditions of moderate liver injury and inflammation. Our findings, however, do agree with proposed protection of a Th2 response at late stages of *C. rodentium* infection, but not at earlier timepoints where the already induced liver injury (Th1 cytokines, neutrophils, monocytes, and T-cell related cytokines and chemokines) appeared to tolerate or prime the liver to subsequent insult with APAP and seemed to play a more important role than the Th2 response initiated by APAP treatment alone.

Sterile inflammation with APAP

Inflammatory responses are critical for eradication of pathogens, but also necessary for tissue and wound repair. Like microbially-induced inflammation, sterile inflammation is characterized by neutrophil and macrophage recruitment coupled with production of pro-inflammatory cytokines and chemokines (Recently reviewed [21]). If in excess or unchecked, however, inflammatory responses can aggravate existing injury. For example, exaggerated neutrophil recruitment and activation in response to sterile inflammatory stimuli contributes to the immunopathology of numerous diseases, such as autoimmunity, DILI, ischemia-reperfusion (I/R), trauma, and others [63, 107, 121-123]. APAP treatment alone resulted in significant elevations in IL-4 (L, S), IL-6 (L, S), KC (L, S), and MCP-1 (L, S) (**Figures 3-3, 3-5, 3-9**). Interestingly, some of the most highly specific targets up-regulated by APAP treatment include IL-4 and IL-5, Th2 cytokines involved in allergic responses and eosinophil activation. Indeed, APAP treatment has gained increased attention for potentially predisposing individuals to allergic responses, especially children [124].

At both 3 and 7 DPI, *C. rodentium* significantly down-regulated IL-4 (L, S) levels induced by APAP (**Figure 3-8 C, Figure 3-9 A and B**). IL-4 is key in cytokine involved in differentiation of naïve helper T-cells (Th0) into Th2 cells. Some of IL-4's other functions include eosinophil activation, neutrophils migration and activation, as well as class switching in B-cells and inducing MHC-II production. The presence of circulating IL-10 and G-CSF were paralleled with lower levels of IL-4 in livers and serum at 3 DPI and 7 DPI, indicating that the cytokine environment induced by *C. rodentium* may have affected the signaling network, attenuating secretion of IL-4. This is in line with evidence that IL-10 inhibits the secretion of IL-4 in peripheral blood monocytes and neutrophils [125]. IL-4 secretion in neutrophils has also been demonstrated in APAP-induced liver injury, and IL-4 has been shown to induce leukocyte migration (monocytes and neutrophils) to sites of inflammation in other disease models, preceded by inflammatory cytokines such as MCP-1 [126]. Indeed, IL-4 and MCP-1 expression in APAP treatment alone was highly correlated but was lost under conditions of *C. rodentium* infection (APAP: $R^2=0.75$; APAP+Citro 3 DPI: $R^2=0.17$, APAP+Citro 7 DPI: $R^2=0.12$) (**Figure 3-8 D**).

Others have shown that MCP-1 can directly enhance synthesis of IL-4 by T cells [127, 128]. More recently, IL-4 was also shown to up-regulate MCP-1 production in vascular endothelium through NADPH-oxidase-mediated ROS production [129, 130]. Regardless of the direct relationship, MCP-1 is also critical in mediating Th2 polarization and proper trafficking of T-cells in addition to its role as a monocyte chemoattractant. Hepatic levels of MCP-1 are also greatly increased during acute liver inflammation, and CCR2^{-/-} (MCP-1 receptor) mice are markedly more sensitive to hepatotoxic effects of APAP compared to WT mice [84]. MCP-1 has also been associated with late monocytes recruitment in APAP injury [56, 83], and, clinically, MCP-1 is highly associated with APAP injury, especially at levels >1000 IU/L [109].

Functionally, the elevated levels of IL-10 and moderate protection observed at 3DPI as a result of *Citro* infection, is in line with IL-10's established hepatoprotective role in APAP-induced injury. IL-10 limits inducible nitric oxide synthase (iNOS) expression and peroxynitrite-induced liver injury after APAP overdose and IL-10 KO animals are more sensitive to APAP [49]. Based on the KO studies it appears that IL-10 in conjunction with IL-4 is required for proper balance of IL-6 responses. This was demonstrated in IL-10^{-/-}/IL-4^{-/-} double knockout mice, which are extremely sensitivity to APAP, attributable to unchecked levels of IL-6 [55]. In APAP-induced liver injury (300 mg/kg i.p), IL-6 knockout results in sustained serum AST elevations at 48 hrs, and did not normalize until 72 hrs; findings coupled with higher levels of MCP-1 and MIP-2 in the liver [131]. Collectively, it appears that IL-4, in conjunction with IL-10, plays a critical role in mediating proper expression of IL-6 and MCP-1, necessary for proper resolution of APAP-induced injury.

Microbially-induced liver injury with *C. rodentium*

Pathogens of the gastrointestinal tract can have hepatic manifestations, as we have demonstrated in **Chapter 2**, but the mechanisms involved in establishing hepatic injury and disease secondary to enteric infection remains poorly understood. Recently, severe necrotizing hepatitis has been observed in IL-10 KO mice infected orally with *Trichinella spiralis*, an enteric parasite [132]. IL-10 in this model was critical in mediating trafficking of intestinally derived CD4⁺ T-cells, and determined the primary source of IL-4 in this model. Furthermore, sequestration of activated neutrophils was shown dependent on IL-4, and while neutrophils depletion alleviated necrosis, they were not required for initiation of injury. This example demonstrates the importance of the enterohepatic cytokine balance for appropriate hepatic immune function. Serum IL-10 is robustly induced in *C. rodentium*-infected animals at 3 DPI and associated with our microbially-induced coagulative necrosis. As a regulatory cytokine, IL-10 exerts influence on numerous immunological activities such as antigen presentation and cytokine production, furthermore is involved in the initiation and maintenance of inflammation [133]. Interestingly, in this study we also confirmed a previous finding that *C. rodentium*-induced necrosis induces both serum and liver RANTES, a chemokine responsible for T-cell activation. RANTES failed to show induction in APAP-induced liver injury and indicates a biomarker for differentiating between drug-induced (sterile) and microbially-induced liver injury. RANTES correlates poorly with ALT levels in *Citro*-

induced injury, but is a good discriminator for the presence of lesions, demonstrated by high correlation and mutual information with lesion bearing animals and correlation with portal inflammation (**Figure 3-9 and Figure 3-10 B, Supplemental Figures 3-1**). Other targets that showed preference in *Citro*-induced injury include IL-1 α / β (L, S), IL-12p40 (L, S). Via TLR4, LPS has been shown to activate type 1 (early, ie IL-1 α / β , RANTES) and type 2 cytokine production (late, ie IL-4) both *in vitro* and *in vivo* in macrophages from C3H/HeJ or C3H/HeOuJ mice [134]. IL-4 production, a prototypical type 2 cytokine, requires both MyD88 and TRAM (adapter molecules) for its secretion 48 hrs after LPS stimulation. If LPS mediated injury with *C. rodentium* at 3 DPI, it would explain the cytokine environment, furthermore, potentially explain the neutralization of Th1/Th2 responses under conditions of APAP+*Citro* treatment at 3 DPI. It is possible that the regulatory state induced by an LPS sets in place a regulatory network less capable of inducing IL-4 secretion.

While animals at 7 DPI did not demonstrate clear pathological necrotic lesions and failed to induce serum transaminases, they remained a state of hepatic inflammation (**see liver pathology Figure 3-4**) with elevations of serum, liver, and colonic cytokines. The contribution of significantly increased circulating levels for IL-17 at 7 DPI implicates colon as the source, with colonic cytokine levels increasing ~10 and 228-fold (average FC at 3 and 7 DPI respectively vs. controls) in animals treated with *Citrobacter*, while IL-17 levels in the liver were decreased at 7 DPI. This hints at a potential mechanism for down-regulation of hepatic cytokine expression under peak colonic inflammation and infection. It has also been documented that IL-17 production in myeloid cells (ie macrophages) is induced by IL-6 and suppressed by IL-10 [116], indicating that perhaps early IL-10 induction with *Citro* infection acts to limit the response of Th17 cells. At 7 DPI, however, circulating IL-17 levels are higher and additive with APAP treatment, correlating with increased ALT when the two were superimposed. Others have also shown a dependence of Th17 responses for recruitment of Th1 cells to inflamed or injured tissues.

Altered cytokine responses under APAP+*Citro* superimposition

There are numerous factors that could explain the altered cytokine environment under APAP+*Citro* conditions, specifically the observed neutralization of Th1/Th2 responses as well as changes in neutrophils and monocytes targets. Transcription factors such as STAT 1, STAT3, STAT6, AP-1, and Nf- κ B are key mediators of inflammatory processes. The role of Nf- κ B on APAP-induced liver injury has been investigated, and the loss of functional p50 subunit of NF- κ B is associated with decreased ability of APAP to up-regulate TNF- α , KC, and IL-10 expression and increased expression of IL-4 and TGF- β , however, gross changes in APAP-induced injury were not observed [135]. This argues that Nf- κ B function alone may not fully explain changes in susceptibility to APAP-induced liver injury associated with various inflammatory mediators, however, does not discount the potential for susceptibility in combination with other transcriptional regulators listed above.

Interestingly, in our study, there were significant changes in IL-10, IL-4, KC, and to some degree TNF- α , which points to altered function of Nf- κ B under *Citro*-induced injury and inflammation. LPS, is a component of *C. rodentium*'s cellular wall, and a known inducer of Nf- κ B transcriptional activity. The role of LPS in APAP-induced liver injury has been examined. LPS pretreatment of male C3H/OuJ mice 24hr prior to APAP treatment (400mg/kg) affords protection but not in male C3H/HeJ (TLR4 deficient), furthermore, protection was mimicked with pretreatment with IL-1 α in both strains [58], a cytokine that we see induced with *C. rodentium* in liver, serum and colon (**Figure 3-3 and 3-5**) but failed to reach significance by mutual information in discriminating all 6 classes but was found to have significant correlations as presented in its total and sub-networks (**Supplemental Figures 3-3, 3-4, and 3-5**). IL-1 α is one of the first effector pro-inflammatory cytokines released upon exposure to LPS by various cell types. LPS binding protein (LPB) KO mice also show protection to APAP-induced liver injury, and a recently used LPB inhibitory peptide demonstrated protection against APAP-induced hepatotoxicity in C57BL/6 mice [59, 60]. LPB is known to assist binding of LPS to receptors CD14 [61] and TLR4/MD2, promoting inflammatory cytokine production. While the effect of LPS delivery 24 prior to APAP has been shown protective, potentially via suppression of CYPs associated with APAP bioactivation, however, a distinctly different local and systemic cytokine profile than may be experienced with APAP delivery 2 hrs-post LPS [62], where LPS pretreatment moved the dose response curve to the left, sensitizing animals to injury. This argues in favor of a temporal dependence of LPS, and inflammatory regulators associated with bacterial host response, in mediating hepatic protection of susceptibility to drug-induced injury. Similarly, at two different timepoints of *Citro*-induced liver injury and of host-pathogen interactions we have two distinct outcomes with APAP treatment in this study.

An acute viral hepatitis model recently showed protection to APAP-induced liver injury characterized by decreased APAP-protein adducts and serum ALT. The authors demonstrated no effect on liver total glutathione, however, attributed protection to decreased bioactivation of APAP \rightarrow NAPQI as mRNA levels of CYP2E1 and CYP1A2 were decreased 3 days post viral infection [136]. We have evaluated the effect of *Citro* infection at 7 DPI on APAP drug exposure (**Chapter 4**) and do not see changes in parent drug exposure due to infection; furthermore, others have demonstrated that *Citro* does not alter hepatic mRNA levels of murine CYP2E1, the primary CYP responsible for APAP bioactivation [8]. This argues that changes in ALT levels with *Citrobacter* infection are likely not attributable to alterations in APAP metabolism or clearance. What is unclear is whether early infection with *C. rodentium* results in gastrointestinal damage, resulting in the release of DAMPs into portal circulation. Future work would look to measure systemic (or portal) concentrations of known DAMPs such as HSPs, HMGB1 etc. The early necrotic lesions may very well be a consequence of both PAMPs (LPS, bacterial products) as well as DAMPs released during early gastrointestinal infections and resultant epithelial damage promoting leakage into portal circulation. Furthermore, examination of

livers at early timepoints would be insightful as to the signaling mechanisms and temporal kinetics of injury under microbially-induced liver injury and inflammation.

Recently, a detailed demonstration of how intravascular danger signals guide neutrophils to sites of sterile inflammation was presented [137]. While the authors induced hepatic necrosis by means of localized thermal injury, the host response to the injury may well translate to drug-induced necrosis seen with APAP. In their model, adenosine triphosphate (ATP) from necrotic cells activated the Nlrp3 inflammasome generating an inflammatory microenvironment (up-regulation of ICAM-1) alerting circulating neutrophils to adhere within liver sinusoids. Subsequent generation of an intravascular chemokine gradient (targets such as MIP-2 and KC) directed neutrophil migration through healthy tissue toward foci of damage. Lastly, formyl-peptide signals released from necrotic cells guided neutrophils through nonperfused sinusoids into the site of injury, overriding the signals from chemokines to reach areas of sterile tissue necrosis. The authors describe this as a potential method to avoid collateral damage of healthy tissue during sterile inflammation. Furthermore, it has recently been demonstrated that APAP treatment in mice results in release of DAMPs such as heat shock protein 70 (HSP70) and high mobility group box-1 (HMGB1) [138]. In our investigation, we saw an up-regulation in numerous neutrophil and monocytes/macrophage associated targets (KC, MCP-1, MIP-1a/b). Moreover, chemokine balance appears important in mediating APAP severity, as CCR2 KO (MCP-1 receptor) exacerbates injury [83, 84] while CXCR2 KO (KC and MIP-2 receptor) is protective [52]. *C. rodentium* infection may provide a physiologically relevant model for the interrogating the role of PAMPs and DAMPs and cytokine/chemokine balance under sterile inflammatory stimuli associated with APAP-treatment.

Mutual information

C. rodentium induced a characteristic signature with direct mutual information for liver pathological states which included IL-12(p40) (L), RANTES (L), and IL-1 α (L), which demonstrated attenuation under co-exposure with APAP at 3 PDI and captures as significant using mutual information (**Figure 3-9**). IL-12p40 production occurs via activation of inflammatory cells, which includes macrophages, neutrophils, microglia and dendritic cells (DCs) upon stimulating by a various inflammatory and pathogenic agents (like LPS) [139, 140]. As a homodimer (IL-12p80), it is known to act as a chemoattractant for macrophages [141, 142] and more recently shown to initiate dendritic cell (DC) migration from the lung to draining lymph nodes in mice challenged with pathogenic mycobacteria. Several other groups have proposed a role for IL-12p40 in fibrosis. Similarly, we have both IL-12p40 in liver and serum upregulated in animals harboring portal venular fibrin thrombi (**Affinity Heatmap, Supplemental Figure 3-2**). It is interesting to note that under APAP treatment at this timepoint, levels of these targets decreased significantly, attributable potentially to IL-4, a Th2 cytokine that can attenuate Th1 responses (**Figure 3-9**). Furthermore, the occurrence of portal vein thrombi was decreased under APAP treatment as well as portal inflammation (missed significance). In other models, IL-4 has been associated with balancing

inflammatory processes as well as modulating tissue factor expression and synthesis in monocytes, a key component for thrombin formation. Given the extent of injury under superimposition of drug and infections, it is difficult to determine whether APAP treatment alleviated *C. rodentium* induced periportal necrosis, however, there was clearly a down regulation of targets associated with such lesions in *Citro* only animals and decreased ALT at 3 DPI. Modulating levels of RANTES, IL-1 α/β and IL-12p40 may be useful in subsequent experiments to determine their role in mediating microbial-induced liver injury in this model.

Mutual information also highlighted IL-17 (CO) as significantly associated with treatment classes and liver pathology, and *C. rodentium* has previously been shown to induce both circulating and colonic elevations at 14 DPI [91, 94]. Activated liver-infiltrating IL-17- producing T helper (Th17) cells are also responsible for neutrophil recruitment into the liver [143]. Furthermore, serum IL-17 levels are increased and serve as a marker of the severity of acute hepatic injury [144]. Here we noticed increased levels of IL-17 in serum and likely attributable to colonic or circulating cells as liver lysates failed to show statistically significant increases. Furthermore, 7DPI was elevated for serum, liver, and colonic G-CSF and KC, two neutrophil-associated targets. While IL-17 levels in the liver were lower in *Citro* and APAP+*Citro* treated animals at 7 DPI in this study, it is possible that the robust Th17 response in the colon (and serum) may have acted to down regulate expression in peripheral tissues or created a systemic cytokine/chemokine environment promoting hepatic inflammation or injury. Similarly, we also saw decreased levels of IL-13, IFN- γ , and IL-10 in liver at 7 DPI for *Citro* and APAP+*Citro* animals, targets believed protective in APAP-induced injury and may have contributed to significantly higher ALT levels at this timepoint. The role of IL-17 has been recently examined in the context in liver injury and in a ConA model of hepatitis; IL-17 plays a role in modifying Nf- κ B mediated responses in a STAT3 dependent manner [116]. Furthermore, increased systemic or liver IL-4 levels (albeit attenuated under *Citro* superimposition) in conjunction with circulating IL-17 may have potentiated neutrophils accumulation and activation in livers at 7 DPI in APAP+*Citro* treated mice in combination with higher G-CSF and KC levels.

Conclusions and Future Work

Inflammatory responses can be both protective and predispose the host to APAP-induced liver injury illustrated by numerous KO models and pharmacological inhibition of immune modulators. In our model of acute inflammatory stress, APAP did not synergize with extrahepatic inflammation induced by *C. rodentium* infection, rather demonstrated moderate protection during the early course of enteric infection while statistically increased serum ALT levels at 7 DPI. We attribute this to an already induced Th1/Th17 response by *C. rodentium*, which we have recently documented (**Chapter 2**) and shown here to induce coagulative necrosis, primarily periportal in distribution early in the infection kinetics. Under co-exposure, the tissue and systemic cytokines levels appear to indicate Th1/Th2 neutralization, as the usual Th2 promoting targets (IL-4 (S, L)) associated with APAP treatment and

Th1 targets with *C. rodentium* (IL-12p40 (L), RANTES (L), IL-a/b (L)) demonstrated attenuated levels as compared to single treatment alone. This can be at least in part attributed to the induction of IL-10, with known immunomodulatory effects on T cell polarization with *C. rodentium* and the anti Th1 effects of IL-4 resulting from APAP treatment. Future work would focus on neutralizing some of the targets obtained in this analysis such as IL-10 to address its role in *Citrobacter*-induced liver injury at 3 DPI, as well as the role in mediating altered signaling states under superimposition with APAP treatment. Cytokines are known signaling molecules in signal transduction pathways, and we previously observed signaling alterations in liver STAT1, STAT3 and I κ B α phosphorylation under *Citro* infection (**Chapter 2, Appendix Chapter B**), important mediators of cytokine signaling and immune responses. Measuring a limited number of intracellular signaling states may help to clarify mechanisms driving altered liver response and changes in T-cell polarizing targets observed here.

We also demonstrate the utility of using multiple computational approaches for interrogating signaling networks in large multi-parameter data sets. Specifically, PLS based methods for correlation determination for a specific target of interest such as ALT, with assumptions of linear dependence, which is useful towards biomarker discovery. We also utilized affinity propagation, a specialized clustering algorithm for visualization of correlations across the entire data set and outlier determination. And finally, in a novel fashion used a hybrid approach harnessing both mutual information and correlation based methods in tandem to create a network architecture that helped us evaluate measured targets with pathological endpoints with a specified number of classes. This method allows statistical evaluation of correlation and dependencies, furthermore, presents data for global and target selective interrogation of interactions using sub-networks.

In summary, we show that drug-induced and microbially-induced liver injury and inflammation have distinct and shared features, furthermore that enterohepatic cytokine balance is involved in mediating appropriate hepatic immune function and responses to both drug and infection-induced insult. Altering the cytokine milieu with *Citro* infection was associated with moderate protection from APAP-induced liver injury 3 DPI, attributable to induced anti-inflammatory mediators such as IL-10 and monocytes chemokines MCP-1 and MIP-1b, however, aggravated injury at 7 DPI correlated with significant elevations in KC and G-CSF and serum IL-17. *C. rodentium* alters APAP-induced cytokine changes, attenuating a Th2 response with demonstrated down-regulation of IL-4 at both early and late stages of infection. Furthermore, we propose non-linear dynamics for IL-4 with respect to liver injury response, indicating its role in hepatic homeostasis may be context dependent.

3.4 Selected methods

Media and Bacterial Strains

Luria-Bertani (LB) agar and broth (Difco Laboratories, Detroit, MI) was used for cultivation of bacteria. MacConkey lactose agar (Difco Laboratories) supplemented with 40 µg/ml of kanamycin was used for quantitative monitoring of bacterial counts in fecal samples. The kanamycin-resistant strain of *C. rodentium* strain, DBS120 (pCRP1:Tn5, Kan^r) [145] was used for all infections.

Animal Housing and Bacterial Infections

Female 8-10 week old C57BL/6J (The Jackson Laboratory, Bar Harbor, ME) mice were housed six per microisolator cage in a specific pathogen-free facility approved by the Association for Assessment and Accreditation of Laboratory Animal Care. Animals were maintained on pelleted rodent chow (LabDiet, Purina Mills, Inc., Richmond, IN) and water ad libitum and allowed to acclimate one week prior to experimentation. Infectious colitis was induced by intragastric inoculation with $\sim 1 \times 10^9$ CFU of DBS120 in 3% sodium bicarbonate (w/v in 1X phosphate buffered saline (PBS), pH 7.4), 100µL volume as described previously [145], while the uninoculated control groups received 100µL of 3% sodium bicarbonate vehicle. Infection kinetics was monitored by fecal shedding determined by plating serial 10 dilutions of fecal slurries (10% [w/v] in 1X PBS, pH 7.4) on LB agar with selection for kanamycin. The Massachusetts Institute of Technology Committee on Animal Care approved all animal experiments prior to investigation.

Fasting and Acetaminophen delivery

Animals were fasted 14-16 hrs to uniformly deplete glutathione stores prior to delivery of either vehicle (0.9% saline solution) or 200mg/kg Acetaminophen (APAP) (Sigma-Adrich, St. Louis, MO) solution delivered via intraperitoneal injection (I.P.) at an infusion volume of 100mL/kg. APAP solution was made fresh for each experiment at 20mg/mL in 0.9% sterile saline (Pheonix Labs) and heated to 55°C in a water bath to dissolve. Animals were sacrificed by CO₂ asphyxiation 24 hours post IP injection. At necropsy, tissues were immediately flash frozen in liquid nitrogen and stored at -80 for subsequent analysis. Blood was collected via terminal cardiac puncture using a 30-gauge needle and transferred to serum separator tubes (Benton Dickinson (BD), Franklin Lakes, NJ), allowed to clot for 30minutes at room temperature, and processed by centrifugation at 8,000 rpm for 10minutes at 4°C. Serum was transferred to a clean eppendorf tube and frozen to -80C until needed for serum chemistry, serum cytokine/chemokine analysis, and total bile acid determination.

Body Weights and Fecal Shedding

Animals weights were monitored every 2-3 days post inoculation with *C. rodentium* or vehicle delivery and at necropsy. Animals losing >20% of initial body weight were euthanized and excluded from subsequent analysis.

Multiplex Detection of Serum Cytokines and Chemokines:

Mouse serum collected at necropsy was processed using mouse 23-plex cytokine panels (Bio-Rad, Hercules, CA) as specified by the manufacturer. Briefly, serum was diluted in species-specific sample diluent (1:4) and 50uL of sample or premixed standards were incubated with pre-washed target capture antibody-conjugated microspheres provided and incubated for 30 minutes with orbital shaking (300 rpm) in a 96-well plate. Upon washing, beads were incubated with detection antibody (30 min), washed, and subsequently incubated with streptavidin-PE (10 min). Beads were washed and resuspended with 125uL assay buffer and read on the Luminex 200 suspension array system using the low RP1 target setting (High PMT) for maximum sensitivity. Data analysis was carried out with the Bio-Plex Manager™ 5.0 software and cytokine or chemokine concentrations calculated against an 8 point standard curve generated by either 4PL or 5PL curve fitting.

Multiplex Detection of Tissue Cytokines and Chemokines

Colon and livers were thawed on ice and ~30-50 mg of tissue was briefly washed with 500uL ice-cold cell wash buffer (Bio-Rad, Hercules, CA). Tissues were then transferred to a clean pre-weighed eppendorf tube and resuspended 12X the tissue weight with cell lysis buffer (Bio-Rad, Hercules, CA). Tissues were homogenized on ice for 1 minute with a Tissue Tearor™ and subsequently frozen to -80°C overnight. Tissues were then thawed on ice and sonicated on level 5 with 5 short (~3 sec) bursts. Upon sonication, lysates were centrifuged for 10 minutes (5,000 rpm, 4°C). Resultant supernatant was carefully removed, protein quantified by BCA protein assay (Thermo Scientific, Rockford, IL), and adjusted to 1ug/uL with 1X PBS + 0.5% BSA (w/v). 50uL of adjusted lysate was subsequently loaded on to a Mouse Group I: 23-Plex panel (Bio-Rad, Hercules, CA) and standards resuspended in the appropriate matrix. Samples were subsequently processed as specified above for serum cytokines and chemokines analysis using the Bio-Plex array system and software manager.

Clinical Chemistries

Serum samples were thawed on ice and diluted 1:4 in water and processed on an Olympus AU 400e serum chemistry analyzer (Beckman Coulter, Inc., Brea, CA) for 18 serum chemistry targets. All samples were run against internal standards and machine calibrated prior to use as specified by the manufacturer. Calcium levels were adjusted to albumin using the following equation: Adjusted CA = (3.5-Albumin) + non-adjusted CA.

Detection of Total Liver Glutathione

40-60 mg of liver was thawed on ice and transferred to a clean pre-weighed eppendorf tube. 5% 5-Sulfosalicylic acid (in ddH₂O, w/v) was added at 5X the liver wet weight and homogenized for one minute with a Tissue Tearor™ (Biospec Products, Inc., Bartlesville, OK), and lysate subsequently frozen at -80°C overnight. Upon thawing at room temperature, lysates were cleared by centrifugation at 8,000 x g for 10 minutes and transferred to a clean eppendorf tube. Supernatant was then

diluted 1:20 in ddH₂O and analyzed for total glutathione (Dojindo Molecule Technologies, Rockville, MD) by monitoring the absorbance of 405nm on a spectrophotometer (Molecular Probes, Sunnyvale, CA) after 10 minutes of incubation at room temperature as specified by the manufacturer. Total glutathione concentration in liver samples was calculated against a glutathione 8-point standard curve using the pseudo-endpoint method and converted to mM/gram tissue.

Total Bile Acids Detection

Serum samples were diluted 1:4 in distilled water and processed using the total bile acids assay kit (BioQuant, San Diego, CA) as specified by the manufacturer. Briefly, the formation of formazan dye was monitored measuring the absorbance at 540nm using a spectrophotometer (Molecular Probes, Sunnyvale, CA). Absorbance was measured at time zero and after 10 minutes of incubation at 37°C. Total serum bile acids were determined by calculating the $((\Delta A_{540} \text{ Sample}/(\Delta A_{540} \text{ Standard})) * \text{Standard (36.1}\mu\text{M/L)})$. All measurements were conducted in duplicate.

Histology and Pathology Scores

At necropsy, blood, fecal, and tissue samples were collected. Distal colon (~0.5 cm) and the left lateral lobe of the liver were snap-frozen in liquid nitrogen and stored at -80°C until needed for protein isolation for western blot and Luminex cytokine/chemokine detection. The remaining colon and liver was fixed in 10% formalin, paraffin embedded, sectioned at 5 μm , and stained with hematoxylin and eosin (H&E), and submitted to a board-certified veterinary pathologist blinded to experimental treatment groups. Colonic tissue sections were scored on a scale of 0 to 4 (0, no lesion; 1, minimal; 2, mild; 3, moderate; and 4, severe) for the categories of inflammation, edema, hyperplasia, dysplasia, and epithelial defects. The sum of all five categorical scores (maximum of 20) resulted in the histological colitis index.

Livers were assessed for both inflammatory and necrotic parameters. Degree of hepatic inflammation was graded on a scale from 0 to 4 based on region (lobular, portal, and interface), and the number of lobes with greater than 5 inflammatory foci was noted. The summation of these scores resulted in a hepatitis index; mice with a score ≥ 4 were defined as having hepatitis. A modified scoring criterion was developed to define the extent, degree, and pattern of liver necrosis. The degree of necrosis was scored from 0 to 4 and the pattern of injury was evaluated as centrilobular, midzonal, or periportal in nature (# = low, ## = medium, ### = high). The distribution of necrosis was evaluated as follows: 0- none, 1 - focal, 2 - multifocal, 3 - translobular, 4 - submassive, involving multiple lobules or entire lobe.

Statistical Analysis:

Statistical significance in body weight change, bacterial load, disease indices, cytokine changes, clinical chemistries, and by comparing control or experimental groups by either student's T-test or by two-way analysis of variance (ANOVA) followed by Bonferroni if group sample sizes were equal or Tukey's post tests if

sample sizes were not equal. Data that demonstrated non-normal distributions or categorical in nature (ex. pathology scores) were assessed by Kruskal-Wallis non-parametric test with Dunn's multiple comparison test against controls unless otherwise indicated. If only two groups were analyzed, Mann Whitney was utilized for non-parametric data. All analyses were done with GraphPad Prism software, version 4.0 and *P* values of <0.05 were considered significant.

PCA and PLSR Analysis

Data was mean centered, variance scaled, \log_{10} transformed, and analyzed by multivariate analysis using SIMCA-P 11.5 software (Umetrics Inc., Kinnelon, New Jersey). Values that were out of range for the assay were set as missing values. PCA analysis was used to reduce the dimensionality of the data set and to assess linear covariation of variance across measured targets. PLS-DA analysis was used to determine the features that best differentiated between selected groups of animals designated as classes (ex. mice harboring necrosis vs non-harboring mice). OPLS analysis was used to determine the features that best correlated with a desired *Y* variable, such as ALT levels or degree of necrosis/hepatitis, resulting in variable importance in the projection (VIP). VIPs greater ≥ 1 were considered significant in their contribution to the model predicting the dependent variable (*Y*) of interest. Model quality was assessed and reported using the following parameters: $R^2 Y$, the fraction of the sum of squares of all *Y* variables explained by the component of the model, and $R^2 Y$ cumulative, the cumulative sum of squares of all *Y* variables explained by all components of the model. Q^2 is the fraction of the total variation in *Y* variables that can be predicted by the component, and Q^2 cumulative is the cumulative Q^2 of the *Y* variables for all components in the model. An R^2 cumulative and Q^2 cumulative of 1 indicate a perfect fit, with 100% of the relationship between *X* variables and *Y* variables explained.

Affinity Propagation and Heat Map Generation

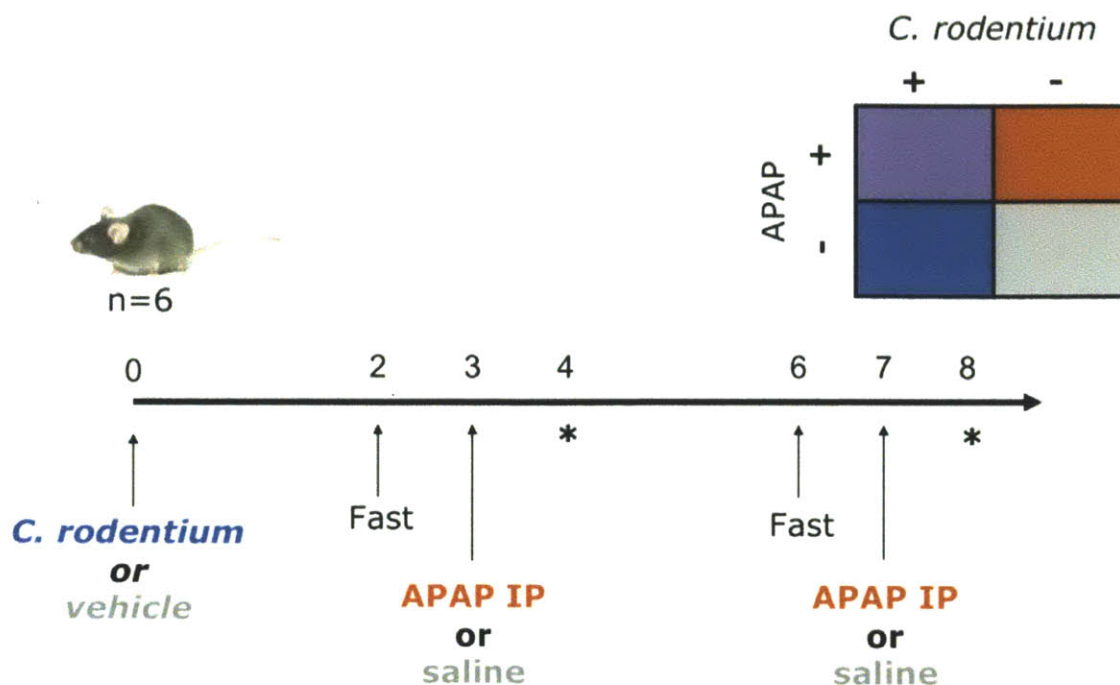
In order to visualize the underlying structures in the data in a heat map, we ordered the data by clustering in both the measurement and the mouse dimensions. Because the dataset contained diverse measurements on incongruent scales, we first mean-centered and variance-scaled each measurement vector. These "z-score" scaled measurement vectors were clustered using the affinity propagation algorithm [146] with a correlation distance metric. To further order the measurements within a cluster, we used hierarchical clustering. Next, the data matrix was clustered in the mouse dimension using the same approach.

Heatmap analysis enabled data quality control and outlier detection. As many of the mice clustered by treatment group, we were able to see that measurements discriminated treatments in an unsupervised manner. We were also able to visualize the measurements that best defined treatment classes.

Mutual Information to detect relationships between measurements, treatment conditions, and pathophysiology

Mutual information is a metric that allows the detection of dependence relationships. Unlike other measures (like PLS-based modeling), mutual information makes no assumptions about linear variable dependence, thereby allowing more diverse detection of functional relationship. Using 3 and 7 DPI data (7 DPI repeat was excluded for validation), our data was discretized using quantile discretization, resulting in optimum levels, essentially converting continuous data to a non-parametric form based on variation between the 6 designated treatment classes. Once the data was in non-parametric form, it was analyzed using MatLab generating mutual information metric determining the interactions that best separated the treatment groups with a required stringency p-value < 0.001. All measurements were analyzed against each other as well as animals resulting in pairwise interactions. We also generated network diagrams using ANOVA correlations with a minimum p-value stringency of 0.001 and organized using Kamada algorithm for optimal separation of targets.

3.5 Figures and Tables



APAP = 200mg/kg IP → Mild Necrosis * Necropsy

Figure 3-1. Experimental design evaluating APAP-induced liver injury under *C. rodentium*-induced inflammatory stress.

At time 0 DPI, 12 female, 8-10 week old C57BL/6 mice were delivered $\sim 10^9$ colony forming units of *C. rodentium* while 12 received 3% sodium bicarbonate (vehicle). The evening prior to dosing, animals were fasted for 14-16 hrs depleting glutathione stores and delivered APAP (200mg/kg, IP) or saline (vehicle). Both 3 and 7 DPI were evaluated with an n=6 for each condition and 24 animals per timepoint. We evaluated the 7DPI timepoint in two separate experiments, yielding an n=12 per condition at 7 DPI in some of our analysis.

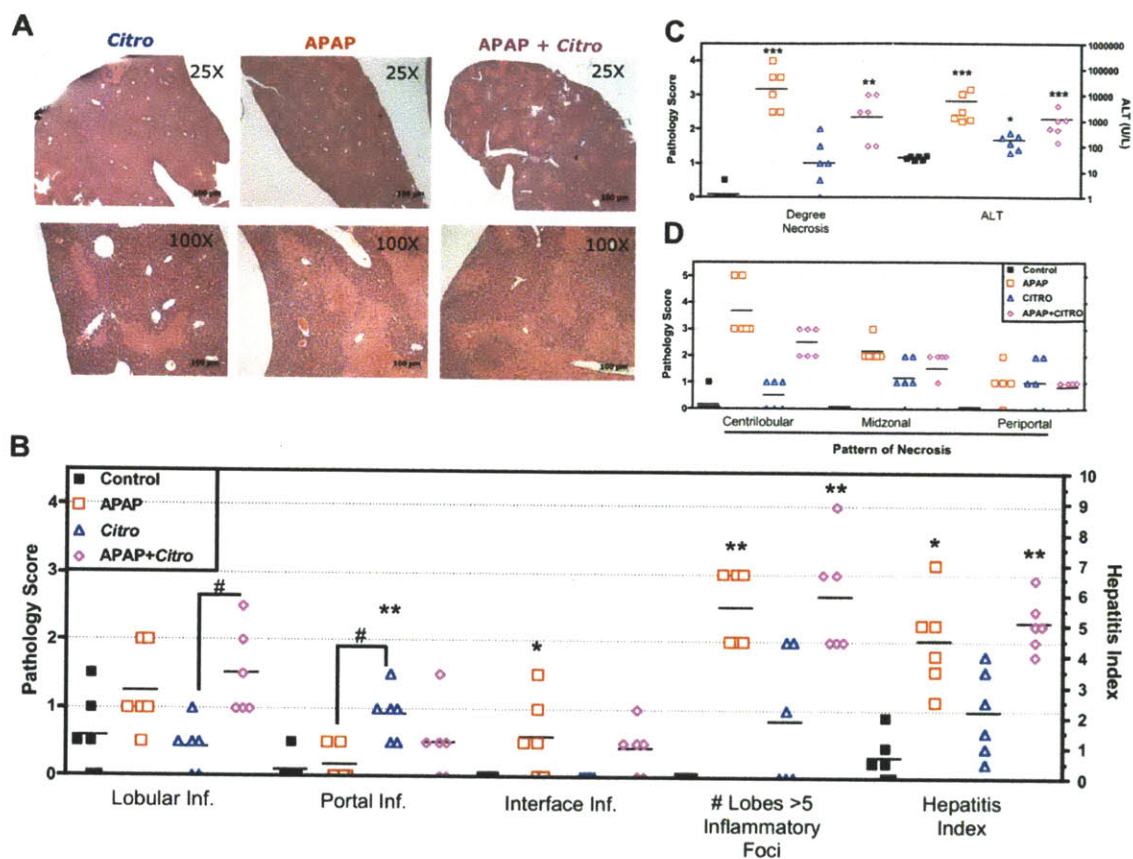


Figure 3-2. *C. rodentium* and APAP-induced liver lesions evaluated by H&E at 3 DPI
 (A) *C. rodentium* treated animals presented periportal coagulative necrosis as previously reported. APAP (200mg/kg) treated animals demonstrate characteristic pattern of centrilobular necrosis. APAP+*Citro* treated livers look very similar to APAP alone. (B) Pathological assessment of liver sections based on lobular inflammation, portal inflammation, interface inflammation, and the number of lobes with greater than 5 inflammatory foci. The total score for each categorical measure of inflammation was summed resulting in the hepatitis index. Animals with a hepatitis index greater than 4 are considered positive for hepatitis. (C) The degree of necrosis and matched serum ALT (U/L). (D) The pattern of necrosis was assessed as centrilobular, midzonal, or periportal in distribution. (Kruskal-Wallis with Dunn's post test compared to controls: for all pathological scores; One-way ANOVA with Bonferroni post tests for ALT (log transformed). * $p < 0.05$, ** $p < 0.01$, *** $p < 0.001$). Symbols indicate individual animals and lines indicate group means (n = 6 for all treatment conditions).

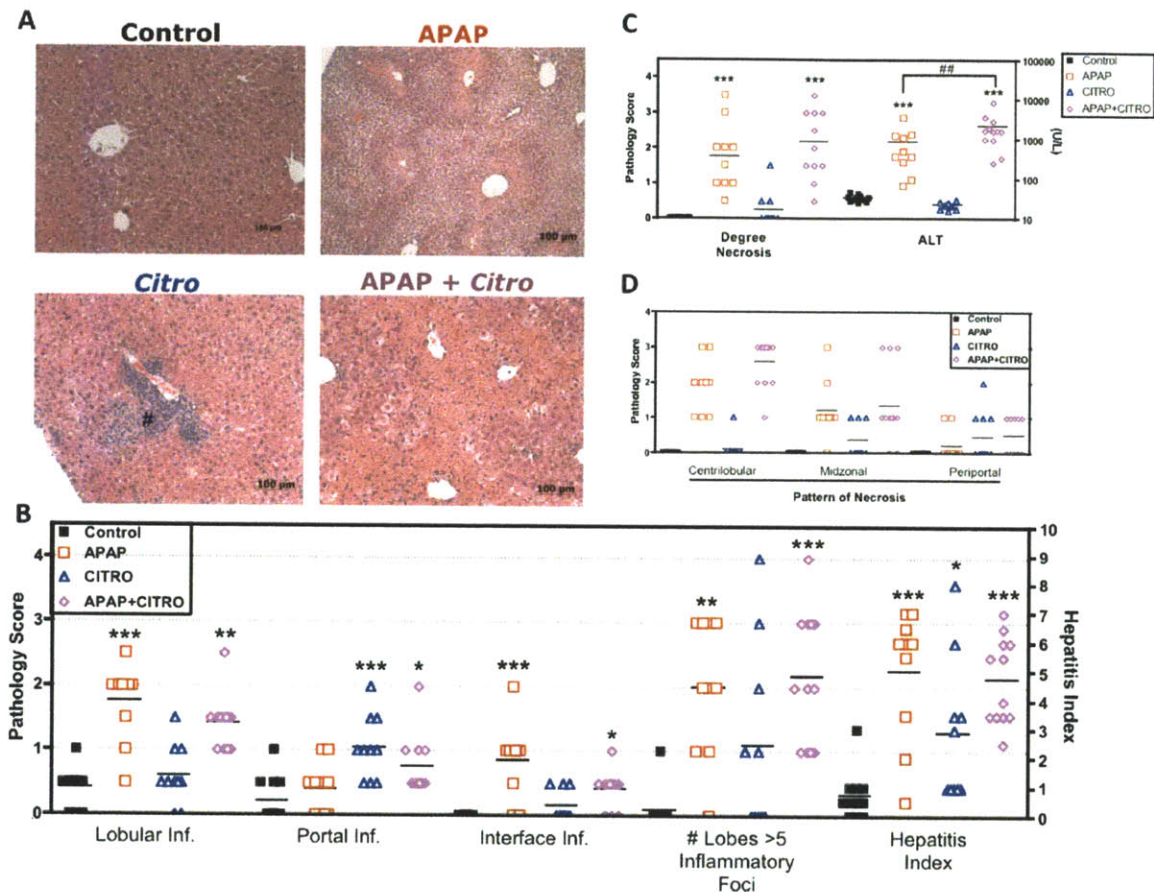


Figure 3-4. *C. rodentium* and APAP-induced liver H&E and inflammation at 7 DPI
(A) Representative H&E liver sections of controls, animals treated with APAP (200mg/kg, ip) treated animals demonstrating characteristic pattern of centrilobular necrosis, *Citro* alone, and APAP+*Citro* at 7 DPI. # indicates region of inflammatory foci **(B)** Pathological assessment of liver sections based on lobular inflammation, portal inflammation, interface inflammation, and the number of lobes with greater than 5 inflammatory foci. The total score for each categorical measure of inflammation was summed resulting in the hepatitis index. Animals with a hepatitis index greater than 4 are considered positive for hepatitis. **(C)** The degree of necrosis and matched serum ALT (U/L). Animals treated with *Citrobacter* alone did not demonstrate elevations in serum ALT, while APAP+*Citro* showed a statistically significant increase at 7 DPI **(D)** The pattern of necrosis was assessed as centrilobular, midzonal, or periportal in distribution. (Kruskal-Wallis with Dunn's post test compared to controls: for all pathological scores; One-way ANOVA with Tukey post tests for ALT (log transformed). * p<0.05, ** p<0.01, *** p<0.001; ## indicates p<0.01 compared to non-*Citro* counterpart). Symbols indicate individual animals and lines indicate group means (n = 10-12 for all treatment conditions).

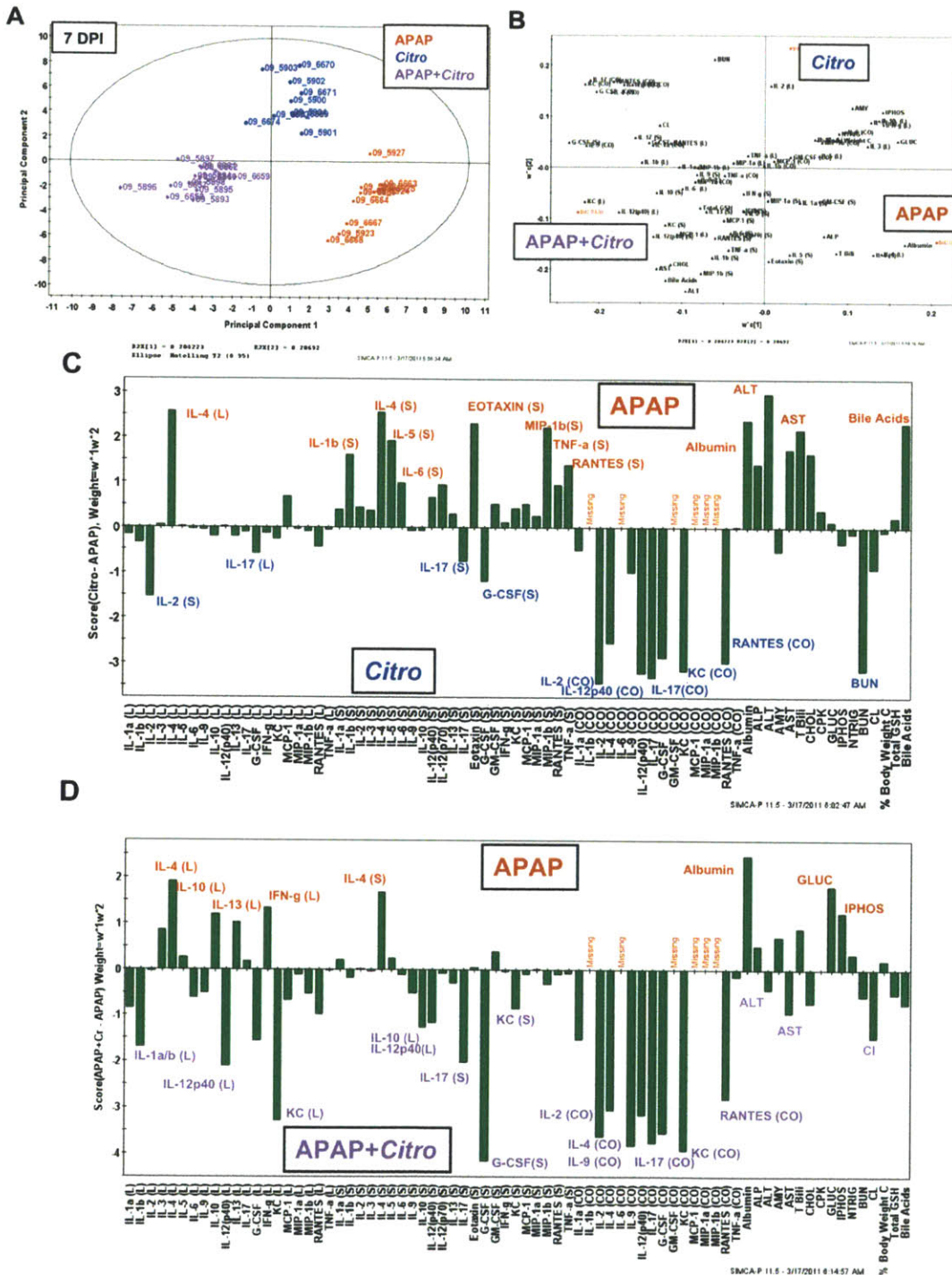


Figure 3-5. PLS-DA analysis at 7DPI

(A) PLS-DA analysis was used to determine optimal discrimination of animals based on the targets measured at 7 DPI. Individual mice are presented and colored based on treatment condition. (B) Scores plot for tissue and serum targets (C) Variable weights discriminating APAP vs *Citro* treated animals at 7DPI. Animals were highlighted and those features that best discriminate between APAP and *Citro* treatment are represented by green bars. (D) Differences between APAP and APAP+*Citro*. For 7 DPI, animals were pooled for analysis resulting in treatment groups of 10-12 animals.

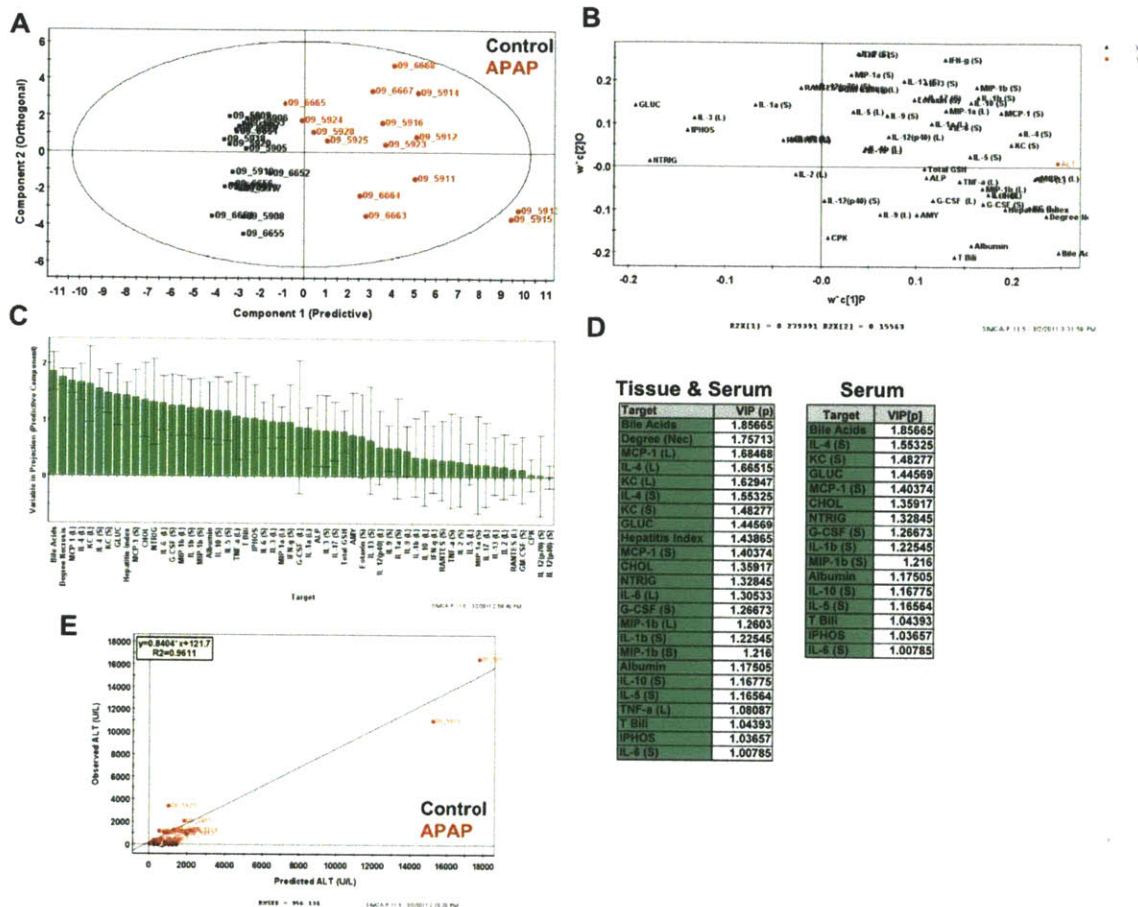


Figure 3-6. OPLS results for prediction of ALT levels for all APAP treated mice.

OPLS analysis of APAP (200mg/kg, ip) treated animals using serum/liver cytokines and chemistries (X) for prediction of ALT levels (Y) (A) Mice segregated well in the predictive component (Principle component 1) with an $R^2X(1) = 0.28$, indicating this component captured ~28% of the variance present in the X variables. (B) The predictive weight and covariation of serum and liver targets (black triangles) in relation to serum ALT (red square). (C) Variables in projection (VIPs) for the predictive component where values >1 are have positive influence in determining ALT levels, and $VIP < 1$ are less predictive. Serum targets were separated from the combined models for ease of viewing (D) Table representing the VIPs for the predictive component for serum ALT. (E) Observed vs predicted plot for ALT resulted in a $R^2 = 0.9611$ with only one predictive and one orthogonal rotation indicating a highly predictive model based on serum and liver targets.

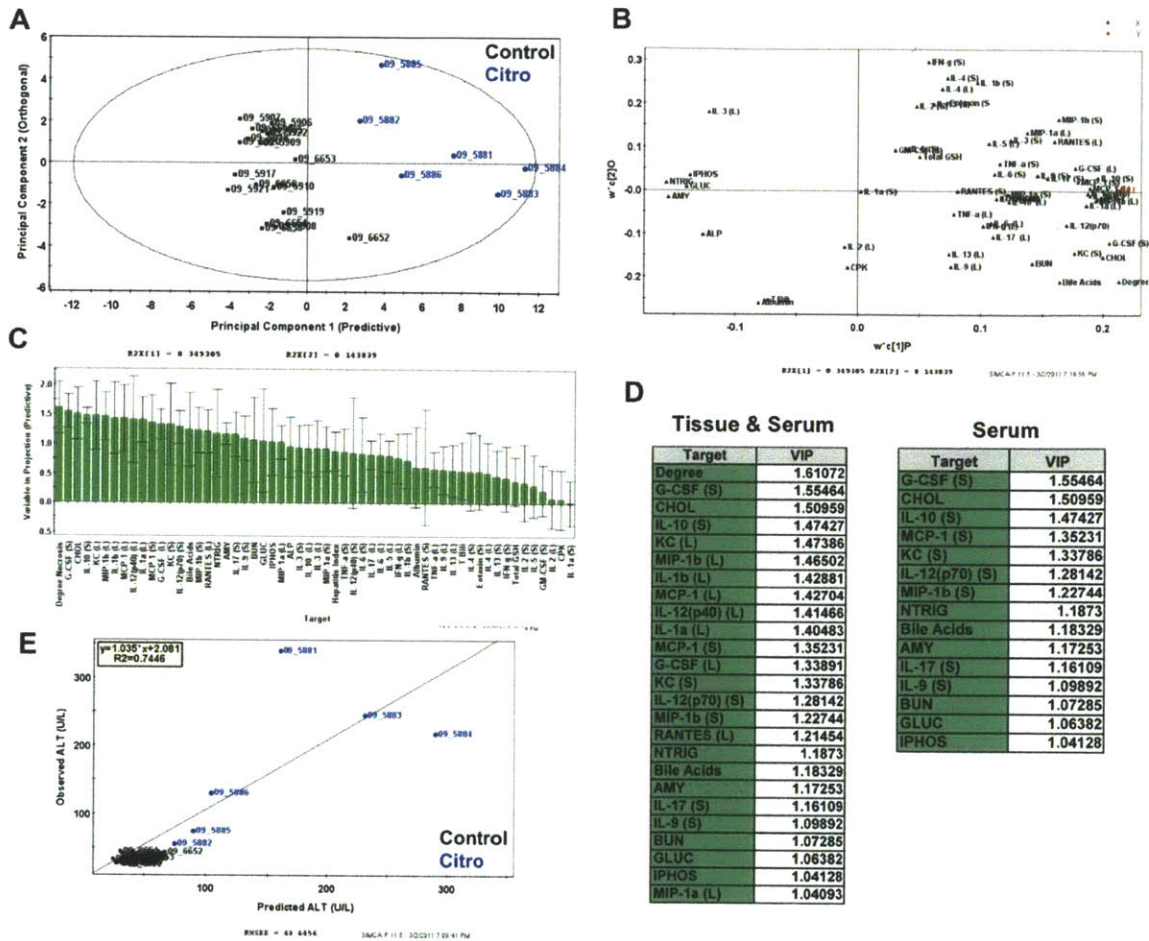


Figure 3-7. OPLS model for prediction of ALT levels for *Citro* (3 DPI) treated mice
 OPLS analysis of *Citro* (3 DPI) treated animals using serum/liver cytokines and chemistries (X) for prediction of ALT levels (Y) (A) Mice segregated well in the predictive component (Principle component 1) with an $R^2X(1) = 0.35$, indicating this component captured ~35% of the variance present in the X variables. (B) The predictive weight and covariation of serum and liver targets (black triangles) in relation to serum ALT (red square). (C) Variables in projection (VIPs) for the predictive component where values >1 are have positive influence in determining ALT levels, and $VIP < 1$ are less predictive. Serum targets were separated from the combined models for ease of viewing (D) Table representing the VIPs for the predictive component for serum ALT. (E) Observed vs predicted plot for ALT resulted in a $R^2 = 0.7446$ with only one predictive and one orthogonal rotation.

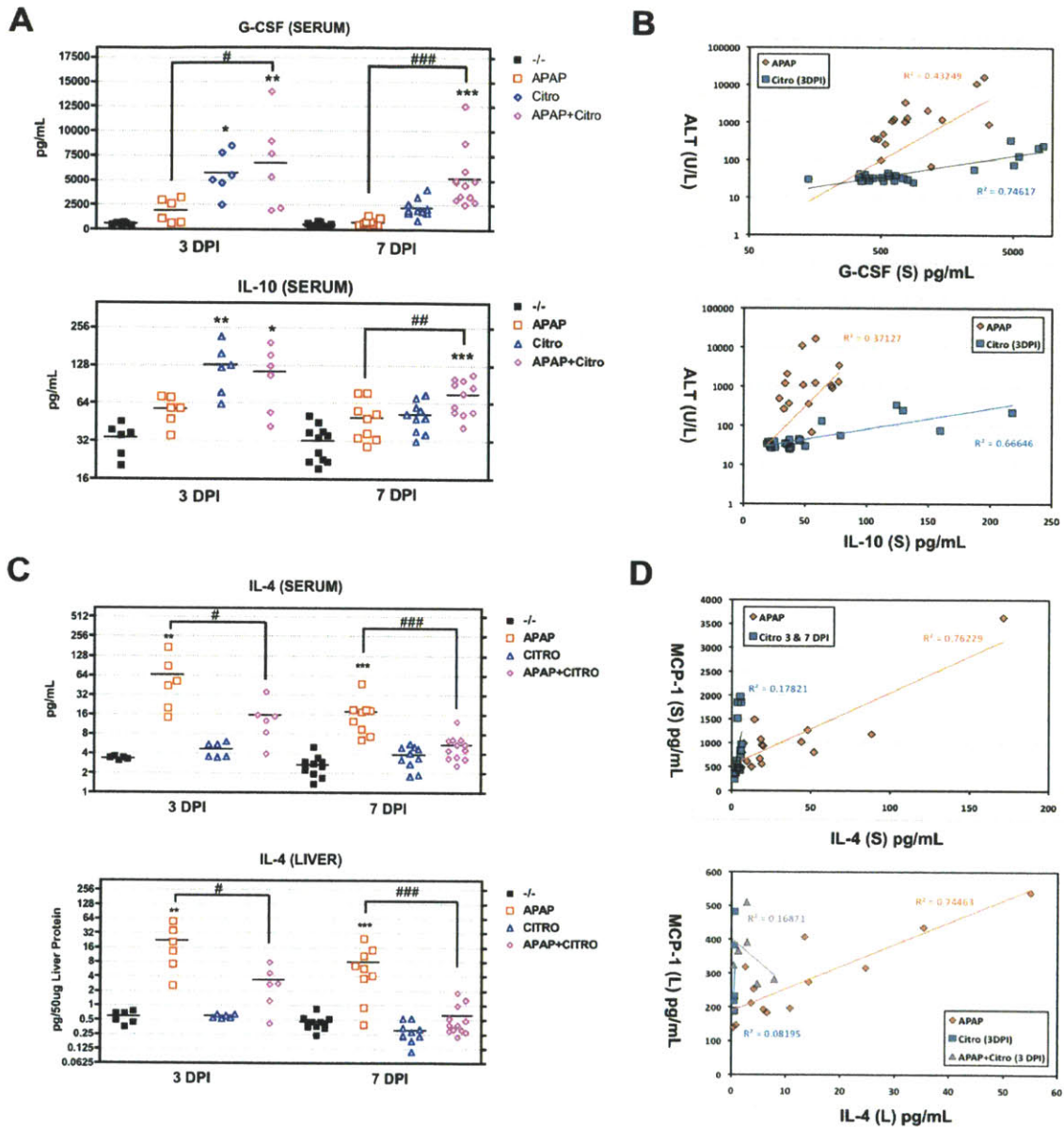


Figure 3-8. Cytokine changes at 3 and 7 DPI with high ALT correlation for Citro or APAP alone.

(A) Cytokine changes at for G-CSF (S) and IL-10 (S), two targets demonstrating higher VIP for *Citro*-induced necrosis at 3 DPI than APAP treatment alone. (B) G-CSF and IL-10 both demonstrate high correlation for ALT and associated with higher circulations at a given level of ALT (C) Serum and Liver IL-4 levels demonstrate down-regulation under conditions of *Citro* infection. (D) IL-4 is highly correlated with MCP-1 in both liver and serum; however, association is lost under conditions of *Citro* infection at both 3 and 7 DI.

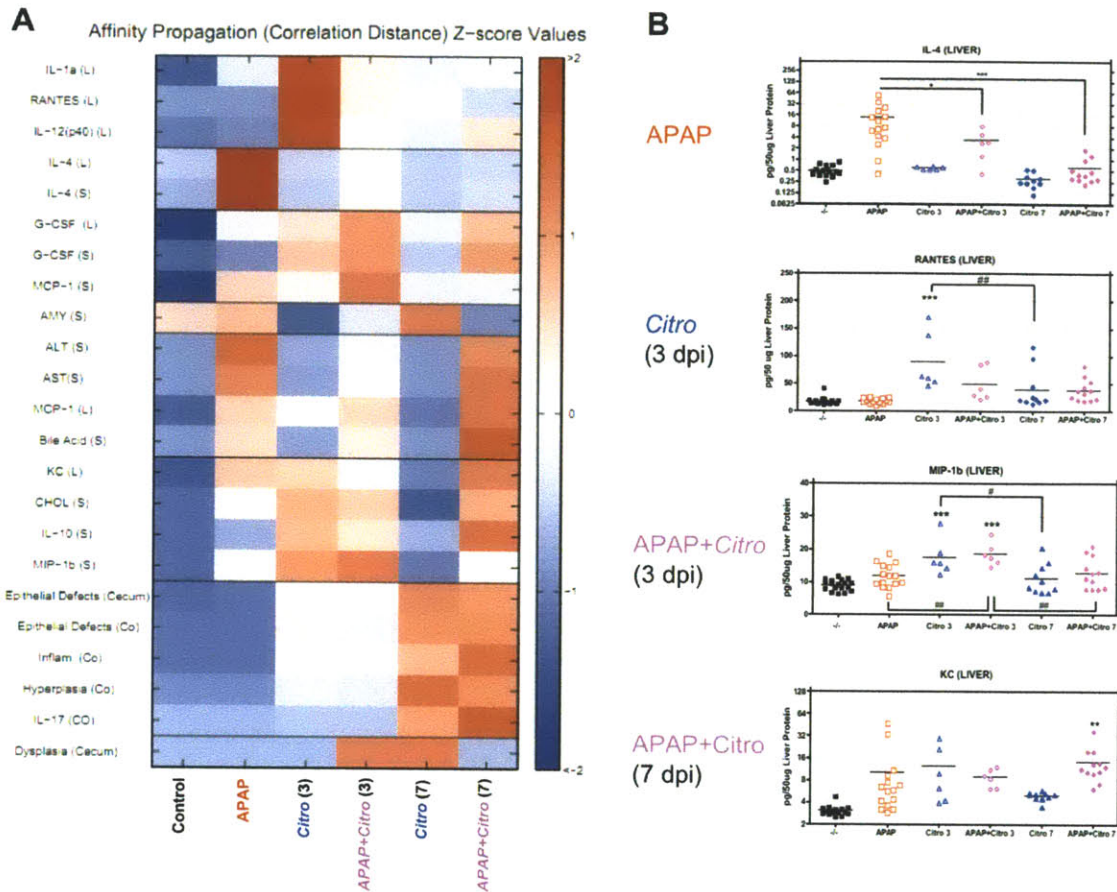


Figure 3-9. Correlations and Mutual information of targets for liver pathologies.
(A) Correlation and mutual information heatmap for targets able to discriminate across our 4 treatment/pathological classes with significance p-value of ≤ 0.001 . Dark red indicates high positive correlation with specific treatment condition, dark blue indicated negative correlation, and white indicates neutral **(B)** Individual animals plotted across 6 determined treatment classes. Significance determined by one-way ANOVA with Tukey's post test (* $p < 0.05$, ** $p < 0.01$, *** $p < 0.001$ compared to controls; # $p < 0.05$, ## $p < 0.01$ compared to non-*Citro* or timepoint counterpart). Lines indicate group means.

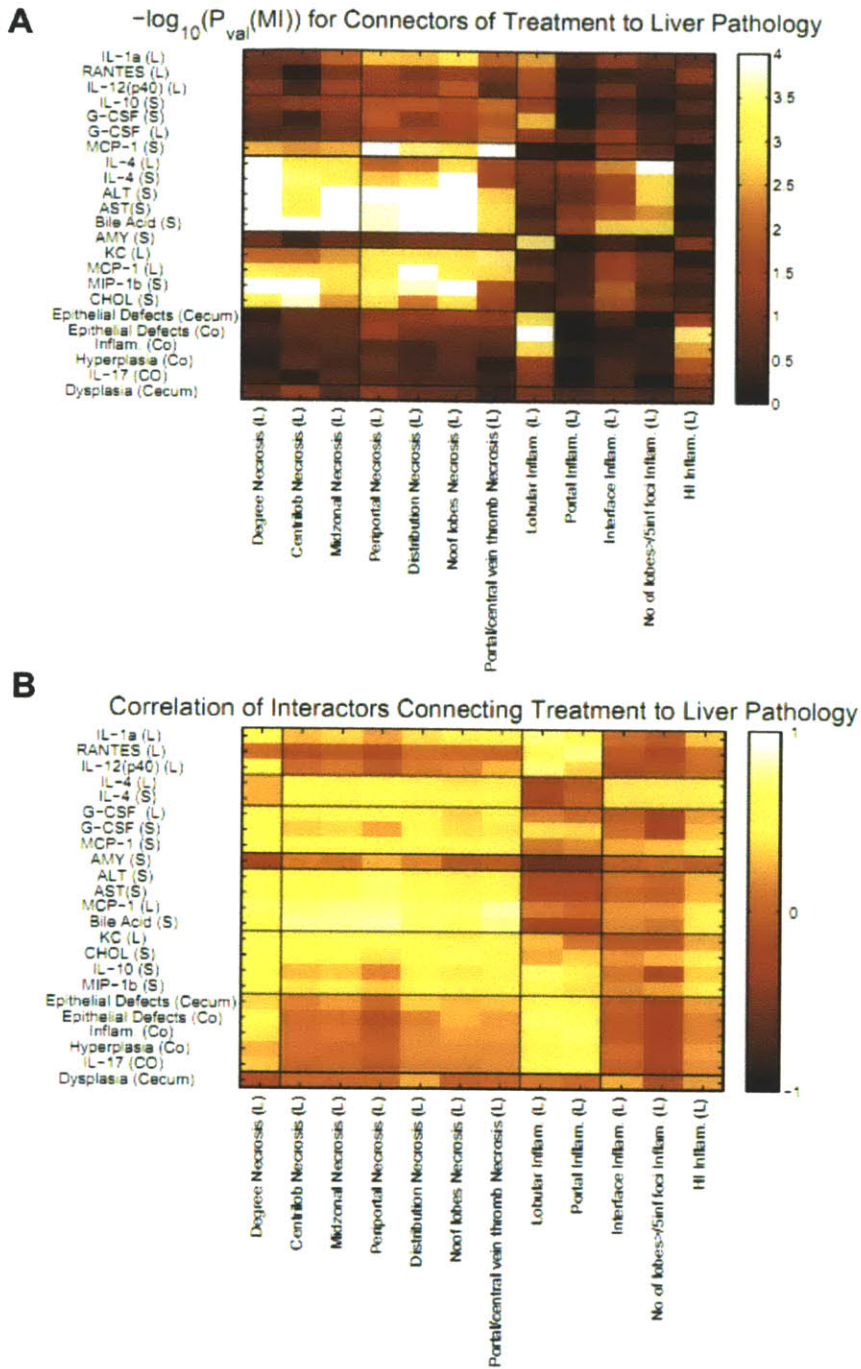


Figure 3-10. Mutual information and correlation maps for liver inflammation and necrosis.

(A) Targets able to discriminate between treatment classes were further analyzed to determine their mutual information for liver pathologies across multiple inflammatory and necrotic parameters. White = high mutual information, black = no mutual information (B) The same targets were analyzed for their respective correlation for liver inflammation and necrosis where white indicates strong positive correlation and black indicates strong negative correlation.

Table 3-1. Data compendium including animal numbers and measurements collected.

Animals were excluded from analysis for the following reasons:

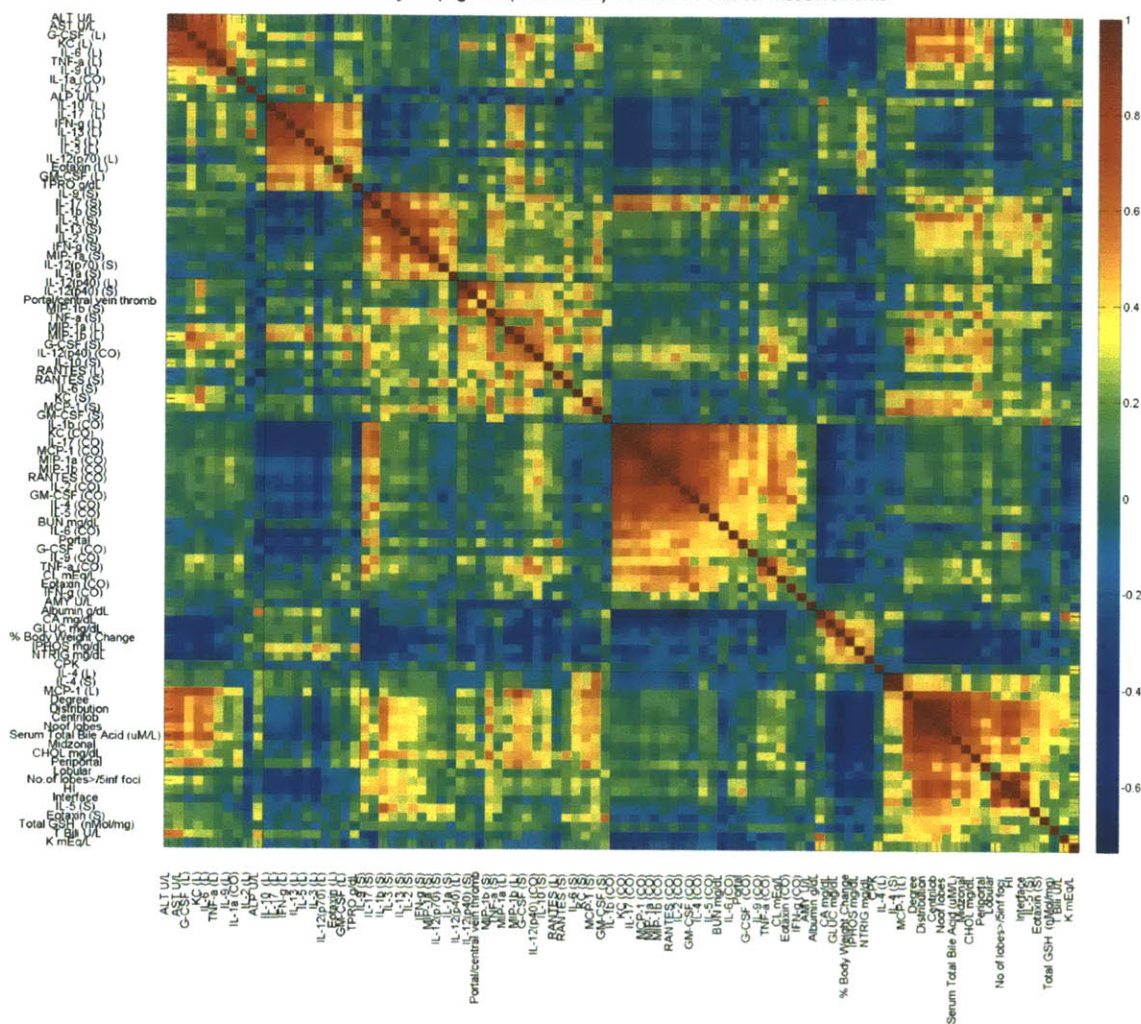
1 animals (*Citro* 7 DPI) was morbid and sacrificed prior to necropsy, while another had lost ~20% of its initial body weight and was excluded from analysis. For the purpose of classification using Mutual Information, 3 APAP-only animals were excluded as they demonstrated less than 2-fold induction of ALT or AST and failed to induce pathological scores in necrosis. Targets were removed from analysis if they were not detectable in at least 5 or more animals or if they failed all three of the following statistical tests: 1) 6-way ANOVA for variance across classification groups with Benjamini-Hochberg multiple hypothesis correction 2) 2-Tailed T-test (unequal variance) between Control and all treatments combined 3) Homogeneity of variance between control and treatments.

Treatment	3 DPI n =	7 DPI n =	7 DPI (r) n =	Measurements	Targets	Data Type
CONTROL	6	6	4	Serum Cytokines	22	Quantitative
				Liver Cytokines	20	Quantitative
APAP	6	4	5	Colon Cytokines	17	Quantitative
CITRO	6	6	4	Serum Chemistries	13	Quantitative
APAP+CITRO	6	6	6	Other Liver Markers (Bile Acids, GSH)	2	Quantitative
TOTAL ANIMALS	24	22	19	Liver Necrosis	7	Pathology Non-parametric
				Liver Inflammation	5	Pathology Non-Parametric
				Colon Inflammation	6	Pathology Non-Parametric
				Cecum Inflammation	6	Pathology Non-Parametric
				TOTAL TARGETS	76	

65 (animals) X 76 (targets) =

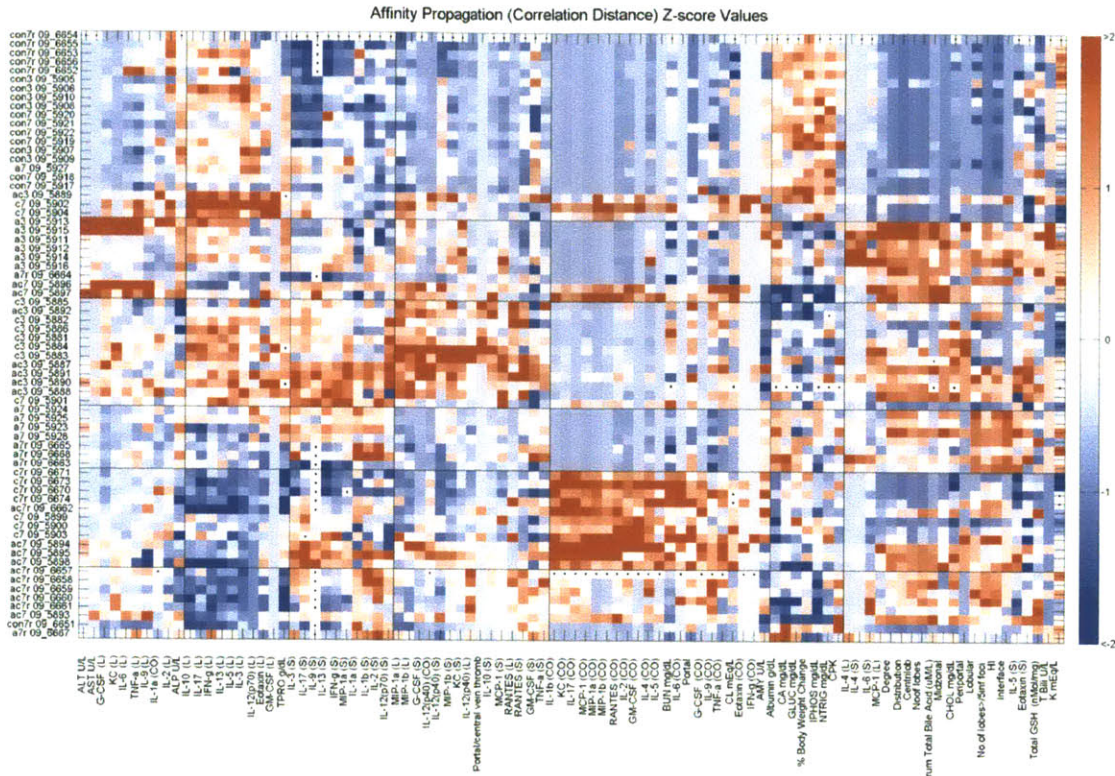
4,940 data points

Affinity Propagation (Correlation) Correlation Values: Measurements



Supplemental Figure 3-1. Affinity propagation clustering of all measurements

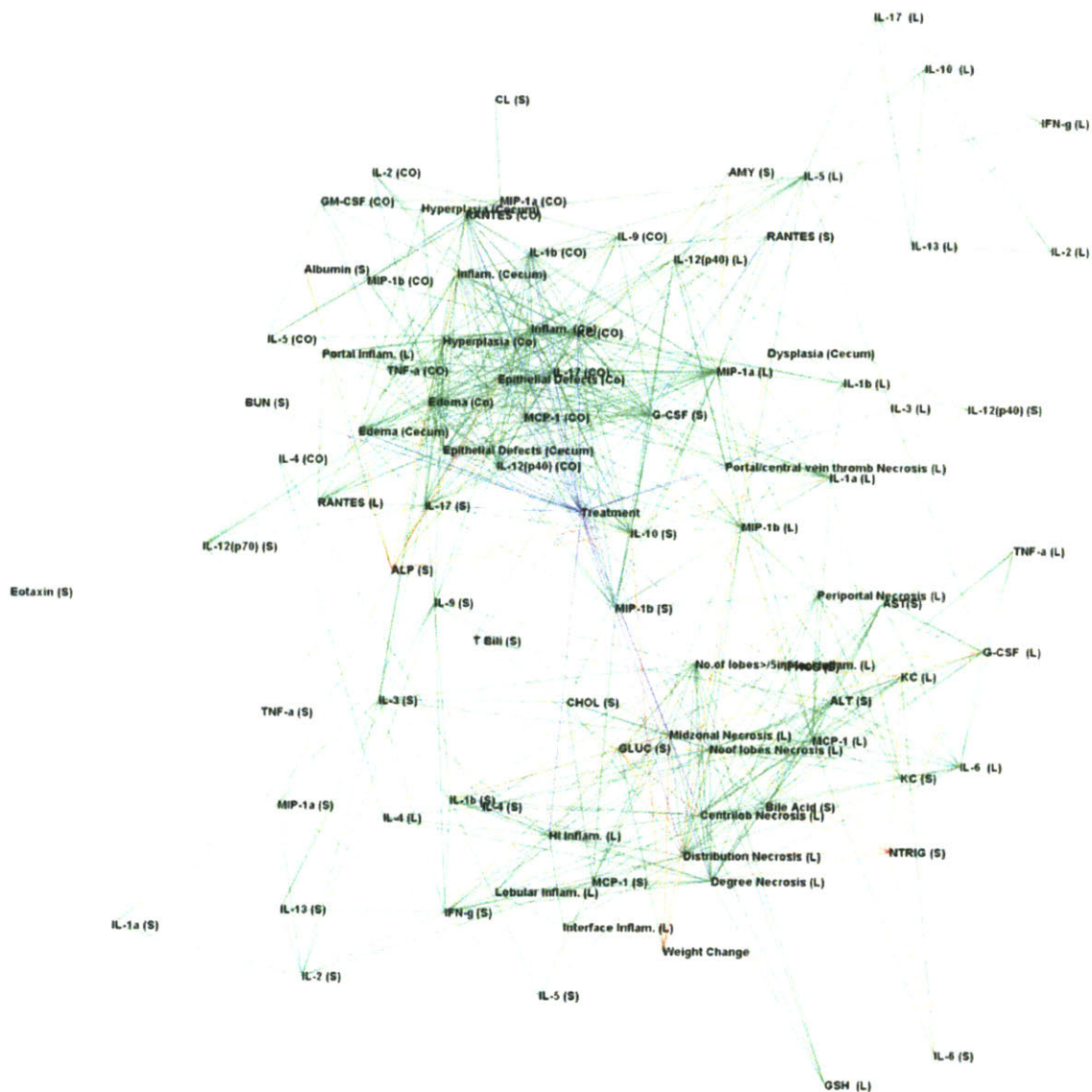
All targets measured were analyzed by affinity propagation clustering algorithm, a correlation based technique. High target correlation is indicated by dark red where 1 = perfect positive correlation. Dark blue indicates negative correlation where -1 equals perfect negative correlations between two targets. Clusters indicate target covariation with inferred association with pathologies such as colitis induction with *C. rodentium* infection (ie, cluster of colon specific targets in middle of figure indicate *Citro*-induced Th17 response with covariation of targets such IL-17 (CO), IL-6 (CO), IL-1β (CO), and neutrophils-related targets such as KC (CO) and G-CSF (CO).



Supplemental Figure 3-2. Animals and measurements clustered by affinity propagation using Z-score values.

All targets and animals were clustered by affinity propagation clustering algorithm using z-score (correlation distance). This allows viewing the weight of the measurement for that particular animal across all targets measured in relation to other animals. High correlation distance (**Red**) indicated a z-score of ≥ 2 indicating high expression compared to the rest of animal measurements. Negative z-scores (**Blue**) indicate expression levels below the average of all animal measurements. (Con = control, A = APAP, C = Citro, AC = APAP+Citro, r = repeat, and 3 and 7 DPI are indicated).

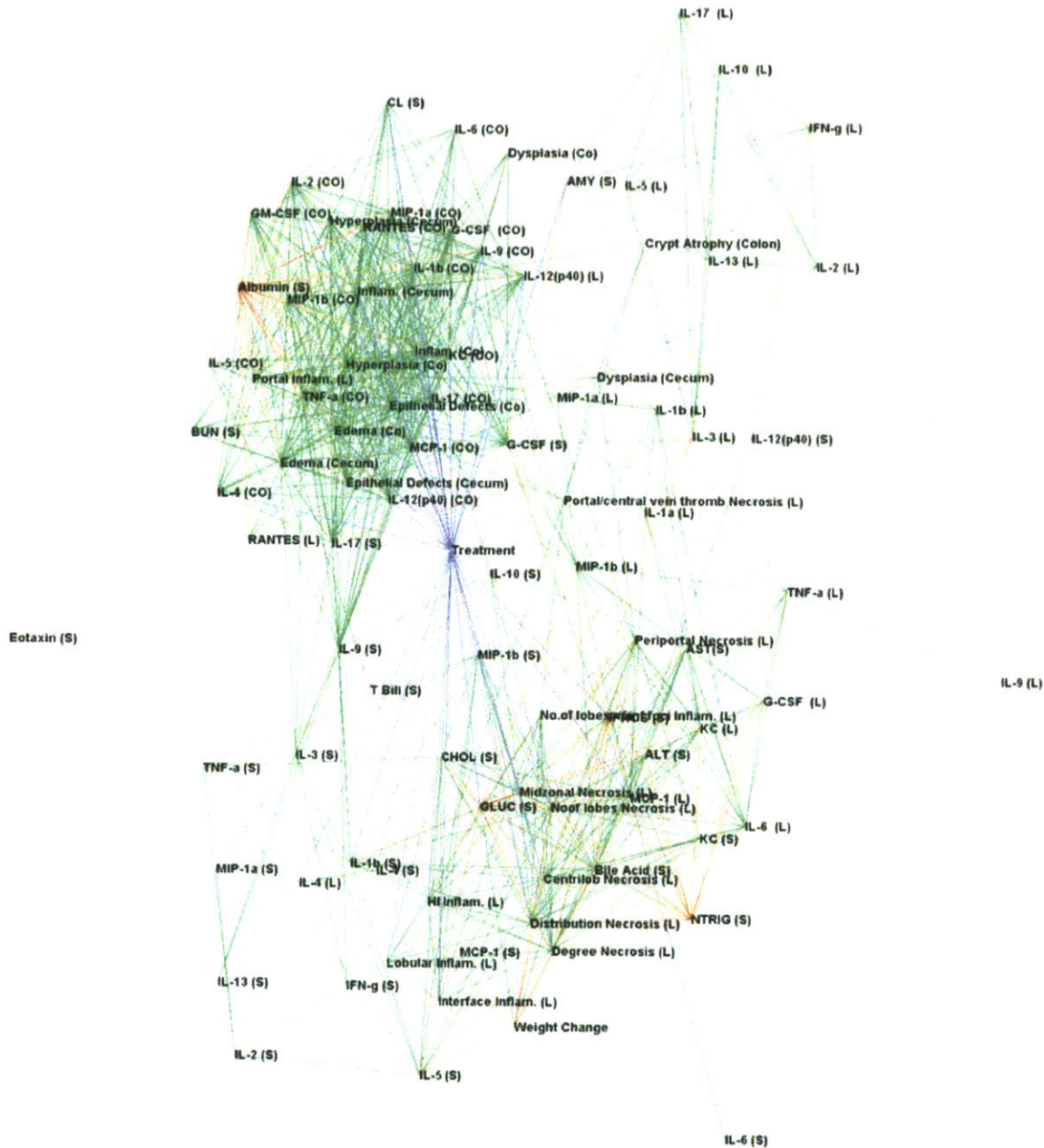
Kamada Plane: MI & Corr Network, DPI3 (MI Sig. ≥ 6)



Supplemental Figure 3-3. Mutual information and correlation network at 3 DPI.

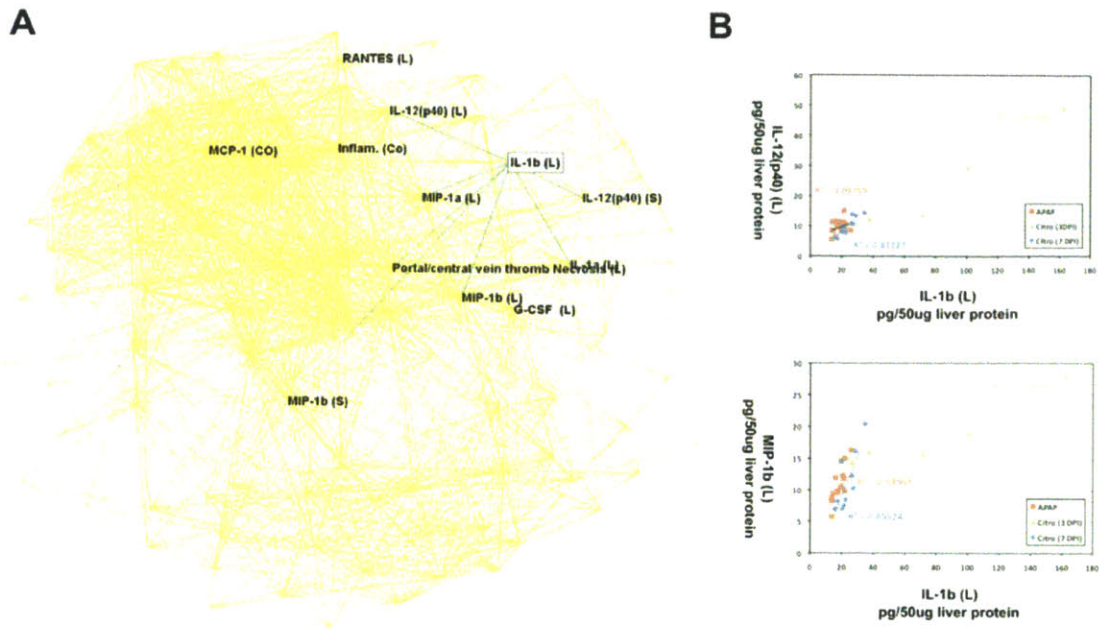
A target interaction network (3 DPI interactions) based on mutual information and ANOVA correlations is presented using the Kamada plane for optimal separation. We assumed 6 discrete classes of treatments/pathological states in generating target selection for this network. Green lines indicate significant positive correlation whereas red lines indicate significant negative correlation between targets, solid purple lines indicate significant ANOVA correlations for treatment class, and dotted purple lines indicate significant mutual information between targets.

Kamada Plane: MI & Corr Network, DPI7, noR (MI Sig. >=6)



Supplemental Figure 3-4. Mutual information and correlation network at 7 DPI.

A target interaction network (7 DPI interactions) based on mutual information and ANOVA correlations is presented using the Kamada plane for optimal separation. We assumed 6 discrete classes of treatments/pathological states in generating target selection for this network. Green lines indicate positive correlation whereas red lines indicate significant negative correlation between targets, solid purple lines indicate significant ANOVA correlations for all six treatment class, and dotted purple lines indicate significant mutual information between targets.



Supplemental Figure 3-5. Sub-network diagram highlighting interactions for liver IL-1β.

(A) In the sub-network, IL-1β (L) demonstrates significant positive correlation to the presence and number or portal vein thrombi, IL-1α (L), IL-12p40 (S, L), MIP-1α (L), MIP-1b (S, L), (ANOVA correlation, green lines), and has significant mutual information with G-CSF (L), MCP-1 (CO), RANTES (L) and colonic inflammation (dotted purple line) but does not significantly discriminate for treatment class. Mutual information does not capture the relationship (seen by ANOVA) between treatment class and IL-1β (L) and demonstrates the utility of using both techniques in evaluating complex data interactions and architecture. (B) Sub-network interactions graphed for correlation coefficient for IL-1β (L) vs IL-12p40 (L) (top) and IL-1β (L) vs MIP-1b (L) for APAP treatment alone, *Citro* 3DPI and *Citro* 7DPI as examples. *Citro* at 3 DPI had the highest correlation at a timepoint/condition where portal vein thrombi were most prevalent and associated with coagulative periportal necrosis.

Chapter 4: Effect of Systemic Inflammation from gastrointestinal infection with *Citrobacter rodentium* on oral drug exposure

Arek Raczynski¹, Tonika Bohnert², Melissa Mobley³, Amanda Potter³, James G. Fox³, Lawrence Gan², Steven Tannenbaum¹, David Schauer^{1,3}

¹Department of Biological Engineering, Massachusetts Institute of Technology, Cambridge, MA, USA ²Biogen Idec Inc, Cambridge, MA, USA ³Division of Comparative Medicine, Massachusetts Institute of Technology, Cambridge, MA, USA

An abridged version of this chapter is to be submitted to *Drug Metabolism and Disposition*

4.1 Introduction

Drug induced liver injury (DILI) is the leading cause of acute liver failure (ALF) in the United States, characterized by low incidence, mechanisms independent of therapeutic target, and is poorly predicted for in currently available animal models. From a pharmaceutical and clinical perspective, DILI is a major concern as it can result in last stage discontinuation of drug development, limit use and distribution of effective therapeutics, or even lead to marketplace withdrawal [31]. Inflammation is one host susceptibility factor contributing to idiosyncratic liver injury [36], as evidenced by numerous knockout studies and endotoxin-induced inflammation (LPS), demonstrating predisposition to injury under immune dysregulation and inflammatory stress [6, 34].

One contributing factor for DILI may be alterations in drug pharmacokinetics (PK) and metabolite profile under inflammatory conditions. Alterations in drug clearance and exposure levels have recently been attributed to LPS [147] and inflammatory disease states such as arthritis. Indeed, a rat animal model of adjuvant arthritis (AA) is currently used in the industrial setting as a proxy for human drug clearance alterations in the rheumatoid arthritis (RA) disease setting [148]. Inflammation and GI infection with *Citrobacter rodentium*, a murine-specific enteric pathogen analogous to *Escherichia coli* (*E. coli*) infection in humans, has been shown to alter the expression of numerous phase I/II metabolic enzymes, necessary for biotransformation and clearance of xenobiotics [7, 8]. The effect of *C. rodentium* on altering cytochrome p450s (CYPs) specifically has been shown to be independent of TLR4 engagement, with *C. rodentium*'s profile of hepatic mRNA CYP450 regulation distinct from those found with the LPS model [8, 77], with cytokine dependent changes associated with both IL-6 and IFN- γ knockout (KO) animals in this infection model [149].

Functional studies, however, have not been conducted demonstrating altered PK and metabolic drug profile under the disease setting of gastrointestinal infection. *C. rodentium* infection in mice provides a reproducible, robust, and physiologically relevant model of inflammation [74] amenable to investigating potential xenobiotic biotransformation and PK differences under human disease settings such as inflammatory bowel disease (IBD), infectious colitis, and pathogenic gastrointestinal infections. Here we evaluated the effect of non-toxic doses of drugs varying in degree of biotransformation and mode of elimination using *C. rodentium* as a source of systemic inflammation. We evaluated propranolol (Inderal®) (high clearance substrate), digoxin (P-glycoprotein (Pgp) substrate), fexofenadine (Allegra®) (organic-anion transporting polypeptide (OATP) substrate, minimal metabolism), acetaminophen (2E1 substrate, Tylenol®), which demonstrates moderate cytochrome p450 mediated clearance, verapamil (3A4 and Pgp substrate) by oral delivery (PO) delivery at 7 days post infection (DPI).

4.2 Results

Acetaminophen and fexofenadine exposure is unchanged by infection with *C. rodentium*

Acetaminophen (APAP) is a commonly used antipyretic and analgesic that demonstrates relatively low clearance in human and mice. Under normal liver conditions, ~90% of APAP is metabolized to non-toxic conjugated metabolites APAP-glucuronide and APAP-sulfate with ~10% metabolized by cytochrome P450 oxidation (CYP 2E1, 3A4, and to a lesser extent 1A2) to form N-acetyl-p-benzoquinoneimine (NAPQI), a highly reactive intermediate [39]. Detoxification of NAPQI normally proceeds by conjugation with intracellular glutathione, either spontaneously or catalyzed by glutathione-s-transferase (GST), the majority of which is excreted into bile via multidrug resistance-associated protein (Mrp2) [40]. APAP was delivered PO at 5mg/kg in the presence and absence of *C. rodentium* infection at 7DPI and plasma processed by LC/MS/MS for detection of parent drug levels (**Figure 4-1**). Both control and *C. rodentium* infected animals demonstrated similar T_{max}, C_{max}, and area under the curve (AUC) (**Table 4-1**), indicating no difference in oral exposure of APAP under conditions of enteric bacterial infection. This is in line with findings by Richardson et al, where mRNA levels of 2E1 in mouse kidney and liver were unchanged with *C. rodentium* infection at both 7 and 10 DPI [8], furthermore, neither IL-6 or IFN- γ deficiency alters CYP2E1 expression under *C. rodentium* infection at 7 DPI [149]. In **Chapter 3** we evaluated the role of enteric infection on APAP hepatotoxicity, and while infection at 7 DPI increased circulating levels of ALT, this is unlikely due to changes in systemic exposure.

We also tested fexofenadine, which demonstrates minimal metabolism and moderate clearance (~40-50% Qh). Fexofenadine is primarily excreted as parent compound by renal clearance in humans, but biliary elimination contributes significantly in mouse. Although fexofenadine has been identified as a Pgp substrate *in vitro* using CACO-2 cells [150], MDR1 polymorphism in fexofenadine disposition is not clearly established [151]. In mice, for example, *mdr1a/1b* KO does not alter biliary clearance but results in 6-fold higher plasma exposure and 3-fold higher brain exposure [152]. Fexofenadine is also an OATP1B1/1B3/2B1 substrate, and OATP1B1 polymorphism affects clearance and AUC, where OATP1B3 is thought to be the main uptake transporter[153]. PO delivery of fexofenadine under conditions of *C. rodentium*-induced inflammatory stress resulted in a shorter T_{max} as compared to uninfected animals (0.08 vs 0.5 hrs respectively) and a higher cMAX (120 vs 45 ng/mL); however, AUC was comparable between infected and non-infected groups (139 vs 132 hr*ng/mL respectively) (**Figure 4-2** and **Table 4-1**).

Increased oral exposure for propranolol and digoxin

Propranolol demonstrates high clearance in human and mouse (>75% Qh). The major drug metabolizing enzymes include 2D6 (4-hydroxypropranolol), 1A2 (N-desisopropyl), and UGT; however, polymorphism has not been shown to have an

effect on propranolol pharmacokinetics. We evaluated propranolol at 10mg/kg and observed an approximate 1.6 and 1.65-fold increase in C_{max} and AUC respectively (**Figure 4-3 B and C**) under infection conditions. Our initial evaluation of propranolol at 5mg/kg resulted in a 2.25-fold increase in AUC; however, due to variability in a few timepoints we repeated at 10mg/kg with comparable results.

Digoxin (Lanoxin®) is a commonly used drug for congestive heart failure, and follows first order kinetics with approximately 50-70% of the dose excreted unchanged in urine, while 25-28% is found in feces via biliary excretion. A small fraction of the drug is metabolized (~16%) resulting in metabolites 3-beta-digoxigenin, 3-keto-digoxigenin and their glucuronide and sulfate conjugates, none of which demonstrate biological activity [154]. It is also a known Pgp substrate[155], and MDR1 polymorphism has been linked to altered oral availability[156, 157]. Under conditions of *C. rodentium* infection, digoxin dosed at 1mg/kg demonstrated moderate increases in exposure with 1.24 and 1.36-fold increases in C_{max} and AUC respectively. While the changes are moderate, they indicate a significant difference between control and inflammatory conditions.

Increased oral exposure of verapamil and its metabolites

Verapamil, a 3A4 substrate, was evaluated as previous work demonstrated 3A11 (homologue of human 3A4) was decreased in hepatic mRNA expression (16% of normal levels) in mice at 7 DPI with *C. rodentium* [8, 77]. 3A4 is the most abundant P450 isoform, partially due to the enzymes broad substrate specificity [158], and is associated with biotransformation of approximately half of therapeutics drugs used by humans today [159]. Infection with *C. rodentium* resulted in approximately a 2-fold increase in oral availability of verapamil compared to vehicle controls (AUC = 657 vs 353) with a delayed T_{max} (**Figure 4-4**). The changes found with verapamil were the greatest of the compounds tested herein. In order to determine if the increased levels of parent drug in plasma were the effect of altered biotransformation (altered levels of 3A4) or other mechanisms, we decided to monitor changes in verapamil metabolites over the timepoints measured (**Figure 4-5**). Since authentic metabolites standards were not available, metabolites were quantified based on Metabolite Area/IS Area response in LC/MS/MS and numbers reflect AUC of these relative ratios (**Figure 4-6A**). All metabolites (except D-617) showed approximately 2-fold higher plasma levels under *C. rodentium* infection, with a paralleled increase to parent drug, arguing against decreased biotransformation by cytochrome P450s as the cause of increased parent levels (**Figure 4-6B**). Individual PK exposure curves for the measured metabolites with and without infection are presented in **Figure 4-7** where norverapamil, the major metabolite and known byproduct of verapamil oxidation by 3A4 (3A11 in mice) was found to be increased by ~2.44-fold (AUC = 12.15 vs 4.98, *C. rodentium* vs control respectively); comparable to changes in parent drug levels.

We conducted a similar analysis for propranolol metabolites and determined a comparable fold-change for its metabolites when compared to parent propranolol (**Table 4-2**). 1'-hydroxypropranolol (+1.7-fold), 2'-hydroxypropranolol (+2.3-fold),

3'-hydroxypropranolol (+2.2-fold) demonstrated approximately 2-fold higher AUC in infected animals as compared to uninfected controls, while desisopropylpropranolol demonstrated only a 140% increase. In humans, desisopropylpropranolol is generated by CYP-mediated N-dealkylation of propranolol by CYP1A2 and is the major metabolite, whereas hydroxylation byproducts are believed generated via oxidation by CYP2D6 [160]. As expected, parent propranolol demonstrated the highest C_{max} as compared to its metabolites in plasma. Collectively, the results indicate that biotransformation by CYPs does not appear responsible for altering plasma levels of parent verapamil and propranolol under conditions of gastrointestinal infection with *C. rodentium*.

4.3 Discussion

Citrobacter rodentium infection in mice provides a reproducible, robust, and physiologically relevant model of inflammation [74] and has been used as an animal model of IBD [93], infectious colitis, and acute diarrheal illness [161]. Infection with *C. rodentium* has also been proposed as a potential model of acute inflammatory stress that alters liver homeostasis, potentially through an altered systemic and local cytokine environment resulting from gastrointestinal infection [7, 8, 77, 149] (**Chapter 2 & 3**). Transcriptional changes in both hepatic and renal phase I and phase II metabolic enzymes demonstrate an altered metabolic state, with the potential to alter exposure and clearance of both endogenous (ie lipids) and exogenous (drugs) substrates from circulation or lead to local accumulation. Metabolic changes associated with *C. rodentium*, furthermore, appear distinct from those associated with LPS treatment alone. More recently, the role of IL-6 and IFN- γ , two commonly associated systemic cytokine targets associated with *C. rodentium* infection were investigated [149]; demonstrating cytokine-specific alterations hepatic CYP450 expression. Using five commonly used pharmaceuticals varying in their degree of metabolism and mode of elimination, we investigated the functional consequence of previously reported transcriptional changes in CYPs associated with *C. rodentium* infection on oral drug exposure.

Increased plasma exposure and gut barrier compromise

Based on our examination we determined a ~2-fold difference in exposure for verapamil, 1.65-fold for propranolol (2.2-fold in initial 5 mg/kg study), and a 1.4-fold higher exposure for digoxin under conditions of *C. rodentium* induced inflammatory stress (Summarized **Table 4-1**). Measuring major metabolites for verapamil and propranolol, we found a similar ~2-fold elevations in plasma of most metabolites measured (except D-617), indicating higher levels of both parent drugs and their respective metabolites, arguing that biotransformation by CYPs was less likely in driving elevations in parent drug exposure after PO drug delivery. If CYPs were the primary contributor in determining increased parent drug exposure levels, we would expect down-regulation of hepatic 3A11 (mouse analogue of human 3A4) to result in decreased levels of metabolites compared to parent drug levels in diseased animals. An alternative hypothesis that we propose is that exposure differences are attributable to increased oral availability due to a leaky GI tract, allowing for increased permeability of certain xenobiotics under conditions of enteric infection with *C. rodentium*. Leaky gut barrier function has been implicated as responsible for translocation of *C. rodentium* to MLNs during infection course [98], and *C. rodentium* has been associated with disruption of tight junctions and barrier function in intestinal epithelial cells *in vitro* and *in vivo* [99, 100]. Clinically, altered epithelial permeability and tight junctions have been associated with IBD [162], and *C. rodentium* infection in mice is an animal model for such disease conditions.

Another potential mechanism could include down-regulation of Pgp in the intestinal tract. Strong evidence exists that Pgp plays a key role in host-bacterial interactions in the gastrointestinal tract contributing to maintenance of intestinal homeostasis [163, 164]. Indeed, *mdr1a*^{-/-} (gene encoding Pgp) mice develop spontaneous colitis [165], and more recently, these animals were characterized as having increased colonic expression of IFN- γ and KC [166]. Furthermore, it is well established that intestinal Pgp located at the apical membrane of enterocytes pumps xenobiotics back into the gut lumen [167], as a mechanism of reducing oral absorption of well established Pgp substrates such as cyclosporine and digoxin [155, 168, 169]. Thus, increased exposure observed with digoxin under *C. rodentium* infection could be attributable to decreased transporter expression of Pgp, as digoxin is not appreciably metabolized by CYPs. Recently, verapamil has also been proposed as a Pgp substrate in rodents [170] and similarly shows increased oral exposure under *C. rodentium* infection. A potential argument against this mechanism may be that we did not see alterations in fexofenadine, however, as mentioned above its role as a Pgp substrate is not clearly established outside of *in vitro* studies. Measuring changes in Pgp protein expression in small intestine and colon seems warranted towards investigating its functional role or contribution in mediating bioavailability of drugs in this model.

APAP and fexofenadine do not demonstrate altered exposure

We did not see changes in exposure of either fexofenadine or acetaminophen. While many of the CYP isoforms examined under *C. rodentium* infection demonstrate some dependence on with IL-6 or IFN- γ , CYP2E1, the primary CYP involved in APAP bioactivation was unchanged in WT and IL-6 and IFN- γ KOs [149]. This indicates that CYP2E1 has a mechanism of transcriptional control unique to that of other CYPs demonstrating alterations under conditions of *C. rodentium* infection. APAP has shown increased AUC, prolonged plasma half-life, and delayed clearance in other diseases associated with chronic inflammation such as cirrhosis, correlating strongly with altered haemodynamic function (systolic and arterial pressures highly associated with AUC) [171, 172]. Furthermore, in a viral hepatitis model, protection from APAP-induced toxicity was attributed to decreased bioactivation of APAP \rightarrow NAPQI as mRNA levels of CYP2E1 and CYP1A2 were decreased 3 days post viral infection [136]. Interestingly, under an acute inflammatory state, characterized with hepatic inflammation (hepatitis-like state, pathological findings **Chapter 2 & 3**) with *C. rodentium*, however, we do not observe changes in systemic exposure after oral delivery for APAP at 7 DPI. This argues that the type of pathogen and resultant cytokine/chemokine response may be vital in determining functional consequences of drug exposure and metabolism for certain substrates.

As mentioned above, pathogenic enteric infection showed increases (~2-fold) of both parent and metabolites of verapamil and propranolol, with slightly less robust changes with digoxin (only parent drug investigated) as quantified by LC/MS/MS in mouse plasma. The changes in exposure, albeit moderate, indicate conditions of GI infection can increase oral bioavailability of certain clinically used therapeutics. While for most therapeutics this is unlikely to be of major clinical impact, there may

be certain instances, like digoxin, for example, where the therapeutic and safety windows may be more sensitive to even modest changes in exposure. While CYP mRNA levels have shown down-regulation under *C. rodentium* infection, CYP activity was not addressed in these studies, furthermore, the contribution of other clearance mechanisms in drug availability such as transporter expression was also not investigated. Cytokines are known to affect the expression of numerous CYPs and transporters, and based in the findings in **Chapter 2** and **Chapter 3**, *C. rodentium* induces a variety of inflammatory mediators at the local and systemic levels that could impact the transcriptional control of CYPs, transporters, as well as other metabolic enzymes required for metabolic homeostasis, particularly for endogenous substrates and xenobiotics. In this regard, a more comprehensive examination of these metabolic regulators in multiple tissues under conditions of *C. rodentium*-induced inflammation would be helpful in fully explaining the findings presented herein.

Future work and conclusions

It has been proposed that changes in phase I/II metabolic enzymes may result in altered exposure and clearance of pharmaceutical and endogenous substrates under inflammatory conditions such as GI infection. Here, using *C. rodentium* infection in C56Bl/6 mice, we demonstrate that changes in oral drug bioavailability, functionally, do not appear dependent on CYP-mediated biotransformation of parent compounds. Rather, observed changes in oral exposure for verapamil, propranolol, and digoxin appear to be driven more by proposed gut barrier compromise. This was illustrated by verapamil, and propranolol, which demonstrated ~2-fold increased exposure under conditions of *C. rodentium* infection, with mirrored changes in numerous metabolites monitored under both infected and uninfected conditions. Interestingly, changes in oral drug availability were only observed in a subset of drugs investigated, as APAP and fexofenadine demonstrated similar oral exposure under normal and disease conditions. Furthermore, examining the expression of both uptake and efflux transporters in the small intestines and liver under conditions of pathogenic enteric infection with *C. rodentium* seems warranted. Specifically, determining the role of Pgp in mediating altered oral bioavailability seen with *C. rodentium* compared to the proposed role of leaky GI. Greater understating of the role of GI infection (and resultant systemic and local inflammation) on drug and endogenous substrate clearance and homeostasis could have implications for patients with disease states such as IBD and pathogenic gastrointestinal infection. Furthermore, could help in the treatment management for patients with similar diseases characterized by either acute or chronic inflammation.

4.4 Selected methods

Media and Bacterial Strains

Luria-Bertani (LB) agar and broth (Difco Laboratories, Detroit, MI) was used for routine cultivation of bacteria. MacConkey lactose agar (Difco Laboratories) supplemented with 40 µg/ml of kanamycin was used for quantitative monitoring of bacterial counts in fecal samples. The kanamycin-resistant strain of *C. rodentium* strain, DBS120 (pCRP1::Tn5, Kan^r) [145] was used for all infections.

Animal Housing and Bacterial Infections

Female 8-10 week old C57BL/6J (The Jackson Laboratory, Bar Harbor, ME) mice were housed six per microisolator cage in a specific pathogen-free facility approved by the Association for Assessment and Accreditation of Laboratory Animal Care. Depending on the particular study, anywhere from 36-42 animals were used in evaluating a particular compound. Animals were maintained on pelleted rodent chow (LabDiet, Purina Mills, Inc., Richmond, IN) and water ad libitum and allowed to acclimate one week prior to experimentation. Infectious colitis was induced by intragastric inoculation with $\sim 1 \times 10^9$ CFU of DBS120 in 3% sodium bicarbonate (w/v in 1X phosphate buffered saline (PBS), pH 7.4), 100µL volume as described previously [145], while the uninoculated control groups received 100µL of 3% sodium bicarbonate vehicle. Infection kinetics was monitored by fecal shedding determined by plating serial 10 dilutions of fecal slurries (10% [w/v] in 1X PBS, pH 7.4) on LB agar with selection for kanamycin. The Massachusetts Institute of Technology Committee on Animal Care approved all animal experiments prior to investigation.

Drug Resuspension and Administration

Acetaminophen (5mg/kg in sterile ddH₂O), fexofenadine (5mg/kg in sterile ddH₂O), digoxin (1mg/kg in ddH₂O with 5% w/v cyclodextrin, pH 7.4), propranolol (5 mg and 10 mg/kg in sterile ddH₂O), verapamil (5mg/kg in sterile ddH₂O) were all made fresh the morning of oral delivery (PO). Compounds were dosed at 10mL/kg using a blunt 22g oral gavage needle. Terminal cardiac bleeds were conducted after euthanasia by CO₂ asphyxiation at 5 min, 0.5, 1, 2, 4, 8, 16, or 24 hrs post delivery of drug using 3 animals per time point (timepoints varied slightly for each drug investigated). Plasma samples were collected (8000 rpm @ 10 minutes, 4C) and levels of parent drug and specified metabolites monitored by LC/MS/MS at Biogen Idec laboratories (Cambridge, MA). Total animals used for each compound under investigation varied between 36 and 42, depending on the number of timepoints evaluated (6-8) for pharmacokinetic analysis.

LC/MS/MS Methodology

Twenty-five to thirty microliters (µL) of plasma samples were precipitated with 100µL 1:1 acetonitrile/methanol and 10µL of 8-cyclopentyl-1,3-dipropylxanthine (CPDPX, internal standard @ 50 ng/mL). After centrifugation, the entire

supernatant was removed 200-300uL 0.1% formic acid added. Samples were analysed by LC/MS/MS using multiple reaction monitoring (MRM). An HPLC, fitted with a Kinetex C18 2.6 μm (3.0 x 50mm) column (Phenomenex, Torrance, CA, USA), was operated in gradient mode from 90% mobile phase A (water/formic acid, 100:0.1, v/v) to 95% mobile phase B (acetonitrile/formic acid, 100:0.1, v/v) over 2 minutes. The analytes along with an internal standard were analyzed on a triple quadrupole mass spectrometer (SCIEX API 5500, Applied Biosystems, Foster City, CA, USA) that was equipped with a Turbo Ion Spray probe and operated in either positive or negative ion mode. In positive ion mode, scans monitored the signal for parent-daughter transitions for verapamil (455>150), propranolol (260>116), acetaminophen (152>110), fexofenadine (502>171) and the internal standard (CPDPX, 305>263). In negative ion mode, scans monitored the signal for parent-daughter transitions for the formic acid adduct of digoxin (825>779) and the internal standard (CPDPX, 303>260). The data was collected and processed using Analyst version 1.5.1 (Applied Biosystems). All calculations were based on peak area ratios between analytes and the internal standard and sample concentrations were determined from the linear range of the standard curve.

Statistical Analysis

Statistical significance was assessed by 2-way ANOVA analysis comparing three animals per timepoint/treatment group.

4.5 Figures and Tables

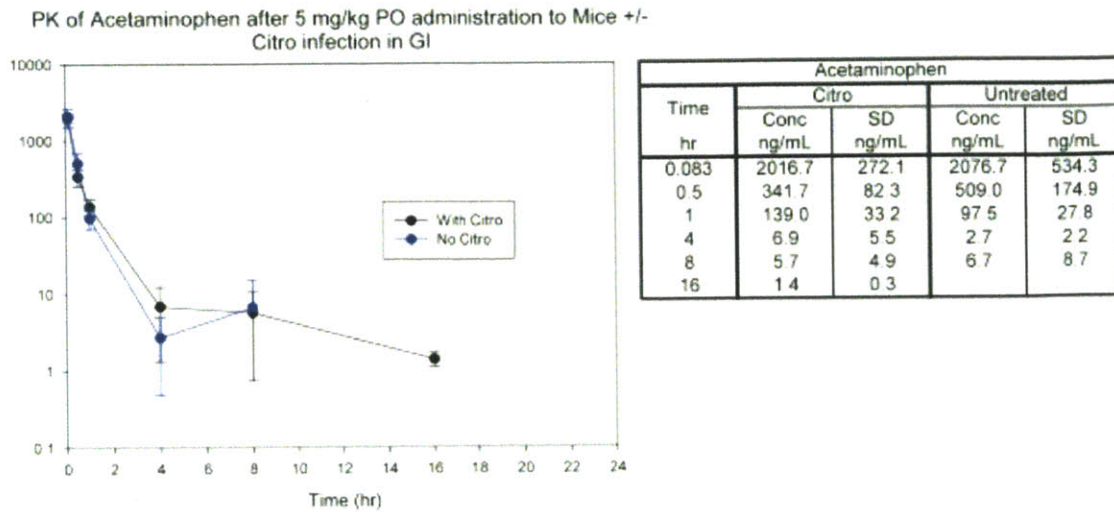


Figure 4-1. Effects of *C. rodentium* infection on Acetaminophen (5mg/kg) exposure. Acetaminophen was delivered PO at 5mg/kg to both control and *C. rodentium* infected mice at 7 DPI. Parent drug levels were measured in plasma by LC/MS/MS at 30min, 1hr, 2 hrs, 4hrs, 8hrs, and 16hrs post delivery (n=3 for each treatment group and timepoint).

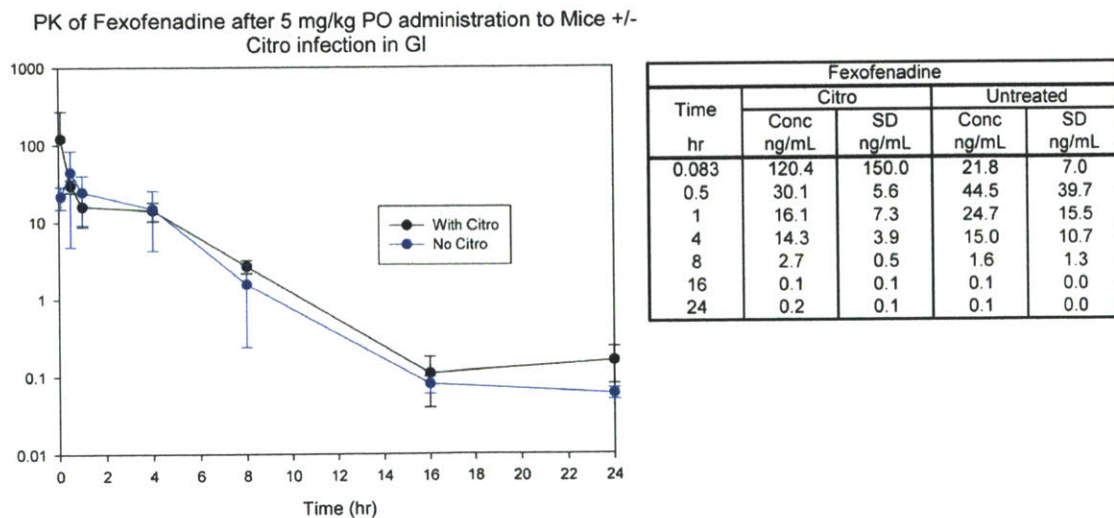
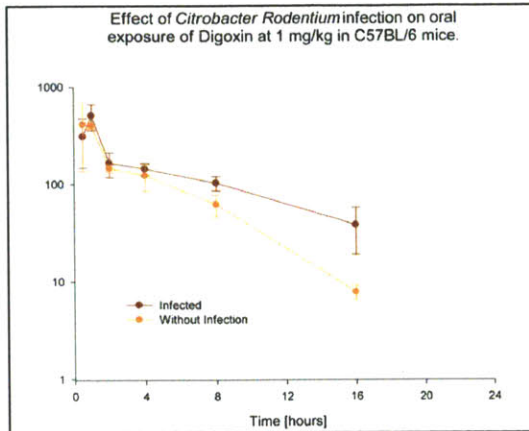
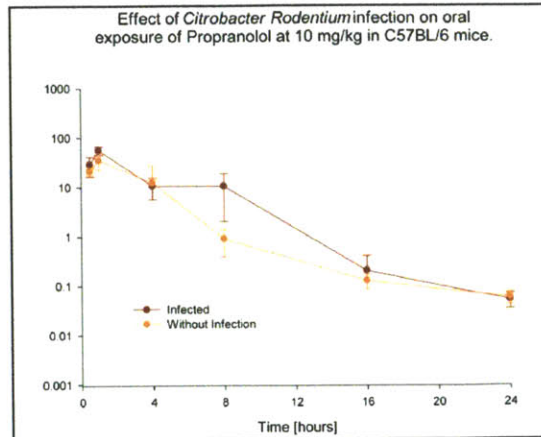
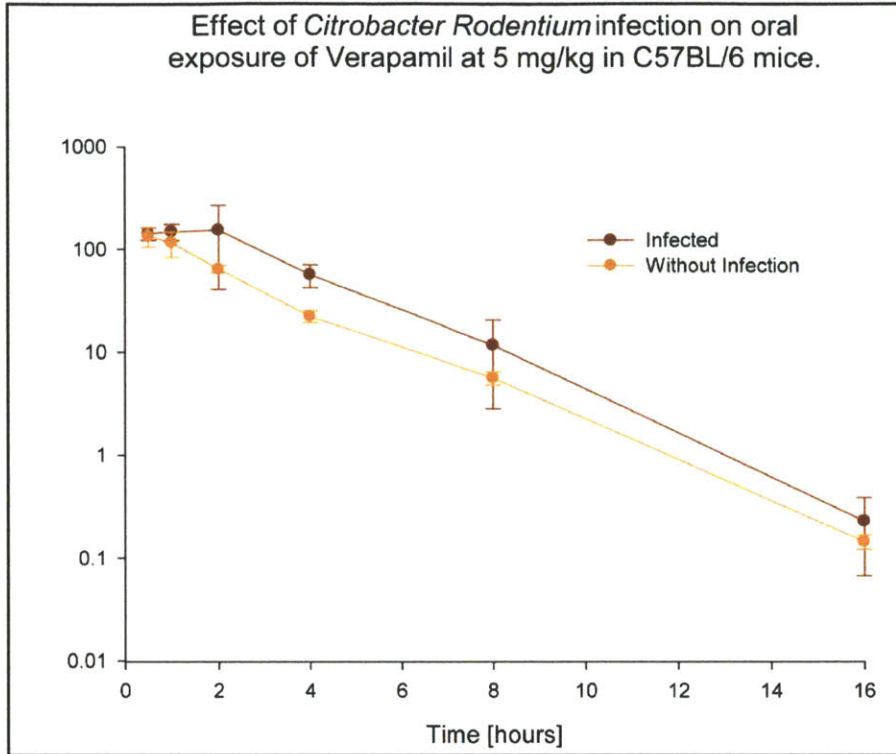


Figure 4-2. Effects of *C. rodentium* infection on Fexofenadine (5mg/kg) exposure. Fexofenadine was delivered PO at 5mg/kg to both control and *C. rodentium* infected mice at 7 DPI. Parent drug levels were measured in plasma by LC/MS/MS at 30min, 1hr, 2 hrs, 4hrs, 8hrs, 16hrs, and 24 hrs post delivery (n=3 for each treatment group and timepoint).

A**B****C**

Compound	Dose (mpk)	Treatment	Tmax (hr)	Cmax (ng/mL)	AUClast (hr*ng/mL)
Digoxin	1	<i>Citro</i>	1	509	2013
	1	control	0.08	410	1469
Propranolol	10	<i>Citro</i>	1	56.4	185
	10	control	1	35.2	112

Figure 4-3. Effect of *C. rodentium* infection on Propranolol and Digoxin exposure. Propranolol (10mg/kg) and digoxin (1mg/kg) were delivered PO to both control and *C. rodentium* infected mice at 7 DPI. Parent drug levels were measured in plasma by LC/MS/MS at 30min, 1hr, 2 hrs, 4hrs, 8hrs, 16hrs, and 24hrs post delivery (n=3 for each treatment group and timepoint).



Treatment	Tmax (hr)	Cmax (ng/mL)	AUClast (hr*ng/mL)	Cl/F (mL/min/kg)	Vz/F (L/kg)
<i>Citro</i>	2	154	657	127	16
control	0.5	134	353	236	32

Figure 4-4. Effects of *C. rodentium* infection on Verapamil (5mg/kg) exposure. Verapamil was delivered PO at 5mg/kg to both control and *C. rodentium* infected mice at 7 DPI. Parent drug levels were measured in plasma by LC/MS/MS at 30min, 1hr, 2 hrs, 4hrs, 8hrs, and 16hrs post delivery (n=3 for each treatment group and timepoint). Increased AUC was observed under infection conditions.

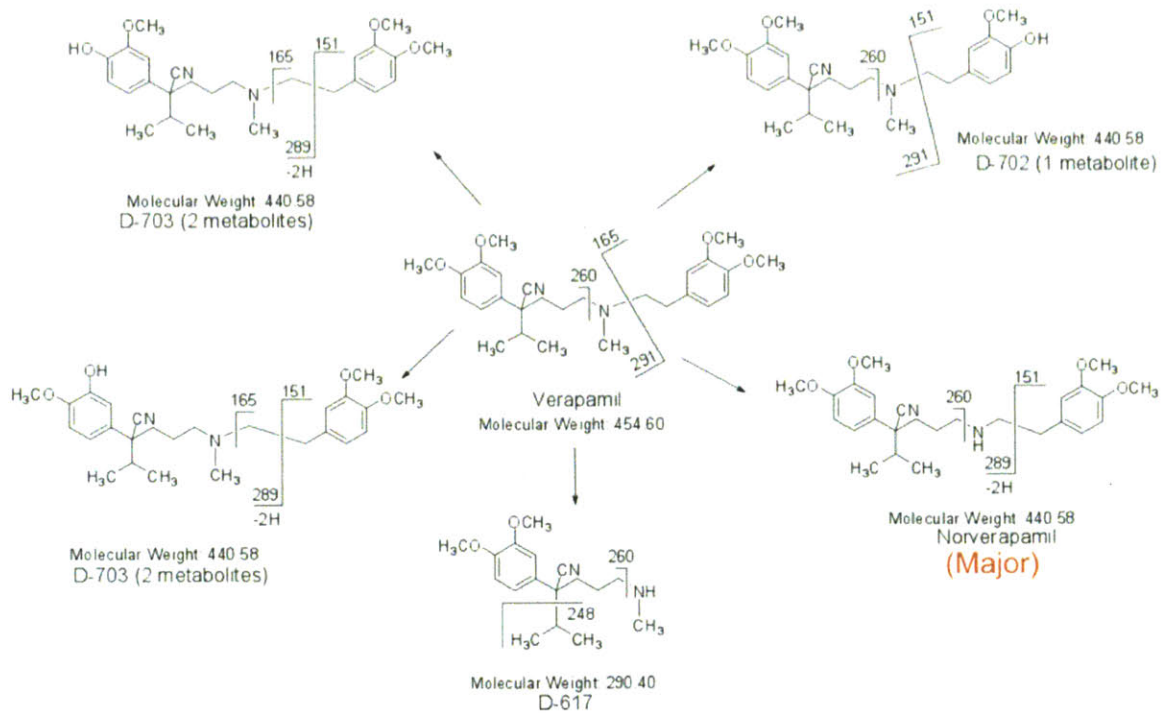


Figure 4-5. Verapamil metabolites monitored after 5mg/kg PO dose

Representative diagram of verapamil metabolites monitored by LC/MS/MS after a PO dose of 5mg/kg in control and *C. rodentium* infected mice at 7 DPI. Norverapamil, the major verapamil metabolite is indicated.

A

Compound	Retention Time	Peaks monitored
Verapamil	3.62 minutes	455>165
		455>260
Norverapamil (Major)	3.57 minutes	441>165
		441>289
		441>260
D-702	3.13 minutes	441>260
		441>291
D-703 (2 metabolites)	2.98 minutes	441>165
	3.22 minutes	441>289
D-617	0.45 minutes	291>260
		291>248

B

Analyte	+/- Citro	AUClast
D-617	+Citro	0.18
	-Citro	0.17
D-702	+Citro	0.2
	-Citro	0.09
D-703 Peak 1	+Citro	1.07
	-Citro	0.44
D-703 Peak 2	+Citro	2.05
	-Citro	1.08
Norverapamil	+Citro	12.15
	-Citro	4.98
Verapamil	+Citro	25.61
	-Citro	14.72

Figure 4-6. Method description and LC/MS/MS results of Verapamil metabolite levels

In order to monitor potential changes in the metabolic profile of verapamil under conditions of *C. rodentium*-induced inflammatory stress, 5 metabolites were monitored and retention times listed (A). AUC results for verapamil metabolites with and without *C. rodentium* infection at 7 DPI (B)

Effect of *Citrobacter Rodentium* infection on the metabolism of Verapamil after a 5 mg/kg oral exposure in C57BL/6 mice.

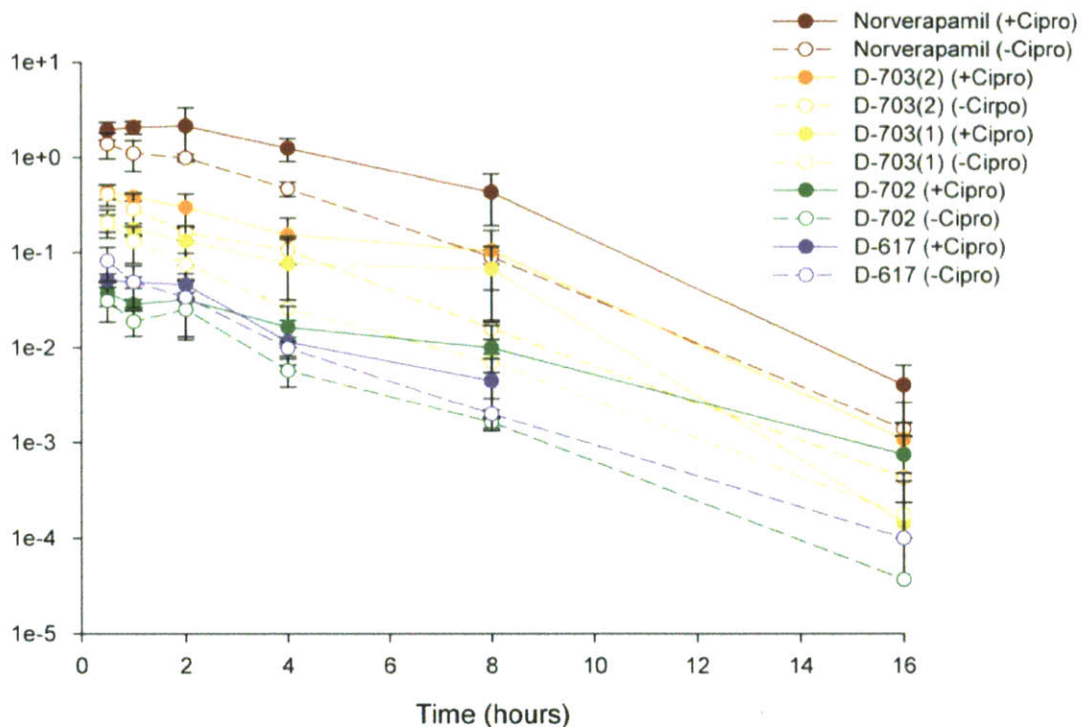


Figure 4-7. Effect of *C. rodentium* on metabolites of Verapamil (5mg/kg)
 Metabolites of verapamil were monitored over the course of 16 hrs with (solid line) and without (dashed line) infection with *C. rodentium*. (n = 3 mice per group per timepoint).

Table 4-1. Summary of compound exposure under *C. rodentium*-induced inflammatory stress

The effect of *C. rodentium*-induced inflammatory stress on drug clearance was assessed in six compounds varying in their biotransformation and mode of elimination. No change was observed with acetaminophen (5mg/kg, PO) and fexofenadine (5mg/kg, PO). Infection resulted in increased oral drug exposure for propranolol, verapamil, and digoxin.

Compound	Dose	Infection Status	Tmax (hrs)	Cmax (ng/mL)	AUClast (hr*ng/mL)	CYP substrate	Transporter substrate
Acetaminophen	5mg/kg	<i>Citrobacter</i>	0.08	2017	968	2E1	MRP2
		Uninfected	0.08	2077	946	"	"
Fexofenadine	5mg/kg	<i>Citrobacter</i>	0.08	120	139	minimal	OATP/(Pgp?)
		Uninfected	0.5	45	132	"	"
Propranolol	10mg/kg	<i>Citrobacter</i>	0.08	103	92	2D6, 1A2	NA
		Uninfected	0.08	32	41	"	"
Digoxin	1mg/kg	<i>Citrobacter</i>	1	509	2014	minimal	Pgp
		Uninfected	0.08	410	1469	"	"
Verapamil	5mg/kg	<i>Citrobacter</i>	2	154	657	3A4	Pgp?
		Uninfected	0.5	134	353	"	"

Table 4-2. LC/MS/MS Results of propranolol metabolites with and without *C. rodentium* Infection

Propranolol and its metabolites; Desisopropyl-propranolol, 1'-hydroxypropranolol, 2'-hydroxypropranolol, 3'-hydroxypropranolol, and parent drug were monitored by LC/MS/MS in plasma after an initial oral dose of 10mg/kg. AUC was determined based on both 0-8 hrs and 0-16 hrs post drug delivery based on detection limits.

Analyte	Treatment	Tmax (hr)	Cmax (ng/ml)	AUC (0-16) (hr*ng/ml)	AUC (0-8) (hr*ng/ml)	Ratio +/-
Desisopropyl-propranolol	<i>Citrobacter</i>	0.5	1.24		1.5	1.4
	uninfected	0.5	1.14		1.09	
1'-hydroxy	<i>Citrobacter</i>	0.5	1.21	6.01	5.25	1.7
	uninfected	0.5	1.01	3.48	3.11	
2'-hydroxy	<i>Citrobacter</i>	0.5	0.53		1.22	2.3
	uninfected	0.5	0.37		0.53	
3'-hydroxy	<i>Citrobacter</i>	0.5	0.31		1.80	2.2
	uninfected	0.5	0.27		0.81	
propranolol	<i>Citrobacter</i>	0.5	3.39	9.61	7.75	2.9
	uninfected	0.5	2.09	3.08	2.67	

Chapter 5: Conclusions and Future Work

The use of *C. rodentium* in various mouse models has contributed greatly to our understanding to pathogenic gastrointestinal infection and inflammatory bowel disease. Here, we investigated liver responses under extrahepatic stress and inflammation resulting from pathogenic enteric infection. While genetic manipulation and pharmacological inhibition has helped greatly in our understanding of hepatic homeostasis under inflammatory stress conditions, there still exist few animal models that can properly predict these pathologies in the human case. Furthermore, understanding the host response to environmental pathogens is critical in order to study how exposure to chemicals amplifies, synthesizes with, or mitigates environmentally induced disease.

Using *C. rodentium*, we show for the first time, to our knowledge, distinct liver pathology associated with enteric infection in C57BL/6 mice, characterized by increased inflammation and hepatitis index as well as periportal necrotic lesions indicative of thrombic ischemic injury during the early course of pathogenic infection (**Chapter 2**). Histologic changes correlate with serum elevation of liver transaminases, systemic and local cytokine and chemokine changes, as well as signal transduction changes prior to peak bacterial colonization and colonic disease. Specifically, using computational approaches we demonstrated systemic targets (cytokines/chemokines and serum chemistry markers) that differentiated animals by PLS-DA. Systemic elevations in ALT, AST, with an upregulation of immune modulators (IL-6, IL-10), monocytes chemokines/activators (MIP-1a, MCP-1), neutrophil chemokines/activators (G-CSF, KC), and t-cell activation (RANTES) at 3PDI correlated with coagulative liver necrosis. Mice harboring lesions also demonstrated induction of STAT3 and I κ B α phosphorylation, coupled with liver specific protein elevations of IL-1 β (L), IL-6 (L) G-CSF (L), KC (L), IL-12p40 (L), MCP-1 (L), MIP-1a (L), and RANTES (L). Future efforts delineating the role of these cytokine targets as well as potential translocation of bacteria (and bacterial products) in mediating injury are warranted.

Having characterized *C. rodentium* infections as a platform for systemic and liver inflammation, we investigated its role in altering susceptibility to drug-induced liver injury (DILI) using APAP, a well-established hepatotoxin (**Chapter 3**). Using computational approaches such as PCA, PLS, affinity propagation, and mutual information, we generated interaction networks to facilitate visualizing of this complex data landscape, but to also interrogate both linear and non-linear dependencies between systemic and tissue specific cytokine/chemokine levels, clinical serum chemistries, and histological scoring metrics. . In our model, APAP did not synergize with extrahepatic inflammation induced by *C. rodentium* infection, rather demonstrated moderate protection during the early course of enteric infection and statistically increased serum ALT levels at 7 DPI. We attribute this to an already induced Th1/Th17 response by *C. rodentium*. Furthermore, under co-

exposure, the tissue and systemic cytokines levels appear to indicate a Th1/Th2 neutralization, as the usual Th2 promoting targets (IL-4 (S, L)) associated with APAP treatment and Th1 targets with *C. rodentium* (IL-12p40 (L), RANTES (L), IL-a/b (L)) demonstrated attenuated levels as compared to single treatment alone. This can be at least in part attributed to the induction of IL-10, with known immunomodulatory effects on T cell polarization with *C. rodentium* and the anti Th1 effects of IL-4 resulting from APAP treatment. Future work would focus on neutralizing some of the targets obtained in this analysis such as IL-10 to address its role in *Citrobacter*-induced liver injury at 3 DPI, as well as the role in mediating altered signaling states under superimposition with APAP treatment. Cytokines are known signaling molecules in signal transduction pathways, and we previously observed signaling alterations in liver STAT1, STAT3 and I κ B α phosphorylation under *Citro* infection (**Chapter 2, Appendix Chapter B**), important mediators of cytokine signaling and immune responses. Measuring a limited number of intracellular signaling states may help to clarify mechanisms driving altered liver response and changes in T-cell polarizing targets observed here.

Finally, we investigated the role of *C. rodentium* in altering oral drug exposure (**Chapter 4**). Based on our examination we determined a ~2-fold systemic exposure for verapamil, propranolol, and a 1.4-fold higher exposure for digoxin under conditions of *C. rodentium* induced inflammatory stress. Upon measuring major metabolites for verapamil and propranolol, we found similar 2-fold elevations in plasma, indicating higher levels of both parent and metabolite indicating that biotransformation was less likely to blame for the elevations in parent drug. We attribute these findings to a leaky GI tract, allowing increased permeability of certain xenobiotics under inflammatory conditions. Furthermore, examining the expression of both uptake and efflux transporters in the small intestines and liver under conditions of pathogenic enteric infection seems warranted. Specifically, determining the role of Pgp in mediating altered oral bioavailability seen with *C. rodentium* compared to the proposed role of leaky GI. Greater understating of the role of GI infection (and resultant systemic and local inflammation) on drug and endogenous substrate clearance and homeostasis could have implications for patients with disease states such as IBD and pathogenic gastrointestinal infection. Furthermore, could help in the treatment management for patients with similar diseases characterized by either acute or chronic inflammation.

A greater appreciation of the liver-gut axis and its role in disease and predisposition at both systemic and tissue specific homeostasis could be critical in developing new therapeutic options or properly mitigating disease. Many liver disease and DILI involve inflammation as a contributing factor to progression and severity; continued examination using models utilizing pathophysiologically relevant sources of stress and inflammation may help towards this understanding. In summary, these findings are important towards helping defining connections between the dynamic interplay of inflammation and systemic/tissue-level homeostasis during enteric infection. Future work focusing on neutralizing antibodies or conditional KO's may help to confirm and expand on the importance of numerous targets implicated herein.

Appendix A: General Methods

Media and Bacterial Strains

Luria-Bertani (LB) agar and broth (Difco Laboratories, Detroit, MI) was used for routine cultivation of bacteria. MacConkey lactose agar (Difco Laboratories) supplemented with 40 µg/ml of kanamycin was used for quantitative monitoring of bacterial counts in fecal samples. The kanamycin-resistant strain of *C. rodentium* strain, DBS120 (pCRP1::Tn5, Kan^r) [145] was used for all infections.

Quantitative real-time PCR

Total RNA was prepared from frozen tissues using Trizol reagent according to manufacturer recommendation (Invitrogen, Carlsbad, CA). cDNA was generated from five micrograms of total RNA using SuperScript II RT (Invitrogen). One hundred nanograms of cDNA were amplified in a 25 µl reaction volume with predesigned primers (Applied Biosystems, Branchburg, New Jersey, USA) and probes (TaqMan Gene Expression Assays) in an ABI Prism Sequence Detection System 7700 (Applied Biosystems, Branchburg, New Jersey, USA) using standard TaqMan protocols: IFN- γ (Mm99999071_m1), IL-17 (Mm00439619_m1), TNF- α (Mm99999068_m1), CCL2 (Mm00441243_g1), IL-1 β (Mm00434228_m1), CCL3 (Mm00441258_m1), CCL5 (Mm01302428_m1), CXCL1 (Mm00433859_m1), CXCL2 (Mm00436450_m1), and glyceraldehyde-3-phosphate dehydrogenase (GAPDH) (Mm99999915_g1). Transcript levels were normalized to GAPDH, and expressed as fold change relative to averaged sodium bicarbonate (vehicle control) inoculated group, which were set at 1, using the Comparative Ct method (Applied Biosystems, User Bulletin no. 2). Reactions were processed in duplicate.

Appendix B: Effect of *Citrobacter rodentium* on early serum and liver responses

Arek R. Raczynski¹, Katherine Schlieper¹, Steven R. Tannenbaum¹, David B. Schauer^{1,2}

¹Department of Biological Engineering, ²Division of Comparative Medicine, Massachusetts Institute of Technology, Cambridge, MA, USA

B.1 Introduction

Citrobacter rodentium (*C. rodentium*) is a mouse specific enteric pathogen that results in varying degrees of inflammation, colonic hyperplasia, and more recently liver-related metabolic dysregulation. We recently found that infection with *C. rodentium* at early timepoints (3-4 DPI) results in coagulative necrosis in the livers of approximately 50% of C57BL/6 mice, correlating with systemic changes in G-CSF, RANTES, IL-10, MCP-1, and IL-6, coupled with STAT3 activation in livers. G-CSF, IL-10, and IL-6 are known upstream activators of STAT3 phosphorylation. In order to better understand the kinetics of injury at this early timepoint, we investigated serum and liver specific effects leading up to these early liver changes by examining *C. rodentium* induced changes at 12,24,48,72, and 96 hrs post inoculation (HPI). We observed a bi-phasic response in serum cytokines and clear induction of acute phase response transcriptional changes in livers as early as 12hr post inoculation with reactivation around 96 HPI (correlating with necrotic lesions described previously in **Chapters 2 & 3**).

To further determine whether this was a *C. rodentium*-specific or simply a non-specific response of the host to inoculation with $\sim 10^9$ bacterial colonies, we inoculated animals with either wild-type (WT) *C. rodentium* (DBS 120), a cloning strain of *E. coli* (DBS 9), or an intimin-deficient, non-pathogenic mutant strain of *C. rodentium* (DBS 255). Intimin is a virulence factor expressed on the surface of bacterial cells and binds to its receptor Tir (translocated intimin receptor) on colonic epithelial cells, an interaction that is critical for attaching and effacing (A/E) lesions, central to the pathogenesis of enteropathogenic *Escherichia coli* (EPEC) and enterohaemorrhagic *Escherichia coli* (EHEC)-mediated diseases in humans and *Citrobacter rodentium* transmissible colonic hyperplasia in mice [98, 173, 174].

Systemic cytokine changes collected were monitored at 12 and 24 hrs post inoculation (HPI). We discovered that all three bacterial strains were able to induce an acute phase response to some degree; however, only infection with WT *C. rodentium* maintains a sustained response at 24 hrs in both cytokine levels and STAT3 phosphorylation.

B.2 Results

***C. rodentium* infection results in early responses in systemic cytokine and chemokines**

Based on previous findings of liver injury at 3DPI, we decided to investigate the host response to *C. rodentium* at time points preceding liver pathology. C57BL/6 mice were infected by intragastric inoculation with $\sim 1 \times 10^9$ CFU of DBS120 (WT *C. rodentium*) and monitored for serum cytokines (Luminex 23-PLEX bead based ELISA), transcriptional changes in liver, and signal transduction in STAT3. As early as 12hrs post inoculation with *C. rodentium*, there was a statistically significant change serum levels of IL-1 α , IL-1 β , IL-5, IL-6, G-CSF, and MIP-1b (**Figure B-3**) ($p < 0.001$ for all targets but IL-1 β which was significant by $p < 0.01$, one way ANOVA with Bonferonni post test).

Quantitative RT-PCR for acute phase and liver targets

Quantitative RT-PCR was performed on RNA isolated from liver tissue to evaluate the expression of some key genes involved in acute phase response (Serum amyloid A and Serpine), immunomodulatory target (CXCL1 (KC)), and metabolic enzyme associated with cholesterol metabolism (CYP7a1) (**Figure B-2**). *C. rodentium* resulted in statistically significant increases in Serum amyloid A transcript (12, 24, and 96 HPI) as well as KC (12 and 96 HPI). Both are associated with the acute phase response, and mediated as least in part by cytokines such as IL-6, IL-10, and G-CSF. Cyp7a1 showed decreases in expression at 12 and 96 HPI but failed to reach significance as a group. Overall this indicates transcriptional changes in acute phase and chemokines associated with neutrophils activation/chemotaxis.

Bacterial clearance of DBS 9, DBS 120, and DBS 255

Oral inoculation with all three strains resulted in detectable colony forming units at both 12 and 24 HPI, with WT *C. rodentium* having the slowest clearance (thus highest bacterial load) at both timepoints, followed by the intimin-deficient strain (DBS 255), and finally *E. coli* (DBS 9) had the lowest colony forming units (CFUs) detected (**Figure B-4**).

Sustained STAT3 Phosphorylation with DBS 120

STAT3 activity was measured by western analysis for phosphorylation at TYR-527 (Cell Signaling Technology, MA). All three strains were able to induce STAT3 activation in livers at 12 HPI, however, only WT *C. rodentium* (DBS 120), the fully pathogenic strains, was able to sustain STAT3 activation at 24 HPI (**Figure B-5**). Bacterial levels at 24 hrs were approximately 3-logs higher at this timepoint.

B.3 Discussion

Here we determined to evaluate the systemic and liver specific cytokine changes associated with *C. rodentium* infection at early timepoints prior to colonic disease (12-96 HPI). Furthermore, we investigated the effect of pathogenic (WT *C. rodentium*), intimin deficient, and *E. coli* strains in their respective abilities of inducing a similar response at 12 and 24 HPI. We discovered that *C. rodentium* is able to induce an acute phase response in mice as early as 12 HPI as indicated by transcriptional activation of Serum amyloid and KC, as well as elevations of pro-inflammatory cytokines IL-1 α , IL-1 β , and IL-6, as well as inflammatory mediators involved in neutrophils activation (G-CSF) and monocytes chemo-attraction (MIP-1b). Furthermore, these changes at both the systemic and tissue levels correlate with signal transduction as monitored by STAT3 activation, a key regulator in acute phase response and tissue injury.

Interestingly, all three bacterial strains were able to induce an acute phase response to some degree; however, only infection with WT *C. rodentium* maintains a sustained response at 24 hrs in both cytokine levels and STAT3 phosphorylation. STAT3 phosphorylation was correlated with systemic cytokine release of pro-inflammatory cytokines (IL-1 α/β), as well as IL-5, IL-6, G-CSF, and MIP-1b. Furthermore, liver specific elevations in serum amyloid A and CXCL1 (KC) were significantly elevated as early as 12 HPI as a result of *C. rodentium* infection.

What remains to be determined is exactly what role these targets may play with respect to the reproducible liver necrosis found in animals approximately 3-4 days post oral inoculation with *C. rodentium*. It is possible that this early response has evolved fairly generically in the face of stress or acute changes in gut physiology or bacterial colonization, and may not necessarily be a predisposition to injury. Although, activating such responses under already injured condition, for example under chronic liver inflammation or drug-induced injury may potentially result in an local and systemic cytokine/chemokine and signaling network with potential synergies or protective effects at play. Indeed, in **Chapter 3** we demonstrate that the injury associated with *C. rodentium* does not synergize with APAP-induced liver injury, rather appears protective. What is unknown is whether the earlier timepoints (12/24 hrs) or even as early as 2-8 HPI would result in a very different response to superimposition with drug-treatment. Indeed others show what appears to be a temporal dependence or LPS to synergize with drug treatment. Much of this could be attributable to the complex mechanism of tolerance and resistance, key to managing and balancing host-pathogen interactions.

B.4 Selected Methods

Mouse Infections

40 female 8-10 week-old, specific pathogen free C57BL/6 mice were (The Jackson Laboratory, Bar Harbor, ME) were housed and maintained as described in Appendix A (General Methods). Infectious colitis was induced by intragastric inoculation with $\sim 1 \times 10^9$ CFU of DBS120 in 3% sodium bicarbonate (in PBS, pH 7.4) using a 100uL volume. Control animals (0 DPI) were sacrificed within 1hr of inoculation while the 12, 24, 48, 72, and 96 hour post inoculation (HPI) animals were monitored for fecal shedding and body weight changes as indicated and euthanized and necropsied at their respective timepoints as described in Appendix A

Immunoblot of Phospho-proteins:

Tissues were thawed on ice, suspended in Bio-Rad cell lysis buffer with provided phosphatase and protease inhibitors, and homogenized with a Tissue Tearor™ for 1 minute. Upon freeze thawing (-80°C), samples were sonicated on level 5 for three 10 second bursts, incubated on ice for 20 minutes, and centrifuged at 4°C at 5000 rpm for 15 minutes to precipitate insolubles. Supernatants were protein quantified by BCA (Thermo Scientific, Rockford, IL) and adjusted to 2ug/uL with Bio-Rad lysis buffer. Equal volumes of 2X SDS loading buffer was added and 20uL loaded (20ug/well) onto 10% SDS Tris-glycine gels (Invitrogen, Carlsbad, CA). Upon transfer to immobolin^{PQ} PVDF membranes, blots were incubated with antibodies (1:2000 P-STAT-3, 1:2000 anti-rabbit monoclonal, **P-38 and ERK1/2**, Cell Signaling Technologies) in TBST-5%BSA, incubated with Santa Cruz luminal reagent, exposed by Kodak MR film, and quantified by NIH imageJ.

Real-time quantitative RT-PCR. Total RNA was prepared from frozen kidney using Trizol reagent according to manufacturer recommendation (Invitrogen, Carlsbad, CA). cDNA was generated from five micrograms of total RNA using SuperScriptII RT (Invitrogen). One hundred nanograms of cDNA were amplified in a 25 μ l reaction volume with predesigned primers (Applied Biosystems, Branchburg, New Jersey, USA) and probes (TaqMan Gene Expression Assays) in an ABI Prism Sequence Detection System 7700 (Applied Biosystems, Branchburg, New Jersey, USA) using standard TaqMan protocols: IFN- γ (Mm99999071_m1), IL-17 (Mm00439619_m1), TNF- α (Mm99999068_m1), CCL2 (Mm00441243_g1), IL-1 β (Mm00434228_m1), CCL3 (Mm00441258_m1), CCL5 (Mm01302428_m1), CXCL1 (Mm00433859_m1), CXCL2 (Mm00436450_m1), and glyceraldehyde-3-phosphate dehydrogenase (GAPDH) (Mm99999915_g1). Transcript levels were normalized to GAPDH, and expressed as fold change relative to averaged sodium bicarbonate (vehicle control) inoculated group, which were set at 1, using the Comparative Ct method (Applied Biosystems, User Bulletin no. 2). Reactions were carried out in duplicate.

B.5 Figures and Tables

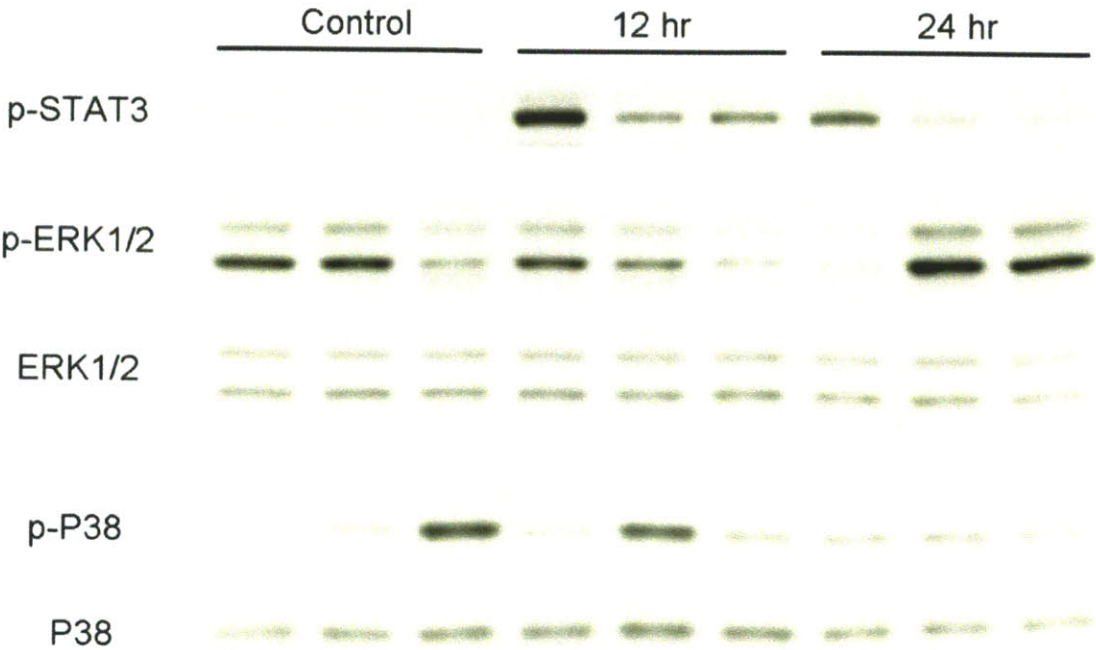


Figure B-1. Signal transduction in liver lysates of *C. rodentium* infected animals at 12 and 24 HPI

Signal transduction was evaluated by western analysis probing for STAT3, ERK, and p-38 phosphorylation at 12 and 24 HPI. Total ERK and p-38 are indicated.

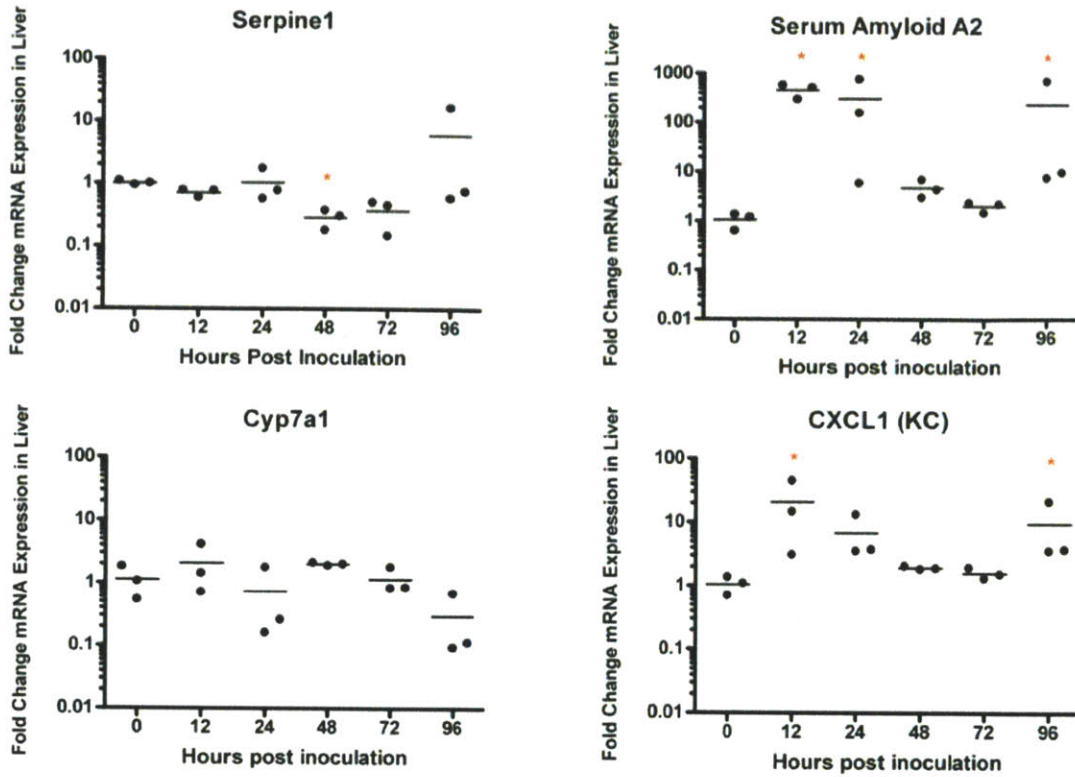


Figure B-2. qRT-PCR for acute phase and liver targets due to *C. rodentium* infection. qRT-PCR (TAQMAN) for Serpine 1, Serum amyloid A2, Cyp7a1, and CXCL1 (KC) were evaluated at 0, 12, 24, 48, 72, and 96 HPI using liver RNA. All targets were normalized to GAPDH presented as Fold-change over the mean of controls (0 HPI). (Kruskal-Wallis with Dunn's post test: * $p < 0.05$, ** $p < 0.01$, *** $p < 0.001$). Lines indicate group means

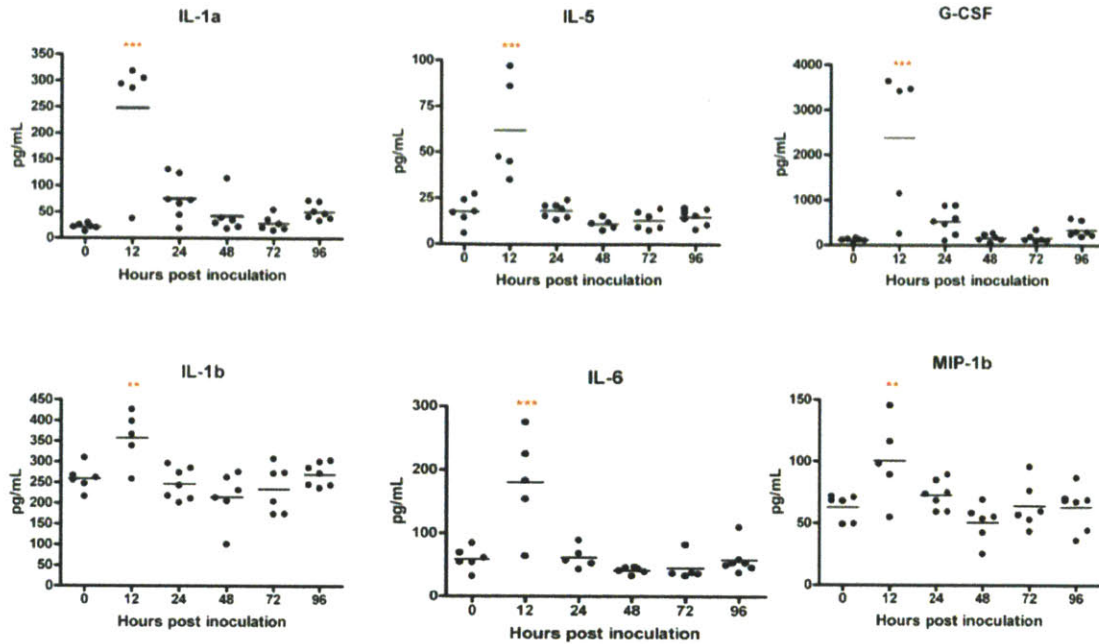


Figure B-3. *C. rodentium* induced systemic cytokines changes at early timepoints
 Multiplex analysis using Bio-Rad cytokine/chemokine panels resulted in significant serum elevations of IL-1 α/β , IL-5, IL-6, G-CSF, and MIP-1b as early as 12-hrs post inoculation. (One-way ANOVA with Bonferonni post test: * p < 0.05, ** p < 0.01, *** p < 0.001). Lines indicate group means

Fecal Shedding Citro_EXP#3

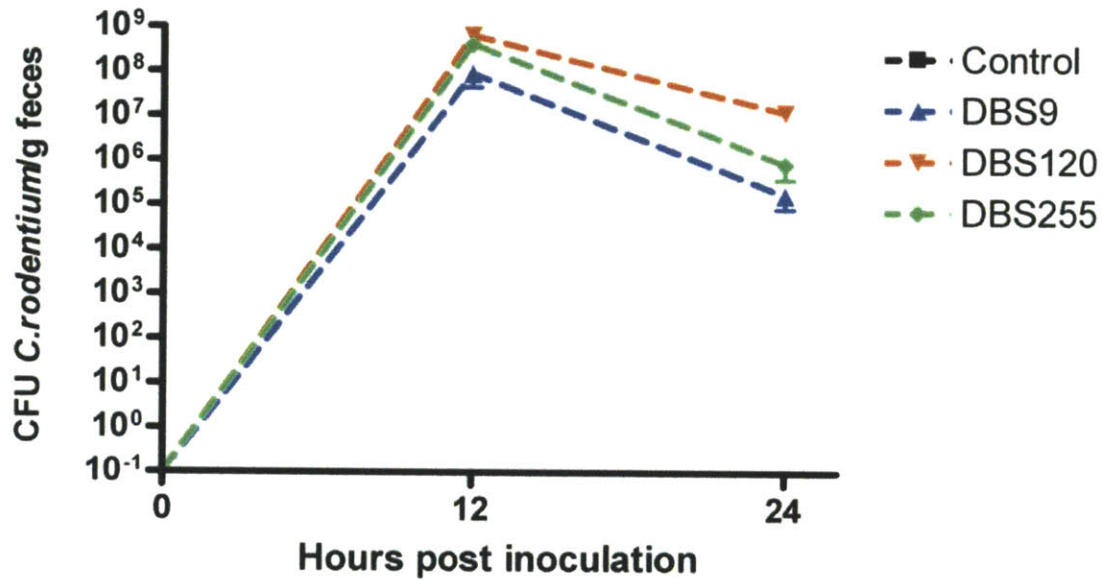


Figure B-4. Infection kinetics of DBS 9, DBS 120, and DBS255 in C57BL/6 mice
 Bacterial load was assessed by fecal shedding by serial dilution at 12 and 24 HPI for DBS 9 (*E. coli*), DBS 120 (WT *C. rodentium*), and DBS 255 (Intimin deficient *C. rodentium*).

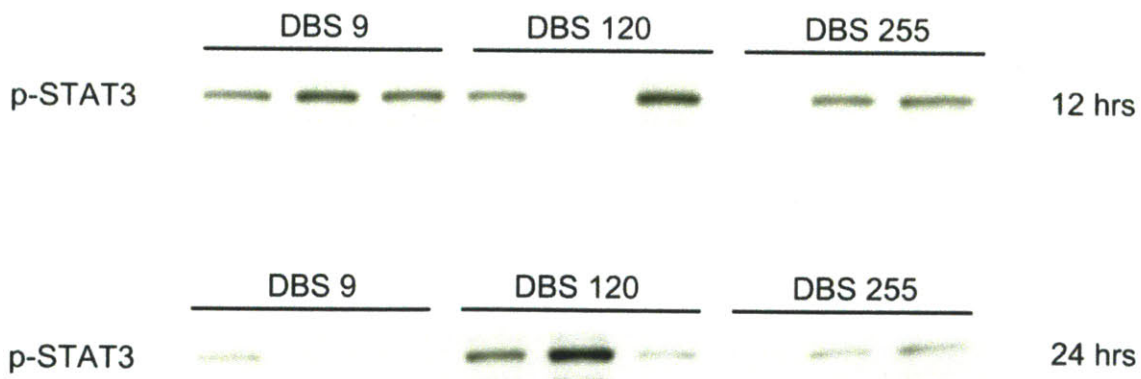


Figure B-5. STAT3 activation in livers of DBS9, DBS120, and DBS255 livers.
 Signal transduction was evaluated by western analysis probing for phosphorylation of STAT3 at 12 and 24 HPI for DBS9, DBS120, and DBS255 inoculated animals (n=3 livers were used for each treatment group).

Appendix C: Biomarkers of Inflammatory Bowel Disease

Knutson CG¹, Raczynski AR¹, Zeng Y¹, Iffrig EM¹, Wishnok JS¹, Korzenik JR² and Tannenbaum SR¹.

¹Department of Biological Engineering, Massachusetts Institute of Technology, Cambridge, MA 02138. ²Crohn's and Colitis Center, Gastrointestinal Unit, Massachusetts General Hospital, Boston, MA 02114.

Sections of this chapter will be used for publication submission.

C.1 Introduction

Ulcerative colitis (UC) and crohn's disease (CD) are two forms of inflammatory bowel disease (IBD) that together affect approximately 2 million people in the United States. Both conditions are multifactorial with unknown etiologies, but can present in very similar fashions clinically, with intermittent and severe activation of the mucosal immune system in the GI tract, promoting a chronic state of inflammation [175]. While many immune regulators have been identified in human analysis as well as animal models of IBD, their respective roles in disease progression, usefulness as biomarkers, and potential for therapeutic intervention remains an uncertainty [176, 177].

Currently, diagnostic evaluation uses erythrocyte sedimentation rate (ESR) and serum C-reactive protein (CRP) levels as early indicators of disease for both forms of IBD. CRP is an acute-phase protein produced in response to infection and inflammation, which activates the classical complement system via c1q binding phosphocholine expressed on the surface of dead or damaged cells (or bacteria), which enhances macrophage phagocytosis. Such biomarkers are used in tandem to evaluate disease severity coupled with symptoms presented by the patient upon physical examination. Typically, patients undergo further evaluation in the form of an endoscopy or colonoscopy as well as tissue biopsy to confirm pathology and severity of disease. Such biomarkers, however, are non-specific; indicating generic activation of inflammatory processes in an individual, providing minimal information with respect to disease specificity, progression, or severity. For this reason, there is growing interest in finding biomarkers more specific to IBD disease subsets, potentially augmenting the current diagnostic process or optimally decreasing the necessity to invasive practices without compromising proper diagnosis.

Here we evaluated patient serum samples from 40 ulcerative colitis (20 active and 20 inactive), 40 crohn's (20 active and 20 inactive), assessing circulating serum cytokines using multiplex cytokine/chemokine panels, coupled with circulating inflammatory stress markers such as Cl-TYR, NO-TYR detected by LC/MS methodology. Using principle components analysis (PCA) and partial least squares regression (PLSR) techniques, we found targets that differentiated between active and inactive individuals based on the clinical disease scores provided by the clinician, yielding biomarkers for both UC and CD individuals that demonstrate high specificity and selectivity for disease activity. Such biomarkers could prove helpful in not only monitoring the disease progression and severity, but also gives insights into potential new therapeutic approaches in controlling both CD and UC disease.

C.2 Results

Details of human patient samples

Patient serum samples from UC, Crohn's, and normal patients were obtained from Mass General Hospital (MGH) from the Gastroenterology department's repository. A total of 40 ulcerative colitis patients (20 active, 20 inactive), 40 Crohn's patients (20 active, 20 inactive), and 30 normal patients were used for analysis. Disease score was provided for all UC and CD patients and based on disease scoring criteria. General patients information was also provided (ex, gender, age, prescribed pharmaceuticals).

OPLS analysis for disease score: active versus inactive

Quantitative data obtained from serum multiplex cytokine/chemokine analysis, CRP, ESR, CL-TYR, and patient disease scores were combined from both study cohorts and OPLS analysis was conducted to determine targets that co-varied best with the clinically ascribed disease scores. UC and CD (four groups, $n = 20$ for each grouping) patients' samples were combined for general IBD assessment and individually to determine if certain variables were better able to differentiate disease activity within the two disease types. Using orthogonormalized partial least squares regression (OPLS) with disease score as the dependent "y" variable, granulocyte colony-stimulating factor (G-CSF), chemokine ligand 10 (IP-10), interleukin-8 (IL-8), IL-17, and IL-1 displayed covariance with the clinical disease score (variable in projection scores (VIP) >1) when UC and CD data sets were combined. When the data was limited to only CD and plotted variables using OPLS (VIP >1) analysis the cytokine profile was unchanged. However, when OPLS (VIP >1) analysis was limited to only UC variables, IL-6 displayed covariation with disease score, but IP-10 and IL-17 did not, which suggests that these factors are less predictive with UC disease score and more predictive of CD disease activity. Using OPLS again, but focusing only on active and inactive disease patients for each IBS type, were able to obtain reasonable separation of patient samples (**Figure C-1**), and determine the observed vs predicted performance of the model resulting in a $R^2 = 0.6231$ (**Figure C-2**). The process was repeated for CD patients as well (**Figure C-3 and C-4**) resulting in reasonable separation of patients, however resulting in a lower $R^2 = 0.3794$.

Mann-Whitney analysis of targets obtained from OPLS

Targets determined to have a VIP score of greater than 1 were analyzed by Mann-Whitney to determine if there were statistically significant differences between circulating levels in active versus inactive (patients in remission) cohorts (**Figure C-6**). We also evaluated CRP and ESR levels measured at the time of disease score assessment and found them to be poor predictors of disease activity, both failing to reach statistical significance in differentiating between groups (**Figure C-5**). From this evaluation the statistical significance between groups demonstrates that cytokines and chemokines are reasonable markers of disease activity.

Total score and selectivity/specificity determination

Total scores were calculated by selecting the top 4 and 5 VIP scores for UC and CD, respectively, normalizing the raw cytokine data to a base-10 spread, scaling by the VIP factor, and summing the total. Patients' samples that resulted in scores above a particular cutoff were designated as active and those below inactive. A selectivity/sensitivity analysis was also conducted to determine the performance of this discrimination.

C.3 Discussion

Using multiplex analysis of serum cytokine/chemokine levels, inflammatory markers of neutrophil activation (CL-Tyr), macrophage activation (NO-TYR), CRP, ESR, and disease indexes collected from patients with active or inactive UC/CD, and normal patients, we present potential biomarkers in the assessment of disease activity for both CD and UC patient populations.

In the case of UC, we utilized OPLS analysis to determine the features that best correlate with clinical disease score and discovered IL-8, CL-Tyr, G-CSF, and IL-6 were best the best performers of the targets measured. By creating a modified disease score based on the four VIP scores and the normalized cytokine values resulted in a total score with a corresponding specificity of 81.8% (Score >40) and sensitivity of 84.2% (Score >40) for UC. For CD, OPLS analysis resulted in CL-TYR, MIP-1b, IP-10, IL-6, and IL-1ra as the best correlates. Calculation of total score for the CD model resulted in a specificity for CD = 87.5% (Score >47) and sensitivity = 75% (Score >47). These new biomarkers serve as potentially valuable complementary tools to existing biomarkers to potentially differentiate between CD, UC, but also monitor disease activity. Recently, disease severity in a mouse model of IBS using *C. rodentium* infection in C57BL/6 mice resulted in the upregulation of serum and colonic cytokines, many paralleling changes we observed in these two forms of IBD (KC (mouse analog of human IL-8), G-CSF, CL-Tyr, and IL-6), indicating a strong neutrophil component to disease severity [94].

UC and CD represent two major form of IBD that affects millions of patients in the United States and abroad. While the current pharmacological inhibitors have been tremendously helpful in managing both conditions, disease relapse and development of resistance and treatment tolerance is a major issue. Here we demonstrate that mediators of the innate immune system appear to be activated in patients with disease activity, furthermore, find sets of biomarkers for both UC and CD that perform quite well in their selectivity and specificity for disease activity. These are markers that irrespective of patient gender age, or current pharmaceutical intervention used, demonstrate a clear enrichment and correlation with disease score and activity.

The current landscape of potentially new biomarkers for IBD has increased recently, with many under clinical investigation [177]. The majorities of biomarkers discovered are associative for either UC or CD and include anti-self antibodies for perinuclear anti-neutrophil cytoplasmic antibodies (pANCA), bacterial products, and glycans. Other general biomarkers of inflammation that have been applied in the IBD settings include calprotectin and CRP [178, 179]. Continued exploration into the role and function of the innate immune system during these disease processes will hopefully lead to a greater understanding of disease etiology and pathogenesis, with an eventual goal of better disease management and intervention.

C.4 Selected Methods

Cl-TYR and N-TYR detection

Nitrotyrosine and chlorotyrosine levels in human serum were measured by negative-ion chemical ionization GC/MS. Briefly, serum (2 mg) was spiked with 1 pmol internal standards (L-3-chloro-[13C9, 15N]-tyrosine and L-3-nitro-[13C9, 15N]-tyrosine). Protein was digested by 1 mg Pronase E (Protease from *Streptomyces griseus*) overnight at pH 7.4, followed by HPLC purification. The purified residue was derivatized with ethyl perfluorobutyrate and N-methyl-N-(*t*-butyldimethylsilyl) trifluoroacetamide + 1% trimethylchlorosilane (MtBSTFA, Regis Technologies, Morton Grove, IL). The derivatized samples were analyzed by negative-ion chemical ionization GC/MS. Separations were carried out on an Agilent 6890N GCMS system equipped with a 30 m HP-5MS capillary column (0.25 mm I.D., 0.25 mm film thickness). The ions were monitored at *m/z* 489 and 499 for chlorotyrosine and L-3-chloro- [13C9, 15N]-tyrosine, and at *m/z* 518 and 528 for nitrotyrosine and L-3-nitro-[13C9, 15N]-tyrosine. Quantification of protein-bound nitrotyrosine and chlorotyrosine were based on the calibration curves (5-points) constructed over the range of 0.1–5.0 pmol for both nitrotyrosine and chlorotyrosine. All analyses were carried out in triplicate.

Multiplex Detection of Serum Cytokines and Chemokines:

Human serum was obtained from Massachusetts General Hospital (MGH) and analyzed using human 27-plex cytokine panels (Bio-Rad, Hercules, CA) as specified by the manufacturer. Briefly, serum was diluted in human-specific sample diluent (1:4) and 50 μ L of sample or premixed standards were incubated with pre-washed target capture antibody-conjugated microspheres provided and incubated for 30 minutes with orbital shaking (300 rpm) in a 96-well plate. Upon washing, beads were incubated with detection antibody (30 min), washed, and subsequently incubated with streptavidin-PE (10 min). Beads were washed and resuspended with 125 μ L assay buffer and read on the Luminex 200 suspension array system using the low RP1 target setting (High PMT) for maximum sensitivity. Data analysis was carried out with the Bio-Plex Manager™ 5.0 software and cytokine or chemokine concentrations calculated against an 8 point standard curve generated by either 4PL or 5PL curve fitting.

Multivariate Data Analysis:

Principal components analysis (PCA) was used as a first-pass, unbiased assessment of global variance in patient data set. To determine serum specific factors that best differentiated normal, UC (active and inactive), CD (active and inactive) patients, supervised multivariate methods were utilized using SIMCA-P software (Umetrics Inc., Kinnelon, New Jersey). Projection to latent structure discriminate analysis (PLS-DA) was conducted based on known classes. The information on class membership allows optimal extraction of particular observations (e.g., serum cytokine targets) that correlate best with disease state and activity. Orthogo-

normalized Partial Least Squares regression (O-PLS) was subsequently used to eliminate systematic variation unrelated to disease score, facilitating the interpretation of disease activity specifically. In this case a cross-matrix correlation between all serum targets (X) and the clinically determined disease score (Y) were used as modeling parameters. Variable importance in the projection (VIP) were computed from influence (weight) on disease score of every term in the model. The average VIP equals 1, therefore VIPs >1 explain Y more than VIP<1. VIPs greater than 1 were used in creating the total score.

Statistical Analysis:

Statistical significance in serum targets between patients groups that demonstrated non-normal distributions or categorical in nature, were assessed by Kruskal-Wallis non-parametric test with Dunn's multiple comparison test against controls unless otherwise indicated. If only two groups were analyzed, Mann Whitney was utilized. All analyses were done with GraphPad Prism software, version 4.0 and *P* values of <0.05 were considered significant.

C.5 Figures and Tables

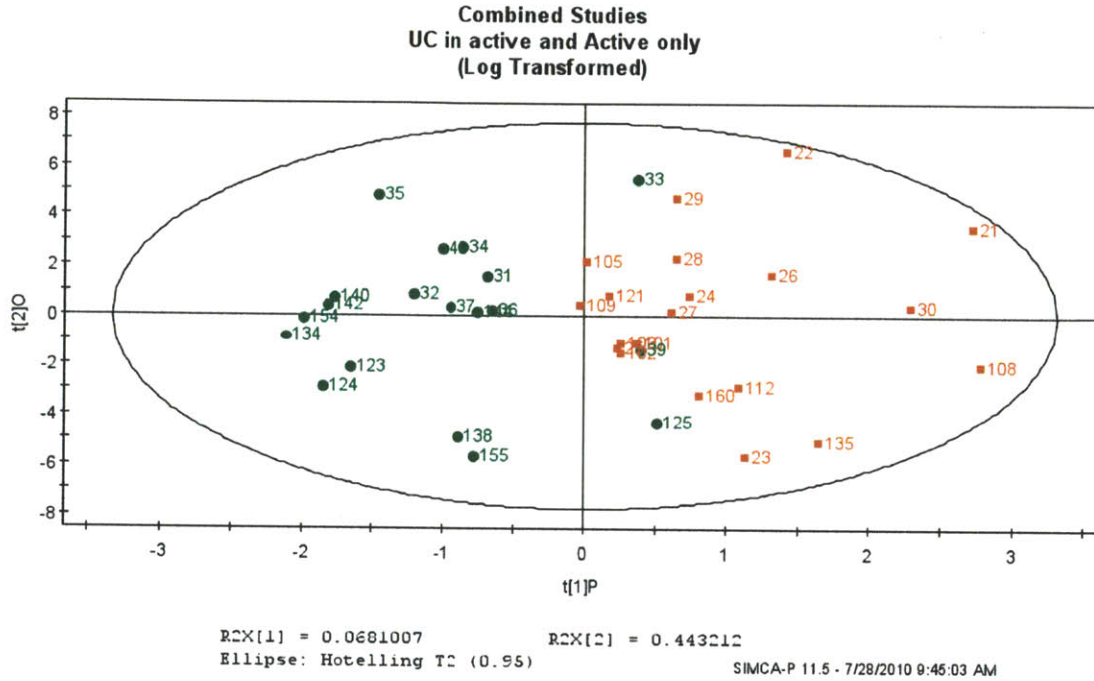


Figure C-1. OPLS for disease score: Ulcerative colitis using active and inactive patients (STUDY 1&2).

Cytokines, chemokines, CRP, ESR, and CL-TYR data (“x”-variables) from UC patients was analyzed by OPLS using disease score as the dependent (“y”) variable. Human controls were not included for this analysis. Individual patients numbers are represented and distinguished as either active (RED) or in remission (GREEN) based on clinical assessment.

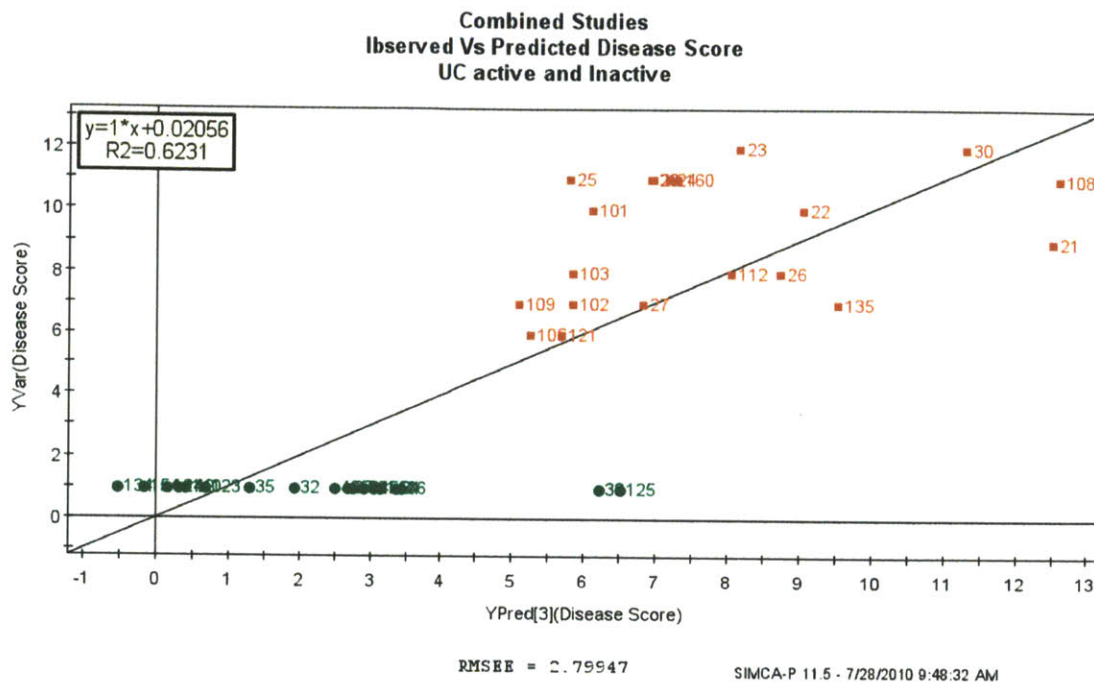


Figure C-2. Observed versus predicted disease score: Ulcerative colitis active and inactive patients (STUDY 1&2)

Observed versus predicted disease score is plotted based on the OPLS analysis of active and inactive patient data. A linear regression as to goodness of fit is shown ($r^2 = 0.6231$). Human controls were not included for this analysis. Individual patients numbers are represented and distinguished as either active (RED) or in remission (GREEN) based on clinical assessment.

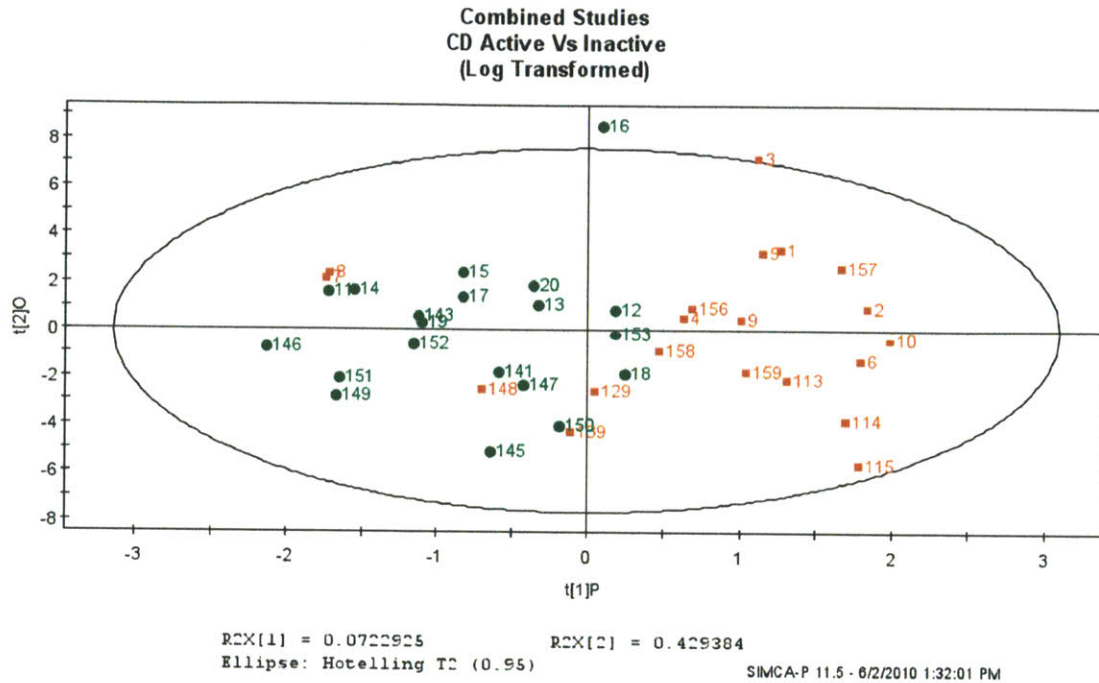


Figure C-3. OPLS for disease score: Crohn's using active and inactive patients (STUDY 1&2).

Log transformed cytokine, chemokine, CRP, ESR, and CL-TYR data ("x"-variables) from CD patients was analyzed by OPLS using disease score as the dependent ("y") variable. Human controls were not included for this analysis. Individual patients numbers are represented and distinguished as either active (RED) or in remission (GREEN) based on clinical assessment.

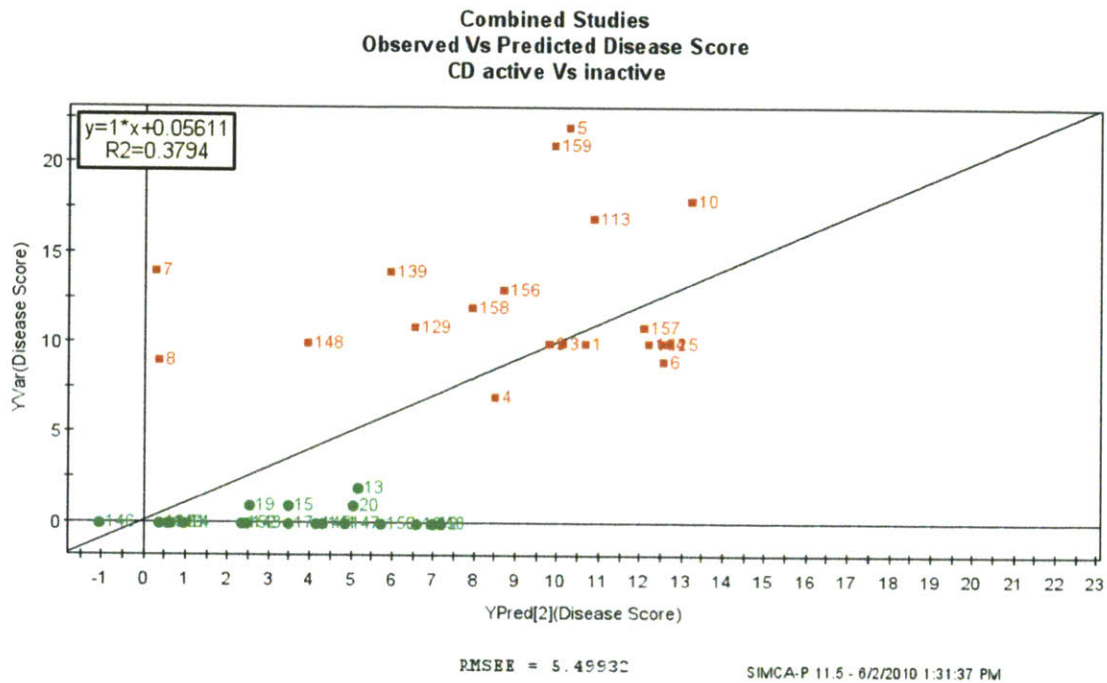


Figure C-4. Observed versus predicted disease score: Crohn’s active and inactive patients (STUDY 1&2).
 Observed versus predicted disease score is plotted based on the OPLS analysis of active and inactive patient data. A linear regression as to goodness of fit is shown ($r^2 = 0.3794$). Human controls were not included for this analysis. Individual patients numbers are represented and distinguished as either active (RED) or in remission (GREEN) based on clinical assessment.

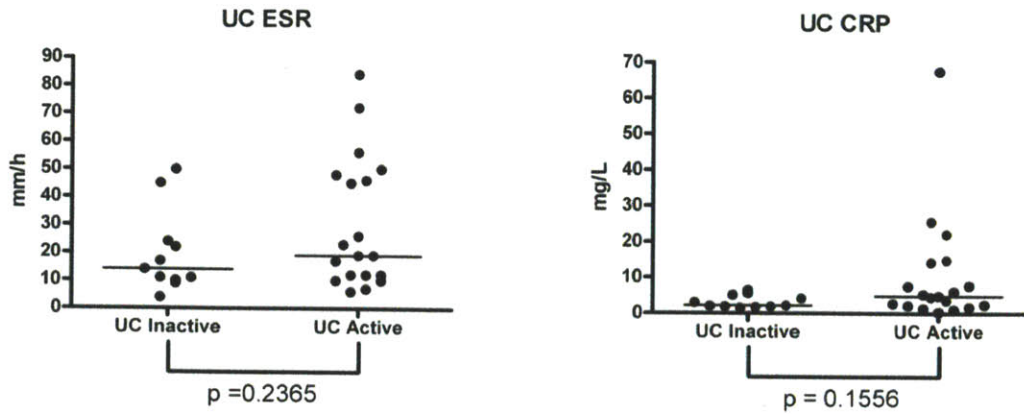


Figure C-5. Mann-Whitney of ESR and CRP values for UC active and inactive patients. ESR and CRP values analyzed from both active and inactive ulcerative colitis patients fail to reach statistical significance for differentiation between groups: ESR ($p = 0.2365$), CRP ($p=0.1556$) (Mann-Whitney non-parametric test).

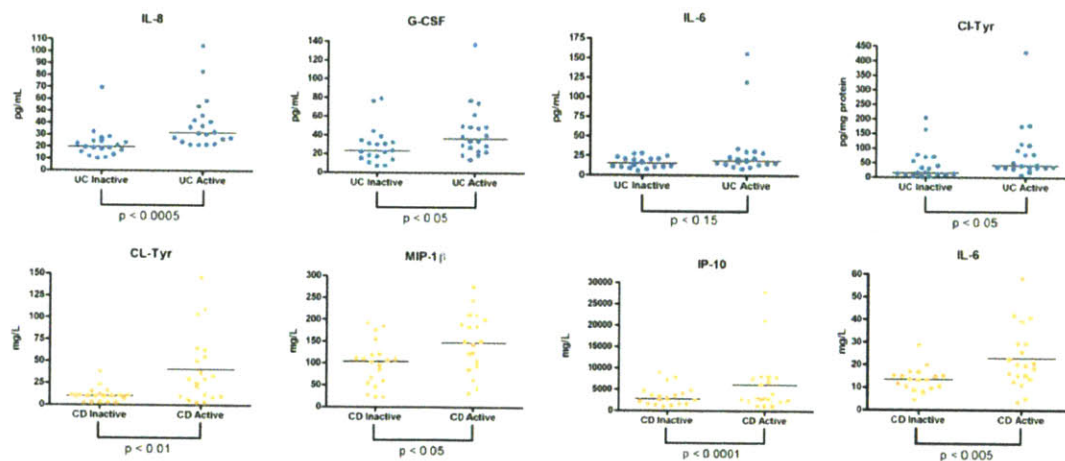


Figure C-6. Potential biomarkers of disease activity obtained from OPLS analysis Mann-Whitney non-parametric t-tests for the top variables obtained from VIP scores for CD and UC patients comparing active and inactive disease populations. All variables were statistically higher in serum of patients with active disease at compared to inactive, or patients in remission ($p < 0.05$).

UC TOTAL SCORES (IL-8, CI-Tyr, G-CFS, IL-6)				CD TOTAL SCORES (CI-Tyr, MIP-1b, IP-10, IL-6, IL-1r)			
	Disease		Total Score		Disease		Total Score
1	UC	Active	67.01	1	CD	Inactive	76.86
2	UC	Active	66.22	2	CD	Active	74.84
3	UC	Inactive	62.06	3	CD	Active	73.90
4	UC	Active	53.26	4	CD	Active	69.96
5	UC	Active	52.04	5	CD	Active	67.11
6	UC	Active	51.25	6	CD	Active	63.94
7	UC	Active	50.68	7	CD	Active	62.00
8	UC	Active	48.32	8	CD	Active	60.98
9	UC	Active	47.31	9	CD	Active	60.01
10	UC	Active	46.39	10	CD	Active	59.44
11	UC	Active	46.29	11	CD	Active	55.74
12	UC	Active	44.02	12	CD	Active	55.51
13	UC	Active	43.79	13	CD	Active	54.34
14	UC	Active	43.75	14	CD	Inactive	48.80
15	UC	Active	43.32	15	CD	Active	48.42
16	UC	Active	42.77	16	CD	Active	47.71
17	UC	Inactive	40.81	17	CD	Inactive	45.01
18	UC	Inactive	40.62	18	CD	Inactive	44.41
19	UC	Active	40.45	19	CD	Inactive	42.11
20	UC	Inactive	39.67	20	CD	Inactive	41.43
21	UC	Active	39.64	21	CD	Inactive	40.03
22	UC	Inactive	37.80	22	CD	Inactive	38.54
23	UC	Active	36.65	23	CD	Active	37.01
24	UC	Active	36.08	24	CD	Active	36.96
25	UC	Inactive	35.55	25	CD	Inactive	36.72
26	UC	Inactive	33.06	26	CD	Inactive	35.99
27	UC	Active	31.96	27	CD	Active	35.51
28	UC	Inactive	31.09	28	CD	Inactive	34.24
29	UC	Inactive	31.03	29	CD	Active	33.79
30	UC	Inactive	30.22	30	CD	Inactive	30.18
31	UC	Inactive	27.61	31	CD	Inactive	29.92
32	UC	Inactive	27.06	32	CD	Inactive	29.33
33	UC	Inactive	26.30	33	CD	Inactive	29.29
34	UC	Inactive	23.46	34	CD	Inactive	28.70
35	UC	Inactive	22.55	35	CD	Active	28.46
36	UC	Inactive	21.13	36	CD	Inactive	27.74
37	UC	Inactive	20.32	37	CD	Active	25.81
38	UC	Inactive	18.08	38	CD	Inactive	24.35
39	UC	Inactive	14.71	39	CD	Inactive	22.92
				40	CD	Inactive	20.14

Figure C-7. Total scores for UC and CD patients based on VIP scores obtained from OPLS.

Calculation of Total Scores for UC and CD patients based on the top 4 UC VIP scores and the top 5 CD VIP scores. Calculated specificity for UC = 81.8% (Score >40) and CD = 87.5% (Score >47). Calculated sensitivity for UC = 84.2% (Score >40) and CD = 75% (Score >47).

Appendix D: Serum and kidney cytokine analysis of STX-expressing *Citrobacter rodentium*

Arek R. Raczynski¹, Katherine Schlieper¹, Steven R. Tannenbaum¹, David B. Schauer^{1,2}

¹Department of Biological Engineering, ²Division of Comparative Medicine, Massachusetts Institute of Technology, Cambridge, MA, USA

John Leong at UMass will use parts of this chapter towards publication.

D.1 Introduction

Citrobacter rodentium (*C. rodentium*) is an enteric bacterial pathogen that results in varying degrees of intestinal inflammation, acute colitis, hyperplasia, and edema in numerous strains of mice [74, 75]. As a human homolog of enteropathogenic *Escherichia coli* (*E. coli*) and enterohemorrhagic *E. coli* (EPEC and EHEC respectively), *C. rodentium* has become a highly utilized animal model of these human infections, providing a reproducible, robust, and physiologically relevant model of inflammation. However, only a subset of Shiga toxin (Stx)-producing *E. coli* (STEC) are human pathogens, resulting in hemorrhagic colitis and hemolytic uremic syndrome (HUS)[180]; a leading cause of acute renal failure in young children [181]. Currently the characteristics driving STEC pathogenicity are yet to be clearly understood and appropriate animal models are lacking.

Here we evaluated intimin-deficient and Stx-expressing *C. rodentium* strains in C57BL/6 mice. Animals were exposed to either sodium bicarbonate vehicle, DBS 807 (Trans Intimin 1), DBS 808 (Trans Intimin 2) DBS 806 (STX(+) strain), or DBS 771 (STX(-) control, non functional clone). Intimin is a virulence factor expressed on the surface of bacterial cells and binds to its receptor Tir (translocated intimin receptor) on colonic epithelial cells, an interaction that is critical for attaching and effacing (A/E) lesions, central to the pathogenesis of EPEC and EHEC (EHEC)-mediated diseases in humans and *Citrobacter rodentium* transmissible colonic hyperplasia in mice [98, 173, 174]. The aim of this study is to determine if a Stx-expressing strain of *C. rodentium* causes a pathogenic signature similar to that found with the human equivalent shigatoxin-expression EPEC and EHEC by measuring inflammatory markers in both circulating protein and kidney transcript levels.

D.2 Results

Luminex serum cytokine analysis

Serum samples collected 8 days post inoculation (DPI) for DBS 806 and DBS 771 (STX (+) and STX (-) strains) and 9 DPI for sodium bicarbonate, DBS 807 and DBS 808 (Intimin 1 and 2-deficient strains of WT *C. rodentium* respectively) were processed for Luminex multiplex detection of cytokine and chemokine levels. The discrepancy in time-point was due to animals demonstrating dehydration and severe body weight loss, particularly in the STX+ (DBS 806) cohort (data not shown). Multiplex analysis of 23 cytokine and chemokine targets (23-PLEX mouse panel, Bio-Rad) resulted in numerous targets demonstrating induction in the STX (+) strain as compared to the STX (-) control (**Figure D2-1**). KC and IL-10 were both elevated in STX (+) sera as compared to STX (-) controls ($p < 0.05$ and $p < 0.01$ respectively), while STX (-) animals demonstrated significantly higher levels of IL-12 (p40) and IL-13 ($p < 0.01$ and $p < 0.05$ respectively). Both strains had substantially higher levels of circulating granulocyte-stimulating factor (G-CSF) ($p < 0.001$) as compared to sodium bicarbonate controls and both demonstrated elevated levels of IL-6, however; only the STX (+) group reached statistical significance. IL-2 and MCP-1 also showed elevations in the STX (+) cohort but failed to reach statistical significance. Intimin deficient strains (DBS 807 and DBS 808) both failed to show statistically significant changes in systemic cytokine or chemokine levels as compared to the sodium bicarbonate control group at 9 DPI.

Expression of pro-inflammatory and immunomodulatory genes in C57BL/6 kidneys

Quantitative RT-PCR was performed on RNA isolated from kidney tissue to evaluate local expression of key pro-inflammatory (IL-1 β , IFN- γ , TNF- α), immune modulatory (IL-17), chemokines CCL2 (monocyte chemoattractant protein-1: MCP-1), CCL3 (macrophage-inflammatory protein 1-alpha: MIP-1a), CCL5 (regulated upon activation, normal T-cell expressed, and secreted: RANTES) and cytokines CXCL1 (neutrophil activating protein: KC), CXCL2 (macrophage inflammatory protein 2-alpha: MIP-2a) (**Figure D2-2**). Expression levels were assessed by one-way ANOVA ($p < 0.01$) followed by Tukey's multiple comparison tests. The presence of Shiga toxin resulted in significant elevations in kidney transcriptional levels for RANTES (CCL5) (3.6-fold, $p < 0.01$ compared to sodium bicarbonate only), TNF- α (5.2-fold, $p < 0.01$), KC (CXCL1) (122-fold, $p < 0.01$), and MIP-1a (CXCL2) (233-fold, $p < 0.01$). Levels of IL-17 were induced in STX (-) and STX (+) strains as compared to sodium bicarbonate controls (19 and 13.5-fold respectively), however, did not reach statistical significance. STX (+) infection was also associated with the down-regulation of IL-1 β , IFN- γ , and CCL3.

D.3 Discussion

The aim of this study was to determine if a Stx-expressing strain of *C. rodentium* causes a pathogenic signature similar to that found with the human equivalent shigatoxin-expression EPEC and EHEC by measuring inflammatory markers in both circulating protein and kidney transcript levels. Shiga toxin producing *E. coli*, such as O157:H7, have been found to induce hemorrhagic colitis and hemolytic uremic syndrome (HUS) in humans, the later characterized by systemic lysis of red blood cells and resultant glomerular dysfunction and acute renal failure in approximately 10% of infected individuals. The interaction of shiga toxin with host endothelium in brain, intestine, and kidney constitutes the majority of histological lesions observed in HUS[182]. Specifically, Stx2-producing *E. coli* strains are more commonly associated with HUS -associated pathology than Stx1-expressing strains [183].

HUS-like injury in C57BL/6 mice treated with STX-expressing *C. rodentium* was evaluated by measuring circulating levels of inflammatory mediators as well as kidney-specific transcriptional changes. Kidney mRNA were induced in STX (+) strain treated C57BL/6 mice at 9DPI in RANTES (CCL5), KC (CXCL1), MIP-2 (CXCL2), and TNF- α , indicating a pro-inflammatory state coupled with a local environment enhanced for recruitment of lymphocytes and activation of both macrophages and neutrophils. Kidney-specific changes were paralleled by serum elevations in KC; however, RANTES and TNF- α did not show statistically significant elevations in mice exposed to the STX (+) strain (circulating MIP-2a not measured). Treatment of human endothelial cells with Stx alone results in increased mRNA levels and protein expression of IL-8 (human analog of murine KC) [184, 185] and confirmed by microarray experiments in human endothelial cells to elucidate responses in gene regulation characteristic to both Stx1 and 2 strains [186]. Most of the genes regulated were for proteins associated with inflammatory responses such as chemokines (IL-8) and cytokines (granulocyte-macrophage colony-stimulating factor [GM-CSF]), findings in line with ours, indicating a contribution to HUS pathogenesis via recruitment of inflammatory cells in the kidney.

In a clinical evaluation of eleven patients with HUS and 9 patients with hemorrhagic colitis at the onset of *E. coli* O157:H7, Yamamoto et al reported significant elevations in serum IL-6 ($p < 0.01$), IL-8 ($p < 0.05$) (KC is the mouse homologue), IL-10 ($p < 0.001$), and endothelin ($p < 0.001$) in patients with HUS compared with those with colitis alone [187]. Here we have complete concordance in results from this clinical work. Inoculation of C57BL/6 mice with a Stx-expressing strain of *C. rodentium* appears to be a potentially useful animal model that mimics the clinically relevant parameters of HUS, furthermore, as a commonly used background for genetic modification, allows for investigation into the molecular mechanisms driving this major public health concern.

D.4 Selected Methods

Culture Preparations and Animal Infections

Specific pathogen free C57BL/6 mice were (The Jackson Laboratory, Bar Harbor, ME) were housed and maintained as described in Appendix A (General Methods). Infections were induced by intragastric inoculation with $\sim 1 \times 10^9$ CFU of DBS 806 (STX(+)), DBS 771 (STX(-)), DBS 807 (intimin 1 deficient), or DBS 808 (intimin 2 deficient) in 3% sodium bicarbonate (in PBS, pH 7.4) using a 100uL volume. DBS 806 and DBS 771 mice were sacrificed 8 DPI for harvesting of tissues and blood for serum collection. Control animals (sodium bicarbonate) and DBS 807 and DBS 808 were sacrificed 9 DPI animals and processed similarly to STX inoculated groups. All animals were monitored for fecal shedding and body weight changes as indicated and euthanized and necropsied at their respective timepoints as described in Appendix A.

Multiplex Detection of Serum Cytokines and Chemokines:

Mouse serum collected at necropsy was processed using mouse 23-plex cytokine panels (Bio-Rad, Hercules, CA) as specified by the manufacturer. Briefly, serum was diluted in species-specific sample diluent (1:4) and 50uL of sample or premixed standards were incubated with pre-washed target capture antibody-conjugated microspheres provided and incubated for 30 minutes with orbital shaking (300 rpm) in a 96-well plate. Upon washing, beads were incubated with detection antibody (30 min), washed, and subsequently incubated with streptavidin-PE (10 min). Beads were washed and resuspended with 125uL assay buffer and read on the Luminex 200 suspension array system using the low RP1 target setting (High PMT) for maximum sensitivity. Data analysis was carried out with the Bio-Plex Manager™ 5.0 software and cytokine or chemokine concentrations calculated against an 8 point standard curve generated by either 4PL or 5PL curve fitting.

Real-time quantitative RT-PCR. Total RNA was prepared from frozen kidney using Trizol reagent according to manufacturer recommendation (Invitrogen, Carlsbad, CA). cDNA was generated from five micrograms of total RNA using SuperScriptII RT (Invitrogen). One hundred nanograms of cDNA were amplified in a 25 μ l reaction volume with predesigned primers (Applied Biosystems, Branchburg, New Jersey, USA) and probes (TaqMan Gene Expression Assays) in an ABI Prism Sequence Detection System 7700 (Applied Biosystems, Branchburg, New Jersey, USA) using standard TaqMan protocols: IFN-g (Mm99999071_m1), IL-17 (Mm00439619_m1), TNF- α (Mm99999068_m1), CCL2 (Mm00441243_g1), IL-1 β (Mm00434228_m1), CCL3 (Mm00441258_m1), CCL5 (Mm01302428_m1), CXCL1 (Mm00433859_m1), CXCL2 (Mm00436450_m1), and glyceraldehyde-3-phosphate dehydrogenase (GAPDH) (Mm99999915_g1). Transcript levels were normalized to GAPDH, and expressed as fold change relative to averaged sodium bicarbonate (vehicle control) inoculated group, which were set at 1, using the Comparative Ct method (Applied Biosystems, User Bulletin no. 2). Reactions were carried out in duplicate.

D.5 Selected Figures

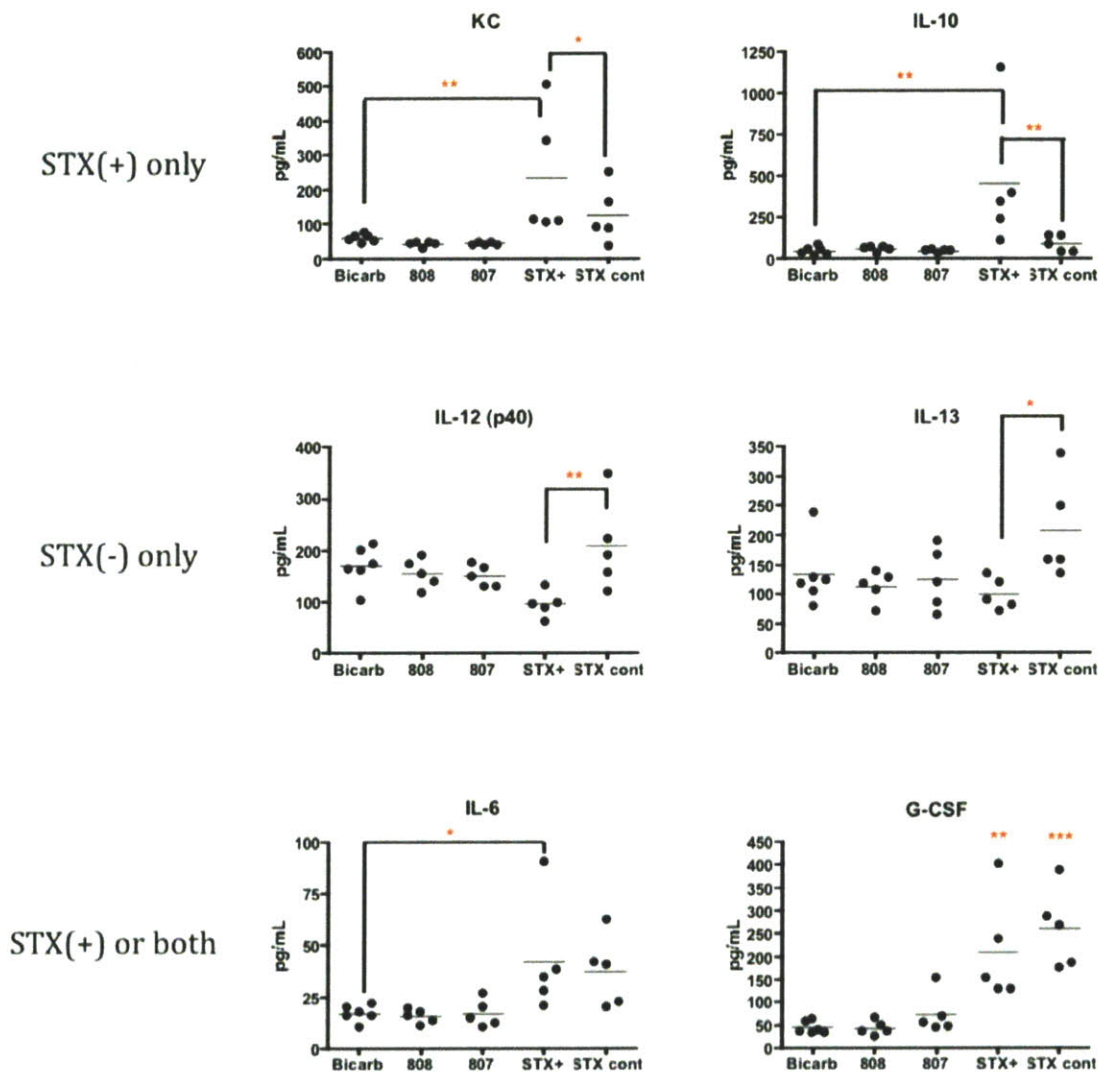


Figure D-1. Serum cytokine and chemokine changes in C57BL/6 mice exposed to intimin-deficient and STX-expressing *C. rodentium*

Serum cytokine and chemokine detection by Luminex at 8 DPI (sodium bicarbonate, DBS807, and DBS 808) and 9DPI (DBS 806 (STX+) and DBS 771 (STX-)). STX-expressing *C. rodentium* had elevated KC, IL-6, and IL-10, while STX controls demonstrated elevations in IL-12p40 and IL-13. Both STX(-) and STX(+) had significantly elevated circulating G-CSF ($p < 0.001$ and $p < 0.01$) as compared to sodium bicarbonate controls. No changes were observed with Intimin deficient strains DBS 807 and DBS 808. (One-way ANOVA with Newman Kleus post test: * $p < 0.05$, ** $p < 0.01$, *** $p < 0.001$).

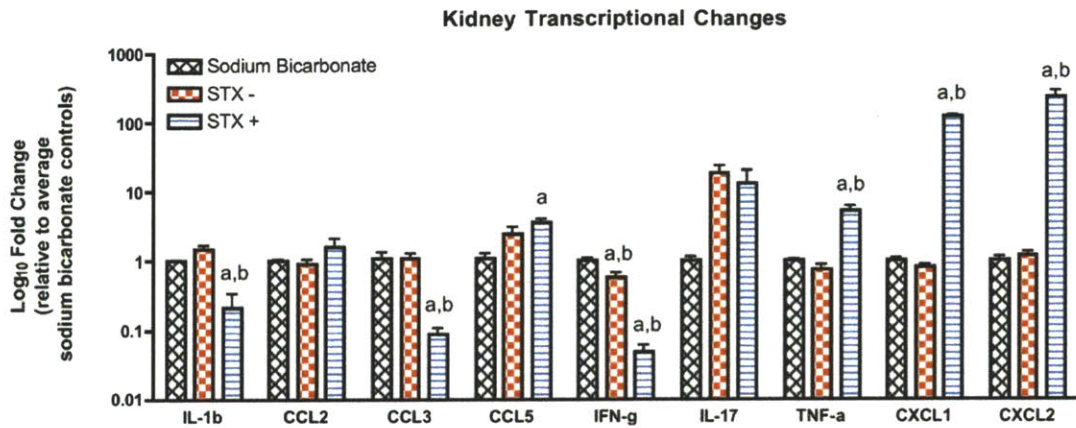


Figure D-2. Quantitative RT-PCR for expression of kidney cytokines and chemokines transcript in C57BL/6 mice inoculated with STX-expressing *C. rodentium*

Kidneys from STX+ treated C57BL/6 mice at 9 DPI demonstrated significantly elevated levels of TNF- α , CXCL1 (KC), and CXCL2 (MIP-2a), and depressed transcriptional levels of IL-1 β , CCL3, and IFN-g as compared to sodium bicarbonate controls and STX (-) deficient counterpart. Both STX(-) and STX(+) cohorts demonstrated elevations in IL-17 but failed to reach significance ($p < 0.01$ level). Top of bars represent means Log₁₀ fold change in expression relative to the average of sodium bicarbonate controls with standard error bars present. One-way ANOVA followed by Tukey's Multiple Comparison Test (**a** = $p < 0.01$ compared to sodium bicarbonate, **b** = $p < 0.01$ compared to STX(-) control).

Appendix E: Abbreviations

A/E:	Attaching and effacing
APAP:	Acetaminophen
ALP:	Alkaline phosphatase
ALT:	Alanine amino transferase
AST:	Aspartate amino transferase
CD:	Crohn's disease
CFU:	Colony forming unit
CITRO:	<i>Citrobacter rodentium</i>
CRP:	C-reactive protein
DAMP:	Damage-associated molecular pattern
DPI:	Days post inoculation
<i>E. coli</i>	<i>Escherichia coli</i>
EHEC:	Enterohemorarrhagic <i>Escherichia coli</i>
EPEC:	Enteropathogenic <i>Escherichia coli</i>
ESR:	Erythrocyte sedimentation rate
G-CSF:	Granulocyte stimulating factor
GM-CSF:	Granulocyte-macrophage colony-stimulating factor
H&E:	Hemotoxylin and eosin
IBD:	Inflammatory bowel disease
IFN-g:	Interferon gamma
LBP:	LPS-binding protein
LPS:	Lipopolysaccharide
MCP-1:	Monocyte chemotactic protein-1
MGH:	Massachusetts General Hospital
OPLS:	Orthogonormalized partial least squares
PAMP:	Pathogen-associated molecular pattern
PBS:	Phosphate buffered saline
PCA:	Principal components analysis
PLS-DA:	Partial least squares discriminate analysis
PLSR:	Partial least squares regression
RT-PCR:	Real-time reverse-transcriptase polymerase chain reaction
STAT:	Signal transducer and activator of transcription
STEC:	Shiga toxin (Stx)-producing <i>E. coli</i>
STX:	Shiga Toxin
Tir:	Translocated intimin receptor
TLR:	Toll-like receptor
TNF- α :	Tumor necrosis factor alpha
UC:	Ulcerative colitis
VIP:	Variable in projection

Appendix F: References

- [1] S. C. Segerstrom and G. E. Miller, "Psychological stress and the human immune system: a meta-analytic study of 30 years of inquiry," *Psychol Bull*, vol. 130, pp. 601-30, Jul 2004.
- [2] R. Medzhitov, "Origin and physiological roles of inflammation," *Nature*, vol. 454, pp. 428-35, Jul 24 2008.
- [3] G. W. Schmid-Schonbein, "Analysis of inflammation," *Annu Rev Biomed Eng*, vol. 8, pp. 93-131, 2006.
- [4] W. S. Garrett, J. I. Gordon, and L. H. Glimcher, "Homeostasis and inflammation in the intestine," *Cell*, vol. 140, pp. 859-70, Mar 19.
- [5] R. A. Roth, J. R. Harkema, J. P. Pestka, and P. E. Ganey, "Is exposure to bacterial endotoxin a determinant of susceptibility to intoxication from xenobiotic agents?," *Toxicol Appl Pharmacol*, vol. 147, pp. 300-11, Dec 1 1997.
- [6] R. A. Roth, J. P. Luyendyk, J. F. Maddox, and P. E. Ganey, "Inflammation and drug idiosyncrasy--is there a connection?," *J Pharmacol Exp Ther*, vol. 307, pp. 1-8, Oct 1 2003.
- [7] T. A. Richardson, M. Sherman, D. Kalman, and E. T. Morgan, "Expression of UDP-glucuronosyltransferase isoform mRNAs during inflammation and infection in mouse liver and kidney," *Drug Metab Dispos*, vol. 34, pp. 351-3, Mar 1 2006.
- [8] T. A. Richardson, M. Sherman, L. Antonovic, S. S. Kardar, H. W. Strobel, D. Kalman, and E. T. Morgan, "Hepatic and renal cytochrome p450 gene regulation during citrobacter rodentium infection in wild-type and toll-like receptor 4 mutant mice," *Drug Metab Dispos*, vol. 34, pp. 354-60, Mar 1 2006.
- [9] L. E. Kuo, J. B. Kitlinska, J. U. Tilan, L. Li, S. B. Baker, M. D. Johnson, E. W. Lee, M. S. Burnett, S. T. Fricke, R. Kvetnansky, H. Herzog, and Z. Zukowska, "Neuropeptide Y acts directly in the periphery on fat tissue and mediates stress-induced obesity and metabolic syndrome," *Nat Med*, vol. 13, pp. 803-11, Jul 1 2007.
- [10] S. Bhusari, Z. Liu, L. B. Hearne, D. E. Spiers, W. R. Lamberson, and E. Antoniou, "Expression profiling of heat stress effects on mice fed ergot alkaloids," *Toxicol Sci*, vol. 95, pp. 89-97, Jan 1 2007.
- [11] Y. Chida, N. Sudo, J. Sonoda, H. Sogawa, and C. Kubo, "Electric foot shock stress-induced exacerbation of alpha-galactosylceramide-triggered apoptosis in mouse liver," *Hepatology*, vol. 39, pp. 1131-40, Apr 1 2004.
- [12] S. Akira, S. Uematsu, and O. Takeuchi, "Pathogen recognition and innate immunity," *Cell*, vol. 124, pp. 783-801, Feb 24 2006.
- [13] M. S. Lee and Y.-J. Kim, "Signaling pathways downstream of pattern-recognition receptors and their cross talk," *Annu Rev Biochem*, vol. 76, pp. 447-80, Jan 1 2007.
- [14] C. van 't Veer, P. S. van den Pangaart, M. A. D. van Zoelen, M. de Kruif, R. S. Birjmohun, E. S. Stroes, A. F. de Vos, and T. van der Poll, "Induction of IRAK-M

- is associated with lipopolysaccharide tolerance in a human endotoxemia model," *J Immunol*, vol. 179, pp. 7110-20, Nov 15 2007.
- [15] J. C. Deng, G. Cheng, M. W. Newstead, X. Zeng, K. Kobayashi, R. A. Flavell, and T. J. Standiford, "Sepsis-induced suppression of lung innate immunity is mediated by IRAK-M," *J Clin Invest*, vol. 116, pp. 2532-42, Sep 1 2006.
- [16] H. B. Yu and B. B. Finlay, "The caspase-1 inflammasome: a pilot of innate immune responses," *Cell Host Microbe*, vol. 4, pp. 198-208, Sep 11 2008.
- [17] E. Meylan, J. Tschopp, and M. Karin, "Intracellular pattern recognition receptors in the host response," *Nature*, vol. 442, pp. 39-44, Jul 6 2006.
- [18] A. Piccini, S. Carta, S. Tassi, D. Lasiglié, G. Fossati, and A. Rubartelli, "ATP is released by monocytes stimulated with pathogen-sensing receptor ligands and induces IL-1beta and IL-18 secretion in an autocrine way," *Proc Natl Acad Sci USA*, vol. 105, pp. 8067-72, Jun 10 2008.
- [19] E. A. Miao, E. Andersen-Nissen, S. E. Warren, and A. Aderem, "TLR5 and Ipaf: dual sensors of bacterial flagellin in the innate immune system," *Semin Immunopathol*, vol. 29, pp. 275-88, Sep 2007.
- [20] M. T. Lotze and K. J. Tracey, "High-mobility group box 1 protein (HMGB1): nuclear weapon in the immune arsenal," *Nat Rev Immunol*, vol. 5, pp. 331-42, Apr 2005.
- [21] G. Y. Chen and G. Nunez, "Sterile inflammation: sensing and reacting to damage," *Nat Rev Immunol*, vol. 10, pp. 826-37, Dec.
- [22] C. Semino, G. Angelini, A. Poggi, and A. Rubartelli, "NK/iDC interaction results in IL-18 secretion by DCs at the synaptic cleft followed by NK cell activation and release of the DC maturation factor HMGB1," *Blood*, vol. 106, pp. 609-16, Jul 15 2005.
- [23] D. Tang, Y. Shi, R. Kang, T. Li, W. Xiao, H. Wang, and X. Xiao, "Hydrogen peroxide stimulates macrophages and monocytes to actively release HMGB1," *J Leukoc Biol*, vol. 81, pp. 741-7, Mar 2007.
- [24] V. Racanelli and B. Rehermann, "The liver as an immunological organ," *Hepatology*, vol. 43, pp. S54-62, Feb 2006.
- [25] T. Luedde, C. Liedtke, M. P. Manns, and C. Trautwein, "Losing balance: cytokine signaling and cell death in the context of hepatocyte injury and hepatic failure," *Eur Cytokine Netw*, vol. 13, pp. 377-83, Oct-Dec 2002.
- [26] C. A. Janeway, Jr. and R. Medzhitov, "Innate immune recognition," *Annu Rev Immunol*, vol. 20, pp. 197-216, 2002.
- [27] H. Malhi, G. J. Gores, and J. J. Lemasters, "Apoptosis and necrosis in the liver: a tale of two deaths?," *Hepatology*, vol. 43, pp. S31-44, Feb 2006.
- [28] L. Galluzzi and G. Kroemer, "Necroptosis: a specialized pathway of programmed necrosis," *Cell*, vol. 135, pp. 1161-3, Dec 26 2008.
- [29] B. D. Cosgrove, C. Cheng, J. R. Pritchard, D. B. Stolz, D. A. Lauffenburger, and L. G. Griffith, "An inducible autocrine cascade regulates rat hepatocyte proliferation and apoptosis responses to tumor necrosis factor-alpha," *Hepatology*, vol. 48, pp. 276-88, Jul 2008.
- [30] E. Seki, S. De Minicis, C. H. Osterreicher, J. Kluwe, Y. Osawa, D. A. Brenner, and R. F. Schwabe, "TLR4 enhances TGF-beta signaling and hepatic fibrosis," *Nat Med*, vol. 13, pp. 1324-32, Nov 2007.

- [31] R. Temple, "Hy's law: predicting serious hepatotoxicity," *Pharmacoepidemiol Drug Saf*, vol. 15, pp. 241-3, Apr 2006.
- [32] G. Ostapowicz, R. J. Fontana, F. V. Schiody, A. Larson, T. J. Davern, S. H. Han, T. M. McCashland, A. O. Shakil, J. E. Hay, L. Hynan, J. S. Crippin, A. T. Blei, G. Samuel, J. Reisch, and W. M. Lee, "Results of a prospective study of acute liver failure at 17 tertiary care centers in the United States," *Ann Intern Med*, vol. 137, pp. 947-54, Dec 17 2002.
- [33] J. Uetrecht, "Idiosyncratic drug reactions: past, present, and future," *Chem Res Toxicol*, vol. 21, pp. 84-92, Jan 2008.
- [34] N. Kaplowitz, "Idiosyncratic drug hepatotoxicity," *Nat Rev Drug Discov*, vol. 4, pp. 489-99, Jun 2005.
- [35] P. E. Ganey, J. P. Luyendyk, J. F. Maddox, and R. A. Roth, "Adverse hepatic drug reactions: inflammatory episodes as consequence and contributor," *Chem Biol Interact*, vol. 150, pp. 35-51, Nov 1 2004.
- [36] X. Deng, J. P. Luyendyk, P. E. Ganey, and R. A. Roth, "Inflammatory stress and idiosyncratic hepatotoxicity: hints from animal models," *Pharmacol Rev*, vol. 61, pp. 262-82, Sep 2009.
- [37] E. T. Morgan, K. B. Goralski, M. Piquette-Miller, K. W. Renton, G. R. Robertson, M. R. Chaluvadi, K. A. Charles, S. J. Clarke, M. Kacevska, C. Liddle, T. A. Richardson, R. Sharma, and C. J. Sinal, "Regulation of drug-metabolizing enzymes and transporters in infection, inflammation, and cancer," *Drug Metab Dispos*, vol. 36, pp. 205-16, Feb 2008.
- [38] W. M. Lee, "Acetaminophen toxicity: changing perceptions on a social/medical issue," *Hepatology*, vol. 46, pp. 966-70, Oct 2007.
- [39] K. K. Wolf, S. G. Wood, J. L. Allard, J. A. Hunt, N. Gorman, B. W. Walton-Strong, J. G. Szakacs, S. X. Duan, Q. Hao, M. H. Court, L. L. von Moltke, D. J. Greenblatt, V. Kostrubsky, E. H. Jeffery, S. A. Wrighton, F. J. Gonzalez, P. R. Sinclair, and J. F. Sinclair, "Role of CYP3A and CYP2E1 in alcohol-mediated increases in acetaminophen hepatotoxicity: comparison of wild-type and Cyp2e1(-/-) mice," *Drug Metab Dispos*, vol. 35, pp. 1223-31, Jul 2007.
- [40] C. Chen, G. E. Hennig, and J. E. Manautou, "Hepatobiliary excretion of acetaminophen glutathione conjugate and its derivatives in transport-deficient (TR-) hyperbilirubinemic rats," *Drug Metab Dispos*, vol. 31, pp. 798-804, Jun 2003.
- [41] P. J. Amar and E. R. Schiff, "Acetaminophen safety and hepatotoxicity--where do we go from here?," *Expert Opin Drug Saf*, vol. 6, pp. 341-55, Jul 2007.
- [42] H. Jaeschke and M. L. Bajt, "Intracellular signaling mechanisms of acetaminophen-induced liver cell death," *Toxicol Sci*, vol. 89, pp. 31-41, Jan 2006.
- [43] B. K. Gunawan, Z. X. Liu, D. Han, N. Hanawa, W. A. Gaarde, and N. Kaplowitz, "c-Jun N-terminal kinase plays a major role in murine acetaminophen hepatotoxicity," *Gastroenterology*, vol. 131, pp. 165-78, Jul 2006.
- [44] C. R. Weston and R. J. Davis, "The JNK signal transduction pathway," *Curr Opin Cell Biol*, vol. 19, pp. 142-9, Apr 2007.

- [45] S. Nemoto, K. Takeda, Z. X. Yu, V. J. Ferrans, and T. Finkel, "Role for mitochondrial oxidants as regulators of cellular metabolism," *Mol Cell Biol*, vol. 20, pp. 7311-8, Oct 2000.
- [46] Q. Zhou, P. Y. Lam, D. Han, and E. Cadenas, "c-Jun N-terminal kinase regulates mitochondrial bioenergetics by modulating pyruvate dehydrogenase activity in primary cortical neurons," *J Neurochem*, vol. 104, pp. 325-35, Jan 2008.
- [47] H. Nakagawa, S. Maeda, Y. Hikiba, T. Ohmae, W. Shibata, A. Yanai, K. Sakamoto, K. Ogura, T. Noguchi, M. Karin, H. Ichijo, and M. Omata, "Deletion of apoptosis signal-regulating kinase 1 attenuates acetaminophen-induced liver injury by inhibiting c-Jun N-terminal kinase activation," *Gastroenterology*, vol. 135, pp. 1311-21, Oct 2008.
- [48] S. B. Yee, M. Bourdi, M. J. Masson, and L. R. Pohl, "Hepatoprotective role of endogenous interleukin-13 in a murine model of acetaminophen-induced liver disease," *Chem Res Toxicol*, vol. 20, pp. 734-44, May 2007.
- [49] M. Bourdi, Y. Masubuchi, T. P. Reilly, H. R. Amouzadeh, J. L. Martin, J. W. George, A. G. Shah, and L. R. Pohl, "Protection against acetaminophen-induced liver injury and lethality by interleukin 10: role of inducible nitric oxide synthase," *Hepatology*, vol. 35, pp. 289-98, Feb 2002.
- [50] Y. Masubuchi, M. Bourdi, T. P. Reilly, M. L. Graf, J. W. George, and L. R. Pohl, "Role of interleukin-6 in hepatic heat shock protein expression and protection against acetaminophen-induced liver disease," *Biochem Biophys Res Commun*, vol. 304, pp. 207-12, Apr 25 2003.
- [51] T. P. Reilly, J. N. Brady, M. R. Marchick, M. Bourdi, J. W. George, M. F. Radonovich, C. A. Pise-Masison, and L. R. Pohl, "A protective role for cyclooxygenase-2 in drug-induced liver injury in mice," *Chem Res Toxicol*, vol. 14, pp. 1620-8, Dec 2001.
- [52] B. Hu and L. M. Colletti, "CXC receptor-2 knockout genotype increases X-linked inhibitor of apoptosis protein and protects mice from acetaminophen hepatotoxicity," *Hepatology*, vol. 52, pp. 691-702, Aug.
- [53] R. D. Goldin, I. D. Ratnayaka, C. S. Breach, I. N. Brown, and S. N. Wickramasinghe, "Role of macrophages in acetaminophen (paracetamol)-induced hepatotoxicity," *J Pathol*, vol. 179, pp. 432-5, Aug 1996.
- [54] C. Ju, T. P. Reilly, M. Bourdi, M. F. Radonovich, J. N. Brady, J. W. George, and L. R. Pohl, "Protective role of Kupffer cells in acetaminophen-induced hepatic injury in mice," *Chem Res Toxicol*, vol. 15, pp. 1504-13, Dec 2002.
- [55] M. Bourdi, D. P. Eiras, M. P. Holt, M. R. Webster, T. P. Reilly, K. D. Welch, and L. R. Pohl, "Role of IL-6 in an IL-10 and IL-4 double knockout mouse model uniquely susceptible to acetaminophen-induced liver injury," *Chem Res Toxicol*, vol. 20, pp. 208-16, Feb 2007.
- [56] M. P. Holt, L. Cheng, and C. Ju, "Identification and characterization of infiltrating macrophages in acetaminophen-induced liver injury," *J Leukoc Biol*, vol. 84, pp. 1410-21, Dec 2008.
- [57] H. C. Yohe, K. A. O'Hara, J. A. Hunt, T. J. Kitzmiller, S. G. Wood, J. L. Bement, W. J. Bement, J. G. Szakacs, S. A. Wrighton, J. M. Jacobs, V. Kostрубsky, P. R. Sinclair, and J. F. Sinclair, "Involvement of Toll-like receptor 4 in

- acetaminophen hepatotoxicity," *Am J Physiol Gastrointest Liver Physiol*, vol. 290, pp. G1269-79, Jun 2006.
- [58] J. Liu, L. E. Sendelbach, A. Parkinson, and C. D. Klaassen, "Endotoxin pretreatment protects against the hepatotoxicity of acetaminophen and carbon tetrachloride: role of cytochrome P450 suppression," *Toxicology*, vol. 147, pp. 167-76, Jul 5 2000.
- [59] G. L. Su, L. M. Hoesel, J. Bayliss, M. R. Hemmila, and S. C. Wang, "Lipopolysaccharide binding protein inhibitory peptide protects against acetaminophen-induced hepatotoxicity," *Am J Physiol Gastrointest Liver Physiol*, vol. 299, pp. G1319-25, Dec.
- [60] G. L. Su, K. Q. Gong, M. H. Fan, W. M. Kelley, J. Hsieh, J. M. Sun, M. R. Hemmila, S. Arbabi, D. G. Remick, and S. C. Wang, "Lipopolysaccharide-binding protein modulates acetaminophen-induced liver injury in mice," *Hepatology*, vol. 41, pp. 187-95, Jan 2005.
- [61] E. Hailman, H. S. Lichenstein, M. M. Wurfel, D. S. Miller, D. A. Johnson, M. Kelley, L. A. Busse, M. M. Zukowski, and S. D. Wright, "Lipopolysaccharide (LPS)-binding protein accelerates the binding of LPS to CD14," *J Exp Med*, vol. 179, pp. 269-77, Jan 1 1994.
- [62] J. F. Maddox, C. J. Amuzie, M. Li, S. W. Newport, E. Sparckenbaugh, C. F. Cuff, J. J. Pestka, G. H. Cantor, R. A. Roth, and P. E. Ganey, "Bacterial- and viral-induced inflammation increases sensitivity to acetaminophen hepatotoxicity," *J Toxicol Environ Health A*, vol. 73, pp. 58-73.
- [63] A. B. Imaeda, A. Watanabe, M. A. Sohail, S. Mahmood, M. Mohamadnejad, F. S. Sutterwala, R. A. Flavell, and W. Z. Mehal, "Acetaminophen-induced hepatotoxicity in mice is dependent on Tlr9 and the Nalp3 inflammasome," *J Clin Invest*, vol. 119, pp. 305-14, Feb 2009.
- [64] M. Enari, H. Sakahira, H. Yokoyama, K. Okawa, A. Iwamatsu, and S. Nagata, "A caspase-activated DNase that degrades DNA during apoptosis, and its inhibitor ICAD," *Nature*, vol. 391, pp. 43-50, Jan 1 1998.
- [65] S. Huck, E. Deveaud, A. Namane, and M. Zouali, "Abnormal DNA methylation and deoxycytosine-deoxyguanine content in nucleosomes from lymphocytes undergoing apoptosis," *FASEB J*, vol. 13, pp. 1415-22, Aug 1999.
- [66] J. Lunec, K. Herbert, S. Blount, H. R. Griffiths, and P. Emery, "8-Hydroxydeoxyguanosine. A marker of oxidative DNA damage in systemic lupus erythematosus," *FEBS Lett*, vol. 348, pp. 131-8, Jul 11 1994.
- [67] I. R. Rifkin, E. A. Leadbetter, L. Busconi, G. Viglianti, and A. Marshak-Rothstein, "Toll-like receptors, endogenous ligands, and systemic autoimmune disease," *Immunol Rev*, vol. 204, pp. 27-42, Apr 2005.
- [68] J. P. Luyendyk, J. F. Maddox, C. D. Green, P. E. Ganey, and R. A. Roth, "Role of hepatic fibrin in idiosyncrasy-like liver injury from lipopolysaccharide-ranitidine coexposure in rats," *Hepatology*, vol. 40, pp. 1342-51, Dec 2004.
- [69] P. J. Shaw, M. J. Hopfensperger, P. E. Ganey, and R. A. Roth, "Lipopolysaccharide and trovafloxacin coexposure in mice causes idiosyncrasy-like liver injury dependent on tumor necrosis factor-alpha," *Toxicol Sci*, vol. 100, pp. 259-66, Nov 2007.

- [70] F. F. Tukov, J. P. Luyendyk, P. E. Ganey, and R. A. Roth, "The role of tumor necrosis factor alpha in lipopolysaccharide/ranitidine-induced inflammatory liver injury," *Toxicol Sci*, vol. 100, pp. 267-80, Nov 2007.
- [71] P. J. Shaw, P. E. Ganey, and R. A. Roth, "Tumor necrosis factor alpha is a proximal mediator of synergistic hepatotoxicity from trovafloxacin/lipopolysaccharide coexposure," *J Pharmacol Exp Ther*, vol. 328, pp. 62-8, Jan 2009.
- [72] X. Deng, J. P. Luyendyk, W. Zou, J. Lu, E. Malle, P. E. Ganey, and R. A. Roth, "Neutrophil interaction with the hemostatic system contributes to liver injury in rats cotreated with lipopolysaccharide and ranitidine," *J Pharmacol Exp Ther*, vol. 322, pp. 852-61, Aug 2007.
- [73] J. P. Luyendyk, P. J. Shaw, C. D. Green, J. F. Maddox, P. E. Ganey, and R. A. Roth, "Coagulation-mediated hypoxia and neutrophil-dependent hepatic injury in rats given lipopolysaccharide and ranitidine," *J Pharmacol Exp Ther*, vol. 314, pp. 1023-31, Sep 2005.
- [74] R. Mundy, T. T. MacDonald, G. Dougan, G. Frankel, and S. Wiles, "Citrobacter rodentium of mice and man," *Cell Microbiol*, vol. 7, pp. 1697-706, Dec 2005.
- [75] D. Borenshtein, M. E. McBee, and D. B. Schauer, "Utility of the Citrobacter rodentium infection model in laboratory mice," *Curr Opin Gastroenterol*, vol. 24, pp. 32-7, Jan 2008.
- [76] S. A. Luperchio and D. B. Schauer, "Molecular pathogenesis of Citrobacter rodentium and transmissible murine colonic hyperplasia," *Microbes Infect*, vol. 3, pp. 333-40, Apr 2001.
- [77] M. R. Chaluvadi, R. D. Kinloch, B. A. Nyagode, T. A. Richardson, M. J. Raynor, M. Sherman, L. Antonovic, H. W. Strobel, D. L. Dillehay, and E. T. Morgan, "Regulation of hepatic cytochrome P450 expression in mice with intestinal or systemic infections of citrobacter rodentium," *Drug Metab Dispos*, vol. 37, pp. 366-74, Feb 2009.
- [78] G. Son, M. Kremer, and I. N. Hines, "Contribution of gut bacteria to liver pathobiology," *Gastroenterol Res Pract*, vol. 2010.
- [79] N. Kaplowitz, "Acetaminophen hepatotoxicity: what do we know, what don't we know, and what do we do next?," *Hepatology*, vol. 40, pp. 23-6, Jul 2004.
- [80] C. J. Henderson, C. R. Wolf, N. Kitteringham, H. Powell, D. Otto, and B. K. Park, "Increased resistance to acetaminophen hepatotoxicity in mice lacking glutathione S-transferase Pi," *Proc Natl Acad Sci U S A*, vol. 97, pp. 12741-5, Nov 7 2000.
- [81] S. S. Lee, J. T. Buters, T. Pineau, P. Fernandez-Salguero, and F. J. Gonzalez, "Role of CYP2E1 in the hepatotoxicity of acetaminophen," *J Biol Chem*, vol. 271, pp. 12063-7, May 17 1996.
- [82] Y. Ishida, T. Kondo, T. Ohshima, H. Fujiwara, Y. Iwakura, and N. Mukaida, "A pivotal involvement of IFN-gamma in the pathogenesis of acetaminophen-induced acute liver injury," *FASEB J*, vol. 16, pp. 1227-36, Aug 2002.
- [83] D. M. Dambach, L. M. Watson, K. R. Gray, S. K. Durham, and D. L. Laskin, "Role of CCR2 in macrophage migration into the liver during acetaminophen-induced hepatotoxicity in the mouse," *Hepatology*, vol. 35, pp. 1093-103, May 2002.

- [84] C. M. Hogaboam, C. L. Bone-Larson, M. L. Steinhauser, A. Matsukawa, J. Gosling, L. Boring, I. F. Charo, K. J. Simpson, N. W. Lukacs, and S. L. Kunkel, "Exaggerated hepatic injury due to acetaminophen challenge in mice lacking C-C chemokine receptor 2," *Am J Pathol*, vol. 156, pp. 1245-52, Apr 2000.
- [85] Z. X. Liu, S. Govindarajan, and N. Kaplowitz, "Innate immune system plays a critical role in determining the progression and severity of acetaminophen hepatotoxicity," *Gastroenterology*, vol. 127, pp. 1760-74, Dec 2004.
- [86] C. M. Hogaboam, K. J. Simpson, S. W. Chensue, M. L. Steinhauser, N. W. Lukacs, J. Gauldie, R. M. Strieter, and S. L. Kunkel, "Macrophage inflammatory protein-2 gene therapy attenuates adenovirus- and acetaminophen-mediated hepatic injury," *Gene Ther*, vol. 6, pp. 573-84, Apr 1999.
- [87] S. Choi and A. M. Diehl, "Role of inflammation in nonalcoholic steatohepatitis," *Curr Opin Gastroenterol*, vol. 21, pp. 702-7, Nov 2005.
- [88] H. Tilg and A. R. Moschen, "Evolution of inflammation in nonalcoholic fatty liver disease: the multiple parallel hits hypothesis," *Hepatology*, vol. 52, pp. 1836-46, Nov.
- [89] S. Wiles, S. Clare, J. Harker, A. Huett, D. Young, G. Dougan, and G. Frankel, "Organ specificity, colonization and clearance dynamics in vivo following oral challenges with the murine pathogen *Citrobacter rodentium*," *Cell Microbiol*, vol. 6, pp. 963-72, Oct 2004.
- [90] B. A. Vallance, W. Deng, K. Jacobson, and B. B. Finlay, "Host susceptibility to the attaching and effacing bacterial pathogen *Citrobacter rodentium*," *Infect Immun*, vol. 71, pp. 3443-53, Jun 2003.
- [91] M. E. McBee, P. Z. Zheng, A. B. Rogers, J. G. Fox, and D. B. Schauer, "Modulation of acute diarrheal illness by persistent bacterial infection," *Infect Immun*, vol. 76, pp. 4851-8, Nov 2008.
- [92] Y. Zheng, P. A. Valdez, D. M. Danilenko, Y. Hu, S. M. Sa, Q. Gong, A. R. Abbas, Z. Modrusan, N. Ghilardi, F. J. de Sauvage, and W. Ouyang, "Interleukin-22 mediates early host defense against attaching and effacing bacterial pathogens," *Nat Med*, vol. 14, pp. 282-9, Mar 2008.
- [93] L. M. Higgins, G. Frankel, G. Douce, G. Dougan, and T. T. MacDonald, "Citrobacter rodentium infection in mice elicits a mucosal Th1 cytokine response and lesions similar to those in murine inflammatory bowel disease," *Infect Immun*, vol. 67, pp. 3031-9, Jun 1999.
- [94] M. E. McBee, Y. Zeng, N. Parry, C. R. Nagler, S. R. Tannenbaum, and D. B. Schauer, "Multivariate modeling identifies neutrophil- and Th17-related factors as differential serum biomarkers of chronic murine colitis," *PLoS One*, vol. 5, p. e13277.
- [95] P. A. Thompson, K. C. Gauthier, A. W. Varley, and R. L. Kitchens, "ABCA1 promotes the efflux of bacterial LPS from macrophages and accelerates recovery from LPS-induced tolerance," *J Lipid Res*, vol. 51, pp. 2672-85, Sep.
- [96] E. A. Deitch, R. Berg, and R. Specian, "Endotoxin promotes the translocation of bacteria from the gut," *Arch Surg*, vol. 122, pp. 185-90, Feb 1987.
- [97] S. Asfaha, W. K. MacNaughton, C. B. Appleyard, K. Chadee, and J. L. Wallace, "Persistent epithelial dysfunction and bacterial translocation after resolution

- of intestinal inflammation," *Am J Physiol Gastrointest Liver Physiol*, vol. 281, pp. G635-44, Sep 2001.
- [98] M. Ghaem-Maghami, C. P. Simmons, S. Daniell, M. Pizza, D. Lewis, G. Frankel, and G. Dougan, "Intimin-specific immune responses prevent bacterial colonization by the attaching-effacing pathogen *Citrobacter rodentium*," *Infect Immun*, vol. 69, pp. 5597-605, Sep 2001.
- [99] A. N. Flynn and A. G. Buret, "Tight junctional disruption and apoptosis in an in vitro model of *Citrobacter rodentium* infection," *Microb Pathog*, vol. 45, pp. 98-104, Aug 2008.
- [100] Q. Zhang, Q. Li, C. Wang, X. Liu, N. Li, and J. Li, "Enteropathogenic *Escherichia coli* changes distribution of occludin and ZO-1 in tight junction membrane microdomains in vivo," *Microb Pathog*, vol. 48, pp. 28-34, Jan.
- [101] S. A. Jones, "Directing transition from innate to acquired immunity: defining a role for IL-6," *J Immunol*, vol. 175, pp. 3463-8, Sep 15 2005.
- [102] R. M. McLoughlin, J. Witowski, R. L. Robson, T. S. Wilkinson, S. M. Hurst, A. S. Williams, J. D. Williams, S. Rose-John, S. A. Jones, and N. Topley, "Interplay between IFN-gamma and IL-6 signaling governs neutrophil trafficking and apoptosis during acute inflammation," *J Clin Invest*, vol. 112, pp. 598-607, Aug 2003.
- [103] C. A. Fielding, R. M. McLoughlin, L. McLeod, C. S. Colmont, M. Najdovska, D. Grail, M. Ernst, S. A. Jones, N. Topley, and B. J. Jenkins, "IL-6 regulates neutrophil trafficking during acute inflammation via STAT3," *J Immunol*, vol. 181, pp. 2189-95, Aug 1 2008.
- [104] D. Feng, Y. Wang, Y. Xu, Q. Luo, B. Lan, and L. Xu, "Interleukin 10 deficiency exacerbates halothane induced liver injury by increasing interleukin 8 expression and neutrophil infiltration," *Biochem Pharmacol*, vol. 77, pp. 277-84, Jan 15 2009.
- [105] M. E. Fuentes, S. K. Durham, M. R. Swerdel, A. C. Lewin, D. S. Barton, J. R. Megill, R. Bravo, and S. A. Lira, "Controlled recruitment of monocytes and macrophages to specific organs through transgenic expression of monocyte chemoattractant protein-1," *J Immunol*, vol. 155, pp. 5769-76, Dec 15 1995.
- [106] N. Hanawa, M. Shinohara, B. Saberi, W. A. Gaarde, D. Han, and N. Kaplowitz, "Role of JNK translocation to mitochondria leading to inhibition of mitochondria bioenergetics in acetaminophen-induced liver injury," *J Biol Chem*, vol. 283, pp. 13565-77, May 16 2008.
- [107] Z. X. Liu, D. Han, B. Gunawan, and N. Kaplowitz, "Neutrophil depletion protects against murine acetaminophen hepatotoxicity," *Hepatology*, vol. 43, pp. 1220-30, Jun 2006.
- [108] J. A. Lawson, A. Farhood, R. D. Hopper, M. L. Bajt, and H. Jaeschke, "The hepatic inflammatory response after acetaminophen overdose: role of neutrophils," *Toxicol Sci*, vol. 54, pp. 509-16, Apr 2000.
- [109] L. P. James, P. M. Simpson, H. C. Farrar, G. L. Kearns, G. S. Wasserman, J. L. Blumer, M. D. Reed, J. E. Sullivan, and J. A. Hinson, "Cytokines and toxicity in acetaminophen overdose," *J Clin Pharmacol*, vol. 45, pp. 1165-71, Oct 2005.

- [110] R. Steuer, J. Kurths, C. O. Daub, J. Weise, and J. Selbig, "The mutual information: detecting and evaluating dependencies between variables," *Bioinformatics*, vol. 18 Suppl 2, pp. S231-40, 2002.
- [111] F. Bertuzzi, S. Marzorati, P. Maffi, L. Piemonti, R. Melzi, F. de Taddeo, V. Valtolina, A. D'Angelo, V. di Carlo, E. Bonifacio, and A. Secchi, "Tissue factor and CCL2/monocyte chemoattractant protein-1 released by human islets affect islet engraftment in type 1 diabetic recipients," *J Clin Endocrinol Metab*, vol. 89, pp. 5724-8, Nov 2004.
- [112] A. Kato, H. Yoshidome, M. J. Edwards, and A. B. Lentsch, "Reduced hepatic ischemia/reperfusion injury by IL-4: potential anti-inflammatory role of STAT6," *Inflamm Res*, vol. 49, pp. 275-9, Jun 2000.
- [113] B. Jaruga, F. Hong, R. Sun, S. Radaeva, and B. Gao, "Crucial role of IL-4/STAT6 in T cell-mediated hepatitis: up-regulating eotaxins and IL-5 and recruiting leukocytes," *J Immunol*, vol. 171, pp. 3233-44, Sep 15 2003.
- [114] S. Higuchi, M. Kobayashi, Y. Yoshikawa, K. Tsuneyama, T. Fukami, M. Nakajima, and T. Yokoi, "IL-4 mediates dicloxacillin-induced liver injury in mice," *Toxicol Lett*, vol. 200, pp. 139-45, Feb 5.
- [115] D. B. Njoku, Z. Li, N. D. Washington, J. L. Mellerson, M. V. Talor, R. Sharma, and N. R. Rose, "Suppressive and pro-inflammatory roles for IL-4 in the pathogenesis of experimental drug-induced liver injury," *Eur J Immunol*, vol. 39, pp. 1652-63, Jun 2009.
- [116] F. Lafdil, H. Wang, O. Park, W. Zhang, Y. Moritoki, S. Yin, X. Y. Fu, M. E. Gershwin, Z. X. Lian, and B. Gao, "Myeloid STAT3 inhibits T cell-mediated hepatitis by regulating T helper 1 cytokine and interleukin-17 production," *Gastroenterology*, vol. 137, pp. 2125-35 e1-2, Dec 2009.
- [117] D. J. Antoine, A. E. Mercer, D. P. Williams, and B. K. Park, "Mechanism-based bioanalysis and biomarkers for hepatic chemical stress," *Xenobiotica*, vol. 39, pp. 565-77, Aug 2009.
- [118] J. Ozer, M. Ratner, M. Shaw, W. Bailey, and S. Schomaker, "The current state of serum biomarkers of hepatotoxicity," *Toxicology*, vol. 245, pp. 194-205, Mar 20 2008.
- [119] H. G. Lavery, D. J. Antoine, C. Benson, M. Chaponda, D. Williams, and B. Kevin Park, "The potential of cytokines as safety biomarkers for drug-induced liver injury," *Eur J Clin Pharmacol*, vol. 66, pp. 961-76, Oct.
- [120] Y. Masubuchi, S. Sugiyama, and T. Horie, "Th1/Th2 cytokine balance as a determinant of acetaminophen-induced liver injury," *Chem Biol Interact*, vol. 179, pp. 273-9, May 15 2009.
- [121] H. Kono and K. L. Rock, "How dying cells alert the immune system to danger," *Nat Rev Immunol*, vol. 8, pp. 279-89, Apr 2008.
- [122] A. Tsung, R. Sahai, H. Tanaka, A. Nakao, M. P. Fink, M. T. Lotze, H. Yang, J. Li, K. J. Tracey, D. A. Geller, and T. R. Billiar, "The nuclear factor HMGB1 mediates hepatic injury after murine liver ischemia-reperfusion," *J Exp Med*, vol. 201, pp. 1135-43, Apr 4 2005.
- [123] H. Jaeschke, "Mechanisms of Liver Injury. II. Mechanisms of neutrophil-induced liver cell injury during hepatic ischemia-reperfusion and other acute

- inflammatory conditions," *Am J Physiol Gastrointest Liver Physiol*, vol. 290, pp. G1083-8, Jun 2006.
- [124] R. Beasley, T. Clayton, J. Crane, E. von Mutius, C. K. Lai, S. Montefort, and A. Stewart, "Association between paracetamol use in infancy and childhood, and risk of asthma, rhinoconjunctivitis, and eczema in children aged 6-7 years: analysis from Phase Three of the ISAAC programme," *Lancet*, vol. 372, pp. 1039-48, Sep 20 2008.
- [125] J. Punnonen, R. de Waal Malefyt, P. van Vlasselaer, J. F. Gauchat, and J. E. de Vries, "IL-10 and viral IL-10 prevent IL-4-induced IgE synthesis by inhibiting the accessory cell function of monocytes," *J Immunol*, vol. 151, pp. 1280-9, Aug 1 1993.
- [126] C. Ratthe, J. Ennaciri, D. M. Garces Goncalves, S. Chiasson, and D. Girard, "Interleukin (IL)-4 induces leukocyte infiltration in vivo by an indirect mechanism," *Mediators Inflamm*, vol. 2009, p. 193970, 2009.
- [127] W. J. Karpus, N. W. Lukacs, K. J. Kennedy, W. S. Smith, S. D. Hurst, and T. A. Barrett, "Differential CC chemokine-induced enhancement of T helper cell cytokine production," *J Immunol*, vol. 158, pp. 4129-36, May 1 1997.
- [128] C. M. Hogaboam, N. W. Lukacs, S. W. Chensue, R. M. Strieter, and S. L. Kunkel, "Monocyte chemoattractant protein-1 synthesis by murine lung fibroblasts modulates CD4+ T cell activation," *J Immunol*, vol. 160, pp. 4606-14, May 1 1998.
- [129] Y. W. Lee, W. H. Lee, and P. H. Kim, "Oxidative mechanisms of IL-4-induced IL-6 expression in vascular endothelium," *Cytokine*, vol. 49, pp. 73-9, Jan.
- [130] Y. W. Lee, B. Hennig, and M. Toborek, "Redox-regulated mechanisms of IL-4-induced MCP-1 expression in human vascular endothelial cells," *Am J Physiol Heart Circ Physiol*, vol. 284, pp. H185-92, Jan 2003.
- [131] L. P. James, L. W. Lamps, S. McCullough, and J. A. Hinson, "Interleukin 6 and hepatocyte regeneration in acetaminophen toxicity in the mouse," *Biochem Biophys Res Commun*, vol. 309, pp. 857-63, Oct 3 2003.
- [132] D. B. Douglas, D. P. Beiting, J. P. Loftus, J. A. Appleton, and S. K. Bliss, "Combinatorial effects of interleukin 10 and interleukin 4 determine the progression of hepatic inflammation following murine enteric parasitic infection," *Hepatology*, vol. 51, pp. 2162-71, Jun.
- [133] M. Saraiva and A. O'Garra, "The regulation of IL-10 production by immune cells," *Nat Rev Immunol*, vol. 10, pp. 170-81, Mar.
- [134] S. Mukherjee, L. Y. Chen, T. J. Papadimos, S. Huang, B. L. Zuraw, and Z. K. Pan, "Lipopolysaccharide-driven Th2 cytokine production in macrophages is regulated by both MyD88 and TRAM," *J Biol Chem*, vol. 284, pp. 29391-8, Oct 23 2009.
- [135] D. M. Dambach, S. K. Durham, J. D. Laskin, and D. L. Laskin, "Distinct roles of NF-kappaB p50 in the regulation of acetaminophen-induced inflammatory mediator production and hepatotoxicity," *Toxicol Appl Pharmacol*, vol. 211, pp. 157-65, Mar 1 2006.
- [136] Y. Getachew, L. James, W. M. Lee, D. L. Thiele, and B. C. Miller, "Susceptibility to acetaminophen (APAP) toxicity unexpectedly is decreased during acute viral hepatitis in mice," *Biochem Pharmacol*, vol. 79, pp. 1363-71, May 1.

- [137] B. McDonald, K. Pittman, G. B. Menezes, S. A. Hirota, I. Slaba, C. C. Waterhouse, P. L. Beck, D. A. Muruve, and P. Kubes, "Intravascular danger signals guide neutrophils to sites of sterile inflammation," *Science*, vol. 330, pp. 362-6, Oct 15.
- [138] B. V. Martin-Murphy, M. P. Holt, and C. Ju, "The role of damage associated molecular pattern molecules in acetaminophen-induced liver injury in mice," *Toxicol Lett*, vol. 192, pp. 387-94, Feb 15.
- [139] G. Trinchieri, S. Pflanz, and R. A. Kastelein, "The IL-12 family of heterodimeric cytokines: new players in the regulation of T cell responses," *Immunity*, vol. 19, pp. 641-4, Nov 2003.
- [140] G. Trinchieri, "Interleukin-12 and the regulation of innate resistance and adaptive immunity," *Nat Rev Immunol*, vol. 3, pp. 133-46, Feb 2003.
- [141] S. J. Ha, C. H. Lee, S. B. Lee, C. M. Kim, K. L. Jang, H. S. Shin, and Y. C. Sung, "A novel function of IL-12p40 as a chemotactic molecule for macrophages," *J Immunol*, vol. 163, pp. 2902-8, Sep 1 1999.
- [142] T. D. Russell, Q. Yan, G. Fan, A. P. Khalifah, D. K. Bishop, S. L. Brody, and M. J. Walter, "IL-12 p40 homodimer-dependent macrophage chemotaxis and respiratory viral inflammation are mediated through IL-12 receptor beta 1," *J Immunol*, vol. 171, pp. 6866-74, Dec 15 2003.
- [143] A. Lemmers, C. Moreno, T. Gustot, R. Marechal, D. Degre, P. Demetter, P. de Nadai, A. Geerts, E. Quertinmont, V. Vercruysse, O. Le Moine, and J. Deviere, "The interleukin-17 pathway is involved in human alcoholic liver disease," *Hepatology*, vol. 49, pp. 646-57, Feb 2009.
- [144] Y. Yasumi, Y. Takikawa, R. Endo, and K. Suzuki, "Interleukin-17 as a new marker of severity of acute hepatic injury," *Hepatol Res*, vol. 37, pp. 248-54, Apr 2007.
- [145] D. Borenshtein, P. R. Nambiar, E. B. Groff, J. G. Fox, and D. B. Schauer, "Development of fatal colitis in FVB mice infected with *Citrobacter rodentium*," *Infect Immun*, vol. 75, pp. 3271-81, Jul 2007.
- [146] B. J. Frey and D. Dueck, "Clustering by passing messages between data points," *Science*, vol. 315, pp. 972-6, Feb 16 2007.
- [147] S. Jaisue, J. P. Gerber, and A. K. Davey, "Pharmacokinetics of fexofenadine following LPS administration to rats," *Xenobiotica*, vol. 40, pp. 743-50, Nov.
- [148] M. Achira, R. Totsuka, and T. Kume, "Differences in pharmacokinetics and hepatobiliary transport of a novel anti-inflammatory agent between normal and adjuvant arthritis rats," *Xenobiotica*, vol. 32, pp. 1139-49, Dec 2002.
- [149] B. A. Nyagode, C. M. Lee, and E. T. Morgan, "Modulation of hepatic cytochrome P450s by *Citrobacter rodentium* infection in interleukin-6- and interferon- γ -null mice," *J Pharmacol Exp Ther*, vol. 335, pp. 480-8, Nov.
- [150] N. Petri, C. Tannergren, D. Rungstad, and H. Lennernas, "Transport characteristics of fexofenadine in the Caco-2 cell model," *Pharm Res*, vol. 21, pp. 1398-404, Aug 2004.
- [151] S. Drescher, E. Schaeffeler, M. Hitzl, U. Hofmann, M. Schwab, U. Brinkmann, M. Eichelbaum, and M. F. Fromm, "MDR1 gene polymorphisms and disposition of the P-glycoprotein substrate fexofenadine," *Br J Clin Pharmacol*, vol. 53, pp. 526-34, May 2002.

- [152] H. Tahara, H. Kusuhara, E. Fuse, and Y. Sugiyama, "P-glycoprotein plays a major role in the efflux of fexofenadine in the small intestine and blood-brain barrier, but only a limited role in its biliary excretion," *Drug Metab Dispos*, vol. 33, pp. 963-8, Jul 2005.
- [153] M. Shimizu, K. Fuse, K. Okudaira, R. Nishigaki, K. Maeda, H. Kusuhara, and Y. Sugiyama, "Contribution of OATP (organic anion-transporting polypeptide) family transporters to the hepatic uptake of fexofenadine in humans," *Drug Metab Dispos*, vol. 33, pp. 1477-81, Oct 2005.
- [154] PhysiciansDeskReference, "PDR guide to drug interactions, side effects, and indications," Montvale, NJ: Thomson PDR, 2006, p. v.
- [155] Y. Tanigawara, N. Okamura, M. Hirai, M. Yasuhara, K. Ueda, N. Kioka, T. Komano, and R. Hori, "Transport of digoxin by human P-glycoprotein expressed in a porcine kidney epithelial cell line (LLC-PK1)," *J Pharmacol Exp Ther*, vol. 263, pp. 840-5, Nov 1992.
- [156] C. Verstuyft, M. Schwab, E. Schaeffeler, R. Kerb, U. Brinkmann, P. Jaillon, C. Funck-Brentano, and L. Becquemont, "Digoxin pharmacokinetics and MDR1 genetic polymorphisms," *Eur J Clin Pharmacol*, vol. 58, pp. 809-12, Apr 2003.
- [157] M. Tanabe, I. Ieiri, N. Nagata, K. Inoue, S. Ito, Y. Kanamori, M. Takahashi, Y. Kurata, J. Kigawa, S. Higuchi, N. Terakawa, and K. Otsubo, "Expression of P-glycoprotein in human placenta: relation to genetic polymorphism of the multidrug resistance (MDR)-1 gene," *J Pharmacol Exp Ther*, vol. 297, pp. 1137-43, Jun 2001.
- [158] D. F. Lewis, "Human cytochromes P450 associated with the phase 1 metabolism of drugs and other xenobiotics: a compilation of substrates and inhibitors of the CYP1, CYP2 and CYP3 families," *Curr Med Chem*, vol. 10, pp. 1955-72, Oct 2003.
- [159] F. P. Guengerich, "Cytochrome P-450 3A4: regulation and role in drug metabolism," *Annu Rev Pharmacol Toxicol*, vol. 39, pp. 1-17, 1999.
- [160] T. M. Baughman, C. L. Talarico, and J. R. Soglia, "Evaluation of the metabolism of propranolol by linear ion trap technology in mouse, rat, dog, monkey, and human cryopreserved hepatocytes," *Rapid Commun Mass Spectrom*, vol. 23, pp. 2146-50, Jul 2009.
- [161] D. Borenshtein, R. C. Fry, E. B. Groff, P. R. Nambiar, V. J. Carey, J. G. Fox, and D. B. Schauer, "Diarrhea as a cause of mortality in a mouse model of infectious colitis," *Genome Biol*, vol. 9, p. R122, 2008.
- [162] D. R. Clayburgh, L. Shen, and J. R. Turner, "A porous defense: the leaky epithelial barrier in intestinal disease," *Lab Invest*, vol. 84, pp. 282-91, Mar 2004.
- [163] G. T. Ho, F. M. Moodie, and J. Satsangi, "Multidrug resistance 1 gene (P-glycoprotein 170): an important determinant in gastrointestinal disease?," *Gut*, vol. 52, pp. 759-66, May 2003.
- [164] G. T. Ho, N. Soranzo, E. R. Nimmo, A. Tenesa, D. B. Goldstein, and J. Satsangi, "ABCB1/MDR1 gene determines susceptibility and phenotype in ulcerative colitis: discrimination of critical variants using a gene-wide haplotype tagging approach," *Hum Mol Genet*, vol. 15, pp. 797-805, Mar 1 2006.

- [165] C. M. Panwala, J. C. Jones, and J. L. Viney, "A novel model of inflammatory bowel disease: mice deficient for the multiple drug resistance gene, *mdr1a*, spontaneously develop colitis," *J Immunol*, vol. 161, pp. 5733-44, Nov 15 1998.
- [166] K. H. Banner, C. Cattaneo, J. L. Le Net, A. Popovic, D. Collins, and J. D. Gale, "Macroscopic, microscopic and biochemical characterisation of spontaneous colitis in a transgenic mouse, deficient in the multiple drug resistance 1a gene," *Br J Pharmacol*, vol. 143, pp. 590-8, Nov 2004.
- [167] A. Sparreboom, J. van Asperen, U. Mayer, A. H. Schinkel, J. W. Smit, D. K. Meijer, P. Borst, W. J. Nooijen, J. H. Beijnen, and O. van Tellingen, "Limited oral bioavailability and active epithelial excretion of paclitaxel (Taxol) caused by P-glycoprotein in the intestine," *Proc Natl Acad Sci U S A*, vol. 94, pp. 2031-5, Mar 4 1997.
- [168] B. Greiner, M. Eichelbaum, P. Fritz, H. P. Kreichgauer, O. von Richter, J. Zundler, and H. K. Kroemer, "The role of intestinal P-glycoprotein in the interaction of digoxin and rifampin," *J Clin Invest*, vol. 104, pp. 147-53, Jul 1999.
- [169] K. S. Lown, R. R. Mayo, A. B. Leichtman, H. L. Hsiao, D. K. Turgeon, P. Schmiedlin-Ren, M. B. Brown, W. Guo, S. J. Rossi, L. Z. Benet, and P. B. Watkins, "Role of intestinal P-glycoprotein (*mdr1*) in interpatient variation in the oral bioavailability of cyclosporine," *Clin Pharmacol Ther*, vol. 62, pp. 248-60, Sep 1997.
- [170] P. Hsiao, L. Sasongko, J. M. Link, D. A. Mankoff, M. Muzi, A. C. Collier, and J. D. Unadkat, "Verapamil P-glycoprotein transport across the rat blood-brain barrier: cyclosporine, a concentration inhibition analysis, and comparison with human data," *J Pharmacol Exp Ther*, vol. 317, pp. 704-10, May 2006.
- [171] P. B. Andreasen and L. Hutters, "Paracetamol (acetaminophen) clearance in patients with cirrhosis of the liver," *Acta Med Scand Suppl*, vol. 624, pp. 99-105, 1979.
- [172] P. Zapater, M. C. Lasso de la Vega, J. F. Horga, J. Such, R. Frances, A. Esteban, J. M. Palazon, F. Carnicer, S. Pascual, and M. Perez-Mateo, "Pharmacokinetic variations of acetaminophen according to liver dysfunction and portal hypertension status," *Aliment Pharmacol Ther*, vol. 20, pp. 29-36, Jul 1 2004.
- [173] W. Deng, B. A. Vallance, Y. Li, J. L. Puente, and B. B. Finlay, "Citrobacter rodentium translocated intimin receptor (Tir) is an essential virulence factor needed for actin condensation, intestinal colonization and colonic hyperplasia in mice," *Mol Microbiol*, vol. 48, pp. 95-115, Apr 2003.
- [174] G. Frankel, A. D. Phillips, M. Novakova, H. Field, D. C. Candy, D. B. Schauer, G. Douce, and G. Dougan, "Intimin from enteropathogenic *Escherichia coli* restores murine virulence to a *Citrobacter rodentium eaeA* mutant: induction of an immunoglobulin A response to intimin and EspB," *Infect Immun*, vol. 64, pp. 5315-25, Dec 1996.
- [175] S. Nikolaus and S. Schreiber, "Diagnostics of inflammatory bowel disease," *Gastroenterology*, vol. 133, pp. 1670-89, Nov 2007.

- [176] J. R. Korzenik and D. K. Podolsky, "Evolving knowledge and therapy of inflammatory bowel disease," *Nat Rev Drug Discov*, vol. 5, pp. 197-209, Mar 2006.
- [177] X. Li, L. Conklin, and P. Alex, "New serological biomarkers of inflammatory bowel disease," *World J Gastroenterol*, vol. 14, pp. 5115-24, Sep 7 2008.
- [178] F. Costa, M. G. Mumolo, L. Ceccarelli, M. Bellini, M. R. Romano, C. Sterpi, A. Ricchiuti, S. Marchi, and M. Bottai, "Calprotectin is a stronger predictive marker of relapse in ulcerative colitis than in Crohn's disease," *Gut*, vol. 54, pp. 364-8, Mar 2005.
- [179] J. Langhorst, S. Elsenbruch, J. Koelzer, A. Rueffer, A. Michalsen, and G. J. Dobos, "Noninvasive markers in the assessment of intestinal inflammation in inflammatory bowel diseases: performance of fecal lactoferrin, calprotectin, and PMN-elastase, CRP, and clinical indices," *Am J Gastroenterol*, vol. 103, pp. 162-9, Jan 2008.
- [180] P. I. Tarr, C. A. Gordon, and W. L. Chandler, "Shiga-toxin-producing *Escherichia coli* and haemolytic uraemic syndrome," *Lancet*, vol. 365, pp. 1073-86, Mar 19-25 2005.
- [181] P. S. Mead and P. M. Griffin, "*Escherichia coli* O157:H7," *Lancet*, vol. 352, pp. 1207-12, Oct 10 1998.
- [182] J. C. Paton and A. W. Paton, "Pathogenesis and diagnosis of Shiga toxin-producing *Escherichia coli* infections," *Clin Microbiol Rev*, vol. 11, pp. 450-79, Jul 1998.
- [183] M. Noris and G. Remuzzi, "Hemolytic uremic syndrome," *J Am Soc Nephrol*, vol. 16, pp. 1035-50, Apr 2005.
- [184] C. M. Thorpe, W. E. Smith, B. P. Hurley, and D. W. Acheson, "Shiga toxins induce, superinduce, and stabilize a variety of C-X-C chemokine mRNAs in intestinal epithelial cells, resulting in increased chemokine expression," *Infect Immun*, vol. 69, pp. 6140-7, Oct 2001.
- [185] C. Zoja, S. Angioletti, R. Donadelli, C. Zanchi, S. Tomasoni, E. Binda, B. Imberti, M. te Loo, L. Monnens, G. Remuzzi, and M. Morigi, "Shiga toxin-2 triggers endothelial leukocyte adhesion and transmigration via NF-kappaB dependent up-regulation of IL-8 and MCP-1," *Kidney Int*, vol. 62, pp. 846-56, Sep 2002.
- [186] A. Matussek, J. Lauber, A. Bergau, W. Hansen, M. Rohde, K. E. Dittmar, M. Gunzer, M. Mengel, P. Gatzlaff, M. Hartmann, J. Buer, and F. Gunzer, "Molecular and functional analysis of Shiga toxin-induced response patterns in human vascular endothelial cells," *Blood*, vol. 102, pp. 1323-32, Aug 15 2003.
- [187] T. Yamamoto, K. Nagayama, K. Satomura, T. Honda, and S. Okada, "Increased serum IL-10 and endothelin levels in hemolytic uremic syndrome caused by *Escherichia coli* O157," *Nephron*, vol. 84, pp. 326-32, Apr 2000.